Ph.D. Thesis in Chemical Science

CHIM02

Resonance Raman Spectroscopy As a Tool To Study The Heme Cavity Structure Of New Discovered Heme Proteins

Francesco Paolo Nicoletti

Ph.D. tutor

Prof. Giulietta Smulevich

Director of the Ph.D. School

Prof. Andrea Goti

UNIVERSITA' DEGLI STUDI DI FIRENZE

Firenze, December 2010

A mia madre Gisella e mio padre Silvio,
a zio Mimmo e zia Patrizia

Preface

During my Ph.D. thesis I have collaborated with:

Prof. P. Ascenzi, Dipartimento di Biologia Università di Roma Tre, Rome, Italy.

Prof. A. Boffi, Dipartimento di Scienze Biochimiche e Istituto CNR di Biologia Molecolare e Patologia, Università di Roma "La Sapienza", Rome, Italy.

Prof. M. Coletta Dipartimento di Medicina Sperimentale e Scienze Biochimiche Università di Roma Tor Vergata, Rome, Italy.

Prof. D. Estrin, Departamento de Química Inorgánica, Analítica y Química Física/INQUIMAE-CONICET, Facultad de Ciencias Exactas y Naturales, Universidad de Buenos Aires, Argentina.

Prof. S. Franzen, Department of Chemistry, North Carolina State University, Raleigh, North Carolina, USA.

Prof. L. Mazzarella and Dr. A. Vergara, Dipartimento di Chimica, Università di Napoli "Federico II", Naples, Italy.

Dr. C. Verde, Istituto di Biostrutture e Bioimmagini, CNR, Naples, Italy

Summary

The research activities during my Ph.D. thesis have been focussed on heme proteins, either in their native state or as site-directed mutants. In order to carry out these studies, I have used spectroscopic techniques of considerable importance in the characterization of the active sites of biomolecules: UV-Vis electronic absorption and resonance Raman (RR).

Heme proteins can play different biological functions, correlated to the different electronic features and structural properties of heme group. Therefore, my studies, which have been carried out over a large temperature range (10 – 300 K), at various pH and ionic strength values, in the presence of exogenous ligands, and in both solution and crystal phases, have provided extensive information on the spin and coordination state of the heme iron and on the heme pocket architecture.

During these years I have characterized hemoproteins of different organisms and functions: a) the complex between heme and Human Serum Albumin (HSA), previously object of my Laurea thesis and then further investigated during my PhD thesis; b) bacterial truncated hemoglobin from *Thermobifida fusca* (Tf-trHb); c) dehaloperoxidase-hemoglobin (DHP) from *Amphitrite ornata* terebellid polychaete; d) fish hemoglobin from *Eleginops Maclovinus* (*E. maclovinus* Hb 1); e) Neuroglobins (Ngbs) from *Chaenocephalus aceratus* and *Dissosticus mawsoni* Antarctic fishes.

a) Heme-Human Serum Albumin

HSA is the most abundant protein in the human serum. It consists of three domains and presents at least seven different binding sites. It is capable to bind heme and many drugs such as ibuprofen and warfarin. Allosteric properties of the monomeric heme-HSA complex under ibuprofen binding have been demonstrated spectroscopically: (Fe^{3+})heme-HSA is consistent with a 5-coordinated high spin (5cHS) heme containing a weak Fe^{3+}-OTyr coordination and becomes 6-coordinated low spin (6cLS) upon ibuprofen binding, with a histidine residue in the sixth coordination position (Tyr-Fe^{3+}-His). Moreover (Fe^{3+})heme-HSA catalyzes the peroxynitrite isomerization when the sixth axial coordination position is free. Since ibuprofen allosterically favours the 6cLS species, the peroxynitrite isomerization is impaired upon drug binding.

Finally, we investigated the pH effect on the Fe^{2+} form and on its complex with CO. At pH 7, the Fe^{2+} form is a mixture of a 5cHS species (with a Tyr coordinated to the iron) and 4-coordinated intermediate spin (4cIS) (due to weak interaction between the Fe^{2+} iron and the oxygen atom of the Tyr), and becomes a pure 6cLS species (His-Fe^{2+}-Tyr) at pH 10. Accordingly, at pH 7 upon addition of CO a CO-(Fe^{2+})heme-HSA adduct with a trans ligand weaker than His (i.e. Tyr), or no ligand at all is formed. At pH 10 a conformational transition occurs, which allows the weak trans ligand to be replaced by a His residue.

b) Truncated hemoglobin from the *Thermobifida fusca* bacterium

Truncated hemoglobins (trHbs) are divided into three groups and *Thermobifida fusca* (Tf) belongs to the II group, characterized by the presence in the distal cavity of three polar residues: TrpG8, TyrB10 and TyrCD1, providing three potential hydrogen bonds to the sixth coordinated heme iron axial ligand. In order to highlight the role of the distal residue(s), I have studied single, double and triple Phe mutants of Tf-trHb at TyrB10, TyrCD1, TrpG8 positions in presence of different exogenous lingand in both Fe^{3+} and Fe^{2+} states.

The WT, single, double and triple mutants carbomonoxy (CO) adduct data suggest that TrpG8 is the key residue in the CO stabilization, providing the strongest hydrogen-bonding, whereas TyrCD1 plays an ancillary role. The existence of two different conformers (form 1 singly H-bonded with TrpG8, and form 2 caged by TrpG8 and the distal TyrCD1 couple) suggest a flexible distal cavity.

Although trHbs can bind oxygen with high affinity, their function is not yet fully understood. Interestingly, it has been found that Tf-trHb Fe^{3+} form binds sulfide with an high affinity (giving rise to stable 6cLS species) and since its encoding gene is contained within a thiol redox pathway, we propose that Tf-trHb might be involved in sulfide metabolism.

At room and low temperatures the interaction between Fe^{3+} Tf-trHb and anionic ligands ($-F^-$, $-OH^-$) is currently under investigation.

c) Dehaloperoxidase-hemoglobin from the *Amphitrite ornata* terebellid polychaete

Dehaloperoxidase-hemoglobin (DHP) is a dimeric globin with a His residue in the distal cavity and shows peroxidase activity. At room temperature in the Fe^{3+} state, the distal histidine is in equilibrium between the open solvent-exposed position (5cHS) and the

closed conformation (aquo 6cHS). The link between the histidine and heme iron coordination extends to the binding of phenols to the protein. In fact, binding of the 4-iodophenol (inhibitor of peroxidase activity) in the distal heme cavity shifts the equilibrium towards the open conformation, as the protein is in a 5cHS state, while the substrate tri-fluorophenol binds externally to the distal side and favours the 6cHS. The 6cHS species is the catalitically active while the 5cHS is inactive: the flexibility of the distal His appears to play a role in a regulatory mechanism in DHP enzymatic function.
Recently it has been found that DHP has sulfide binding properties. Furthermore, a complete reduction of the Fe^{3+} heme occurring after sulfide exposure suggests an important role in the catabolism of sulfide, a toxic environmental threat.

d) Hemoglobin from the *Eleginops Maclovinus* fish

E. maclovinus is a member of the Nothoteinoidei family living in temperate waters and it possesses a tetrameric Hb. The *E. maclovinus* Hb 1 was studied in the Fe^{3+} form (in the absence and in presence of anionic ligands: $-OH^-$, $-F^-$, $-CN^-$), and in the Fe^{2+} form (deoxy, oxy- and –CO) in solution. In addition, the study of single crystals by microRaman spectroscopy was performed for *E. maclovinus* Hb1, in the Fe^{3+} state, deoxy, -CO and oxy in order to have a direct comparison with data obtained in solution and the X-ray diffraction patterns.

The aim of the project was to elucidate heme binding pocket structural features and to compare the *E. maclovinus* Hb 1 ligand properties with those of *T. bernacchii* Hb which belongs to the same family, but lives in Antarctic waters, in order to give an insight into structural features determining the cold adaptability.

The Fe^{3+} form is an equilibrium between a 6cLS hemicrome species (His-Fe^{3+}-His) and 6cHS aquo (His-Fe^{3+}-H_2O). Upon reduction to the Fe^{2+} form, a pure 5cHS deoxy species is obtained with a $\nu_{(Fe\text{-}Im)}$ at 213 cm^{-1} (typical frequency of Hb). In presence of CO two conformers are revealed: form 1 is consistent with a bound CO stabilized by a weaker H-bonding interaction with the distal histidine compared to human Hb A-CO; form 2 is a conformer having no polar interactions with the surrounding amino acids.

In conclusion, a hemichrome species is present in *E. maclovinus* Hb1 (Fe^{3+}) around pH 7 as previously observed in the antartic Hb from *T. bernacchi*, possibly due to the common origin from Nothoteinoidei family. Moreover the heme cavity properties of *E. maclovinus* Hb1 are essentially identical to those of *T. bernacchi* Hb and human HbA.

e) Neuroglobins from *C. aceratus* and *D. mawsoni* antarctic fishes

I have carried out a detailed comparative analysis of Ngbs isolated from the brain of the *C. aceratus* icefish, and from the retina of the closely related, but red-blooded, *D. mawsoni* Antarctic notothenioid, both in the Fe^{3+} and Fe^{2+} states and in presence of CO and O_2. In the absence of exogenous ligands the Fe^{3+} and Fe^{2+} forms of Ngbs are 6cLS being the distal and proximal histidines coordinated to the heme iron, similar to human and murine Ngbs. Moreover upon addition of O_2 and CO, the comparison of the $\nu_{(Fe\text{-}XO)}$ stretching frequencies clearly indicate that the exogenous ligands bind the different Ngbs in a similar manner, suggesting similar distal cavity properties.

Publications related to this thesis

1. **Francesco P. Nicoletti**, Barry D. Howes, Maria Fittipaldi, Gabriella Fanali, Mauro Fasano, Paolo Ascenzi, and Giulietta Smulevich.
   Ibuprofen Induces an Allosteric Conformational Transition in the Heme Complex of Human Serum Albumin with Significant Effects on Heme Ligation
   J. Amer. Chem. Soc. (2008) 130, 11677-11688
   (This study was started during my Laurea Thesis).

2. Paolo Ascenzi, Alessandra di Masi, Massimo Coletta, Chiara Ciaccio, Gabriella Fanali, **Francesco P. Nicoletti**, Giulietta Smulevich, and Mauro Fasano.
   Ibuprofen Impairs Allosterically Peroxynitrite Isomerization by Ferric Human Serum Heme-Albumin
   J. Biol. Chem. (2009) 284, 31006-31017.

3. **Francesco P. Nicoletti**, Alessandra Comandini, Alessandra Bonamore, Leonardo Boechi, Fernando Martin Boubeta, Alessandro Feis, Giulietta Smulevich, and Alberto Boffi.
   Sulfide Binding Properties of Truncated Hemoglobins
   Biochemistry (2010), 49, 2269-2278.

4. **Francesco P. Nicoletti**, Matthew K. Thompson, Barry D. Howes, Stefan Franzen, and Giulietta Smulevich.
   New Insights into the Role of Distal Histidine Flexibility in Ligand Stabilization of Dehaloperoxidase-hemoglobin from Amphitrite ornata
   Biochemistry (2010), 49, 1903-1912.

5. Matthew K. Thompson, Michael F. Davis, Vesna de Serrano, **Francesco P. Nicoletti**, Barry D. Howes, Giulietta Smulevich, and Stefan Franzen.
   Two-site competitive inhibition in dehaloperoxidase-hemoglobin
   Biophys. J. (2010), 99, 1586-1595.

6. Antonello Merlino, Luigi Vitagliano, Anna Balsamo, **Francesco P. Nicoletti**, Barry D. Howes, Daniela Giordano, Daniela Coppola, Guido di Prisco, Cinzia Verde, Giulietta Smulevich, Lelio Mazzarella, and Alessandro Vergara.
   Crystallization, preliminary X-ray diffraction studies and Raman microscopy of the major hemoglobin from the sub-Antarctic fish Eleginops maclovinus in the carbomonoxy form
   Acta Crystallogr. Sect. F: Struct. Biol. Cryst. Commun. (2010) F66, 1536-1540.

7. Enrica Droghetti, **Francesco P. Nicoletti**, Alessandra Bonamore, Leonardo Boechi, Pau Arroyo Mañez, Dario A. Estrin, Alberto Boffi, Giulietta Smulevich, and Alessandro Feis. *Heme pocket structural properties of a bacterial truncated hemoglobin from Thermobifida fusca*
   Biochemistry (2010), 49, 10394-10402.

Seminar presented by myself at National and International Conferences

August 2008: 21st International Conference on Raman Spectroscopy (ICORS 2008). Brunel University, Uxbridge, London (UK), (poster).
The allosteric effect of Ibuprofen on the axial coordination of the heme-Fe-atom in heme-human serum albumin.
F.P. Nicoletti, B.D. Howes, M. Fittipaldi, G. Fanali, M. Fasano, P. Ascenzi, G. Smulevich

August 2009: XIII European Conference on the Spectroscopy of Biological Molecules (ECSBM 2009). Palermo (Italy), (poster).
The key role of the distal histidine in dehaloperoxidase.
Francesco P. Nicoletti, Matthew K. Thompson, Barry D. Howes, Stefan Franzen, and Giulietta Smulevich

August 2010: 30th European Congress of Molecular Spectroscopy (EUCMOS 2010). Firenze (Italy), (poster).
Resonance Raman and UV-vis absorption spectra of *Thermobifida fusca* truncated hemoglobin in its ferric state.
F. P. Nicoletti, E. Droghetti, A. Feis, A. Boffi, and G. Smulevich

September 2010: XX National Conference of Italian School of Pure and Applied Biophysics (SIBPA 2010). Arcidosso (Italy), (oral presentation).
UV-vis and Resonance Raman structural characterization of Thermobifida fusca truncated hemoglobin
F. P. Nicoletti, E. Droghetti, A. Feis, A. Boffi, and G. Smulevich

Seminar presented by coworkers at National and International Conferences

July 2008: V International Conference on Porphyrins and Phthalocyanines (ICPP). Moscow (Russia), (oral presentation).
Ibuprofen binding to heme-Human Serum Albumin induces marked conformational changes: an allosteric modulation.
F.P. Nicoletti, B.D. Howes, M. Fittipaldi, G. Fanali, M. Fasano, P. Ascenzi, **G. Smulevich**

February 2009: XXI Congresso Nazionale GNRS. Milano (Italy), (oral presentation).
The intriguing world of truncated hemoglobins
Alessandro Feis, Barry D. Howes, Enrica Droghetti, Francesco P. Nicoletti, **Giulietta Smulevich**

July 2009: XXIII congresso nazionale della Società Chimica Italiana. Sorrento (Italy), (poster).
Ibuprofen modulates allosterically peroxynitrite isomerization by ferric human serum heme-albumin
Paolo Ascenzi, Alessandra di Masi, Massimo Coletta, Chiara Ciaccio, **Gabriella Fanali**, Francesco P. Nicoletti, Giulietta Smulevich, Mauro Fasano

August 2009: XIII European Conference on the Spectroscopy of Biological Molecules (ECSBM 2009). Palermo (Italy), (oral presentation).
Heme pocket structural properties of bacterial truncated hemoglobins as revealed by resonance Raman spectroscopy
A. Feis, E. Droghetti, B.D. Howes, F.P. Nicoletti, A. Boffi, C. Verde, **G. Smulevich**

April 2010: Proteine 2010. Parma (Italy), (poster).
Structural and functional characterisation of hemoglobins of *Eleginops maclovinus*, a sub-Antarctic notothenioid fish
D. Coppola, A. Vergara, F.P. Nicoletti, B.D. Howes, S. Bruno, R. Russo, D. Giordano, C. Ciaccio, A. Merlino, L. Vitagliano, C. Viappiani, M. Coletta, G. Smulevich, L. Mazzarella, G. di Prisco, C. Verde

July 2010: VI International Conference on Porphyrins and Phthalocyanines (ICPP). New Mexico (USA), (oral presentation).
The heme cavity structure of truncated bacterial hemoglobins as envisaged by resonance Raman spectroscopy.
A. Feis, E. Droghetti, B. D. Howes, F. P. Nicoletti, L. Boechi A. Boffi, C. Verde, and **G. Smulevich**

August 2010: XVIth International Conference on Oxygen Binding and Sensing Proteins (O2BIP). Antwerp Belgium), (poster).
Neuroglobin from brain and retina of Antarctic fish.

R. Russo, D. Giordano, W.V. Leuven, A. Nadra, F.P. Nicoletti, S. Bruno, A. Riccio, D.A. Estrin, G. Smulevich, L. Moens, C-H.C. Cheng, S. Dewilde, G. di Prisco, G. Hui Bon Hoa, S. Abbruzzetti, C. Viappiani, C. Verde.

August 2010: XVIth International Conference on Oxygen Binding and Sensing Proteins (O2BIP). Antwerp Belgium), (oral presentation).
Ligand binding properties of Thermobifida fusca truncated hemoglobin
Enrica Droghetti, Francesco P. Nicoletti, Alberto Boffi, Alessandro Feis and **Giulietta Smulevich**

September 2010: 10 Int. Conf. on Fundamental and Applied Aspects of Physical Chemistry. Belgrade (Serbia), (oral presentation)
Structural properties of truncated hemoglobins from unicellular organisms as revealed by resonance Raman Spectroscopy
E. Droghetti, A. Feis, B.D. Howes, F.P. Nicoletti, **G. Smulevich**

October 2010: Tenth workshop on pharmacobiometallics. Pozzuoli (NA, Italy), (oral presentation).
Resonance Raman spectroscopy of bacterial truncated hemoglobins
G. Smulevich, A. Feis, E. Droghetti, F.P. Nicoletti, B.D. Howes, A. Boffi, C. Verde

Abbreviations

Hb: hemoglobin

Mb: myoglobin

HSA: human serum albumin

trHbs: truncated hemoglobins

Tf-trHb: truncated hemoglobin from *Thermobifida fusca*

Bs-trHb: truncated hemoglobin from *Bacillus subtilis*

DHP: dehaloperoxidase-hemoglobin from *Amphitrite ornata*

E. maclovinus Hb1: hemoglobin from *Eleginops maclovinus*

P. urvillii Hb: hemoglobin from *Pseudaphiritis urvillii*

T. bernacchii Hb: hemoglobin from *Trematomus bernacchii*

T. newnesi Hb: hemoglobin from *Trematomus newnesi*

Ngb: neuroglobin

C. aceratus Ngb: neuroglobin from *Chaenocephalus aceratus*

D. mawsoni Ngb: neuroglobin from *Dissosticus mawsoni*

CCP: cytochrome c peroxidase

HRP: horseradish peroxidase

Ibu: ibuprofen

WF: warfarin

4IP: 4-iodophenol

TFP: 2,4,6-trifluorophenol

UV-Vis: ultraviolet-visible

RR: resonance Raman

EPR: electron paramagnetic resonance

HS: high spin

LS: low spin

IS: intermediate spin

4c: 4-coordinated

5c: 5-coordinated

6c: 6-coordinated

RT: room temperature

LT: low temperature

WT: wild type

CT: porphyrin(π)→iron (d_z^2) charge transfer band

CT1: long wavelength (>600 nm) (π)→iron (d_π) charge transfer band

$\nu_{(Fe\text{-}Im)}$: iron-imidazole stretching mode

$\nu_{(Fe\text{-}CO)}$: iron-carbon monoxide stretching mode

$\nu_{(CO)}$: carbomonoxide stretching mode

$\nu_{(Fe\text{-}O2)}$: iron-oxygen stretching mode

$\nu_{(Fe\text{-}OH)}$: iron-hydroxide stretching mode

$\nu_{(Fe\text{-}F)}$: iron-fluoride stretching mode

$\nu_{(Fe\text{-}CN)}$: iron-cyanide stretching mode

TRIS: hydroxymethyl-aminomethane

PBS: phosphate-buffered saline

MOPS: 3-(N-morpholino)propanesulfonic acid

pdb: protein data bank

Chapter 1

Heme characterization: spectroscopic techniques

1.1 The heme group

The biochemical activity of hemoproteins derives in part from the structural properties of heme group. It is well accepted that heme is of considerable biological importance, being the active centre for ligand binding, electron transfer and catalytic activity. Several biologically different types of heme exist, the most important being the heme b (or protoporphyrin IX). In the thesis I studied protoporphyrin IX containing proteins.

The heme contains one iron atom coordinating the nitrogens of the protoporphyrin IX in the equatorial positions (Figure 1.1). The protoporphyrin IX is a tetrapyrrole macrocycle containing different peripheral substituents: two vinyl groups in positions 2 and 4, four methyl groups in 1, 3, 5 and 8 and two propionyl chains in positions 6 and 7. The iron can assume two stable oxidation state, the ferric (Fe^{3+}) and ferrous (Fe^{2+}) forms.

Whereas free iron-protoporphyrin IX adopts a planar structure, the protein matrix can exert constraints that diminish the planarity of the chromophore.

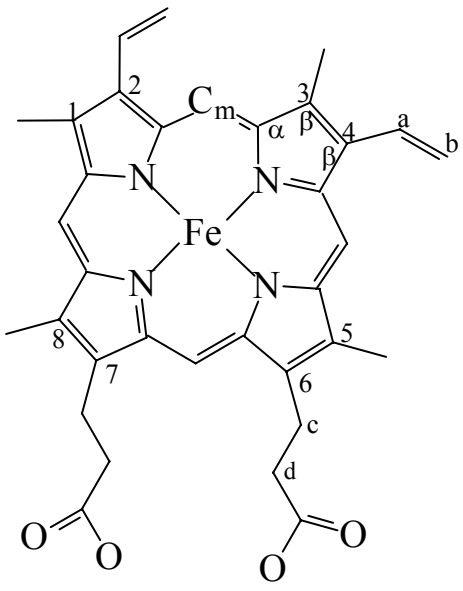

Figure 1.1 Structure of Fe-protoporphyrin IX: the heme.

1.2 Electronic absorption spectroscopy

In quantum mechanics, a radiative transition between two states *m* and *n* can occur only if the transition moment, a vector quantity given by the integral

$$\int \Psi_n^* \mu \Psi_m d\tau \qquad (1.1)$$

is different from zero; Ψ_m and Ψ_n are the wavefunctions associated with the ground and the excited states, respectively, and μ is the electric dipole moment operator.

It is possible to evaluate whether the (1.1) is different from zero by symmetry considerations. When electronic transitions are considered, if vibrations are not excited either in the lower or in the upper electronic states, assuming that the Born-Oppenheimer approximation holds, the general requirement is that the product

$$\Psi_n^* \mu_i \Psi_m \qquad (1.2)$$

(where $i = x, y, z$) is totally symmetric for at least one orientation.

The transition is allowed when the direct product of the species (Γ) of Ψ_n, Ψ_m, and μ has a totally symmetric component (TS), *i.e.*: $\Gamma(\Psi_n) \times \Gamma(\mu_i) \times \Gamma(\Psi_m) \cap \Gamma_{TS}$. When the peripheral substituents are approximated as point masses and axial ligands are neglected, the idealized protoporphyrin IX chromophore has pseudosymmetry D_{4h}.

The optical properties of the iron-protoporphyrin IX complexes have been studied since many years (1) and are considered deriving from the highly conjugated π electron system. Two electronic transitions (giving rise to B and Q bands) dominate the UV-Vis region of the absorption spectrum of iron-porphyrin complex, that correspond to the porphyrin $\pi \rightarrow \pi^*$ singlet transitions. The B band corresponds to the $a_{1u} \rightarrow e_g$ transition and the Q band to the $a_{2u} \rightarrow e_g$ transition (Figure 1.2). There is a strong interaction between these two transitions, so that the transition dipoles are summed for the intense B band (also called Soret) and nearly cancelled for the Q band. Some intensity is regained by the Q transition via vibronic mixing (*1*), giving rise to the Q_0 (α) band and its vibronic envelope, Qv (β) band.

When the conjugation of the porphyrin ring is extended to the vinyl groups the energy of the Q and B transitions is lowered and consequently the absorption bands can be red shifted by 4-10 nm, depending on the degree of conjugation between the porphyrin aromatic system and the vinyl double bonds (*2*).

Applying the Huckel approximation method, Gouterman discovered an interaction between the π orbitals of the porphryn and d orbitals of the iron, due to their comparable

energetic levels and favourable symmetry (*3*). Therefore, information about the oxidation, the spin and the coordination states of the heme iron can be obtained by the wavelength of the Soret, β and α bands of the UV-Vis spectra. In fact, (Fe^{2+}) has six valence electrons in its 3d orbitals while (Fe^{3+}) has five valence electrons. The two axial positions of the iron atom can be occupied by ligands and they could introduce an external perturbation. If the interaction with ligands is weak or the sixth position is not occupied, the d orbitals are quasi-degenerate and the occupancy follows the Hund's rule, thus producing a high spin (HS) configuration: S = 5/2 for (Fe^{3+}) and S = 2 for (Fe^{2+}). On the other hand, a strong interaction with the ligands can alter the relative energies of the 3d orbitals removing their degeneracy (the well-known process of ligand field splitting) and produce a low spin (LS) configuration. In this case the two 3d orbitals that point directly to the approaching ligands, i.e. the dz^2 and the dx^2-dy^2**,** are lifted in energy above the remaining three 3d orbitals (d_{xy}, d_{xz} and d_{yz}), and the electrons occupy only the lower orbitals generating the configuration S = 1/2 for (Fe^{3+}) and S = 0 for (Fe^{2+}). Since in the LS configuration the higher energy orbitals are unoccupied, the size of the core containing the iron atom is smaller than in the HS configuration and the metal lies in the plane of the tetrapyrrole ring, while the HS iron sits out of plane.

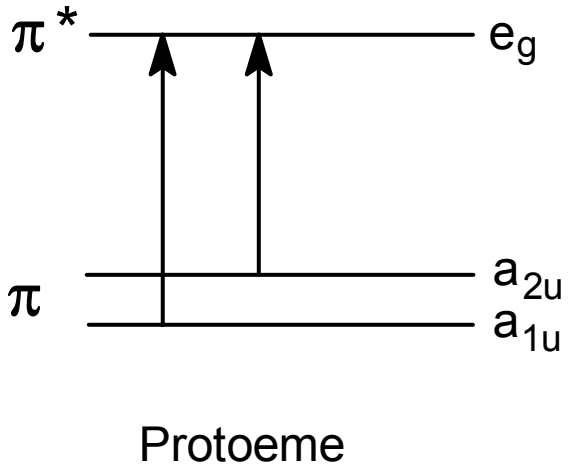

Figure 1.2 Gouterman's four orbital diagram.

Furthermore, an extra band at longer wavelength (in the 600-700 nm region) is observed only for high-spin (HS) Fe^{3+} heme proteins, assigned to a charge-trasfer transition (CT1) from the porphyrin to the iron orbitals [$a_{2u}(\pi) \rightarrow e_g(d_\pi)$] (Figure 1.3). The intensity and the wavelength of the CT1 band are related to the energy difference between the d

orbitals of the metal and the π orbitals of the porphyrins, which in turn, depend on the nature of the axial ligands.

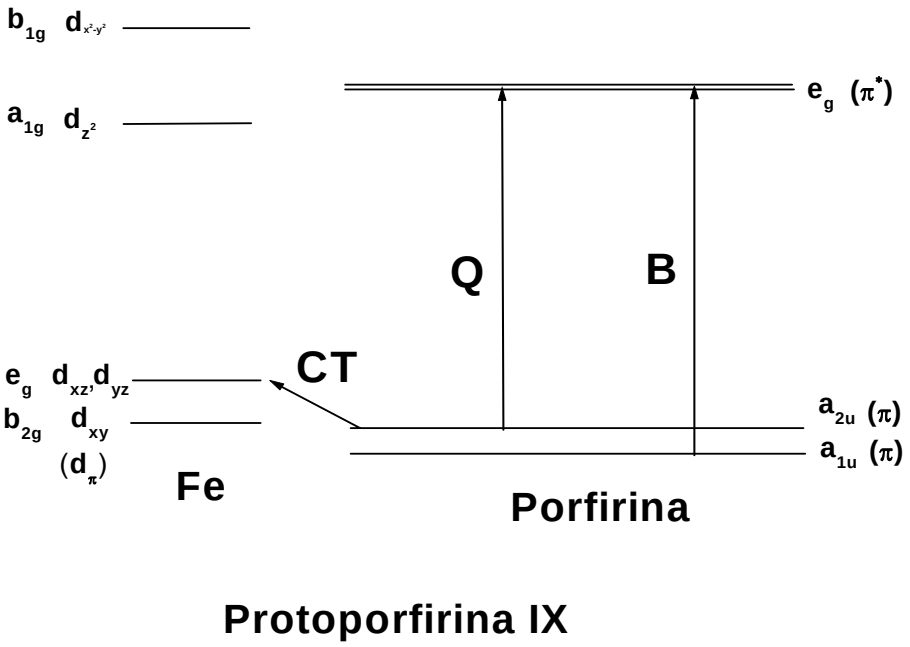

Figure 1.3 Electronic transitions observed in a heme protein. On the left: energy levels for the iron atom; on the right: energy levels for the protoporphyrin.

1.3 Raman and Resonance Raman spectroscopy theory

Vibrational spectroscopy deals with the processes of interaction of light with matter which produce a variation in the vibrational motions of the atoms. Light is an electromagnetic wave which consists of an electric field vector and a magnetic field vector which are perpendicular to each other. For Raman scattering only the electric field vector is important. The electric field varies with the time according to the following relation (*4*):

$$E_z(t) = E_{max}\cos 2\pi\nu_0 t$$

- E_z = electric field along z direction
- E_{max} = maximum magnitude of electric field
- ν_0 = frequency of incident light
- t = time

Vibrational spectra contain important information at molecular level, the frequencies of molecular vibrations depending upon the masses of the atoms, the molecular geometry and the forces binding the atoms together.

The basic requirement for Raman and resonance Raman (RR) scattering is the induction of an instantaneous dipole moment into the electron cloud of the molecule. The induced dipole moment μ depends on the strength of the electric field, E, of the light wave and on the electric polarizability, α, of the molecule: $\mu = \alpha E$. The electric polarizability α is an anisotropic characteristic, i.e. it depends on the direction of the molecule bonds respect to the electronic field direction.

For a quantum mechanical description of Raman and RR scattering the wave particle dualism, the Boltzmann distribution and the consideration of discrete energy levels instead of continuous energy levels have to be taken into account. If a photon strikes a molecule, the photon will be scattered either in elastic or inelastic way. If the photon is elastically scattered, what is more probable than inelastic, then no energy transfer occurs and the frequency of the incident photon and of the scattered photon will be the same (Rayleigh scattering; Figure 1.4). If inelastic scattering occurs, then energy can be transferred from the photon to the molecule or from the molecule to the photon. Upon the energy transfer from the photon to the molecule, the molecule will go into a higher energy state. Instantaneously a photon will be re-emitted with a lower energy (Stokes scattering; Figure 1.4). In the case of Stokes scattering a molecule is already in a vibrational excited state. Upon scattering of the incident light by the molecule, the molecule goes to a lower vibrational state and energy is transferred from the molecule to the photon, so that the frequency of the photon is higher after the scattering than before the scattering (anti-Stokes scattering; Figure 1.4).

The difference between Raman and RR consists of the energy level of the excited state: in Raman process the molecule is excited to an unstable state, called virtual level, since it does not correspond to any real electronic state of the system. In RR, the excitation wavelength is close to an allowed electronic transition with frequency $(\nu_{ei}) = (E_e - E_i)/h$ (Figure 1.4).

The difference between Raman and RR spectroscopies from other spectroscopies like fluorescence is that a radiationless relaxation process does not occur before the radiative transition.

Laser sources provide the exciting line for Raman and RR spectroscopies.

The transition between two vibrational levels *j* and *k* can occur only if the integral

$$\int \Psi_{fv} \, \alpha \, \Psi_{iv} \, d\tau$$

is different from zero, where Ψ_{iv} and Ψ_{fv} are the vibrational functions associated with the initial and final states. In the harmonic approximation, only fundamental transitions are allowed in the Raman and RR spectra. Anharmonic motions of the nuclei must be taken into account to explain the activity of overtone and combination transitions.
It is possible to use symmetry considerations to evaluate when the integral is different from zero. The general requirement is $\Gamma(\Psi_{fv}) \times \Gamma(\alpha) \times \Gamma(\Psi_{iv}) \cap \Gamma_{TS}$, where α is a second-order tensor.
I have analyzed only Stokes lines, therefore, only transitions where the lower vibrational level is the zero-point level must be taken into account, that is to say (Ψ_{iv}) = Γ_{TS} and the general requirement for a transition to be allowed becomes $\Gamma(\Psi_{fv}) \times \Gamma(\alpha) \cap \Gamma_{TS}$. Moreover, I performed only RR experiments.

Compared to other technique, Raman and RR spectroscopies offer many advantages:
1. A very small amount of sample is necessary. Experiments are carried out on small sample volumes (down to 30 μl), protein concentration being in the range between 5 x 10^{-6} and 5 x 10^{-4} M.
2. Experiments are carried out under physiological conditions. It is possible to dissolve proteins in appropriate buffers, because, unlikely infrared spectroscopy, there is only little interference from the water bands.
3. Minimal or no sample damage are caused when appropriate experimental conditions are chosen.
4. Spectra can be obtained also at low temperatures that prevent the sample damage and increase spectral resolutions. Moreover low temperatures measurements can be directly compared with data obtained by electronic paramagnetic resonance (EPR) and X-ray diffraction that usually work at low temperatures.
5. In comparison to Raman spectroscopy, RR spectroscopy has the advantage that only the totally symmetric vibrations (A_{1g}) of the chromophore are enhanced. Moreover, the intensities of the RR bands are significantly stronger then in the Raman spectrum (intensity enhancement by 2 or 3 order of magnitude).

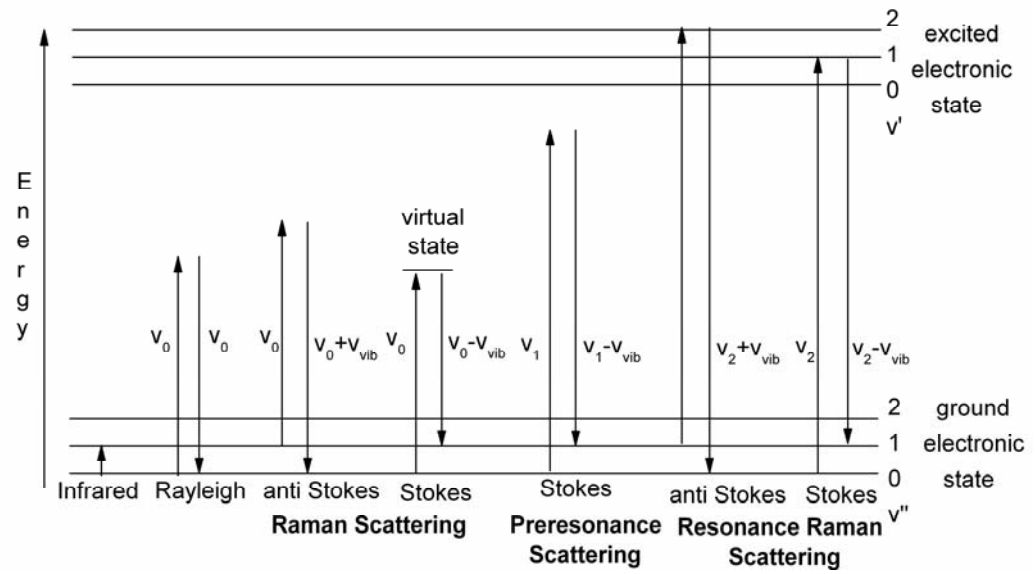

Figure 1.4 Energy level scheme for IR, Raman scattering, pre-resonance Raman scattering and resonance Raman scattering. If the energy of the incoming does not correspond to the energy difference between an excited electronic state and ground electronic state, i.e. the incoming light is not in resonance with an excited electronic state, then Raman scattering will occur. The figure is adapted from reference (*4*).

1.3.1 The polarization of Raman bands

The depolarization ratio ρ of a Raman band gives information regarding the symmetry of the vibration. This quantity is a measure of the degree to which the polarization properties of the incident radiation change after scattering has occurred.

The laser beam incident radiation is in plane polarized. The depolarization ratio ρ is defined as follows: $\rho = I_{\perp}/I_{//}$

where $I_{\perp}$ and $I_{//}$ are the intensity of scattered light with the electric vector perpendicular and parallel to the polarization of the incident light, respectively.

Under the pseudo-symmetry D_{4h} totally symmetric vibrations (A_{1g}) are characterized by $\rho = 1/8$ and are called polarized. For vibrations whose symmetry is B_{1g} or B_{2g} it comes out that $\rho = 3/4$ and the Raman bands are called depolarized. For A_{2g} modes $\rho = 3/4$ and the Raman bands are called inversely or anomalously polarized.

1.4 Resonance Raman spectroscopy of heme proteins: core-size modes

RR spectroscopy is well suited to characterize heme proteins and can occur either by exciting in the Soret band or in the α, β bands (Figure 1.5). Excitation close to the Soret band results in Franck-Condon scattering and enhances totally symmetric vibrations (A_{1g} modes). Excitation in the α, β region results in the enhancement of non-totally symmetric vibrations (B_{1g}, B_{2g} and A_{2g}). However, due to the Jahn-Teller effect (which occurs when two electronic transitions become degenerate) non-totally symmetric modes are also observed in the RR spectra upon Soret excitation. In fact, the Jahn-Teller effect is a limiting case of vibronic scattering and, therefore, the mixing vibrations (of B_{1g} and B_{2g} symmetry) are strongly enhanced.

An idealized metalloporphyrin with D_{4h} symmetry, where the peripheral substituents are approximated as point masses and axial ligands are neglected, has 37 atoms, which result in 105 (3N-6) normal modes of vibration: 71 (2N-3) in the porphyrin plane and 34 (N-3) out of the porphyrin plane (*5*). The symmetry species of the 105 normal vibrations of the porphyrin ring are:

$\Gamma_{(inplane)} = 9\ A_{1g} + 8\ A_{2g} + 9\ B_{1g} + 9\ B_{2g} + 18\ E_u$

$\Gamma_{(outofplane)} = 3\ A_{1u} + 6\ A_{2u} + 5\ B_{1u} + 4\ B_{2u} + 18\ E_g$

Upon Soret excitation, the RR spectrum in the high frequency region from about 1300 to 1700 cm^{-1} consists of in-plane porphyrin vibrations. This region contains the oxidation marker band ν_4, which provides information about the oxidation state of the metal atom, the core size marker bands, ν_2, ν_3, ν_{10} which provide information about the coordination and the spin state of the metal, and the vinyl $\nu_{(C=C)}$ stretches between 1600-1640 cm^{-1} (Table 1.1).

The frequency of the core size marker bands is markedly affected by the coordination and the spin state of the metal atom. The frequencies of these bands are observed at higher wavenumbers for the low-spin than for the high-spin configurations of the iron atom. This is due to the fact that in the low-spin complexes the valence electrons are accommodated in the low-lying energy orbitals and the antibonding orbital $d_{x^2-y^2}$, which points towards the nitrogen atom of the porphyrin ring, is empty. The bonds between

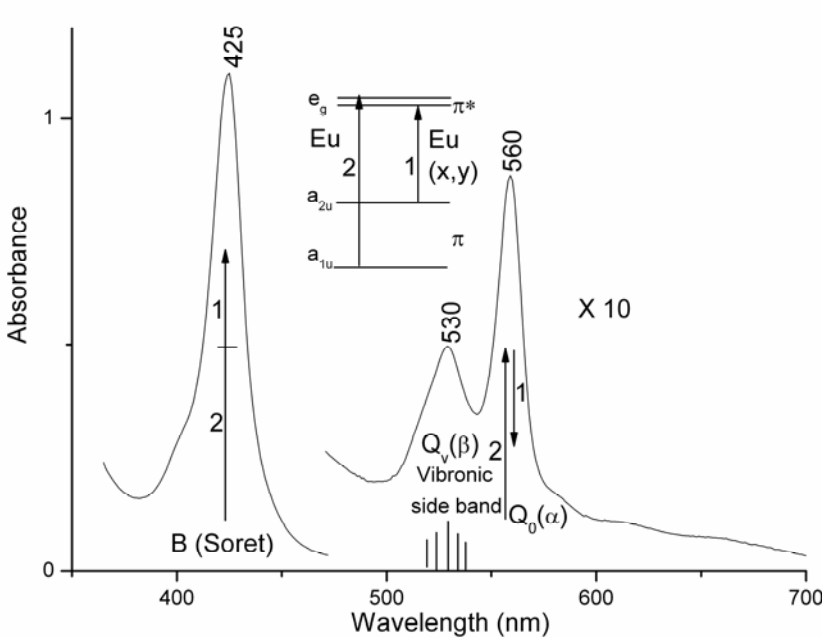

Figure 1.5 UV-Vis spectrum of Ngb (Fe^{2+}) from *D. aceratus*. The schematic representation of the Gouterman four orbital model for a metalloporphyrin is also reported. The electronic transitions which give rise to the Soret band and the $Q_o(\alpha)$ band are indicated by the arrows. In the case of the Soret band the two electronic transitions 1 and 2 are additive and in the case of the α band the transitions are subtractive. The $Q_v(\beta)$ band is an envelope of 0-1 vibronic transitions induced by mixing of the Soret and Q transition.

the iron atom and the porphyrin ligand are consequently shortened, thus inducing a contraction of the porphyrin ring. On the contrary, when the electronic configuration of the iron atom is high spin, both the d_z^2 and $d_{x^2-y^2}$ orbitals contain an electron and consequently the bonds between the iron atom and the ligands are lengthened and the macrocycle core expanded (*5*).

Moreover, the frequencies of these bands are lower for 6cHS complexes than for the 5cHS forms, due to the fact that, while in the former the iron atom is located in the heme plane, in the latter the iron atom is displaced from the heme cavity towards the fifth ligand, thus inducing the contraction of the macrocycle cavity and the consequent upshift of the frequency.

In the 1610-1640 cm^{-1} region, the vinyl stretches occur. On the basis of RR spectra and local density functional calculations on mono- and divinyl-hemes, it has been proposed that two distinct $\nu_{(C=C)}$ stretching modes occur when the protein matrix exerts no constraints on the vinyl groups: one band at about 1620 cm^{-1} is assigned to the nearly in-plane vinyl group whereas the other band, around 1630 cm^{-1}, to an out-of-plane vinyl group (*2, 6*). A direct relationship between the $\nu_{(C=C)}$ stretching wavenumber and the orientations of the vinyl groups (i.e., their torsional angles), as induced by specific

protein interactions, has been established for heme-containing peroxidases and myoglobin (*2*).

Vinyl groups are known to induce Raman activity in E_u modes and to remove their degeneracy (*7*). For example, in the spectrum of Fe^{3+} aquo Mb ν_{37} is seen with significant intensity at 1583 cm^{-1} (*8*). Moreover ν_{38} is splitted in two components at 1511 and 1521 cm^{-1}. Vinyl groups also induce a significant change in the normal mode composition of ν_2 and ν_{11}.

To assign most of the bands of a metalloporphyrin the ^{14}N atoms of the pyrrole rings were substituted by ^{15}N atoms (*8*), the hydrogen atoms of the porphyrin ring, the propionate groups and the vinyl groups were substituted by deuterium (*8*) and the ^{56}Fe, in the case of myoglobin, was substituted as well by ^{54}Fe (*9*).

Table 1.1 Core size marker bands of a general hemoglobin in the region from 1300-1700 cm^{-1}

			(Fe^{2+})		**(Fe^{3+})**		
Mode	**Sym.**	**Pol.**	**5cHS**	**6cHS**	**6cHS**	**5cHS**	**6cLS**
ν_4	A_{1g}	p	1357	1359	1370	1373	1373
ν_3	A_{1g}	p	1471	1493	1480	1491	1502
ν_{11}	B_{1g}	dp	1547	1539	1545	1553	1562
ν_2	A_{1g}	p	1562	1584	1559	1570	1579
ν_{19}	A_{2g}	ap	1550	1583	1560	1571	1586
ν_{10}	B_{1g}	dp	1604	1617	1610	1626	1640

1.5 Modes active in the low frequency region

In the low frequency region in-plane porphyrin vibrations, out-of -plane vibrations, the bending modes of the vinyl and the propionate groups and metal ligand vibrations can be found (*10, 11*). In particular if the heme is distorted, the spectra are particularly rich of bands, since many modes which in the D_{4h} symmetry were not enhanced become active. Therefore, RR spectroscopy can provide information about the interactions between the prosthetic group peripheral substituents and the heme environment.

The low frequency region of the heme proteins RR spectra contains heme-ligand vibrational modes that allow the identification of the axial ligands of the heme and can give relevant information on the interaction between the ligand and the residues of the heme cavity.

1.5.1 Endogeneous ligand: iron imidazole stretching mode $\nu_{(Fe\text{-}Im)}$

Information on the proximal heme cavity can be obtained by the RR spectra of 5cHS Fe^{2+} heme proteins. In the 200-250 cm^{-1} region, the frequency of a strong band due to the iron imidazole stretching mode, $\nu_{(Fe\text{-}Im)}$, occurs, identified on the basis of isotopic substitution (^{56}Fe replaced by ^{54}Fe). It is still unclear the reason why in the 6cLS Fe^{2+} species, the $\nu_{(Fe\text{-}Im)}$ is not detected.

The $\nu_{(Fe\text{-}Im)}$ stretching mode frequency is very sensitive to the strength of the bond between the iron atom and the imidazole N_ε. Studies of 5cHS Fe^{2+} porphyrins model compounds containing 2-methylimidazole (2-MeIm) ligand (the 2-methyl group providing steric hindrance to the Fe moving into the porphyrin plane and forming a 6c complex) demonstrated that a shift of this band maybe indicative of a change of the H-bonding of the proton of the proximal histidine N_δ-H (*12, 13*). The $\nu_{(Fe\text{-}2\text{-}MeIm)}$ stretching is observed at 219 cm^{-1} in a simple aqueous solution but it shifts to lower frequency (208 - 209 cm^{-1}) in presence of detergent. It is thought that the micelle formation by detergent reduces the water molecule--H-N_1(2-MeIm) contact, reducing the basicity of 2-MeIm and thus lowering the $\nu_{(Fe\text{-}2\text{-}MeIm)}$ frequency. Moreover in non-H-bonding solvents (CH_2Cl_2), in which the H-N_1(2-MeIm) deprotonation is avoided, $\nu_{(Fe\text{-}2\text{-}MeIm)}$ frequency is at the lowest frequency (200 cm^{-1}) (*14*). Unlikely, in presence of a strong base such as NaH, the 2-MeIm is ionized to 2-$MeIm^-$ and the band at 233 cm^{-1} was assigned to $\nu_{(Fe\text{-}2\text{-}MeIm)}$ (*14*). The frequency shift observed in 5cHS Fe^{2+} porphyrins model compounds well explains the difference between $\nu_{(Fe\text{-}Im)}$ frequencies of deoxy Mb and peroxidases. In myoglobin (Mb), where the N_δ proton is H-bound to a neutral backbone carbonyl group, $\nu_{(Fe\text{-}Im)}$ is at 220 cm^{-1} (*15*). Interestingly in peroxidases, the N_δ-H is H-bound to the carboxylate group of a conserved aspartic residue, imparting an imidazole character to the proximal histidine and thus shifting the $\nu_{(Fe\text{-}Im)}$ stretching to higher frequency (230-246 cm^{-1}) (*16*).

Furthermore the $\nu_{(Fe\text{-}Im)}$ frequency can depend on the π^*_{por} and $\sigma^*Fe_{\text{-}His}$ orbitals overlapping. Three σ electrons are involved in the Fe-His bond; two of these are donated by the sp^2 histidine to dz^2 iron orbital and they lie in $\sigma_{Fe\text{-}His}$. The third electron derives from the iron and is localized on the $\sigma^*_{Fe\text{-}His}$ antibonding, that points towards Fe-His vector, which is described by the tilting (θ) and the rotation (Φ) angles. The θ is defined by the histidine inclination respect to the heme normal (z axis, Figure 1.6 left); the Φ angle measures the rotation of the imidazole plane respect to the axis passing through N(1)-Fe-N(3) porphryn plane (Figure 1.6 left). An increasing of the θ angle induced by protein matrix gives rise to a weakness of the Fe-His bond due to the repulsion between the porphyrin nitrogens and the proximal histidine hydrogens, resulting in a lower $\nu_{(Fe\text{-}Im)}$ frequency (*17*). An example of this concept has practically been found in the difference between the $\nu_{(Fe\text{-}Im)}$ stretching frequency in the T (low affinity for O_2) and R states (high affinity for O_2) of deoxy Hb at 215 and 222 cm^{-1}, respectively (*18*). In the T structure the proximal histidine is more tilted from the heme normal than in the R structure (*19*), causing a strained and less stable bond, and thus the $\nu_{(Fe\text{-}Im)}$ frequency is lower.

On the other side, to a lower ϕ value it corresponds an high repulsion between the π_{por} and the $\sigma^*_{Fe\text{-}His}$ electrons. Since there is an interaction between π^*_{por} and $\sigma^*Fe_{\text{-}His}$ (Figure 1.6 right), and in particular the $\sigma^*Fe_{\text{-}His}$ donates an electron to the LUMO of porphyrin (*20*), thus the repulsion diminishes and the $\nu_{(Fe\text{-}Im)}$ frequency increases.

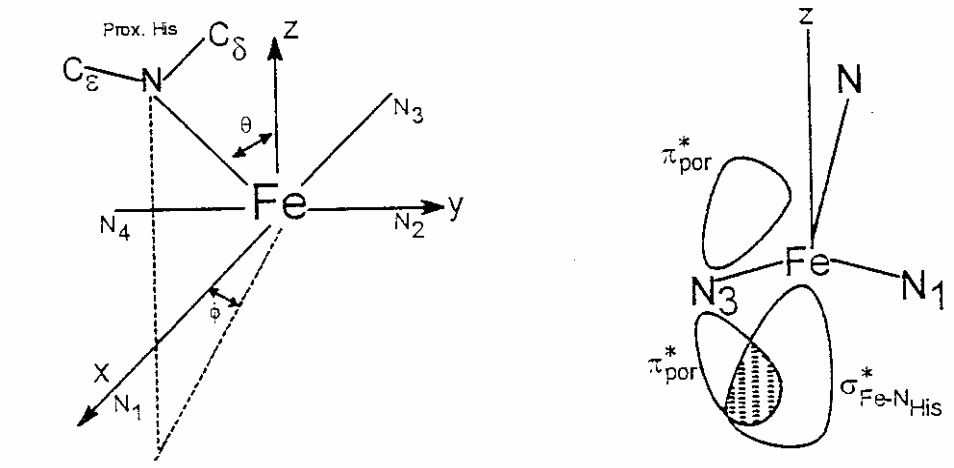

Figure 1.6 Schematic description of ϕ and θ angles (left), and the interaction between porphyrin, iron and histidine antibonding orbitals (right). The figure is adapted from reference (*17*).

1.5.2 Exogeneous ligands

In the low frequency region the $\nu_{(Fe\text{-}exogenous\ ligand)}$ modes (i.e. exogenous ligands are: -CO, $-O_2$, $-F^-$, $-OH^-$, $-SH^-$) can be detected and their frequencies are influenced by the nature, the geometry and the orientation of the distal residues of the heme cavity interacting with exogenous ligands. To identify the vibrations of exogenous ligands, isotopic substitution is frequently used. In fact a shift in frequency is expected upon substitution of an atom which participates in the vibration, according to the formula $\nu = (1/\pi) \times (k/\mu)^{1/2}$, where ν is the frequency, k = force constant and μ is the reduced mass. Isotopic substitution is used for the assignment of the metal ligand vibrations for exogenous ligands such as $-O_2$, -CO, $-OH^-$ and $-CN^-$.

New hemoproteins binding properties were compared to those of globins (Mb and Hb) and peroxidases (HRP) taken as references due to their different polarity of the distal cavity. In fact in the globins, the distal histidine controls the coordination in the sixth axial position through its N_ε hydrogen bonding, meanwhile in peroxidase along with an histidine, a positive charged guanidinium group of an arginine increases the polarity of the distal cavity and plays the key role in ligand binding.

1.5.2.1 Carbon monoxide (CO)

The CO ligand has been used to probe the structure and bonding in transition metal carbonyl complexes, including CO adducts of the heme group. When bound to heme, the frequency of the $\nu_{(CO)}$ stretch diminishes by 200 cm^{-1} as compared to its frequency, 2143 cm^{-1}, as free gas. This frequency falls in a region of the vibrational spectrum which is relatively free of interferences from other molecular vibrations. At the same time the $\nu_{(CO)}$ infrared intensity is greatly augmented. These effects are due to the back bonding donation. Fe^{2+} d_π electrons are donated to the empty CO π^* orbitals, thereby diminishing the CO bond order and increasing the $\nu_{(Fe\text{-}CO)}$ frequency; at the same time the transition dipole moment is increased because compressing and expanding the CO bond shifts electrons back and forth between the CO and Fe^{2+} orbitals.

The $\nu_{(Fe\text{-}CO)}$ and $\nu_{(CO)}$ stretching frequencies for a number of carbonmonoxy complexes of metalloporphyrins and hemoproteins are listed in Table 1.2. The data are also shown in Figure 1.7 as a plot of $\nu_{(Fe\text{-}CO)}$ versus $\nu_{(CO)}$ stretching frequencies. The slopes of the plots are negative due to the back-bonding phenomenon.

By the analysis of these results, it is possible understanding the factors that control the relation between the $\nu_{(Fe-CO)}$ and $\nu_{(CO)}$. Considering the set of points labelled 1 through 15, they represent a wide variety of carbomonoxy heme complexes with an histidine residue as trans ligand and, they exhibit a strong correlation between the $\nu_{(Fe-CO)}$ and $\nu_{(CO)}$ stretching frequencies (Figure 1.7 red line). Meanwhile points 18 through 21 represent a variety of cytochrome P-450 enzymes, each with a thiolate sulfur as the trans ligand of the iron. The strong σ-donating effect of mercaptide ligand in the trans position to the CO ligand weakens the Fe-CO bond and leads to a lowering position of the plot line (Figure 1.7 blue trace). On the other hand, the absence of a trans ligand (point 16) or the presence of a weak histidine bound as in the case of cytochrome c oxidase (point 17) increases the back-bonding donation and the $\nu_{(Fe-CO)}$ frequency and, the plot shifts to an higher position (Figure 1.7 black line). Thus Figure 1.7 suggests that the nature of the trans ligand of CO heme complexes determines the position of the $\nu_{(Fe-CO)}$ and $\nu_{(CO)}$ plot lines and that there is a strong correlation between the $\nu_{(Fe-CO)}$ and $\nu_{(CO)}$ stretching frequencies in CO complexes when the trans(fifth) ligands are similar.
Moreover it is interesting to illustrate the factors that govern the back-bonding donation and thus determine the position along the plot when the trans ligand is a histidine residue:

i) Hydrogen-bonding

This is the most important contribution to the back-bonding effect. This is well illustrated by the $\nu_{(Fe-CO)}$ and $\nu_{(CO)}$ stretching frequencies at 540 and 1905 cm^{-1}, respectively observed for HRP at pH 7 (point 1). They fall on the higher position of the plot (red line in Figure 1.7). This adduct corresponds to a bent Fe-CO unit respect to the heme plane, and the oxygen is hydrogen bonded to a distal Arg38. A second form is observed (point 3) in HRP at pH 7, with $\nu_{(Fe-CO)}$ at 518 $cm^{-1}$and $\nu_{(CO)}$ at 1933 cm^{-1}, in which the CO lost the interaction with Arg and is weakly hydrogen bonded to the His42. By lowering the pH to 3 (point 15) the $\nu_{(Fe-CO)}$ at 492 cm^{-1} and $\nu_{(CO)}$ at 1967 cm^{-1} are similar to those of the FePP(DME)(ImH) model compound [$\nu_{(Fe-CO)}$ = 495 cm^{-1}, $\nu_{(CO)}$

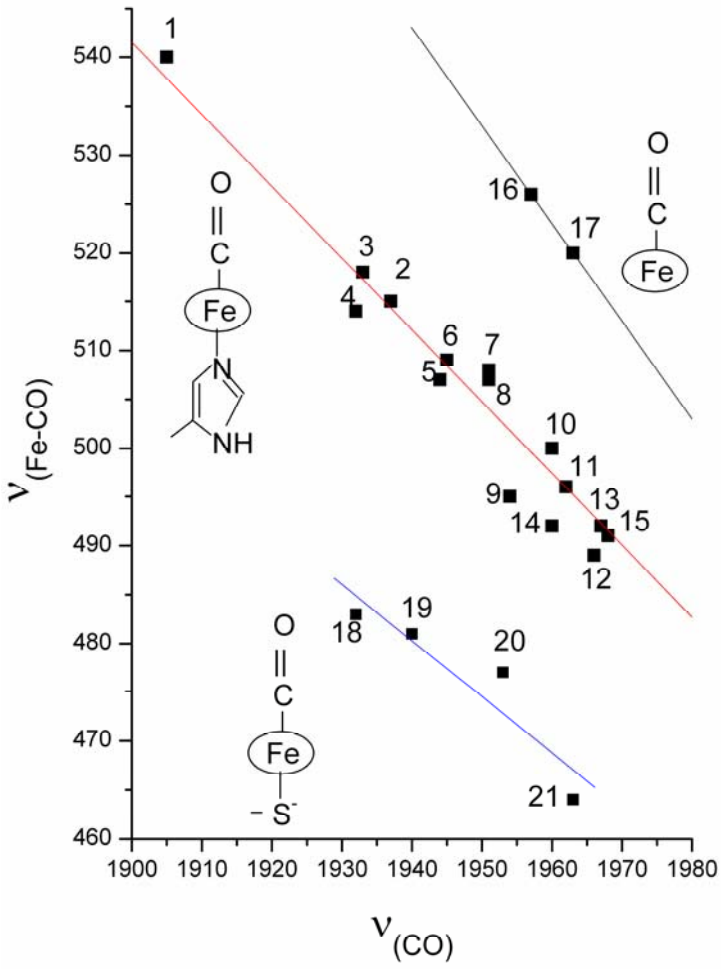

Figure 1.7 Canonical back-bonding correlations between the $\nu_{(Fe-CO)}$ and $\nu_{(CO)}$ stretching frequencies. Data and references are in Table 1.2.

= 1960 cm^{-1}] (point 14). Thus, at acid pH the distal cavity is open, the CO lost interactions with the distal residues. Therefore, it binds linearly and the back-bonding decreases giving rise to frequency lowering of the $\nu_{(Fe-CO)}$ and increasing of the $\nu_{(CO)}$.

ii) polar interaction

Since back-bonding increases the negative charge on the oxygen atom, the presence of positive residues on the distal cavity can favours the retro-donation. This effect is clear by the comparison of the stretching frequencies of the CO adduct of SW (point 6) and Elephant Mb (point 2). The latter presents a distal histidine properly orientated to displace the CO off the heme axis due to a polar interaction. The frequencies observed for the CO are: $\nu_{(Fe-CO)}$ = 507 cm^{-1}, $\nu_{(CO)}$ = 1944 cm^{-1}. On the other side Elephant Mb falls on an higher position in the plot ($\nu_{(Fe-CO)}$ = 515 cm^{-1} and $\nu_{(CO)}$ = 1937 cm^{-1}) suggesting that the glutamine residue (present on the place of the distal histidine)

determines a lower steric hindrance but it simultaneously establishes a stronger polar interaction.

iii) steric hindrance

The steric hindrance gives the lower contribution in Fe-CO back-bonding. The attempts to understand the variation in heme-CO vibrations were performed employing a series of sterically unhindered and hindered synthetic iron porphyrins. One simple iron porphyrin (heme 5) without groups to hinder the CO binding was studying along with three "constrained" hemes; 2-MeIm was used as an axial ligand in the fifth position (Figure 1.8). The heme free of any steric hindrance (point 9) presents $\nu_{(Fe\text{-}CO)}$ and $\nu_{(CO)}$ at 495 and 1954 cm^{-1}, respectively. The "costrained" hemes with 15- (point 5) and 13-atoms (point 4) hydrocarbon chain across one face of the heme exert varying degrees of sideway shearing strain to the CO ligand. As the chain length is decreased, the degree of steric hindrance is increased and points shift on the left of the plot (Figure 1.7).

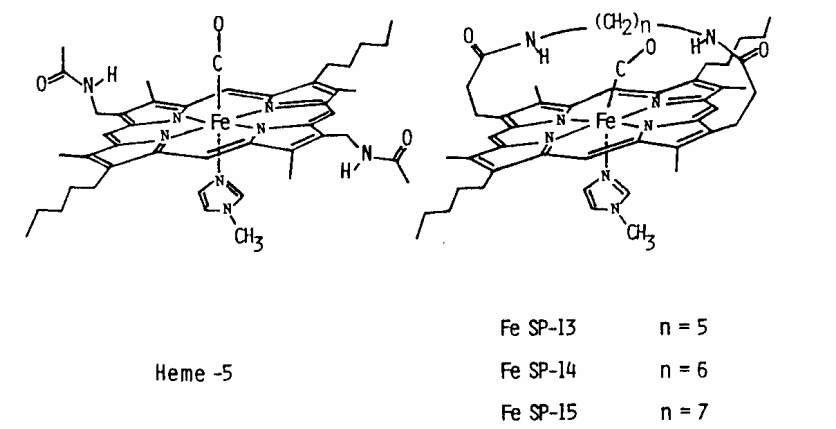

Figure 1.8 Chemical structure of the carbonmonoxy complexes of unhindered (heme 5) and hindered hemes with 2-MeIm as an axial base. The figure is adapted from reference (*21*).

In addition to the $\nu_{(Fe\text{-}CO)}$ and $\nu_{(CO)}$ vibrations, the RR spectrum sometimes reveals a band near 570 cm^{-1}, assignable to $\delta_{(Fe\text{–}C\text{–}O)}$ bending (*36*). Actually this mode is an out-of-phase combination of Fe–C–O bending and Fe–C tilting coordinates, as described by Ghosh and Bocian (*37*), whose DFT calculation revealed a large bend–tilt interaction constant. This interaction accounts for the elevated $\delta_{(Fe\text{–}C\text{–}O)}$ frequency (which had been a source of controversy over the assignment (*10*)). The observation of $\delta_{(Fe\text{–}C\text{–}O)}$ in FeSP-13 (point 4) suggested that distortion of the Fe-C-O linkage serves to enhance the RR intensity of the Fe-C-O bending mode relative to that of $\nu_{(Fe\text{-}CO)}$.

Table 1.2 Frequencies (in cm^{-1}) of $\nu_{(Fe-CO)}$ and $\nu_{(CO)}$ Stretching Vibrations in CO Complexes of Metalloporphyrin and Hemoproteins.

	$\nu_{(Fe-CO)}$	$\nu_{(CO)}$	Complexes	Ref.
1	540	1905	HRP (pH 7)	(*22, 23*)
2	515	1937	Elephant Mb	(*24*)
3	518	1933	HRP (pH 7)	(*23*)
4	514	1932	FeSP-13 (2-MeIm)	(*21*)
5	509	1945	FeSP-15 (2-MeIm)	(*21*)
6	507	1944	Sperm Whale Mb	(*25*)
7	508	1951	Carp Hb	(*26-28*)
8	507	1951	Human Hb A	(*28*)
9	495	1954	Heme-5 (2-MeIm)	(*21*)
10	500	1960	Insect Hb CTT III	(*29*)
11	496	1962	Fe(TpivPP) (1,2-Me_2Im)	(*30*)
12	489	1968	Fe(TpivPP) (2-MeIm)	(*30*)
13	491	1968	Carp Hb IHP	(*26-28*)
14	495	1960	FePP(DME)(ImH)	(*22*)
15	492	1967	HRP (pH 3)	(*31*)
16	526	1957	Fe(TpivPP) (THF)	(*30*)
17	520	1963	Cytochrome C Oxidase	(*32, 33*)
18	483	1932	Cytochrome P-450 (camphor) (putidaredoxin from P. putida)	(*34*)
19	481	1940	Cytochrome P-450 (camphor) from P. putida	(*34*)
20	477	1953	Cytochrome $P\text{-}450_{SCC}$ from bovine adrenocortical mitochondria	(*35*)
21	464	1963	Cytochrome P-450 from P. putida	(*34*)

1.5.2.2 Dioxygen (O_2)

The nature of O_2 bonding in hemoproteins has been extensively investigated (*38-42*). The X-ray crystal structure of oxymyoglobin (*43*) and oxyhemoglobin (*44*) have revealed that the Fe-O_2 bond has a bent geometry.

The Fe-O_2 moiety provides three vibrational modes: $\nu_{(Fe-O2)}$ stretching, $\delta_{(Fe-O-O)}$, and $\nu_{(O-O)}$ stretching. In principle, the determination of these frequencies with different isotopes in oxy hemoproteins should permit one to estimate the Fe-O-O angle and Fe-O_2 bond-stretching force constant (hence bond distance or bond strength). Unfortunately, $\delta_{(Fe-O-O)}$, and $\nu_{(O-O)}$ are usually not detected in RR and only the $\nu_{(Fe-O2)}$ is revealed. There is only one oxygen isotope-sensitive band at ~ 570 cm^{-1} in the RR spectra of Mb-O_2 and Hb-O_2, which was assigned to the $\nu_{(Fe-O2)}$ stretching mode (*45-47*), suggesting a similar stabilization played by the distal His and possibly related to the common oxygen transport and storage functions. Interestingly in truncated Hbs, the $\nu_{(Fe-O2)}$ was found at lower frequencies (between 554 and 560 cm^{-1}) since the heme-bound ligand is stabilized by interactions with the distal residues through an interlaced H-bonding network with the distal as well as the proximal oxygen (i.e. the oxygen directly coordinated to the iron) atoms of the dioxygen, resulting in a very strong H-bond (*48*) that reduces the Fe-O_2 strength bond.

1.5.2.3 Hydroxide (-OH^-)

Mb can bind –OH^-, giving rise to electronic absorption and RR spectra that show a thermal spin state equilibrium between a 6cHS and a 6cLS species (*49*). By lowering the temperature (to 10-15 K), the equilibrium is completely shifted towards the LS species (*50*), as revealed in the UV-Vis spectrum that shows a 6 nm red-shifted of the Soret band (from 413 to 419 nm) and the disappearance of the β and CT1 bands at 485 and 600 nm, respectively. On the contrary the HRP-OH complex is a pure 6cLS complex both at room and low temperatures (Soret at 415 nm, β band at 543 nm, and α band at 575 nm) (*50, 51*). Since that, in Mb RR spectra two $\nu_{(Fe-OH)}$ modes are expected, that are reduced to only one in the case of HRP. The $\nu_{(Fe-OH)}$ modes are assigned on the basis of isotopic shift observed in H_2O, D_2O and $H_2{}^{18}O$ buffers.

The (Fe^{3+}) Mb at alkaline pH and room temperature shows the presence of two $\nu_{(Fe-OH)}$ at 491 and 550 cm^{-1} (477 and 538 cm^{-1} in D_2O, and 468 and 525 cm^{-1} in $H_2{}^{18}O$) assigned to the HS and LS species, respectively (*50*). The frequency of the HS form is at lower values respect to that of the LS, since in the former there is a partial occupancy of the iron antibonding $d_z{}^2$ orbital (*50*).

On the other side, the HRP-OH complex presents the LS $\nu_{(Fe-OH)}$ at 503 cm^{-1} (509 cm^{-1} in D_2O and 484 cm^{-1} in $H_2{}^{18}O$) (*50*). Studies on the hydroxide complex of Arg38 and

His41 HRP variants allowed to identify these two distal residues as involved in the $-OH^-$ stabilization (*52*). In fact the His42Leu and His42Arg mutants determine the formation of the 6cHS species with $\nu_{(Fe-OH)}$ at 493 and 501 cm^{-1}, respectively and the $\nu_{(Fe-OH)}$ LS species decreases in amount up to become very weak to be detected (*52*). Similarly the Arg38 mutation to Gly or Leu induces the lost of the 6cLS species, proving that Arg residue is essential for the Fe-OH bond to form. These results indicate that the LS species is favoured in presence of a strong hydrogen bond and positive charged residues such as Arg, that determine a decrease of the force costant Fe-O bond a thus a 50 cm^{-1} downshift of the $\nu_{(Fe-OH)}$ frequency respect to Mb. The strong H-bonding interaction between distal residues and hydroxide in HRP is also useful to explain why a 6 cm^{-1} upshift upon D isotopic substitution is observed despite the increasing mass. In fact an increase of the H-bond strength induces a loss of Fe-OH biatomic oscillator character (via vibrational coupling with the Fe-OH bending and torsion and the O--HX stretch modes) and thus the Fe-OD stretch can experience a lesser downshift or even an upshift compared with the corresponding Fe-OH stretch (*50*).

1.5.2.4 Fluoride ($-F^-$)

The Fe^{3+} hemoproteins bind fluoride at acid pH giving rise to 6cHS species as indicated by the UV-Vis absorption spectra (Soret at 402-406 nm, β at 491-494 nm, and CT1 at 610-620 nm) (*53*) and core-size frequencies in RR spectra.

The marker bands that are informative of the hydrogen bonding stabilization between fluoride and distal residues are the CT1 [$2u(\pi) \rightarrow eg(d_\pi)$] in the UV-Vis (*53*) and the $\nu_{(Fe-F)}$ in the RR spectra. As the strength and the number of hydrogen bond increase as a red-shift of the CT1 (*53*) and a downshift in the $\nu_{(Fe-F)}$ frequencies occur (*54*).

In Mb-F the CT1 band is at 610 nm (*53*) and in the RR low frequency region two $\nu_{(Fe-F)}$ stretching modes are observed: at 461 and 422 cm^{-1} and have been assigned to the Fe-F stretch to a non H-bonded form and to a form, respectively (*55-58*). In particular, based on the X-ray crystal structure (*59*) the band at 420 cm^{-1} has been assigned to a hydrogen-bonded form to the distal HisE7 and to a water molecule (*53*). The band 460 cm^{-1} is pH sensitive, as it shifts down by about 60 cm^{-1} upon acidification. This result was interpreted as being due to protonation of the distal HisE7, that directly is hydrogen bond to the fluoride ligand (*55*).

In HRP-F $\nu_{(Fe-F)}$ is at lower frequency (385 cm^{-1}, (*60*)). The great difference of the frequencies of the $\nu_{(Fe-F)}$ stretching modes between Mb and HRP suggests that the fluoride is H-bonded differently in the two proteins and in particular the ligand is more strongly H-bonded (probably Arg, H_2O (*53*)) in HRP. Consequently a significant CT1 red-shift is expected to occur in its UV-Vis absorption spectrum. Nevertheless, in HRP the CT1 band is red-shifted only by 1 nm (611 nm) as compared to Mb (*53*). This small shift can be explained taking the $\nu_{(C=C)}$ stretching into account. Unlike Mb, which is characterized by two coincident $\nu_{(C=C)}$ stretching modes at 1621 cm^{-1} (*8*), two polarized bands are observed for HRP at 1621 and 1632 cm^{-1} (with the latter more intense) which are assigned to two vinyl stretching modes. The CT1 band is due to a transition from the $a_{2u}(\pi)$ porphyrin orbitals to d_π iron orbitals. The energy of the d_π orbitals depends on the coordination/spin state of the heme and the degree of conjugation between the heme group and its two vinyl substituents. A lower frequency of the $\nu_{(C=C)}$ stretching mode corresponds to a higher degree of conjugation between the vinyl group and the porphyrin π system. Increased conjugation with the vinyl group should shift the energy of $a_{2u}(\pi) \rightarrow d_\pi$ transitions to lower energy, thus shifting the CT1 maximum to the red. As a consequence, the only 1 nm red-shift of the CT1 band observed in the HHP-F complex as compared to Mb-F can be explained with a different orientation of the two vinyl groups.

1.5.2.5 Sulfide (H_2S/-HS^-)

At pH 7 sulfide may coordinate to the heme iron in the monoprotonated (HS^-) or diprotonated (H_2S) form since the pK_a for this equilibrium is reportedly 6.9, generating a 6cLS species. Heme proteins bind sulfide in its Fe^{3+} state, giving rise to UV-Vis (Soret band centered at 425-427 nm and a broad visible band at 550-575 nm) and RR spectra characteristic of a 6cLS adduct (*61*).

The structural determinants for sulfide binding can be traced back to the properties of the distal heme cavity. The presence of an aromatic cage and a H-bond donor appear to account for the structural determinant that govern the thermodynamic properties of sulfide binding in hemoglobins. The structure of the sulfide avid HbI from *L. pectinata*

has shown that two phenyalanine residues occupy the positions corresponding to CD1 and E11 in myoglobin and the distal E7 residue is glutamine instead of the common histidine of vertebrate Mb and Hb (*62*). The structure of sulfide-bound HbI suggest two different kinds of interactions between the bound ligand and the relevant residues within the distal heme pocket, namely, H-bonding between sulfide and Gln64, and sulfide-aromatic ring electrostatic interactions with Phe43 and Phe68 (*63, 64*). The electrostatic interactions can be regarded as a major determinant of the high H_2S affinity of HbI on the basis of the reported weakness of H-bonds involving S atoms (*65*). On the other hand, Fe-sulfide has been described as a relatively strong H-bond acceptor in DFT calculations on thiolate-bound model porphyrins (*66*).

In the low frequency region the $\nu_{(Fe-S)}$ stretching mode is assigned to the band at ~ 375 cm^{-1} and its frequency is not affected by variations in the nature of distal cavity residues (*61*).

References

(1) Gouterman, M. (1979) The Porphyrins. D. Dolphin Ed. Academic Press.

(2) Marzocchi, M. P., and Smulevich, G. (2003) Relationship between heme vinyl conformation and the protein matrix in peroxidases. *J. Raman Spectr. 34*, 725-736.

(3) Zerner, M., and Gouterman, M. (1966) *Theoret. Chim. Acta (Berlin) 4*, 44.

(4) Carey, P. R. (1982) Biochemical Applications of Raman and Resonance Raman Spectroscopies. *Academic Press*, chapter 2, pages 11–47.

(5) Spiro, T. G. (1985) Resonance Raman spectroscopy as a probe of heme protein structure and dynamics. *Adv. Protein Chem. 37*, 111-159.

(6) Kalsbeck, W. A., Robertson, D. E., Pandey, R. K., Smith, K. M., Dutton, P. L., and Bocian, D. F. (1996) Structural and electronic properties of the heme cofactors in a multi-heme synthetic cytochrome. *Biochemistry 35*, 3429-3438.

(7) Choi, S., Spiro, T. G., Langry, K. G., Smith, K. M., Budd, D. L., and La Mar, G. N. (1982) Structural correlations and vinyl influences in the Resonance Raman spectra of protoheme complexes and proteins. *J. Am. Chem. Soc. 104*, 4345-4351.

(8) Hu, S., Smith, K. M., and Spiro, T. G. (1996) Assignment of Protoheme Resonance Raman Spectrum by Heme Labeling in Myoglobin. *J. Am. Chem. Soc. 118*, 12638-12646.

(9) Argade, P. V., Sassaroli, M., Rousseau, D. L., Inubushi, T., Ikeda-Saito, M., and Lapidot, A. (1984) Confirmation of the Assignment of the Iron-Histidine Stretching Mode in Myoglobin. *J. Am. Chem. Soc. 106*, 6593-6596.

(10) Kincaid, J. R. (2000) in: K. M. Kadish, K. M. Smith, R. Guilard (Eds.), The Porphyrin Handbook,. *Academic Press, San Diego 7*, 227-291.

(11) Spiro, T. G., and Li, X.-Y. (1988) in Biological application of Raman Spectroscopy (Spiro, T.G.,Ed.) *Vol. 3*, pp. 1-37, Wiley Interscience, New York.

(12) Hori, H., and Kitagawa, T. (1980) Iron-ligand stretching band in the resonance Raman spectra of ferrous iron porphyrin derivatives. Importance as a probe band for quaternary structure of hemoglobin. *J. Am. Chem. Soc. 102* 3608-3613.
(13) Stein, P., and Spiro, T. G. (1980) Hydrogen-bond and deprotonation effects on the resonance Raman iron-imidazole mode in deoxy hemoglobin models: implication for hemoglobin cooperativity. *J. Am. Chem. Soc. 102*, 7795-7797.
(14) Teraoka, J., and Kitagawa, T. (1981) Structural implication of the heme-linked ionization of horseradish peroxidase probed by the Fe-histidine stretching Raman line. *J. Biol. Chem. 256*, 3969-3977.
(15) Kitagawa, T., Nagai, K., and Tsubaki, M. (1979) Assignment of the Fe-Nepsilon (His F8) stretching band in the resonance Raman spectra of deoxy myoglobin. *FEBS Lett. 104*, 376-378.
(16) Smulevich, G., Feis, A., and Howes, B. D. (2005) Fifteen years of Raman spectroscopy of engineered heme containing peroxidases: what have we learned? *Acc. Chem. Res. 38*, 433-440.
(17) Friedman, J. M., Campbell, B. F., and Noble, R. W. (1990) A possible new control mechanism suggested by resonance Raman spectra from a deep ocean fish hemoglobin. *Biophys. Chem. 37*, 43-59.
(18) Kitagawa, T. (1988) in: T.G. Spiro (Ed.), Biological Applications of Raman Spectroscopy: Resonance Raman Spectra of Hemes and Metalloproteins, Wiley, New York,. 97-131.
(19) Perutz, M. F. (1979) Regulation of oxygen affinity of hemoglobin: influence of structure of the globin on the heme iron. *Annu. Rev. Biochem. 48*, 327-386.
(20) Bangcharoenpaurpong, O., Schomacker, K. T., and Champion, P. M. (1984) Resonance Raman investigation of myoglobin and hemoglobin. *J. Am. Chem. Soc. 106*, 5688-5698.
(21) Yu, N. T., Kerr, E. A., Ward, B., and Chang, C. K. (1983) Resonance Raman detection of Fe-CO stretching and Fe-C-O bending vibrations in sterically hindered carbonmonoxy "strapped hemes". A structural probe of Fe-C-O distortion. *Biochemistry 22*, 4534-4540.
(22) Evangelista-Kirkup, R., Smulevich, G., and Spiro, T. G. (1986) Alternative carbon monoxide binding modes for horseradish peroxidase studied by resonance Raman spectroscopy. *Biochemistry 25*, 4420-4425.
(23) Uno, T., Nishimura, Y., Tsuboi, M., Makino, R., Iizuka, T., and Ishimura, Y. (1987) Two types of conformers with distinct Fe-C-O configuration in the ferrous CO complex of horseradish peroxidase. Resonance Raman and infarared spectroscopic studies with native and deuteroheme-substituted enzymes. *J. Biol. Chem. 262*, 4549-4556.
(24) Kerr, E. A., Yu, N. T., Bartnicki, D. E., and Mizukami, H. (1985) Resonance Raman studies of CO and O2 binding to elephant myoglobin (distal His(E7)----Gln). *J. Biol. Chem. 260*, 8360-8365.
(25) Ramsden, J., and Spiro, T. G. (1989) Resonance Raman evidence that distal histidine protonation removes the steric hindrance to upright binding of carbon monoxide by myoglobin. *Biochemistry 28*, 3125-3128.
(26) Onwubiko, H. A., Hazzard, J. H., Noble, R. W., and Caughey, W. S. (1982) Demonstration of inositol hexaphosphate induced changes in structure at ligand binding sites in carp hemoglobin carbonyl. *Biochem. Biophys. Res. Commun. 106*, 223-228.
(27) Rousseau, D. L., Tan, S. L., Ondrias, M. R., Ogawa, S., and Noble, R. W. (1984) Absence of cooperative energy at the heme in liganded hemoglobins. *Biochemistry 23*, 2857-2865.

(28) Tsubaki, M., Srivastava, R. B., and Yu, N. T. (1982) Resonance Raman investigation of carbon monoxide bonding in (carbon monoxy)hemoglobin and -myoglobin: detection of Fe-CO stretching and Fe-C-O bending vibrations and influence of the quaternary structure change. *Biochemistry 21*, 1132-1140.

(29) Yu, N. T., Benko, B., Kerr, E. A., and Gersonde, K. (1984) Iron-carbon bond lengths in carbonmonoxy and cyanomet complexes of the monomeric hemoglobin III from Chironomus thummi thummi: a critical comparison between resonance Raman and x-ray diffraction studies. *Proc. Natl. Acad. Sci. U S A 81*, 5106-5110.

(30) Kerr, E. A., Mackin, H. C., and Yu, N. T. (1983) Resonance Raman studies of carbon monoxide binding to iron "picket fence" porphyrin with unhindered and hindered axial bases. An inverse relationship between binding affinity and the strength of iron-carbon bond. *Biochemistry 22*, 4373-4379.

(31) Smulevich, G., Paoli, M., De Sanctis, G., Mantini, A. R., Ascoli, F., and Coletta, M. (1997) Spectroscopic evidence for a conformational transition in horseradish peroxidase at very low pH. *Biochemistry 36*, 640-649.

(32) Argade, P. V., Ching, Y. C., and Rousseau, D. L. (1984) Cytochrome a3 structure in carbon monoxide-bound cytochrome oxidase. *Science 225*, 329-331.

(33) Volpe, J. A., O'Toole, M. C., and Caughey, W. S. (1975) Quantitative infrared spectroscopy of CO complexes of cytochrome c oxidase, hemoglobin and myoglobin: evidence for one CO per heme. *Biochem. Biophys. Res. Commun. 62*, 48-53.

(34) Makino, R., Iizuka, T., and Ishikawa, Y. (1984) in Proc. IXth Int. Conf. Raman Spectrosc., Tokyo, Japan, August 27-September. 492.

(35) Tsubaki, M., Matsusaka, K., and Ichikawa, Y. (1984) in Proc. IXth Int. Conf. Raman Spectrosc., Tokyo, Japan, August 27-September 1w. 752.

(36) Kerr, E. A., and Yu, N. T. (1988) in: T.G. Spiro (Ed.), Biological Applications of Raman Spectroscopy, vol. 3, Wiley-Interscience, New-York. 39-95.

(37) Ghosh, A., and Bocian, D. F. (1996) The Carbonyl Tilting and Bending Potential Energy Surface of Carbonmonoxyhemes. *J. Phys. Chem. 100*, 6363-6367.

(38) Cerdonio, M., Congiu-Castellano, A., Calabrese, L., Morante, S., Pispisa, B., and Vitale, S. (1978) Room-temperature magnetic properties of oxy- and carbonmonoxyhemoglobin. *Proc. Natl. Acad. Sci. U S A 75*, 4916-4919.

(39) Huynh, B. H., Case, D. A., and Karplus, M. (1977) Nature of the iron-oxygen bond in oxyhemoglobin. *J. Am. Chem. Soc. 99*, 6103-6105.

(40) Maxwell, J. C., Volpe, J. A., Barlow, C. H., and Caughey, W. S. (1974) Infrared evidence for the mode of binding of oxygen to iron of myoglobin from heart muscle. *Biochem. Biophys. Res. Commun. 58*, 166-171.

(41) Pauling, L. (1977) Magnetic properties and structure of oxyhemoglobin. *Proc. Natl. Acad. Sci. U S A 74*, 2612-2613.

(42) Wittenberg, J. B., Wittenberg, B. A., Peisach, J., and Blumberg, W. E. (1970) On the state of the iron and the nature of the ligand in oxyhemoglobin. *Proc. Natl. Acad. Sci. U S A 67*, 1846-1853.

(43) Phillips, S. E. (1980) Structure and refinement of oxymyoglobin at 1.6 A resolution. *J. Mol. Biol. 142*, 531-554.

(44) Shaanan, B. (1982) The iron-oxygen bond in human oxyhaemoglobin. *Nature 296*, 683-684.

(45) Hirota, S., Ogura, T., Appelman, E. H., Shinzawaitoh, K., Yoshikawa, S., and Kitagawa, T. (1994) Observation of a New Oxygen-Isotope-Sensitive Raman

Band for Oxyhemoproteins and Its Implications in Heme Pocket Structures. *J. Am. Chem. Soc. 116*, 10564-10570.

(46) Potter, W. T., Tucker, M. P., Houtchens, R. A., and Caughey, W. S. (1987) Oxygen infrared spectra of oxyhemoglobins and oxymyoglobins. Evidence of two major liganded O2 structures. *Biochemistry 26*, 4699-4707.

(47) Van Wart, H. E., and Zimmer, J. (1985) Resonance Raman evidence for the activation of dioxygen in horseradish oxyperoxidase. *J Biol Chem 260*, 8372-7.

(48) Egawa, T., and Yeh, S. R. (2005) Structural and functional properties of hemoglobins from unicellular organisms as revealed by resonance Raman spectroscopy. *J. Inorg. Biochem. 99*, 72-96.

(49) Beetlestone, J., and George, P. (1964) A Magnetochemical Study of Equilibria between High and Low Spin States of Metmyoglobin Complexes. *Biochemistry 3*, 707-714.

(50) Feis, A., Marzocchi, M. P., Paoli, M., and Smulevich, G. (1994) Spin state and axial ligand bonding in the hydroxide complexes of metmyoglobin, methemoglobin, and horseradish peroxidase at room and low temperatures. *Biochemistry 33*, 4577-4583.

(51) Sitter, A. J., Shifflett, J. R., and Terner, J. (1988) Resonance Raman spectroscopic evidence for heme iron-hydroxide ligation in peroxidase alkaline forms. *J. Biol. Chem. 263*, 13032-13038.

(52) Howes, B. D., Rodriguez-Lopez, J. N., Smith, A. T., and Smulevich, G. (1997) Mutation of distal residues of horseradish peroxidase: influence on substrate binding and cavity properties. *Biochemistry 36*, 1532-1543.

(53) Neri, F., Kok, D., Miller, M. A., and Smulevich, G. (1997) Fluoride binding in hemoproteins: the importance of the distal cavity structure. *Biochemistry 36*, 8947-8953.

(54) Schonbaum, G. R., Houtchens, R. A., and Caughey, W. S. (1979) in Biochemical and Clinical Aspects of Oxygen (Caughey, W. S., Ed.) p 195, Academic Press, New York.

(55) Asher, S. A., Adams, M. L., and Schuster, T. M. (1981) Resonance Raman and absorption spectroscopic detection of distal histidine--fluoride interactions in human methemoglobin fluoride and sperm whale metmyoglobin fluoride: measurements of distal histidine ionization constants. *Biochemistry 20*, 3339-3346.

(56) Asher, S. A., and Schuster, T. M. (1981) Differences in iron-fluoride bonding between the isolated subunits of human methemoglobin fluoride and sperm whale metmyoglobin fluoride as measured by resonance Raman spectroscopy. *Biochemistry 20*, 1866-1873.

(57) Asher, S. A., Vickery, L. E., Schuster, T. M., and Sauer, K. (1977) Resonance Raman spectra of methemoglobin derivatives. Selective enhancement of axial ligand vibrations and lack of an effect of inositol hexaphosphate. *Biochemistry 16*, 5849-5856.

(58) Desbois, A., Lutz, M., and Banerjee, R. (1979) Low-Frequency Vibrations in Resonance Raman Spectra of Horse Heart Myoglobin. Iron-Ligand and Iron-Nitrogen Vibrational Modes. *Biochemistry 18*, 1510-1518.

(59) Aime, S., Fasano, M., Paoletti, S., Cutruzzola, F., Desideri, A., Bolognesi, M., Rizzi, M., and Ascenzi, P. (1996) Structural determinants of fluoride and formate binding to hemoglobin and myoglobin: crystallographic and 1H-NMR relaxometric study. *Biophys. J. 70*, 482-488.

(60) Yu, N. T. (1986) Resonance Raman studies of ligand binding. *Methods Enzymol Vol. 130*, pp. 350-409.

(61) Nicoletti, F. P., Comandini, A., Bonamore, A., Boechi, L., Boubeta, F. M., Feis, A., Smulevich, G., and Boffi, A. (2010) Sulfide Binding Properties of Truncated Hemoglobins. *Biochemistry 49*, 2269–2278.

(62) Rizzi, M., Wittenberg, J. B., Coda, A., Ascenzi, P., and Bolognesi, M. (1996) Structural bases for sulfide recognition in Lucina pectinata hemoglobin I. *J. Mol. Biol. 258*, 1-5.

(63) Cerda-Colon, J. F., Silfa, E., and Lopez-Garriga, J. (1998) Unusual rocking freedom of the heme in the hydrogen sulfide-binding hemoglobin from Lucina pectinata. *J. Am. Chem. Soc. 120*, 9312-9317.

(64) Kraus, D. W., and Wittenberg, J. B. (1990) Hemoglobins of the Lucina pectinata/bacteria symbiosis. I. Molecular properties, kinetics and equilibria of reactions with ligands. *J. Biol. Chem. 265*, 16043-16053.

(65) Biswal, H. S., Shirhatti, P. R., and Wategaonkar, S. (2009) O-H...O versus O-H...S hydrogen bonding I: Experimental and computational studies on the p-cresol x H2O and p-cresol x H2S complexes. *J. Phys. Chem. A 113*, 5633-5643.

(66) Dey, A., Okamura, T. A., Ueyama, N., Hedman, B., Hodgson, K. O., and Solomon, E. I. (2005) Sulfur K-edge XAS and DFT calculations on P450 model complexes: effects of hydrogen bonding on electronic structure and redox potentials. *J. Am. Chem. Soc. 127*, 12046-12053.

Chapter 2

Materials and Methods

2.1 Materials

Ascorbic acid was obtained from Carlo Erba (Milan, Italy), sodium dithionite from Fluka Chemicals (Buchs, Switzerland), Sephadex G-25 from Pharmacia Biotech (Uppsala, Sweaden), human serum albumin (HSA), hemin chloride, warfarin, sodium sulfide, hydrogen peroxide and $^{18}O_2$ from Sigma Aldrich (Steinheim, Germany). Gaseous ^{12}CO and ^{13}CO were purchased from Rivoira (Milan, Italy) and FluoroChem (Derbyshire, UK), respectively. Sodium cyanide was obtained from Cambridge Isotope Laboratories (Andover, US). All the other chemicals were obtained from Merck AG (Darmstadt, Germany). All chemicals were analytical or reagent grade and were used without further purification.

2.1.1 Heme-Human Serum Albumin (HSA)

Heme (hemin or (Fe^{3+}) protoporphyrin IX (Fe-PPIX)) was dissolved in 0.1 M NaOH to give a final concentration of 2-3 mM. The heme concentration was determined spectrophotometrically at 535 nm, after converting heme to the heme-bisimidazolate derivative by adding 1.0 M imidazole, in 20% p/v SDS micelles (ε_{535nm} = 14.5 $mM^{-1}cm^{-1}$) (*1*). An appropriate amount of this solution was added to HSA in phosphate buffer to give a final (Fe^{2+})-heme-HSA ratio of 1:1.7. Samples at pH 5.8 and 10 were prepared diluting the sample at pH 7 in the appropriate 0.1 M phosphate and glycine buffers, respectively. (Fe^{2+})-heme-HSA samples were prepared by addition of 5% volume freshly prepared sodium dithionite (20 mg/mL) to deoxygenated (Fe^{3+}) solutions. All CO-heme complexes were prepared by degassing the heme-HSA solution by flushing first with nitrogen and then with CO or ^{13}CO and reducing the heme by addition of a 5% volume freshly prepared sodium dithionite (20 mg/mL) solution.

The heme concentration of the heme-HSA samples was determined using the molar absorptivity of 99.2 mM^{-1} cm^{-1} at 404 nm (*2*).

The Warfarin (WF) stock solution (final concentration, 5.0×10^{-2} M) was prepared by dissolving the drug in water at pH 10.0, then the pH was adjusted to 7.0 with diluted HCl (*3*).

CO-(Fe^{2+})-heme-HSA and (Fe^{2+})-heme-HSA-WF solutions were prepared by equilibrating a HSA-hemeFe(Fe^{3+}) solution (about 1.0×10^{-5} M), in the presence of 5 mg/ml of sodium dithionite, with either 1.0×10^{-4} M CO or 1.0×10^{-2} M warfarin for 1 hour. The unusually-long equilibration time was necessary for the completion of the reactions, which are characterized by very slow phases.

2.1.2 Truncated hemoglobin from *Thermobifida fusca* (Tf-trHb)

Tf-trHb was expressed as recombinant proteins in E. coli cells and purified as described previously (*4*).

The protein concentration was determined on the CO derivative in the presence of 10-20 mM sodium dithionite by using an extinction coefficient at 421 nm of 174000 M^{-1} cm^{-1} for Tf-trHb (*5*). The Fe^{3+} derivatives were prepared by oxidation of the Fe^{2+} form using excess potassium ferricyanide followed by gel filtration on a Sephadex G-25 column equilibrated with 0.1 M phosphate buffer (for room temperature) and 0.1 M 3-(N-morpholino)propanesulfonic acid (MOPS) buffer (for low temperature) at pH 7 to remove the oxidant.

The fluoride adducts were prepared by adding 1 M fluoride solution to protein in 0.1 M phosphate buffer at pH 7.

The pH titrations of Tf-trHb WT and mutants were perfomed adding appropriate volumes of 1 M NaOH to a 1800 μL of sample in 1 cm cuvette. The pH was checked before and after the spectrum acquisition.

The hydroxide complex was prepared diluting the Fe^{3+} sample in 0.1 M glycine buffer at appropriate pH_{alk} (i.e. a complete alkaline transition occurs as determined by titration). The hydroxyl complexes in isotopically enriched water were prepared by adding 5 μL of Fe^{3+} sample, in 0.1 M natural abundance potassium phosphate, to 50 μL of 0.1 M glycine buffer in D_2O at final $pD = pH_{alk} + 0.2$.

2.1.3 Dehaloperoxidase-hemoglobin (DHP)

DHP was expressed in Escherichia coli and purified as previously described (*6*). Of the two DHP isoenzymes identified to date [A and B forms] (*7*) in the thesis we have characterized the isoform A, indicated hereafter as DHP.

DHP samples are at pH 6 in 0.15 M phosphate buffer. The deoxy form was prepared by addition of a freshly prepared 5% volume ascorbic acid (12 mg/mL) solution (previously flushed with nitrogen) to the Fe^{3+} forms previously degassed with nitrogen for 30 minutes. The DHP-$^{16}O_2$ complex was prepared by reducing the protein with a 5% volume addition of a fresh ascorbic acid (12 mg/mL) solution in aerobic condition as previously reported for the DHP B isoenzyme (*7*). The DHP-$^{18}O_2$ complex was prepared by first flushing the Fe^{3+} protein solution with nitrogen for 30 minutes, then flushing with $^{18}O_2$ and then reducing the protein with a 5% volume addition of freshly prepared ascorbic acid (previously flushed with nitrogen).

The sulfide complexes were prepared by addition of the Fe^{3+} protein to a solution containing sodium sulfide in a range 20-200-fold excess, both in aerobic and anaerobic conditions. An excess of sulfide was necessary for ensuring complete binding of the protein and to compensate for the progressive release of sulfide and its oxidation that unavoidably occurs during the relatively long time needed for the RR measurements. The samples with sulfide were cooled by a gentle flow of nitrogen gas passed through liquid nitrogen during RR experiments. Protein concentration was 35 μM for both the electronic absorption and RR samples. The sulfheme sample was prepared by mixing solutions of the Fe^{3+} DHP with solutions of sulfide and H_2O_2 in a ratio of 1:20:0.1 (DHP: sulfide: H_2O_2).

2.1.4 hemoglobin from *E. maclovinus* Hb1

Purification of *E. maclovinus* Hb 1 and the amino-acid sequencing of globins were carried out as described previously (*8*).

E. maclovinus Hb 1 (Fe^{3+}) derivatives were prepared by oxidation of the CO-Fe^{2+} form using excess potassium ferricyanide followed by gel filtration on a Sephadex G-25 column equilibrated with 50 mM Tris-HCl buffer at pH 7.6 to remove the oxidant. Samples at alkaline pH were obtained diluting a concentrated sample in 50 mM Glycine at pH 9.3. The hydroxyl complexes in isotopically enriched water were prepared by adding 3 μl of 0.5 mM *E. maclovinus* Hb 1 (Fe^{3+}), in natural abundance 50 mM hydroxymethyl)aminomethane (Tris)-HCl at pH 7.6, to 48 μL of 50 mM glycine at pD

9.6. The imidazole adduct was prepared adding a 600-fold final excess of ligand to *E. maclovinus* Hb 1 (Fe^{3+}). The cyanide adduct was prepared adding a grain of the ligand to 50 μl of 30 μM *E. maclovinus* Hb 1 (Fe^{3+}) in 50 mM Tris-HCl at pH 7.6.

E. maclovinus Hb 1 was isolated in the CO form; the CO samples were prepared by simply diluting concentrated protein in 50 mM Tris-HCl at pH 7.6. The *E. maclovinus* Hb 1 (Fe^{2+}) deoxy samples were prepared by adding 2 μl of sodium dithionite (30 mg/ml) to 50 μL of deoxygenated *E. maclovinus* Hb 1 (Fe^{3+}) in 50 mM Tris-HCl at pH 7.6. Both solutions of dithionite and *E. maclovinus* Hb 1 (Fe^{3+}) were degassed with nitrogen for thirty minutes. The oxy *E. maclovinus* Hb 1 (Fe^{2+}) samples were obtained by gel filtration of the deoxy samples on a Sephadex G-25 column equilibrated with 50 mM Tris-HCl at pH 7.6 to remove the dithionite

2.1.5 Neuroglobins (Ngbs) from *Chaenocephalus aceratus* and *Dissosticus mawsoni*

Expression and purification of Ngbs were performed by Dr. Cinzia Verde and coworkes at CNR of Naples. Recombinant expression plasmid was successfully transformed in the *E. Coli* strain BL21(DE3)pLysS (Invitrogen). The growth of the transformed bacteria and the overexpression of *C. aceratus* and *D. mawsoni* Ngbs was performed as described by Dewilde (*9*).

D. mawsoni and *C. aceratus* Ngbs were isolated in the Fe^{3+} form. The Ngbs (Fe^{2+}) samples were prepared by adding 2 μl of sodium dithionite (20 mg/ml) to 50 μL of deoxygenated Ngbs (Fe^{3+}) in 50 mM Tris-HCl at pH 7.6. Both solutions of dithionite and Ngbs (Fe^{3+}) were degassed with nitrogen for thirty minutes.

All CO-heme complexes were prepared by degassing Fe3+ samples by flushing first with nitrogen and then with CO or ^{13}CO and reducing the heme by addition of a 5% volume freshly prepared sodium dithionite (20 mg/mL) solution.

The oxy Ngbs samples were obtained by gel filtration of the deoxy samples on a Sephadex G-25 column equilibrated with 50 mM Tris-HCl at pH 7.6 to remove the dithionite.

2.2 Methods

Electronic absorption spectra were measured with a double-beam Cary 5 spectrophotometer (Varian, Palo Alto, CA).

The RR spectra were obtained by excitation with the 406.7 and 413.1 nm lines of a Kr^+ laser (Coherent, Innova 300 C, Santa Clara, CA), 441.6 nm line of a HeCd laser (Kimmon IK4121RG, Tokyo Japan) and 514.5 nm line of an Ar^+ laser (Coherent, Innova 90/5, Santa Clara, CA). Backscattered light from a slowly rotating NMR tube was collected and focused into a triple spectrometer (consisting of two Acton Research SpectraPro 2300i and a SpectraPro 2500i in the final stage with a 1800 or 3600 grooves/mm grating) working in the subtractive mode, equipped with a liquid nitrogen-cooled CCD detector. It should be noted that the spectral resolution of the RR spectra cited in the figure captions is that calculated theoretically on the basis of the optical properties of the spectrometer. However, for the moderately broad experimental RR bands observed in the present study (ca. 10 cm^{-1}), the effective spectral resolution will in general be lower.

2.2.1 Room temperature

Absorption spectra were obtained using a 5-mm NMR tube or a 1 cm cuvette, and a 600 nm/min scan rate.

RR spectra were acquired using a 5-mm NMR tube. To improve the signal/noise ratio, a number of spectra were accumulated and summed only if no spectral differences were noted. The RR spectra were calibrated with indene, CCl_4, dimethyl sulfoxide, acetone, and acetonitrile as standards to an accuracy of 1 cm^{-1} for intense isolated bands. The deviation of the calibrated wavenumber for a peak from the real wavenumber was always lower than 0.5 cm^{-1}. Spectra were normalized on the ν_7 band in the low frequency region and ν_4 in the high frequency region, if no differently stated. All spectra were edited by using Labcalc version 2.22. To determine peak intensities and positions a curve-fitting program (Lab Calc, Galactic) was used to simulate the spectra using a Lorentzian line shape.

2.2.2 Low temperature

The low-temperature experiments were carried out using an Air Products Displex closed-cycle He refrigerator with automatic temperature control. The absorption spectra were obtained using a 3-mm quartz microcuvette (100 μL) and a 120 nm/min scan rate. The cuvette was mounted on the coldfinger of the cryostat and filled with the protein solution at 90 K under nitrogen flow. The temperature was then lowered to 10-15 K

under vacuum. The temperature was allowed to stabilize for 30 min before recording the spectrum.

For the low-temperature RR measurements, 20 μL of the protein solution was deposited on the copper cold finger of the refrigerator at 90 K under a nitrogen flow. The temperature was then slowly decreased to 10-15 K under vacuum, and RR spectra were obtained at this temperature.

References

(1) Boffi, A., Das, T. K., della Longa, S., Spagnuolo, C., and Rousseau, D. L. (1999) Pentacoordinate hemin derivatives in sodium dodecyl sulfate micelles: model systems for the assignment of the fifth ligand in ferric heme proteins. *Biophys. J. 77*, 1143-1149.

(2) Kamal, J. K., and Behere, D. V. (2002) Spectroscopic studies on human serum albumin and methemalbumin: optical, steady-state, and picosecond time-resolved fluorescence studies, and kinetics of substrate oxidation by methemalbumin. *J. Biol. Inorg. Chem. 7*, 273-283.

(3) Baroni, S., Mattu, M., Vannini, A., Cipollone, R., Aime, S., Ascenzi, P., and Fasano, M. (2001) Effect of ibuprofen and warfarin on the allosteric properties of haem-human serum albumin. A spectroscopic study. *Eur. J. Biochem. 268*, 6214-6220.

(4) Bonamore, A., Ilari, A., Giangiacomo, L., Bellelli, A., Morea, V., and Boffi, A. (2005) A novel thermostable hemoglobin from the actinobacterium Thermobifida fusca. *Febs J. 272*, 4189-4201.

(5) Nicoletti, F. P., Comandini, A., Bonamore, A., Boechi, L., Boubeta, F. M., Feis, A., Smulevich, G., and Boffi, A. (2010) Sulfide Binding Properties of Truncated Hemoglobins. *Biochemistry 49*, 2269–2278.

(6) Belyea, J., Gilvey, L. B., Davis, M. F., Godek, M., Sit, T. L., Lommel, S. A., and Franzen, S. (2005) Enzyme function of the globin dehaloperoxidase from Amphitrite ornata is activated by substrate binding. *Biochemistry 44*, 15637-15644.

(7) D'Antonio, J., D'Antonio, E. L., Thompson, M. K., Bowden, E. F., Franzen, S., Smirnova, T., and Ghiladi, R. A. (2010) Spectroscopic and mechanistic investigations of dehaloperoxidase B from Amphitrite ornata. *Biochemistry 49*, 6600-6616.

(8) Coppola, D., Giordano, D., Vergara, A., Mazzarella, L., di Prisco, G., Verde, C., and Russo, R. (2010) The hemoglobins of sub-Antarctic fishes of the suborder Notothenioidei. *Polar Sci. 4*, 295-308.

(9) Dewilde, S., Mees, K., Kiger, L., Lechauve, C., Marden, M. C., Pesce, A., Bolognesi, M., and Moens, L. (2008) Expression, purification, and crystallization of neuro- and cytoglobin. *Methods Enzymol 436*, 341-357.

Chapter 3

Heme-Human Serum Albumin: a monomeric protein with allosteric properties

Francesco P. Nicoletti, Barry D. Howes, Maria Fittipaldi, Gabriella Fanali, Mauro Fasano, Paolo Ascenzi, and Giulietta Smulevich.
Ibuprofen Induces an Allosteric Conformational Transition in the Heme Complex of Human Serum Albumin with Significant Effects on Heme Ligation.
J. Amer. Chem. Soc. (2008) 130, 11677-11688.

Paolo Ascenzi, Alessandra di Masi, Massimo Coletta, Chiara Ciaccio, Gabriella Fanali, **Francesco P. Nicoletti**, Giulietta Smulevich, and Mauro Fasano.
Ibuprofen Impairs Allosterically Peroxynitrite Isomerization by Ferric Human Serum Heme-Albumin.
J. Biol. Chem. (2009) 284, 31006-31017.

3.1 State of art

Human serum albumin (HSA), the most prominent protein in plasma, is best known for its extraordinary ligand binding capacity. The most strongly bound compounds are hydrophobic organic anions of medium size such as long-chain fatty acids, heme and bilirubin. Smaller and less hydrophobic compounds (e.g. tryptophan) are held less strongly, but their binding can still be highly specific. HSA provides a depot for many compounds. Therefore, they can be available in quantities well beyond their solubility in plasma. Moreover, HSA abundance (concentration of 45 mg × mL^{-1} in the serum of human adults) makes it an important determinant of the pharmacokinetic behaviour of

many drugs. HSA holds some ligands in a strained orientation, allowing their metabolic modification, and renders potential toxins harmless by transporting them to disposal sites. HSA also accounts for most of the antioxidant capacity of human serum, either binding and carrying radical scavengers, or by sequestering transition metal ions with pro-oxidant activity. Finally, HSA acts as a nitric oxide depot and carrier, leading to covalent modification(s) of (macro)molecules (*1-7*).

HSA displays a modular structure containing three homologous domains (named I, II, and III). Each domain consists of two separate helical sub-domains (named A and B) connected by random coils. Terminal regions of sequential domains contribute to the formation of interdomain helices linking domain IB to IIA, and IIB to IIIA, freely linked by extended random coils (Figuere 3.1A) (*6, 8-14*). It is, thus, reasonable to hypothesize allosteric conformational transition(s) occurring in HSA upon ligand binding. Note that the flexibility of the HSA structure allows it to adapt readily to ligands and that its three-domain design provides a variety of binding sites. In particular, the conformational adaptability of HSA involves more than the immediate vicinity of the binding site(s), affecting both the structure and the ligand binding properties of the whole HSA molecule (*2-7, 12, 15-17*). The interaction of ligands with HSA occurs mainly in two regions. According to the Sudlow's nomenclature, bulky heterocyclic anions bind to site I (located in subdomain IIA), whereas site II (located in subdomain IIIA) is preferred by aromatic carboxylates with an extended conformation. Remarkably, ibuprofen, a nonsteroidal anti-inflammatory agent (*18*), and warfarin, an anticoagulant drug (*18*), are considered as stereotypical ligands for Sudlow's site II and Sudlow's site I, respectively (*19, 20*). Ibuprofen (ibu) binds to Sudlow's site II with Kd: 3.7×10^{-7} M (*21*), whereas warfarin (WF) binds to Sudlow's site I with Kd: 3.0×10^{-6} M (*22-24*). Secondary binding clefts have been found for ibu and WF to be located on domain I. Remarkably, the ibu secondary site corresponds to the WF primary cleft (i.e. to Sudlow's site I) (*3, 6, 17*). Moreover, multiple recognition sites for binding of anaesthetics, fatty acids, and triiodobenzoic acid to HSA have also been identified (*19, 25*). Among hydrophobic molecules, heme binding to HSA is of peculiar relevance for the heme iron reuptake following hemolytic events (*26*). The heme binding site has been located primarily at the interface between domains I and II of HSA, while on domains II and III secondary binding clefts have been found (*3, 4, 16*). The heme bound to its primary site in HSA is buried in a hydrophobic pocket within domain I delimited by Tyr138 and Tyr161 that interact with the porphyrin by π-π stacking. The heme

propionates protrude from the pocket pointing toward the interface between domains I and III and are stabilized by salt bridges with His146 and Lys190 (Figure 3.1B) (*27*).

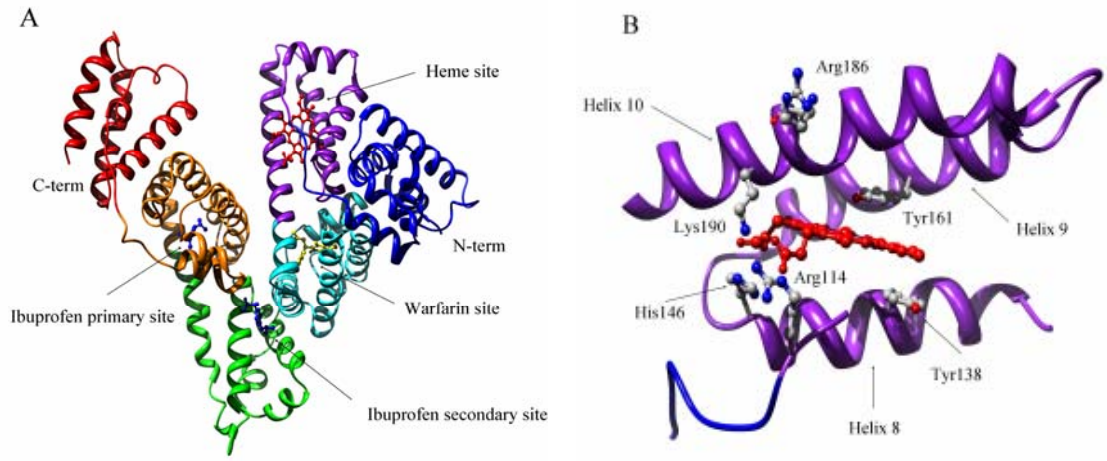

Figure 3.1 Panel A: HSA structure. The six subdomains of HSA are coloured as follows: subdomain IA, blue; subdomain IB, purple; subdomain IIA, cyan; subdomain IIB, green; subdomain IIIA, orange; subdomain IIIB, red. The heme (red) binds in the primary cleft of subdomain IB. Ibuprofen (blue) is shown in both its primary (Sudlow's site 2) and secondary binding sites. Warfarin (yellow) occupies its primary binding site (Sudlow's site 1). N- and C-termini are labelled. Atomic coordinates are taken from PDB entries 1N5U, (*27-29*). Panel B: Zoom of the heme binding pocket. Heme (red) is bound in the cleft formed by helices 8, 9 and 10. Residues Arg114, Tyr138, His146, Tyr161 (coordinating heme Fe^{3+}), Arg186, and Lys190 are shown.

3.2 Effects of ibuprofen binding on heme-HSA complex

3.2.1 Heme-HSA

During the first months of my Ph.D. thesis, I continued the spectroscopic characterization of the heme-HSA complex, previously object of my Laurea thesis (*30*). The crystallographic studies have revealed that (Fe^{3+})heme is pentacoordinated high spin (5cHS) coordinated to Tyr161 (Figure 3.1B) (*27*). The distance between the iron and the phenolic oxygen is 2.73 Å suggesting a week coordination. The spectroscopic data (UV-Vis and RR) in solution, confirmed that (Fe^{3+})heme is a 5cHS, characterized by the presence of a weak bond between an axial oxygen anionic ligand and the Fe atom (*30, 31*). The weakness of Fe-O bond was also confirmed by the RR spectrum of (Fe^{2+})heme-HSA that shows two species: a 5cHS state with Tyr161 coordinated to the heme iron, and a four coordinate intermediate spin (4cIS) state deriving from the dissociation of the weakly bound Tyr upon reduction. To understand the nature of the fifth ligand, the (Fe^{2+})heme-HSA complex was studied in presence of 2-metil-imidazole

(2-MeIm). It is known that 2-MeIm coordinates to the (Fe^{2+})heme to give rise a 5cHS species. The comparison of the low frequency RR spectra of (Fe^{2+})heme-HSA in the presence and absence of 2-MeIm clearly indicates the $\nu_{(Fe-Im)}$ band at 208 cm^{-1} in the complex with 2-MeIm. These results clearly demonstrated that Tyr161, and not a His residue, is coordinated to the Fe^{2+} iron (*30, 31*).

3.2.2 Heme-HSA-Ibuprofen

Among the various drugs which bind to HSA, I have tested the ibu binding. Ibu binding to heme-HSA affects allosterically the heme affinity for HSA: the 5c tyrosine-bound heme coordination of heme-HSA, observed in the absence of ibu, becomes 6-coordinate low spin (6cLS) upon drug binding (*30, 31*). The g values of the low spin species observed in the corresponding EPR spectrum suggested that a His residue is one of the low spin axial ligands, the sixth ligand probably being Tyr161 (*30, 31*).

The first experiments of my Ph.D. thesis were focused on the CO-(Fe^{2+})heme-HSA adducts, in the presence and absence of ibu. The comparison between the electronic absorption spectrum of the CO-heme-HSA and CO-heme-HSA-ibu complexes together with their $\nu_{(Fe-CO)}/\nu_{(CO)}$ vibrational frequencies clearly indicate that in the CO-heme-HSA-ibu complex two CO-(Fe^{2+})heme-HSA forms are present. One form is characterized by a CO complex with a weak (such as Tyr161) or absent trans ligand (the only species present in the adduct in the absence of ibu) whereas the second conformer is typical of a CO complex with a His residue coordinated to the iron in the trans position. This conclusion was also confirmed by the observation of the $\nu_{(Fe-Im)}$ mode at 218 cm^{-1} in the heme-HSA-ibu complex upon photolysis of the CO (*31*). These results supported the ligation of a His to the heme iron upon ibu binding.

3.2.3 Peroxynitrite isomerization by (Fe^{3+})-heme-HSA

(Fe^{3+})heme-HSA catalyzes peroxynitrite isomerization to NO^{3-} and prevents peroxynitrite-mediated nitration of free added L-tyrosine (*32*). The (Fe^{3+})heme-HSA catalyzed isomerization of peroxynitrite has been ascribed to the reactive 5c (Fe^{3+})heme species. Since the ibuprofen induces the formation of the 6cLS specie (Tyr-Fe^{3+}-His), the drug impairs dose-dependently peroxynitrite isomerization by (Fe^{3+})heme-HSA and facilitates the nitration of free added L-tyrosine. These results represent the first evidence for peroxynitrite isomerization by (Fe^{3+})heme-HSA, highlighting the allosteric modulation of (Fe^{3+})heme-HSA reactivity by heterotropic interaction(s), and outlining the role of drugs in modulating HSA functions (*32*).

3.3 (Fe^{2+})-heme-HSA and CO adduct in dependence of pH

3.3.1 (Fe^{2+})-heme-HSA

In agreement with previous results (*31, 33*), the UV-vis spectrum of (Fe^{2+})-heme-HSA at pH 7 is characterized by a broad Soret band centred at 418 nm, with two shoulders at 405 and 424 nm, and β and α bands at 536 and 572 nm, respectively (Figure 3.2A). The 413.1 nm excitation RR spectrum (Figure 3.2B), in resonance with the Soret band at 418 nm, shows the presence of a predominant 4cIS (ν_4 at 1370 cm^{-1}, ν_3 at 1502 cm^{-1}, ν_2 at 1580 cm^{-1}, ν_{10} at 1635 cm^{-1}) in equilibrium with a 5cHS (ν_4 at 1358 cm^{-1}, ν_3 at 1472 cm^{-1}, ν_2 at 1557 cm^{-1}, ν_{10} at 1602 cm^{-1}). This latter has been proposed to correspond to a 5cHS species containing a tyrosinate coordinated to the heme iron while the formation of a 4cIS species is a consequence of the weakness of the Fe^{2+}-OTyr bond (*31*). A small amount of a 6cLS (Fe^{2+})-heme species (Soret band at 424 nm, α band at 559 nm and ν_3 at 1492 cm^{-1}) is also revealed.

Upon decreasing the pH to 5.8, the relative intensities of the RR bands change (Figure 3.2B) clearly indicating that the 4cIS form increases while the 6cLS species diminishes as the Soret band sharpens at 424 nm (Figure 3.2A). It is not clear if any change in the amount of the 5cHS species occurs. At pH values lower than 5.5 the heme-HSA complex is not stable and, in agreement with previous findings, free heme has been detected (*34*).

At pH 10.0, the 6cLS species becomes the predominant form while the 4cIS and 5cHS species remain in traces. The UV-Vis spectrum of the 6cLS species (Figure 3.2A) resembles very closely to that obtained upon complexation of (Fe^{2+})heme with 2-methyl-imidazole (*31*) as well as that of ferrous *Herbaspirillum seropedicae* truncated hemoglobin (Hs-trHb) (*35*). Therefore, we assign the 6cLS form to a heme-Fe-atom coordinated to the oxygen atom of a tyrosinate (Tyr 161) and the N atom of a histidine (His146). This hypothesis agrees with our previous finding that an allosteric conformational transition, induced by ibuprofen binding, moves the His146 residue close to the (Fe^{3+})-heme atom (*31*). This residue is at a distance of about 9 Å from the Fe-heme atom, therefore, significant changes in the heme cavity site can be foreseen. The crystal structure of (Fe^{3+})-heme-HSA in the presence of ibu is not available yet, but a model study, made by energy minimization of the heme structure within the heme

binding cleft of the HSA-ibu complex (*28*), has revealed an appreciable tilt of α-helix 10 and a reorientation of α-helix 7 (*31*). Accordingly, we suggest that at alkaline pH the formation of the His-Fe-Tyr 6cLS species derives from a shift of α-helix 8 (as a consequence of the tilt of the α-helix 10 and of the reorientation of the α-helix 7); this leads to a rotation of the His146 residue toward the heme-Fe atom.

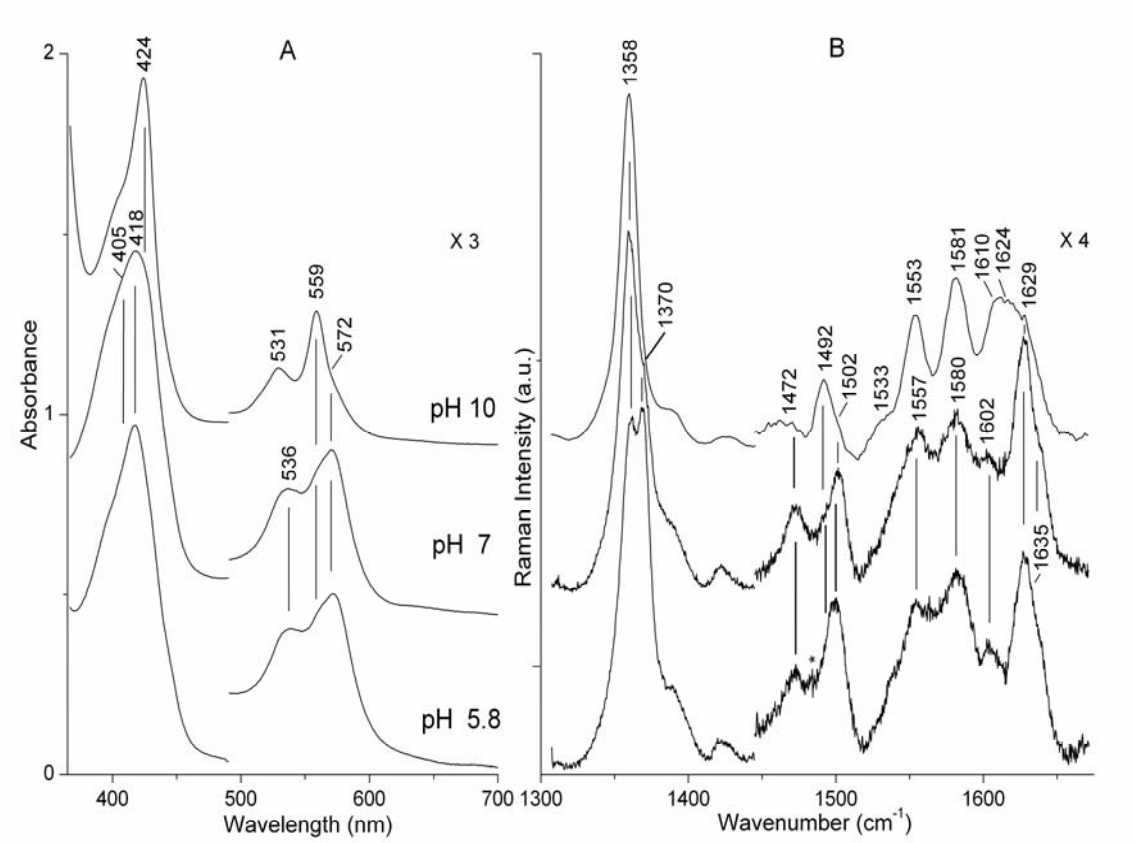

Figure 3.2 Electronic absorption (panel A) and RR spectra (panel B) of (Fe^{2+})-heme-HSA at pH 10 (in 0.1 M glycine buffer), 7 and 5.8 (in 0.1 M phosphate buffer). Experimental conditions: Panel A: 600 nm/min scan time. Panel B: 413.1 nm excitation wavelength, 3.8 cm^{-1} spectral resolution (pH 10), 1.1 cm^{-1} spectral resolution (pH 7 and 5.8). (pH 10): 10 mW laser power at the sample, average of four spectra with 120 s integration time; (pH 7): 17 mW laser power at the sample, average of six spectra with 300 s integration time; (pH 5.8): 2 mW laser power at the sample, average of 30 spectra with 120 s integration time. The intensities are normalized to that of ν_4 band. Spectra have been shifted along the ordinate axis to allow better visualization. The asterisk indicates the small amount of the Fe^{3+} form due to the easy oxidation of the sample at pH 5.8.

3.3.2 (Fe^{2+})-heme-HSA-CO

On the basis of the findings that a conformational change occurs in the (Fe^{2+})-heme-HSA upon pH change (altering the ligand coordination state of (Fe^{2+})-heme-HSA), I have extended the previous study of the CO-(Fe^{2+})-heme-HSA adduct (*31*) at pH 7 to different pH values in order to gain insight on the pH-dependent conformational changes occurring at the heme-Fe binding site (*i.e.*, at FA1).

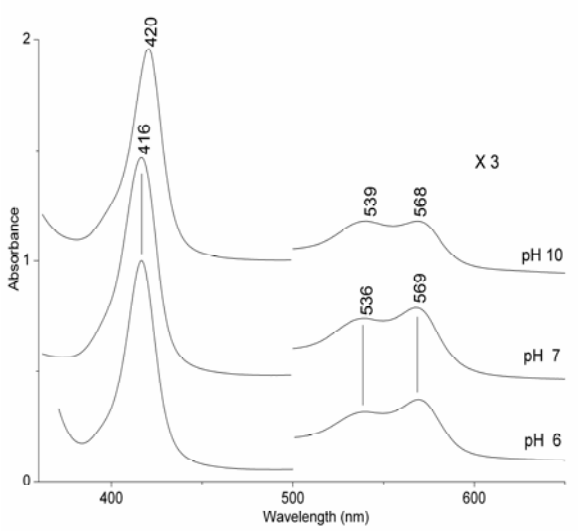

Figure 3.3 Electronic absorption spectra of CO-(Fe^{2+})-heme-HSA at pH 6 and 7 (in 0.1 M phosphate buffer), and pH 10 (in 0.1 M glycine buffer). Spectra have been shifted along the ordinate axis to allow better visualization. Scan time of 600 nm/min.

Upon addition of CO to (Fe^{2+})-heme-HSA at pH 7.0, similarly to what previously reported (*31, 36*), the electronic absorption spectrum is characterized by a sharp Soret band centred at 416 nm and β and α bands at 536 and 569 nm, respectively (Figure 3.3). The blue-shift of the Soret absorption band, as compared to that of the CO complexes of heme proteins having an imidazole as fifth ligand (Soret at 420 nm), has been interpreted as a CO-(Fe^{2+})-heme adduct with a trans ligand weaker than His, or no ligand at all (*31*). At pH 10, the 4 nm red shift of Soret band (Figure 3.3) strongly suggests a conformational transition which allows the weak trans CO-(Fe^{2+})-heme ligand to be replaced by an amino acid residue coordinating the (Fe^{2+})-heme atom with a N atom. Accordingly, the RR spectra of CO-(Fe^{2+})-heme-HSA at pH 7 and 10 (Figure 3.4), clearly show a change in the relative intensity of the $\nu_{(Fe\text{-}CO)}$ and $\nu_{(CO)}$ stretching modes (Table 3.1). At pH 10, the strong bands at 524 cm^{-1} [$\nu_{(Fe\text{-}CO)}$] and at 1960 cm^{-1} [$\nu_{(CO)}$], observed at pH 7.0 (*31*), decrease in intensity. Concomitantly a band at 498 cm^{-1} [$\nu_{(Fe\text{-}CO)}$] becomes clearly evident. The corresponding [$\nu_{(CO)}$] stretch could possibly be

assigned to the shoulder at 1970 cm^{-1}. It must be noted that a very weak band at 498 cm^{-1} is also present in a very low amount at pH 7. Accordingly, a change of the excitation wavelength from 413.1 to 441.6 nm, i.e in resonance with the Soret band at 420 nm (Figure 3.3), leads to a substantial enhancement of the 498 cm^{-1} band relative to the 524 cm^{-1} band (Figure 3.5).

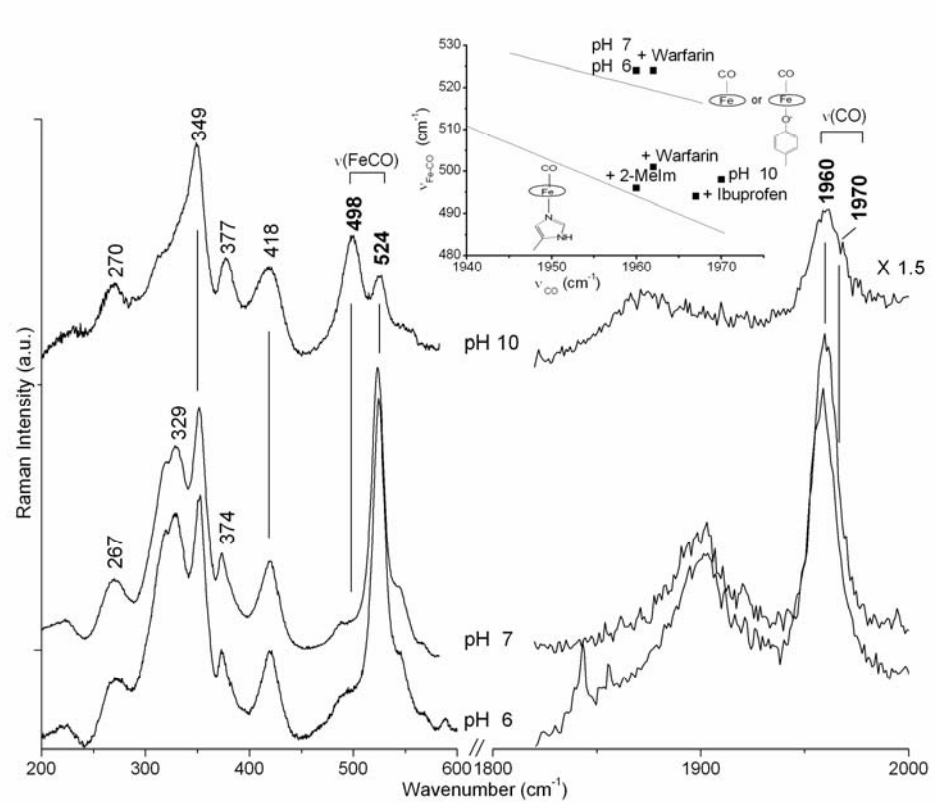

Figure 3.4 RR spectra of CO-(Fe^{2+})-heme-HSA pH 6 and 7 (in 0.1 M phosphate buffer), and pH 10 (in 0.1 M glycine buffer). Experimental conditions: 413.1 nm excitation wavelength; 1 cm^{-1} and 3.3 cm^{-1} spectral resolution for the low and high frequency region, respectively. (pH 6 and 7): 2 mW laser power at the sample; average of 32 spectra with 140 s integration time (low frequency region); average of three spectra with 600 s integration time (high frequency region). (pH 10): 2 mW laser power at the sample; average of 6 spectra with 300 s integration time (low frequency region); average of eight spectra with 600 s integration time (high frequency region). The intensities are normalized to that of the ν_4 band (not shown). Spectra have been shifted along the ordinate axis to allow better visualization. The inset plot shows the correlation of the $\nu_{(FeCO)}$ versus $\nu_{(CO)}$ frequencies observed in the CO complexes of heme-HSA under various experimental conditions. The lower line indicates the back-bonding correlation line for six-coordinate CO heme proteins with imidazole as sixth ligand, as given in ref (*37*). The upper line represents five-coordinate, with no trans ligand, or six-coordinate CO heme proteins with weak trans ligands. Data and references are reported in Table 3.1.

In the inset of Figure 3.4, a plot of the $\nu_{(Fe\text{-}CO)}$ and $\nu_{(CO)}$ frequencies for CO adducts of a variety of heme proteins and model compounds having either a His residue as the fifth ligand or a weaker/absent trans ligand is shown. The lines are obtained according to eq. 1 reported in ref (*37*). The $\nu_{(Fe\text{-}CO)}$ stretching mode at 524 cm^{-1} and the $\nu_{(CO)}$ stretch at 1960 cm^{-1} of the CO-(Fe^{2+})Heme HSA complex at pH 7 are located above the histidine

line of the $\nu_{(Fe\text{-}CO)}/\nu_{(CO)}$ backbonding correlation, since the proximal ligand is either weak (*38*) or absent (*39*). This result is consistent with the presence of a Tyr ligand as the axial ligand. However, the correlation plot cannot effectively separate a 5c CO-(Fe^{2+})Heme system from a 6c species with a weak proximal ligand, such as water or Tyr (*37, 40*). Furthermore, the spectroscopic features of the CO-(Fe^{2+})heme-HSA adduct at pH 6 (Figures 3.3 and 3.4) are identical to those at pH 7 although at lower pH the 4cIS species increases.

The $\nu_{(Fe\text{-}CO)}/\nu_{(CO)}$ stretch values of the alkaline form at pH 10 fall on the histidine $\nu_{(Fe\text{-}CO)}/\nu_{(CO)}$ back-bonding correlation line (Figure 3.4), closer to the values of the CO-(Fe^{2+})-HSA complex in presence of 2-metil-imidazole or ibu, in which the trans ligand is an imidazole (*31*). These data confirm that at alkaline pH a major conformational change occurs in the CO-(Fe^{2+})-heme-HSA heme pocket allowing the His146 residue to coordinate to the heme Fe atom via its nitrogen atom, both in presence and in absence of CO.

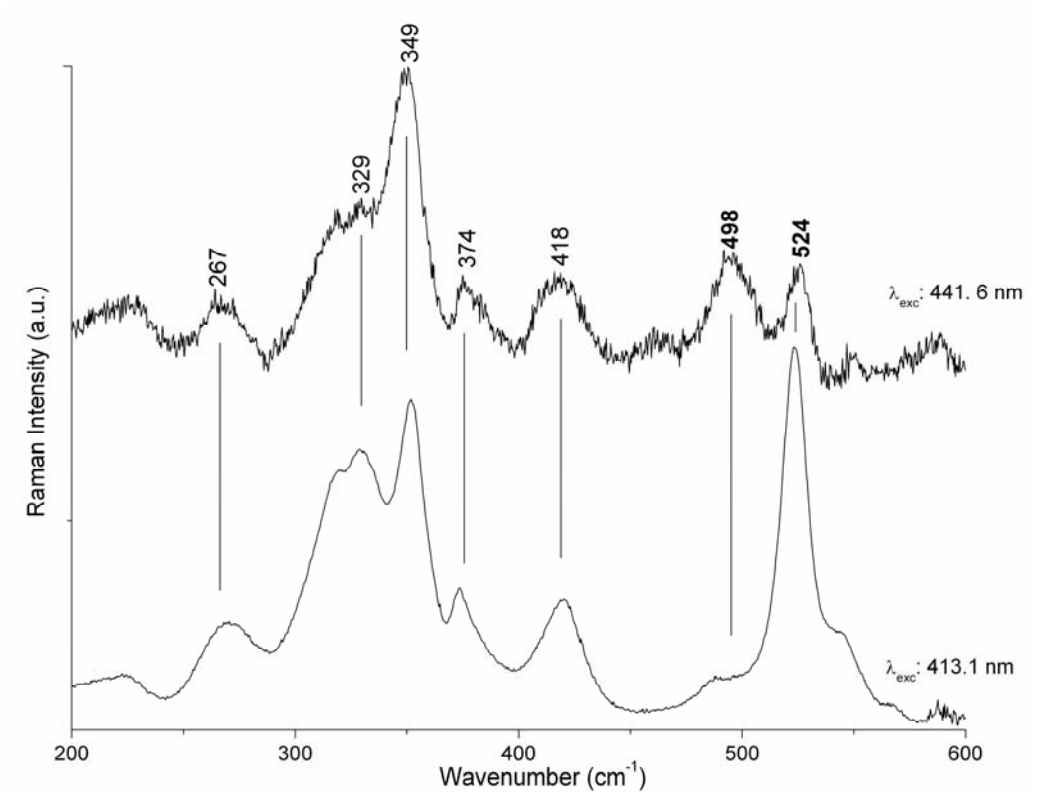

Figure 3.5 RR spectra of CO-(Fe^{2+})-heme-HSA at pH 7 in 0.1 M phosphate buffer. Experimental conditions: 1 cm^{-1} spectral resolution, 2 mW laser power at the sample, average of 32 spectra with 140 s integration time (λ_{exc}: 413.1 nm); 0.9 cm^{-1} spectral resolution, 1 mW laser power at the sample, average of 30 spectra with 900 s integration time (λ_{exc}: 441.6 nm). The intensities are normalized to that of the 349 cm^{-1} band. Spectra have been shifted along the ordinate axis to allow better visualization.

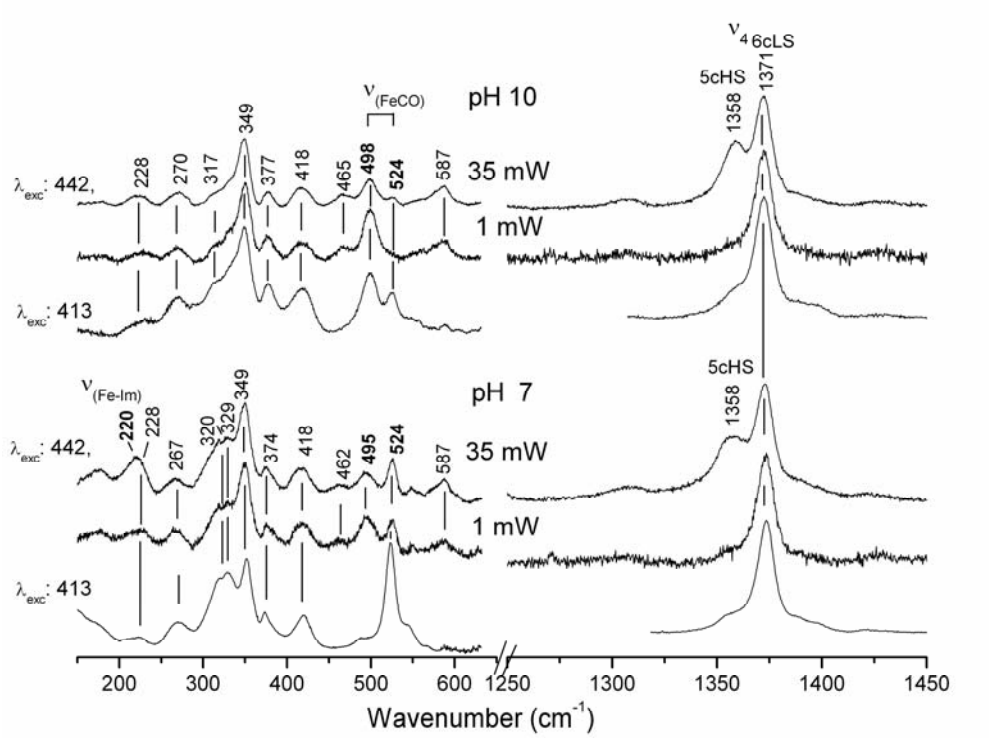

Figure 3.6 RR spectra in the low (LF) and high frequency (HF) regions of CO-(Fe^{2+})-heme-HSA at pH 7 (0.1 M phosphate buffer) and at pH 10 (0.1 M glycine buffer) with 413.1 and 441.6 nm excitation wavelength. Experimental conditions: λ_{exc}: 413.1 nm, 1 cm^{-1} spectral resolution, 2 mw laser power at the sample, average of ten spectra with 180 s integration time (LF), average of four spectra with 200 s integration time (HF). λ_{exc}: 441.6 nm, 0.9 cm^{-1} spectral resolution, 1 mW laser power at the sample, average of twenty spectra with 300 s integration time (LF), average of eight spectra with 260 s integration time (HF); 35 mW laser power at the sample, average of five spectra with 300 s (LF), average of three spectra with 180 s integration time (HF). The intensities are normalized to that of ν_7 and ν_4 for LF and HF regions, respectively. Spectra have been shifted along the ordinate axis to allow better visualization.

The formation of the Fe-N bond is convincingly confirmed by the presence of the $\nu_{(Fe\text{-}Im)}$ stretching mode upon photolysis of the CO in the laser beam. Figure 3.6 shows the low frequency region RR spectra obtained with 441.6 nm excitation of the CO-(Fe^{2+})heme-HSA complex at pH 7 and 10 upon increasing the laser power. At 1 mW laser power (Figure 3.6), when CO is fully bound (ν_4 at 1371 cm^{-1}) the $\nu_{(Fe\text{-}CO)}$ at 495 and 498 cm^{-1}, at pH 7 and 10, respectively, are fairly strong. At higher laser power (35 mW, Figure 3.6), CO is partially photolyzed. Therefore, the CO mode decreases in intensity and the vibrations of the ferrous 5c species grow in (ν_4 at 1358 cm^{-1}). The strong band which appears at 220 cm^{-1} for sample at pH 7 is therefore assigned to the $\nu_{(Fe\text{-}Im)}$ mode and demonstrates the coordination of an imidazole ring to (Fe^{2+})heme-HSA at neutral pH. At higher pH, we are not able to observe any $\nu_{(Fe\text{-}Im)}$ stretching mode because a fast rebiding of Tyr161 occurs at pH 10 to regenerate the 6cLS species (Tyr-Fe^{2+}-His) as described above.

3.4 CO-(Fe^{2+})-heme-HSA-Warfarin

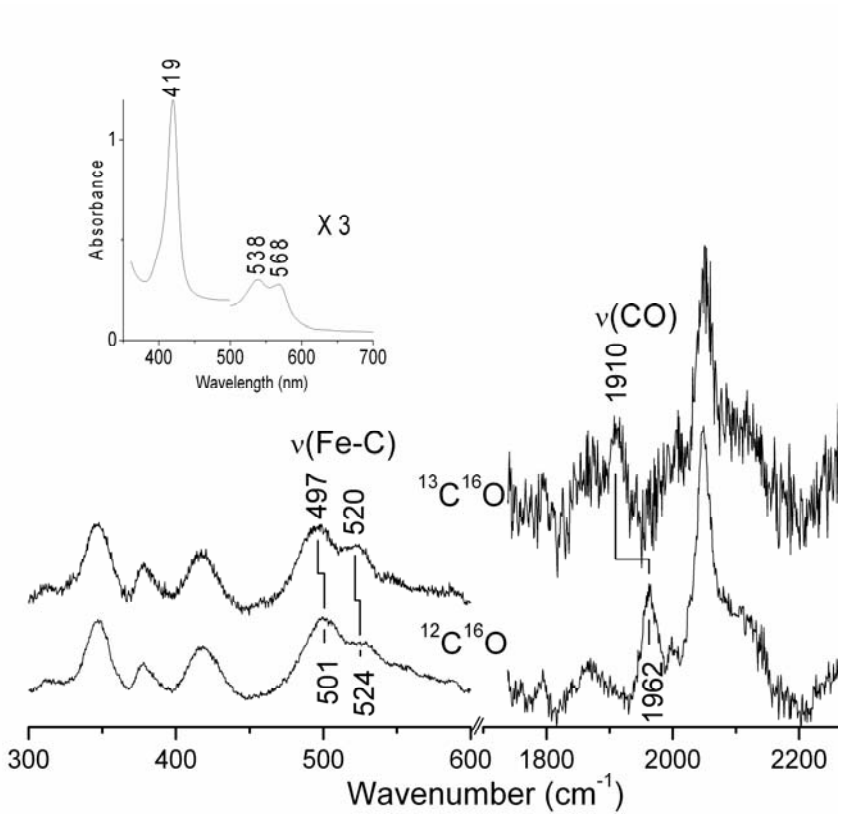

Figure 3.7 RR spectra of CO-(Fe^{2+})-heme-HSA-WF at pH 7 in 0.1 M phosphate buffer, 413.1 nm excitation wavelength, 2 mW laser power at the sample. Experimental conditions: 1 and 3.3 cm^{-1} spectral resolution for LF and HF frequency regions, respectively. Average of seven spectra with 300 s integration time (LF), average of four spectra with 3600 s integration time (HF) [$^{12}C^{16}O$]. Average of three spectra with 300 s integration time (LF), average of two spectra with 3600 s integration time (HF) [$^{13}C^{16}O$]. The intensities are normalized to that of ν_7 and ν_4 for LF and HF regions, respectively. The inset reports the UV-Vis spectrum of CO-(Fe^{2+})-heme-HSA-WF at pH 7 in 0.1 M phosphate buffer. The HF region was expanded by 1.5 times.

In the inset of Figure 3.7 it is reported the absorption spectrum of CO-(Fe^{2+})-heme-HSA in presence of WF. The maximum of the Soret band at 419 nm (β and α bands at 538 and 568 nm, respectively) suggests an heme iron coordinated to a His residue in the fifth coordination position, trans to the CO molecule, similarly to the species formed upon ibu binding at neutral pH (*31*) or at pH 10 without any drug (Figure 3.3). The RR spectra confirmed this results (Figure 3.7). A conformer with $\nu_{(Fe\text{-}CO)}$ at 501 cm^{-1} and $\nu_{(CO)}$ at 1962 cm^{-1} is found which falls on the histidine $\nu_{(Fe\text{-}CO)}/\nu_{(CO)}$ back-bonding correlation line (Figure 3.4). Moreover, a second conformer is present, characterized by $\nu_{(Fe\text{-}CO)}$ at 524 cm^{-1}, while the $\nu_{(CO)}$ mode overlaps with the band at 1962 cm^{-1} of the first conformer. This result is consistent with the presence of a 6c species containing a Tyr ligand as the axial ligand or a 5c CO-(Fe^{2+}) species (Figure 3.7).

The presence of a histidine as trans ligand to the CO has been confirmed by CO photolysis (Figure 3.8). By increasing the power of the beam focused on the sample, a 5cHS species is formed (ν_4 band at 1356 cm^{-1}) , thus the intensity of the $\nu_{(Fe\text{-}CO)}$ mode at 501 cm^{-1} weakens and a new band at 218 cm^{-1} appears (at the same frequency of the photolyzed CO-(Fe^{2+})-heme-HSA-ibu (*31*). This band is assigned to the $\nu_{(Fe\text{-}Im)}$ stretching mode.

The conformational change induced upon WF binding can be easily explained since the drug binds to the Sudlow's I site (the secondary ibu binding site) (*3, 6*) which is considered to trigger the allosteric changes in the heme cavity (FA1 site).

Table 3.1 Vibrational Frequencies (cm^{-1}) of the FeCO Stretching Modes in CO adducts of Selected Iron Porphyrins and Heme Proteins.[a]

protein[b]	$\nu_{(Fe\text{-}CO)}$	$\nu_{(CO)}$	axial ligation	reference
6c CO complexes with weak trans ligand or 5c complexes with no ligand				
1. Heme-HSA + ibu	525 (519)	1962 (1924)	CO-Fe	(*31*)
2. Heme-HSA + 2-MeIm	524 (520)	1960 (1912)	CO-Fe-O_{Tyr}	(*31*)
3. *Heme-HSA pH 7*	524 (520)	1960 (1912)	CO-Fe-O_{Tyr}	(*31*)
4. $HasA_{SM}$	532 (523)	1954 (1905)	CO-Fe-O_{Tyr}	(*41*)
5. Human HO-1(H25Y)	529 (524)	1962 (1917)	CO-Fe-H_2O	(*42*)
6. Heme-CO in PBS, pH 6.9	525	1962	CO-Fe	(*31*)
6c CO complexes with imidazole trans ligand and apolar distal environment				
7. *Heme-HSA pH 10*	498 (494)	1970 (1927)	CO-Fe-N_{His}	This thesis
8. Heme-HSA +Ibu	494 (488)	1967 (1924)		(*31*)
9. Heme-HSA +2-MeIm	496 (492)	1960 (1912)	CO-Fe-N_{His}	(*31*)
10. Heme-HSA +WF	501 (497)	1962 (1902)	CO-Fe-N_{His}	This thesis
11. Fe(PPDME)(Im)	495	1960	CO-Fe-N_{His}	(*43*)
12. Sperm whale Mb, pH 2.6	491	1967	CO-Fe-N_{His}	(*44, 45*)

[a] The frequencies obtained with ^{13}CO are given in parentheses. [b]$HasA_{SM}$, hemophore HasA from *Serratia marcenscens*, HO-1, heme oxygenase-1; Mb, myoglobin; PPDME, protoporphyrin IX dimethyl ester.

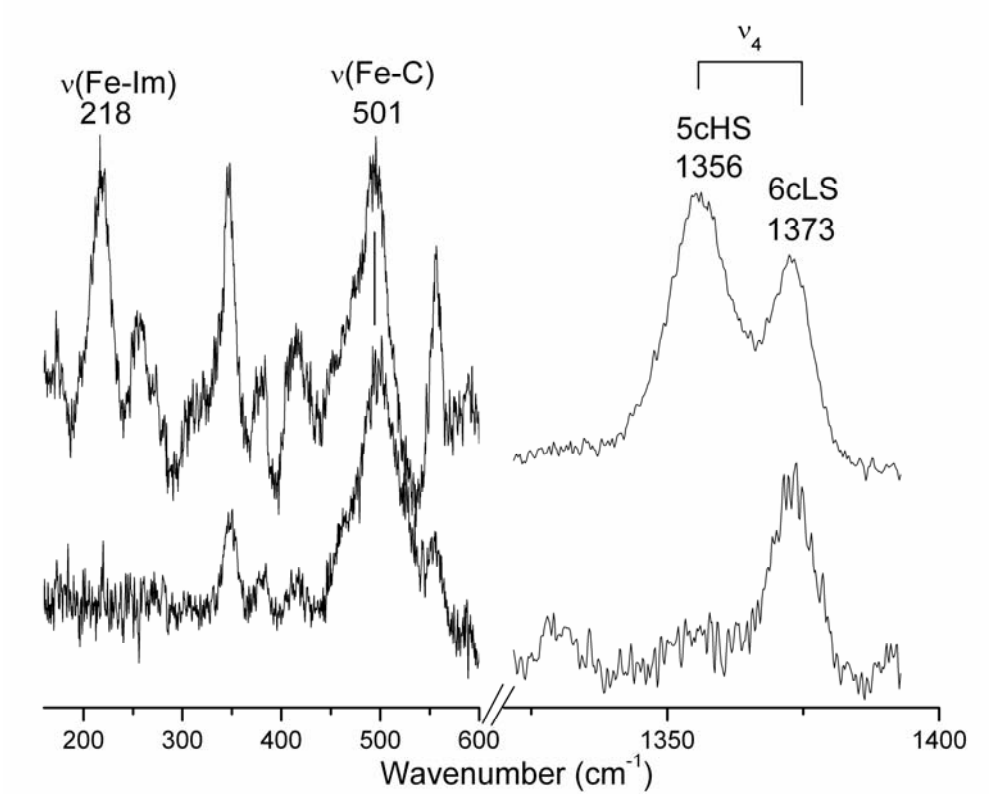

Figure 3.8 RR spectra of CO-(Fe^{2+})heme-HSA-WF in 0.1 M phosphate buffer at pH 7. Experimental conditions: 441.6 nm excitation wavelength, 0.9 cm^{-1} spectral resolution, (bottom):1 mW laser power at the sample, average of five spectra with 1800 s integration time (low frequency region), average of three spectra with 1800 s integration time (high frequency region); (top): 35 mW laser power at the sample, average of two spectra with 400 s integration time (low frequency region), average of two spectra with 132 s integration time (high frequency region). The intensities are normalized to that of the ν_4 band. The LF region was expanded by three times.

3.5 Conclusions

The effect of ibu and WF binding to the Sudlow's I on the electronic absorption and RR properties of CO-(Fe^{2+})-heme-HSA is keeping in with the allosteric conformational transition(s) induced by these therapeutic drugs in HSA. Interestingly, the binding of the drugs to the Sudlow's I site induces the same effect exerted by the pH, changing from the N (normal, at neutral pH) to B (basic, at alkaline pH) conformer transition in HSA (*46*). In fact, the spectroscopic properties of the CO adducts in presence of WF and ibu are quite similar to that observed at pH 10 in absence of drug. Moreover the affinity of therapeutic drugs for the B-form of HSA is higher than that observed for the N-form (*47, 48*). Finally, drug-dependent spectroscopic properties of CO-(Fe^{2+})-heme-HSA may be helpful in investigating ligand binding and allosteric properties of HSA since the therapeutic use of WF and ibu may affect heme transfer to hemopexin and

consequently its plasma level. In parallel, heme may affect pharmacokinetics of drugs carried out by HSA.

References

(1) Bhattacharya, A. A., Grune, T., and Curry, S. (2000) Crystallographic analysis reveals common modes of binding of medium and long-chain fatty acids to human serum albumin. *J. Mol. Biol. 303*, 721-732.

(2) Curry, S., Mandelkow, H., Brick, P., and Franks, N. (1998) Crystal structure of human serum albumin complexed with fatty acid reveals an asymmetric distribution of binding sites. *Nat. Struct. Biol. 5*, 827-835.

(3) Dockal, M., Carter, D. C., and Ruker, F. (1999) The three recombinant domains of human serum albumin. Structural characterization and ligand binding properties. *J. Biol. Chem. 274*, 29303-29310.

(4) Fasano, M., Baroni, S., Vannini, A., Ascenzi, P., and Aime, S. (2001) Relaxometric characterization of human hemalbumin. *J. Biol. Inorg. Chem. 6*, 650-658.

(5) Mattu, M., Vannin, A., Coletta, M., Fasano, M., and Ascenzi, P. (2001) Effect of bezafibrate and clofibrate on the heme-iron geometry of ferrous nitrosylated heme-human serum albumin: an EPR study. *J. Inorg. Biochem. 84*, 293-296.

(6) Peters, T. J. (1996) All About Albumin: Biochemistry, Genetics and Medical Applications. Academic Press, San Diego and London.

(7) Sugio, S., Kashima, A., Mochizuki, S., Noda, M., and Kobayashi, K. (1999) Crystal structure of human serum albumin at 2.5 A resolution. *Protein Eng. 12*, 439-446.

(8) Ascenzi, P., Bocedi, A., Notari, S., Fanali, G., Fesce, R., and Fasano, M. (2006) Allosteric modulation of drug binding to human serum albumin. *Mini Rev. Med. Chem. 6*, 483-489.

(9) Carter, D. C., and Ho, J. X. (1994) Structure of serum albumin. *Adv. Protein Chem. 45*, 153-203.

(10) Curry, S. (2002) Beyond expansion: structural studies on the transport roles of human serum albumin. *Vox Sang 83 Suppl 1*, 315-319.

(11) Fasano, M., Curry, S., Terreno, E., Galliano, M., Fanali, G., Narciso, P., Notari, S., and Ascenzi, P. (2005) The extraordinary ligand binding properties of human serum albumin. *IUBMB Life 57*, 787-796.

(12) He, X. M., and Carter, D. C. (1992) Atomic structure and chemistry of human serum albumin. *Nature 358*, 209-215.

(13) Sakurai, Y., Ma, S. F., Watanabe, H., Yamaotsu, N., Hirono, S., Kurono, Y., Kragh-Hansen, U., and Otagiri, M. (2004) Esterase-like activity of serum albumin: characterization of its structural chemistry using p-nitrophenyl esters as substrates. *Pharm. Res. 21*, 285-292.

(14) Zunszain, P. A., Ghuman, J., McDonagh, A. F., and Curry, S. (2008) Crystallographic analysis of human serum albumin complexed with 4Z,15E-bilirubin-IXalpha. *J. Mol. Biol. 381*, 394-406.

(15) Bhattacharya, A. A., Curry, S., and Franks, N. P. (2000) Binding of the general anesthetics propofol and halothane to human serum albumin. High resolution crystal structures. *J. Biol. Chem. 275*, 38731-38738.

(16) Carter, D. C., Ho, J. X., and Ruker, F. (1999) Oxygen-transporting albumin-based blood replacement composition and blood volume expander. US Patent 5948609.
(17) Dockal, M., Chang, M., Carter, D. C., and Ruker, F. (2000) Five recombinant fragments of human serum albumin-tools for the characterization of the warfarin binding site. *Protein Sci. 9*, 1455-1465.
(18) James, E., and Reynolds, F. (1996) Martindale: The Extra Pharmacopoeia, 31st edn. The Pharmaceutical Press, London.
(19) Petitpas, I., Bhattacharya, A. A., Twine, S., East, M., and Curry, S. (2001) Crystal structure analysis of warfarin binding to human serum albumin: anatomy of drug site I. *J. Biol. Chem. 276*, 22804-22809.
(20) Sudlow, G., Birkett, D. J., and Wade, D. N. (1975) The characterization of two specific drug binding sites on human serum albumin. *Mol. Pharmacol. 11*, 824-832.
(21) Whitlam, J. B., Crooks, M. J., Brown, K. F., and Pedersen, P. V. (1979) Binding of nonsteroidal anti-inflammatory agents to proteins--I. Ibuprofen-serum albumin interaction. *Biochem. Pharmacol. 28*, 675-678.
(22) Diana, F. J., Veronich, K., and Kapoor, A. L. (1989) Binding of nonsteroidal anti-inflammatory agents and their effect on binding of racemic warfarin and its enantiomers to human serum albumin. *J. Pharm. Sci. 78*, 195-199.
(23) Loun, B., and Hage, D. S. (1994) Chiral separation mechanisms in protein-based HPLC columns. 1. Thermodynamic studies of (R)- and (S)-warfarin binding to immobilized human serum albumin. *Anal. Chem. 66*, 3814-3822.
(24) Pinkerton, T. C., and Koeplinger, K. A. (1990) Determination of warfarin-human serum albumin protein binding parameters by an improved Hummel-Dreyer high-performance liquid chromatographic method using internal surface reversed-phase columns. *Anal. Chem. 62*, 2114-2122.
(25) Berman, H. M., Westbrook, J., Feng, Z., Gilliland, G., Bhat, T. N., Weissig, H., Shindyalov, I. N., and Bourne, P. E. (2000) The Protein Data Bank. *Nucleic Acids Res. 28*, 235-242.
(26) Pasternack, R. F., Gibbs, E. J., Hoeflin, E., Kosar, W. P., Kubera, G., Skowronek, C. A., Wong, N. M., and Muller-Eberhard, U. (1983) Hemin binding to serum proteins and the catalysis of interprotein transfer. *Biochemistry 22*, 1753-1758.
(27) Wardell, M., Wang, Z., Ho, J. X., Robert, J., Ruker, F., Ruble, J., and Carter, D. C. (2002) The atomic structure of human methemalbumin at 1.9 A. *Biochem Biophys. Res. Commun. 291*, 813-819.
(28) Ghuman, J., Zunszain, P. A., Petitpas, I., Bhattacharya, A. A., Otagiri, M., and Curry, S. (2005) Structural basis of the drug-binding specificity of human serum albumin. *J. Mol. Biol. 353*, 38-52.
(29) Zunszain, P. A., Ghuman, J., Komatsu, T., Tsuchida, E., and Curry, S. (2003) Crystal structural analysis of human serum albumin complexed with hemin and fatty acid. *BMC Struct. Biol. 3*, 6.
(30) Nicoletti, F. P. (2007) Proprietà spettroscopiche del complesso eme-albumina umana in presenza di ibuprofene. *Tesi di laurea per Chimica e Tecnologia Farmaceutiche*.
(31) Nicoletti, F. P., Howes, B. D., Fittipaldi, M., Fanali, G., Fasano, M., Ascenzi, P., and Smulevich, G. (2008) Ibuprofen induces an allosteric conformational transition in the heme complex of human serum albumin with significant effects on heme ligation. *J . Am. Chem. Soc. 130*, 11677-11688.

(32) Ascenzi, P., di Masi, A., Coletta, M., Ciaccio, C., Fanali, G., Nicoletti, F. P., Smulevich, G., and Fasano, M. (2009) Ibuprofen impairs allosterically peroxynitrite isomerization by ferric human serum heme-albumin. *J. Biol. Chem. 284*, 31006-31017.

(33) Komatsu, T., Ohmichi, N., Nakagawa, A., Zunszain, P. A., Curry, S., and Tsuchida, E. (2005) O2 and CO binding properties of artificial hemoproteins formed by complexing iron protoporphyrin IX with human serum albumin mutants. *J. Am. Chem. Soc. 127*, 15933-15942.

(34) Monzani, E., Bonafe, B., Fallarini, A., Redaelli, C., Casella, L., Minchiotti, L., and Galliano, M. (2001) Enzymatic properties of human hemalbumin. *Biochim. Biophys. Acta 1547*, 302-312.

(35) Razzera, G., Vernal, J., Baruh, D., Serpa, V. I., Tavares, C., Lara, F., Souza, E. M., Pedrosa, F. O., Almeida, F. C., Terenzi, H., and Valente, A. P. (2008) Spectroscopic characterization of a truncated hemoglobin from the nitrogen-fixing bacterium Herbaspirillum seropedicae. *J. Biol. Inorg. Chem. 13*, 1085-1096.

(36) Kamal, J. K., and Behere, D. V. (2002) Spectroscopic studies on human serum albumin and methemalbumin: optical, steady-state, and picosecond time-resolved fluorescence studies, and kinetics of substrate oxidation by methemalbumin. *J. Biol. Inorg. Chem. 7*, 273-283.

(37) Spiro, T. G., and Wasbotten, I. H. (2005) CO as a vibrational probe of heme protein active sites. *J. Inorg. Biochem. 99*, 34-44.

(38) Ray, G. B., Li, X. Y., Ibers, J. A., Sessler, J. L., and Spiro, T. G. (1994) How far can proteins bend the FeCO unit? Distal polar and steric effects in heme proteins and models. *J. Am. Chem. Soc. 116*, 162–176.

(39) Vogel, K. M., Kozlowski, P. M., Zgierski, M. Z., and Spiro, T. G. (2000) *297*, 11–17.

(40) Ye, X., Yu, A., Georgiev, G. Y., Gruia, F., Ionascu, D., Cao, W., Sage, J. T., and Champion, P. M. (2005) CO rebinding to protoheme: investigations of the proximal and distal contributions to the geminate rebinding barrier. *J. Am. Chem. Soc. 127*, 5854-5861.

(41) Lukat-Rodgers, G. S., Rodgers, K. R., Caillet-Saguy, C., Izadi-Pruneyre, N., and Lecroisey, A. (2008) Novel heme ligand displacement by CO in the soluble hemophore HasA and its proximal ligand mutants: implications for heme uptake and release. *Biochemistry 47*, 2087-2098.

(42) Liu, Y., Moenne-Loccoz, P., Hildebrand, D. P., Wilks, A., Loehr, T. M., Mauk, A. G., and Ortiz de Montellano, P. R. (1999) Replacement of the proximal histidine iron ligand by a cysteine or tyrosine converts heme oxygenase to an oxidase. *Biochemistry 38*, 3733-3743.

(43) Ling, J., Li, T., Olson, J. S., and Bocian, D. F. (1994) Identification of the iron-carbonyl stretch in distal histidine mutants of carbonmonoxymyoglobin. *Biochim. Biophys. Acta 1188*, 417-421.

(44) Ramsden, J., and Spiro, T. G. (1989) Resonance Raman evidence that distal histidine protonation removes the steric hindrance to upright binding of carbon monoxide by myoglobin. *Biochemistry 28*, 3125-3128.

(45) Sage, J. T., Morikis, D., and Champion, P. M. (1991) Spectroscopic studies of myoglobin at low pH: heme structure and ligation. *Biochemistry 30*, 1227-1237.

(46) Baroni, S., Mattu, M., Vannini, A., Cipollone, R., Aime, S., Ascenzi, P., and Fasano, M. (2001) Effect of ibuprofen and warfarin on the allosteric properties of haem-human serum albumin. A spectroscopic study. *Eur. J. Biochem. 268*, 6214-6220.

(47) Janssen, L. H., Van Wilgenburg, M. T., and Wilting, J. (1981) Human serum albumin as an allosteric two-state protein. Evidence from effects of calcium and warfarin on proton binding behaviour. *Biochim. Biophys. Acta 669*, 244–250.
(48) Kragh-Hansen, U. (1981) Molecular aspects of ligand binding to serum albumin. *Pharmacol. Rev. 33*, 17-53.

Chapter 4

The truncated hemoglobin from *Thermobifida fusca*

Francesco P. Nicoletti, Alessandra Comandini, Alessandra Bonamore, Leonardo Boechi, Fernando Martin Boubeta, Alessandro Feis, Giulietta Smulevich, and Alberto Boffi.
Sulfide Binding Properties of Truncated Hemoglobins.
Biochemistry (2010), 49, 2269-2278.

Enrica Droghetti, **Francesco P. Nicoletti**, Alessandra Bonamore, Leonardo Boechi, Pau Arroyo Mañez, Dario A. Estrin, Alberto Boffi, Giulietta Smulevich, and Alessandro Feis.
Heme pocket structural properties of a bacterial truncated hemoglobin from Thermobifida fusca.
Biochemistry (2010), 49, 10394-10402.

4.1 The truncated Hb family: an overview

More than three hundreds of truncated haemoglobin (trHb) genes have been documented in the last 10-20 years in bacteria, unicellular eukaryotes and plants (*1, 2*).
The first evidence of hemoproteins in unicellular organisms was reported by T. Sato and H. Tamiya in 1937 (*3*), when spectroscopic studies on the suspensions of the ciliated protozoa *Paramecium caudatum* revealed the occurrence of hemoglobin-like protein. In 1953 Keilin and Riley confirmed the presence of hemoglobin in protozae (*4*). The globin from *P. caudatum* was sequenced by Iwasaa four decades later (1989) (*5*), revealing 116 amino acid residues and a quite lower sequence identity respect to vertebrate Hbs. The first 3D structure of trHb from *P. caudatum* was determined by Bolognesi and coworkers (*6*), and in Figure 4.1 it is compared to the sperm whale Mb

fold. The crystal structure shows that the *P. caudatum* globin fold is based on a subset of the "classical" globin fold (the so called 3-on-3 α-helical sandwich (3/3)) typical of sperm whale myoglobin (Mb) (Figure 4.1 left) (*7*). Indeed, *P. caudatum* globin fold hosts the heme in a 2-on-2 α-helical sandwich ("2/2 fold") based on four α-helices, corresponding to the B-, E-, G-, and H-helices of the classical globin fold. The antiparallel helix pairs (B/E and G/H) are arranged in a sort of α-helical bundle which surrounds and protects the heme group from the solvent phase (Fig. 4.1 right) (*8*).

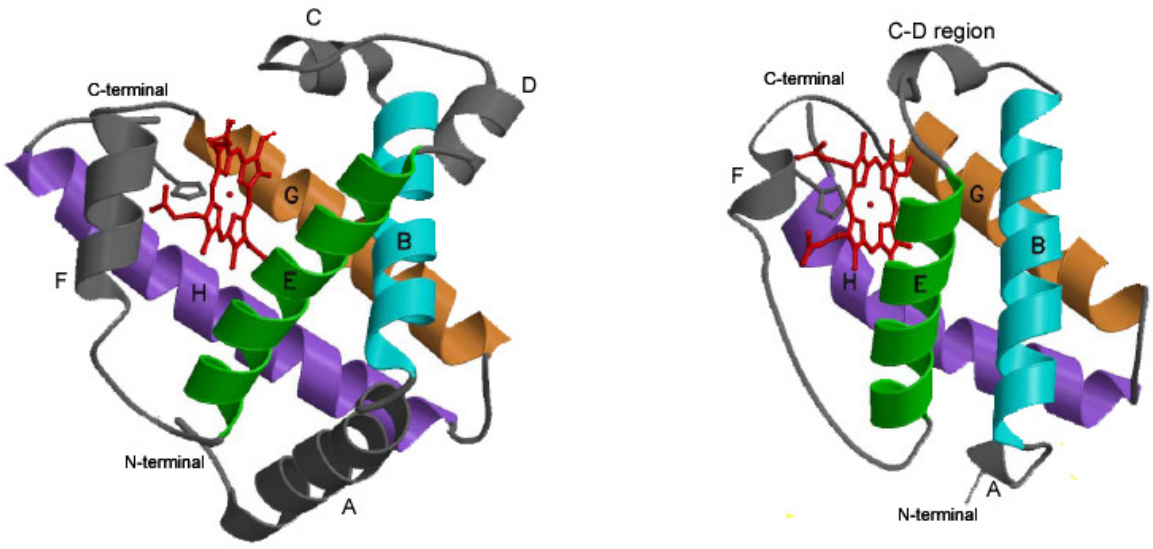

Figure 4.1 The α-helical sandwich fold in sperm whale Mb (3/3Hb, left) (pdb 1ebc) and in trHb from *P.caudatum* (2/2Hb, right) (pdb 1dlw). The figure has been taken from lecture by Prof. Bolognesi during the XII School of Pure and Applied Biophysics (*The ever changing world of (hemo)globins*, Venice 28 January - 2 February 2008).

Thereafter many genes codifying for these globins have been found, most occurring in bacterial genomes. Phylogenetic analysis based on amino acid sequences shows that this new globin family branches into three groups, designed as I, II and III (also distinguished by the N, O and P characters, respectively) (*1*). The affiliation of each group depends on the internal sequence conservation. It is noticed that the patterns of amino acid conservation in the heme pocket of each of these groups differ from that of vertebrate or invertebrate 3/3Hbs and that the sequence identity between trHbs from different groups is lower than 20% of the overall identity, while it is very high within a given group. 2/2Hbs from more than one group can coexist in the same organism, indicating a diversification of their functions.

From this picture it emerges that in the trHbs family the deviation from the 3/3 classical globin fold is only partly common to the three group. Specific structural features are

typical for each group. Among the general features, the trHbs are small hemoproteins, typically 20-40 residues shorter than mammalian Hbs. Their A-helix is drastically shorter, the D-helix is absent and an extended polypeptide segment (pre-F), followed by a short F-helix (one helix turn) is present. The reduced size of the polypeptide chain, combined with the ability to bind diatomic exogenous ligand (such as O_2 and CO) earned this protein and its relatives the name of "truncated hemoglobins".

The helices are labelled according to the conventional globin fold nomenclature, A through H, starting from the N-terminal. Moreover, the C-D region is trimmed to about three residues, linking directly the C- and E-helices. Three Gly-motifs are individuated at the AB, at the EF inter-helical corners and just before the short F-helix, they have been suggested to contribute to the stabilization of the 2/2 fold, helping in locating the short A-helix onto the B- and E-helices. Besides the bend of H-helix, this one and the G-helix match the globin fold topology. These structural features are common in groups I and II; the only relevant difference is the presence of the pre-F helix in group II, see Figure 4.2. In fact, in group II the pre-F segment region hosts 15 residues, as the result of two amino acid insertions. This modification is reflected in the presence of a novel six-residue α-helix (the Φ-helix), involved in interactions with the heme propionate (Figure 4.2 left) (*9*). The deviation of the pre-F segment relative to group I trHbs may be related to a significant shift of the whole heme group within the heme crevice of trHbO (group II trHbs).

In group III 2/2Hbs the A-helix is completely deleted, the AB hinge Gly-Gly motif is missing, thus forcing the protein residues preceding the B-helix to extend towards the GH region. An elongation of 7 amino acids is observed between the C- and E- helices. Such elongation of the CD region spans the C- and E-helices, but does not shift the position of the E-helix relative to the heme distal site (Figure 4.2 right).

In all 2/2 globins, the fold establishes a scaffold sufficient to efficiently bury the heme group, and the hydrophobic residues at topological positions provide a network of van der Waals contacts to the heme. Interactions between the heme and polar residues are known to provide further stabilization; additional salt bridges link heme propionates and positively charged residues. The unique heme-protein covalent interaction has been revealed in *Synechocystis* sp. 2/2HbN, occurring between the 2-vinyl group of the heme and an histidine residue (*10*).

A particular feature of this kind of proteins contrary to Mb of vertebrate is that, due to the shortened C-D region, the distal E-helix falls very close to the prosthetic group, thus

causing side chain crowding of the distal site residues at topological position, such as B10, CD1, E7, E11 and G8. The topological positions within the globin fold of a single protein are referred to the tertiary structure of sperm whale Mb and are shown in Figure 4.3. Some of these residues are polar, allowing the formation of a network of hydrogen bonds, functional to an efficient stabilization of the exogenous ligand, but also to the rebinding of dissociated ligands.

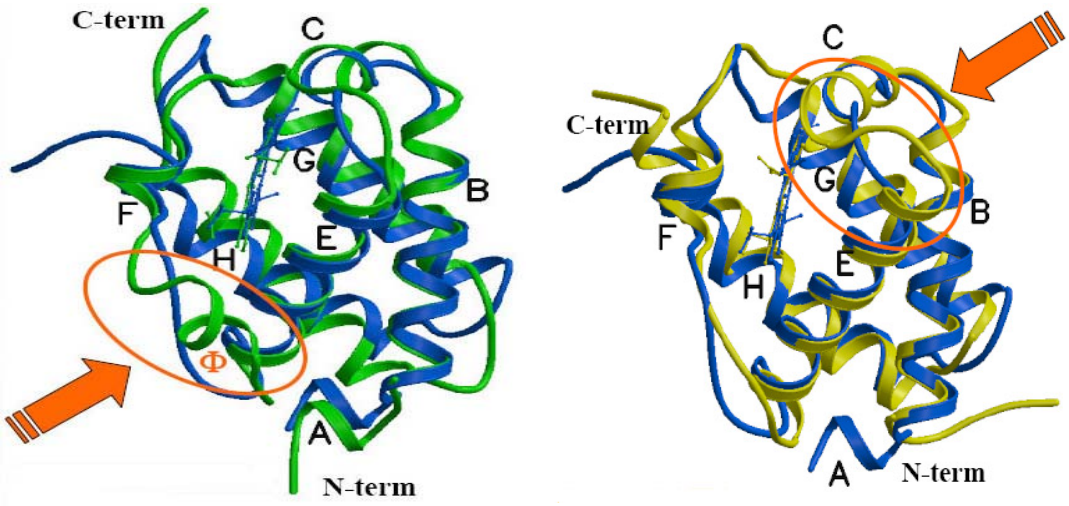

Figure 4.2 Comparative views of structural overlay between group I *Chlamydomonas eugametos* trHb (blue trace, pdb 1dly), group II *Mycobacterium tuberculosis* trHb (green trace, pdb 1ngk) and group III *Campylobacter jejuni* trHb (yellow trace, pdb 2ig3). (Figures taken from reference (*8*)).

The polarity of the distal residues is the common properties of the 2/2Hbs, but the residues involved in the building of the heme architecture switch over the three groups. In group I, for example, the hydrogen-bond network involves residues at B10, E7 and E11 topological positions. The strongly conserved tyrosine (YB10) in position B10 plays a key role in the ligand stabilization through its OH group pointing directly to the heme ligand. Normally, the complete stabilization by hydrogen-bond network is realized by a glutamine residue (Q) located at E7 or E11, or at both positions. In group II, another residue, the tryptophan (WG8) is fully conserved; it contributes to the heme-bound ligand stabilization by the hydrogen bond linking the indole nitrogen atom and the ligand. Furthermore, the presence of a tyrosine at position CD1 in some 2/2HbO proteins drastically modifies the interaction network. In particular, structure and sequence analysis suggests that the nature of residues at CD1 is correlated with the nature of the site E11, at least for the group II trHbs.

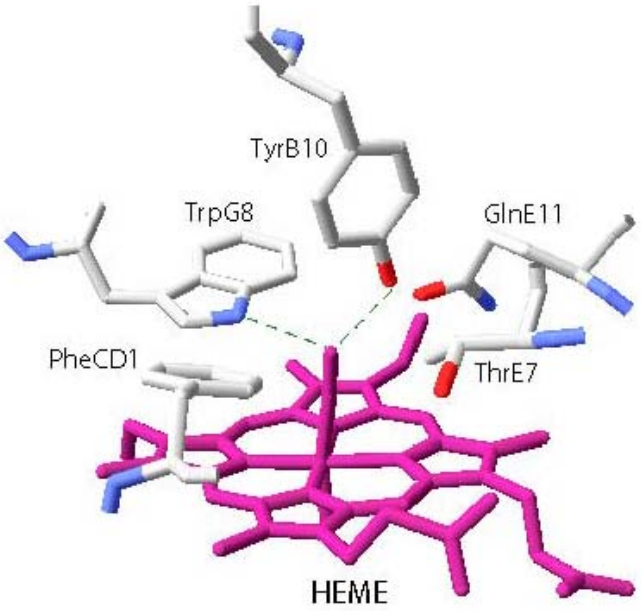

Figure 4.3 Scheme of the distal site of the CO complex of *Bacillus subtilis* 2/2HbO, in which the main residues discussed in the text and their topological positions are displayed. The green dashed lines show possible hydrogen-bonding interactions.

Table 4.1 Comparison of the topological site amino acids of selected trHbs, the first two rows refer to myoglobin from sperm whale and flavohemoglobin from E.coli, respectively. The trHbs are indicated by the name of the organism in which they occur. In bold type, the proteins studied in this thesis are highlighted. The Protein Data Bank (PDB) codes are also reported.

Group	Organism	B10	CD1	E7	E11	F8	G8	pdb	Ref.
	SW Mb	L	F	H	V	H	I	1ebc	(*11*)
	Escherichia coli/HMP	Y	F	G	L	H	V	1gvh	(*12*)
	Paramecium caudatum	Y	F	Q	T	H	V	1dlw	(*6*)
	Chlamydomonas eugametos	Y	F	Q	Q	H	V	1dly	(*6*)
I	Synechocystis sp.	Y	F	Q	Q	H	V	1mwb	(*13*)
	Mycobacterium tuberculosis N	Y	F	L	Q	H	V	1idr	(*14*)
	Mycobacterium tuberculosis O	Y	Y	A	L	H	W	1ngk	(*9*)
II	Bacillus subtilis	Y	F	T	Q	H	W	1ux8	(*15*)
	Thermobifida fusca	Y	Y	A	L	H	W	2bmm	(*16*)
III	Campylobacter jejuni	Y	F	H	I	H	W	2ig3	(*17*)

L = leucine; F = phenylalanine; H = histidine; V = valine; I = isoleucine; Y= tyrosine; Q = glutamine; T = threonine; A = alanine; W = tryptophan

When the protein has a Y at CD1, a non polar residue is found at E11 position; conversely, when a non-hydrogen bond donor replaces the YCD1, a hydrogen bond donor is present in E11. YB10 and WG8 are invariant residues also in group III 2/2HbPs and are directly hydrogen bonded to the ligand. Contrary to group II, the group III truncated proteins display an invariantly F residue in CD1 position and a hydrophobic residue at position E11.

All the consideration reported in this paragraph are discussed in the critical review by Pesce et al. (*18*) and references inside. In table 4.1, the occupancy of the topological sites in different trHbs is summarized and compared with the sperm whale Mb and with the flavohemoglobin from E.coli.

4.2 *Thermobifida fusca*: a novel thermostable hemoglobin

The identification of "hemoglobin-like" proteins in *Thermobifida fusca* thermophilic actinobacterium was reported in 2005 by Boffi and coworkers (*16*). The presence of hemoglobins in thermophilic micro-organism brings out fundamental questions concerning the structural parameters that lead to thermostability of these proteins. Four genes within the genome of the bacterium *Thermobifida fusca* have been identified for as many proteins: a protoglobin (Tf-Pgb), a truncated hemoglobin (Tf-trHb), a flavohemoglobin (Tf-FHb) and an additional globin-like protein. The biochemical functionality and the physiological significance of these most intriguing hemoproteins are still unknown. The crystal structure of the Fe^{3+}, acetate-bound derivative was obtained at 2.48 Å resolution (*16*). Its three dimensional structure is reported in Figure 3.4 (pdb code: 2BMM): it consists of a 2/2 α-helical structure belonging to group II truncated hemoglobins.

The distal heme pocket architecture (Figure 4.5) shows that the acetate ion ligand is stabilized by interactions with residues YCD1(67) and WG8(119). The carbonyl oxygen of the acetate ion is hydrogen-bonded to the -OH group of YCD1 and to the indole group of WG8 (distances = 2.86 and 2.52 Å, respectively). WG8 is rigorously conserved in the three hemoglobins showed in Figure 4.5, i.e., Tf-trHb, from *Mycobacterium tuberculosis* (Mt-trHbO) and Bacillus subtilis (Bs-trHb), all classified as group II trHbs. In Tf-trHb the W119 (G8) is essentially parallel to the heme plane. In

addition the Y54 is present at position B10. In the proximal region the H106 (F8) is bonded to the Fe^{3+} of the heme with an unusually short distance (N-Fe = 1.92 Å).

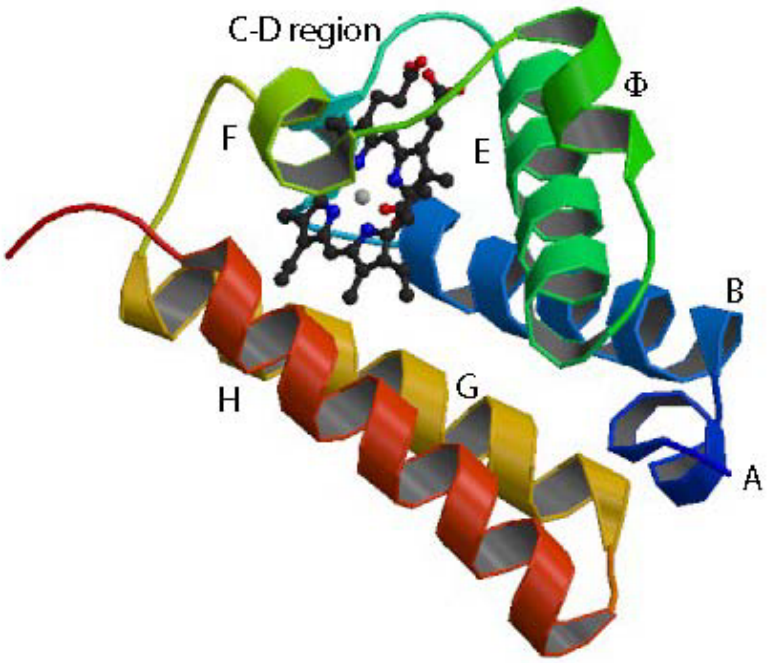

Figure 4.4 Three-dimensional structure of Tf-trHb. It displays a 2/2 α-helical sandwich fold formed by the helices B, E, G and H; shorter F and A helices than in the classic globin fold; absence of helices C and D; presence of an additional phi-helix between helices E and F.

We performed UV-Vis and RR experiments on wild-type (WT) and an acidic surface variant (ASV) of the Tf-trHb, which was designed with the aim of creating a versatile globin scaffold endowed with thermostability and high recombinant expression level in soluble form. This engineered protein was obtained by mutating the surface-exposed residues F107 and R91 to E. Furthermore, the ASV was used in a combinatorial mutagenesis of the distal heme pocket residues in which one, two or three of the conserved polar residues: YB10(54), YCD1(67), WG8(119) were substituted by F.

In this chapter the spectroscopic characterization of the Fe^{3+} WT and its variants, in the presence and in the absence of exogenous ligands such as fluoride, sulfide and hydroxide, at 298 and 15 K, will be presented. The study of single, double, and triple F mutants at positions G8, B10 and CD1 allowed us to highlight the role of the distal residue(s) for ligand stabilization.

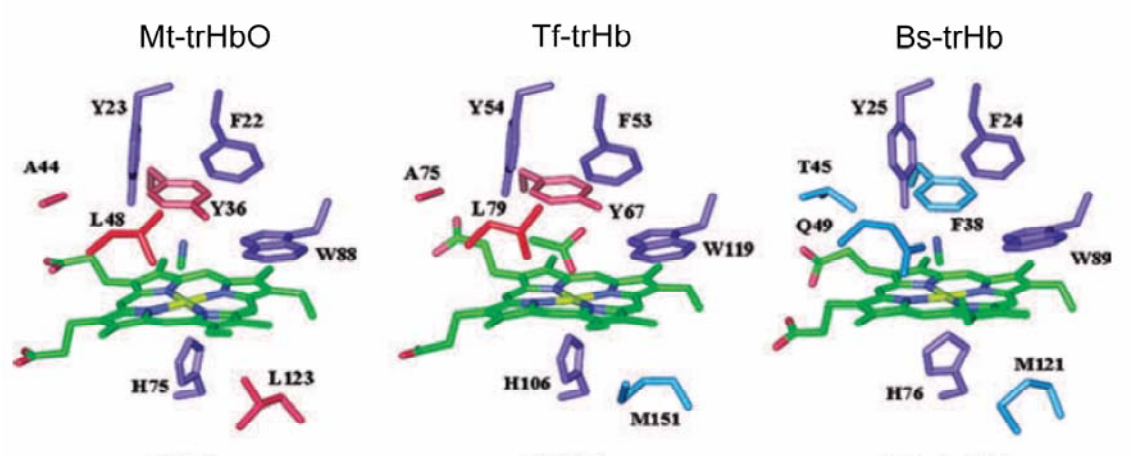

Figure 4.5 close-up view of the active sites of Tf-trHb (in the center, pdb code: 2BMM), Mt-trHbO (on left, pdb code: 1NGK) and Bs-trHb (on right, pdb code: 1UX8). Residues that are conserved in all three structures are marked in violet, Tf-trHb residues conserved with respect to Mt-trHbO and Bs-trHb are red and cyan, respectively (from (*16*)).

4.3 The ferric state

4.3.1 Results

Figure 4.6 shows the UV-Vis (left) and RR spectra (right) of the WT, ASV and selected variants of WG8, YCD1 and YB10 in the Fe^{3+} state at pH 7.

i) WT and ASV

The UV-Vis spectrum of WT Tf-trHb shows the maximum of the Soret at 408 nm, and bands at 493, 540, 577, 609 and 630 nm in the visible region. The corresponding RR spectrum indicates the presence of a 6cHS (ν_3 at 1480 cm^{-1}, ν_2 at 1563 cm^{-1} and ν_{10} at 1503 cm^{-1}), a 5cHS (ν_3 at 1492 cm^{-1}) and a 6cLS (ν_3 at 1503 cm^{-1}, ν_2 at 1580 cm^{-1} and ν_{10} at 1638 cm^{-1}) species. Thus, the WT Tf-trHb at pH 7 is an equilibrium of three different species: i) the 5cHS corresponds to a form with no ligand in the six axial coordination position of the heme iron; ii) the 6cHS species is characterized by a water molecule in the sixth coordination position (CT1 band at 630 nm, β band at 493 nm); iii) the 6cLS species corresponds to a form containing an $-OH^-$ into sixth coordination position. Furthermore, the UV-Vis spectrum suggests the presence of an equilibrium between a 6cHS and 6cLS species, since together with the β and α bands at 540 and 577 nm, respectively a band at 609 nm is present, due to the CT1 band of a hydroxo-6cHS (*19*).

The UV-Vis spectrum of the ASV sample shows a 2 nm blue-shift of the Soret band indicating an increase of the HS species respect to the LS species. Accordingly the RR spectrum confirms a slight increase of the 5cHS species while the 6cHS remains essentially unchanged.

ii) Singly mutated variants

Upon mutation of **WG8 to F**, the Soret band is observed at 404 nm, the β and the α bands of the HS species are at 498 and 533 nm, respectively, and the CT1 of the aquo-6cHS species is at 630 nm. Interestingly, the α band of the 6cLS species is 5 nm blue-shifted compared to the WT and ASV, suggesting the presence of a different ligand coordinated in the sixth axial position. The corresponding RR spectrum clearly indicates the disappearance of the 5cHS species, and the presence of a 6cHS species (ν_3 at 1483 cm^{-1}) and 6cLS (ν_3 at 1504 cm^{-1}).

YB10F and YCD1F show very similar UV-Vis (except for 1 nm shift of the Soret and CT1 bands) and RR spectra. The Soret bands are centred at 407-408 nm, the β band of the 6cHS aquo species is at 493 nm, the β and the α bands of the $–OH^-$ species are at 541 and 578 nm, the CT1 bands are at 608-609 and 630 nm for the $–OH^-$ and aquo species, respectively, similar to the maxima observed in the WT and ASV samples. The RR spectra indicate an equilibrium of a 6cHS (ν_3 at 1480 cm^{-1}) and 6cLS (ν_3 1503-1504 cm^{-1}), with a smaller amount of 5cHS (ν_3 at 1492 cm^{-1}), as compared to WT and ASV. Therefore, mutation of the tyrosines with F does not appear to markedly affect the coordination and spin states as compared to WT and ASV

iii) Doubly mutated variants

YB10F/WG8F and YCD1F/WG8F variants present similar spectroscopic features. The Soret band is observed at 404 nm, the β and α bands at 498-502 nm and 531 nm, respectively, CT1 bands at 628 nm (YB10F/WG8F) and 632 nm (YCD1F/WG8F). The RR spectra are a mixture of a 6cHS (ν_3 at 1482 cm^{-1}) and 6cLS (ν_3 at 1505 cm^{-1}) species. The 5cHS is not observed.

The **YB10F/YCD1F** variant, in which both distal Tyr residues are missing, is the sample containing the higher amount of 5cHS (ν_3 at 1492 cm^{-1}) with respect to the WT and the other variants. Thus, the Soret band is blue-shifted (404 nm) and the β and α bands of the HS species are at 502 and 534 nm, respectively. The CT1 band at 632 nm is indicative of the presence of a 6cHS aquo species.

Accordingly the RR spectra are characteristic of an equilibrium between a 6cHS (ν_3 at 1482 cm^{-1}) and 5cHS (ν_3 at 1492 cm^{-1}).

iv) Triply mutated variant. The 6cHS aquo form is the predominant species as indicated by the CT1 band at 632 nm and the ν_3 at 1486 cm^{-1}. Nevertheless, since the ν_3 bandwidth is 7 cm^{-1} broader respect to the WG8F ν_3 band, the presence of a certain amount of 5cHS can not be ruled out.

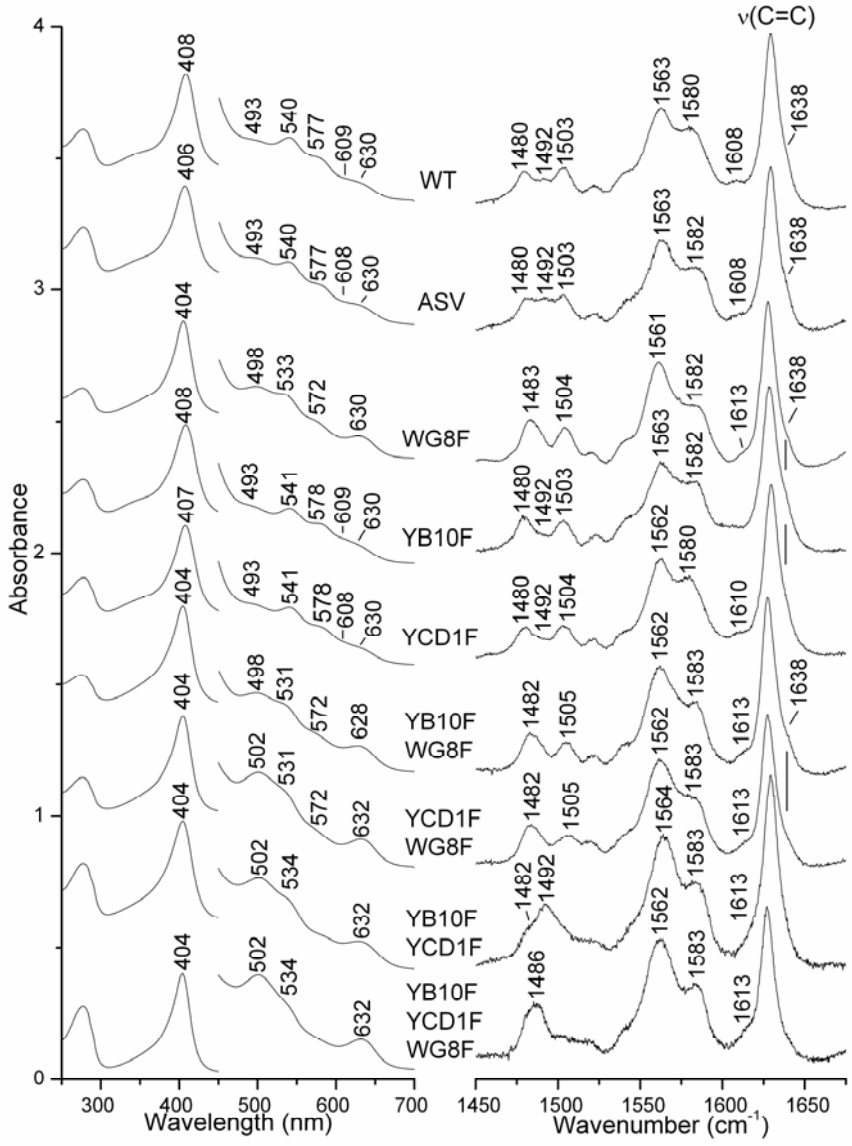

Figure 4.6 UV-Vis (left) and RR (right) spectra of Fe^{3+} WT, ASV, and distal variants of Tf-trHb, at pH 7, in 0.1 M phosphate buffer. UV-Vis: scan time of 600 nm/min, 10-15 μM sample concentration. RR: 413.1 nm excitation wavelength, 1.2 cm^{-1} spectral resolution, 10 mW laser power at the sample, 30-35 μM sample concentration, average of three spectra with 246 s integration time (WT), average of two spectra with 900 s integration time (ASV), average of six spectra with 540 s integration time (WG8F), average of six spectra with 330 s integration time (YCD1F), average of five spectra with 360 s integration time (YB10F), average of six spectra with 540 s integration time (YB10F/WG8F), average of six spectra with 540 s integration time (YCD1F/WG8F), average of six spectra with 300 s integration time (YB10F/YCD1F), and average of five spectra with 420 s integration time (YB10F/YCD1F/WG8F). The region between 450-700 nm was expanded by ten fold. Spectra have been shifted along the ordinate

axis to allow better visualization. The position of the CT1 band due to the hydroxo-6cHS form has been assigned on the basis of the second derivative of the absorption spectra (data not shown).

The other core size RR modes are assigned as followed: 6cHS (ν_2 at 1561-1564 cm^{-1}, ν_{10} at 1608-1613 cm^{-1}); 6cLS (ν_2 at 1580-1583 cm^{-1}, ν_{10} at 1638 cm^{-1}). The two $\nu_{(C=C)}$ stretching modes merge into a single band ranging between 1627 and 1629 cm^{-1}.

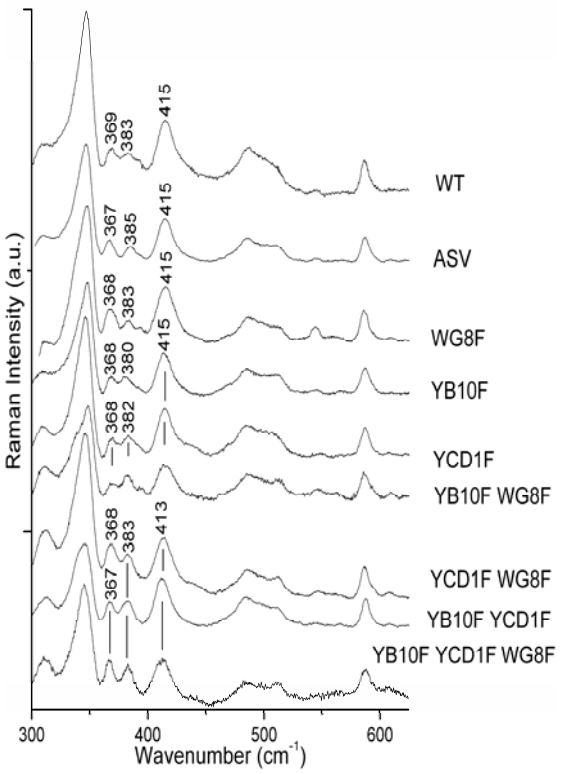

Figure 4.7 RR spectra in the low frequency region of Fe^{3+} WT, ASV, and distal variants of Tf-trHb, at pH 7, in 0.1 M phosphate buffer. RR: 413.1 nm excitation wavelength, 1.2 cm^{-1} spectral resolution, 10 mW laser power at the sample, 30-35 μM sample concentration, average of six spectra with 900 s integration time (WT), average of four spectra with 750 s integration time (ASV), average of ten spectra with 740 s integration time (WG8F), average of eight spectra with 700 s integration time (YCD1F), average of six spectra with 660 s integration time (YB10F), average of eight spectra with 740 s integration time (YB10F/WG8F), average of nine spectra with 740 s integration time (YCD1F/WG8F), average of eight spectra with 500 s integration time (YB10F/YCD1F), and average of five spectra with 420 s integration time (YB10F/YCD1F/WG8F). Spectra have been shifted along the ordinate axis to allow better visualization.

The RR spectra in the low frequency region are reported in Figure 4.7. The band at 413-415 cm^{-1} was assigned to the bending vibration of the vinyl groups [δ(CβCaCb)] and the two bands at 367-369 and 380-383 cm^{-1} are tentatively assigned to heme propionyl bending vibrations [δ(CβCcCd)] (*20*). The different frequencies of the two propionyl bending modes suggest that while one propionyl has a weaker H-bonding interaction (367-369 cm^{-1}), the other experiences a stronger H-bonding network (380-383 cm^{-1}). In fact, the frequencies of these modes have been proposed to shift to higher frequencies as

a result of hydrogen bonding between the propionyl groups of the heme and nearby amino acid side chains, although there is not a fixed relationship between a given frequency and the number of hydrogen bonds (*21, 22*). Inspection of the crystal structures of Tf-trHb (*16*) provides a rationale for the observed frequencies. In particular, while the 7-propionyl group interacts with a water molecule at 2.7 Å, the 6-propionyl group is involved in a wider hydrogen bonding network (R105, R97, and Y93 at 3.2, 2.9, and 2.7 Å, respectively). Thus, the modes at 380-383 cm^{-1} can be assigned to the bending vibrations of the heme substituent at position 6.

4.3.2 Discussion

The WT Tf-trHb in the Fe^{3+} state at pH 7 is a mixture of three forms, 5cHS, 6cHS, 6cLS species.

i) The 5cHS becomes predominat in the YB10F/YCD1F variant, suggesting that the water molecule coordination is prevented by the presence of a strong H-bonding interaction with the WG8. A similar result was previously observed in cytochrome c peroxidase (CCP), since the presence of the W51 in the WT protein favours the 5cHS species in the Fe^{3+} form. In the W51F mutant, the loss of the H-bond allows the water molecule to coordinate to the heme iron giving rise to a 6cHS species *(23)*. This results may derive from a slight structural rearrangement of the TrpG8, due to the lack of both distal tyrosines, favouring the H-bond with the distal water molecule. Accordingly, the slight higher amount of 5cHS in ASV with respect to WT might be due to a different orientation of the tyrosines, that prevents the ligand stabilization in the sixth axial position of the heme iron.

ii) the coordination of a water molecule in the sixth axial position gives rise to a 6cHS species. The presence of a water molecule coordinated to the Fe^{3+} in trHb of group II has been previously observed in trHbs from *Herbaspirillum seropedicae* (*24*) and *Pseudoalteromonas haloplanktis TAC125* (*25*) as well as in Mb (*26*).

The coordination of the water is conserved in all variants, although in different amounts. Since the YB10F/YCD1F/WG8F retains the 6cHS aquo species, we suggest that the water molecule does not require of a stabilization by the distal residues;

iii) the other ligand present in the sixth axial position is the $–OH^-$, which exists as an equilibrium between a 6cHS and a 6cLS forms, similarly to Mb at alkaline pH (*19*). The coordination of the hydroxide is maintained in the ASV, YB10F and YCD1F variant.

These results indicate that the TrpG8 and at least one Tyr (as tyrosinate form) are the key residues for the binding of this anionic ligand and cooperate for its stabilization.
Interestingly, in the WG8F, YB10F/WG8F and YCD1F/WG8F mutants, together with the 6cHS aquo species, a 6cLS form is also present with a maximum at 572 nm versus 577 nm of WT. Accordingly the second derivatives of WG8F, YB10F/WG8F and YCD1F/WG8F absorption spectra reveal the band at 572 nm broader and 7 nm blue-shifted respect to that of WT, ASV, YB10F and YCD1F variant. A band at 572 nm is reminiscent of the α band (570 nm) present in the Fe^{3+} trHb from *Pseudoalteromonas haloplanktis TAC125* at pH 7.6 corresponding to the ligation of a tyrosinate (either YCD1 or YB10 tyrosinate residues) to the heme iron (*25*). Therefore, it cannot be rule out that the small amount of the 6cLS present in these three variant of Tf-trHb could arise from the readjustement with the subsequent coordination to the heme iron, of one of the two Tyr when WG8 is absent in the cavity. These results indicate that between these three distal residues exist a mutual influence, and that the two Y are flexible residues. Nevertheless, an excitation profile in order to confirm the coordination of a tyrosine in these variant is necessary. In fact, a Y coordinated to a heme iron can often be identified by RR experiments, since the excitation in the tyrosinate-(Fe^{3+}) CT band (near 500 nm) yields characteristic vibrational frequencies of the bound phenolate (*27*). The most prominent of these polarized modes are $\nu(C=C)_{ring}$ at ca. 1600 and ca. 1500 cm^{-1}, ν(C-O) at ca. 1300 cm^{-1} and ν(Fe-O) at ca. 590 cm^{-1} (*28-33*).

4.4 The ferrous state

The reduction of the (Fe^{3+}) heme to the ferrous state in WT, ASV and distal mutants of Tf-trHb brings to analogous results: the formation of a 5cHS species as revealed by the UV-Vis absorption maxima at 428-431 and 558 nm. Consistently, the RR spectra in high frequency region are typical of 5cHS form (ν_3 at 1470 cm^{-1}, ν_{38} at 1524 cm^{-1}, ν_{11} at 1547 cm^{-1}, ν_2 at 1560 cm^{-1}, ν_{37} at 1580 cm^{-1}, ν_{10} at 1605 cm^{-1}).
Interestingly in the low frequency region, a band at 323 cm^{-1} (γ_6) is present and it is assigned to an out-of-plane mode. This mode lacks in enhancement in D_{4h} symmetry but becomes active if the porphyrin undergoes an out-of-plane distortion (*34*). The activation of out-of-plane modes was previously observed in Mycobacterium trHbO, a truncated haemoglobin belonging to the same class of Tf-trHb, but is not observed for

class I Mycobacterium trHbN. This kind of distortion is possibly a consequence of the strain induced on the relatively rigid heme tetrapyrrole ring by the interaction with the protein matrix.

In 5cHS Fe^{2+} heme with an His residues coordinated in the fifth axial position, it appears in the region between 200-250 cm^{-1} a mode assignable to the $\nu_{(Fe-His)}$ stretching (Chapeter 1). In WT and in mutated Tf-trHb the $\nu_{(Fe-His)}$ is at 223 cm^{-1}, intermediate between those of sperm whale Mb (220 cm^{-1}) (*35*) and Mycobacterium trHbO (226 cm^{-1}) (*36*). Similarly to the latter protein, the relatively short Fe-His bond (1.9 Å) can be ascribed to the staggered orientation of the imidazole plane of the proximal His with respect to the heme nitrogen atoms, in contrast to the eclipsed orientation in Mb and human adult Hb (*37*). The higher frequency of the Fe-His stretching modes, thus, could in part be a consequence of the reduction of the repulsive interactions between heme and the proximal His, which would allow a stronger Fe coordination.

In conclusion, the RR spectra of the Tf-trHb Fe^{2+} forms are typical of trHbs class II. Mutations at the distal side of the cavity do not influence the heme distortion nor the strength of the proximal His-Fe coordination bond, suggesting that the distal and the proximal sides are not coupled for these proteins, as it occurs, for example, in peroxidases (*38*).

4.5 The ferric state in presence of fluoride

4.5.1 Results

Figure 4.8 compares the UV-Vis spectra of the fluoride adducts of the WT Tf-trHbO and its distal mutants in the visible region. The addition of fluoride to WT Tf-trHbO resulted in an absorption spectrum typical of a 6cHS heme, with Soret band at 405 nm and CT1 at 613 nm. Some differences are observed in the wavelength of the absorption maxima of the spectra of the mutants. In particular, while the Soret maximum is found at 405-407 nm, the wavelength of the CT1 band markedly changes, ranging between 614 and 603 nm.

The UV-Vis spectrum of the ASV sample clearly shows a blue-shift of the CT1 band by 3 nm. The same change has been observed for the single YCD1F and for the double YB10F/YCD1F mutants. Similar results have also been observed for the single WG8F mutant (CT1 at 609 nm), while a further blue-shift of the CT1 band has been observed by the double YCD1F/WG8F (606 nm) and the triple YB10F/WG8F/YCD1F (603 nm) mutants. Interestingly, two variants show a red-shifted CT1 band, namely the YB10F (614 nm) and YB10F/WG8F (611 nm).

It must be noted that the spectrum of the triple YB10F/WG8F/YCD1F (603 nm) mutant clearly shows the presence of unligated protein, being the CT1 very broad due to the presence of a shoulder at 632 nm, due to the CT1 band of the Fe^{3+} aquo 6cHS heme (Figure 4.6), indicating that the absence of any polar distal residue marked decrease the affinity for the ligand.

The high frequency region RR spectra of all the fluoride adducts (Figure 4.9) are typical of a 6cHS heme with ν_3 at 1478 cm^{-1} ν_2 at 1561 cm^{-1}, ν_{10} at 1607-1608 cm^{-1}. The two $\nu_{(C=C)}$ stretching modes merge into a single band ranging between 1626 and 1628 cm^{-1} (Figure 4.9). According to the UV-Vis spectrum, the triple mutant is not fully bound, being clearly observed a shoulder at 1486 cm^{-1} due to ν_3 of the 6cHS aquo Fe^{3+} protein (Figure 4.6).

Usually, the $\nu_{(Fe-F)}$ stretching mode is strongly enhanced upon excitation in the CT1 band in the low frequency region between 380 and 470 cm^{-1} (*39-41*). However, the Fe-F stretch of the Mb-F adduct has been also observed upon excitation in the Soret region

(*42*). Therefore, we attempted to find the $\nu_{(Fe-F)}$ stretching mode of the fluoride complexes using Soret excitation which is available to us.

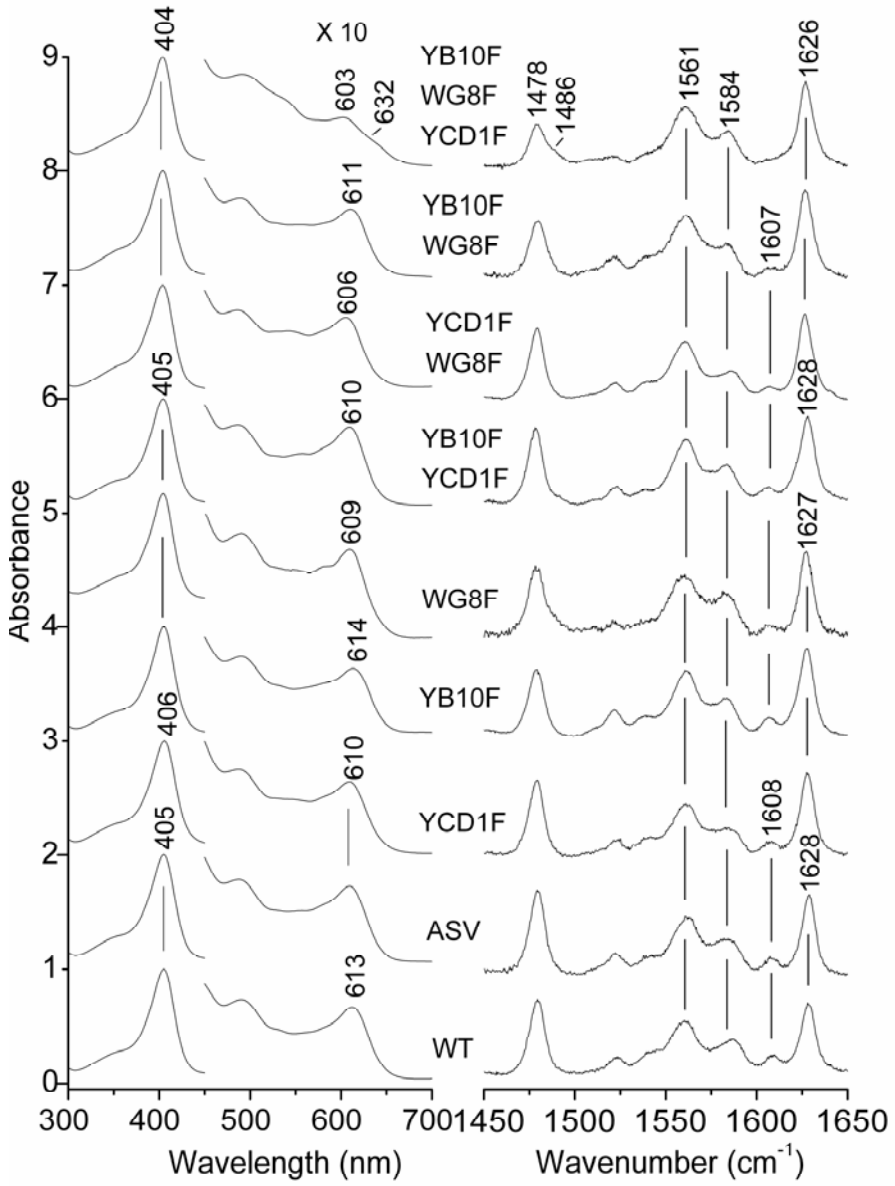

Figure 4.8 WT, ASV, and mutated Fe^{3+} Tf-trHb, at pH 7 in 0.1 M phosphate buffer, in presence of 0.5 M fluoride. Left: UV-Vis spectra, scan time of 600 nm/min, 10-15 μM sample concentration.
Right: RR spectra in the high frequency region. 406.7 nm excitation wavelength, 1.3 cm^{-1} spectral resolution, 10 mW laser power at the sample, 30-35 μM sample concentration, average of three spectra with 246 s integration time (WT), average of two spectra with 900 s integration time (ASV), average of six spectra with 540 s integration time (WG8F), average of six spectra with 330 s integration time (YCD1F), average of five spectra with 360 s integration time (YB10F), average of six spectra with 540 s integration time (YB10F/WG8F), average of six spectra with 540 s integration time (YCD1F/WG8F), average of six spectra with 300 s integration time (YB10F/YCD1F), and average of five spectra with 420 s integration time (YB10F/YCD1F/WG8F). Spectra have been shifted along the ordinate axis to allow better visualization.

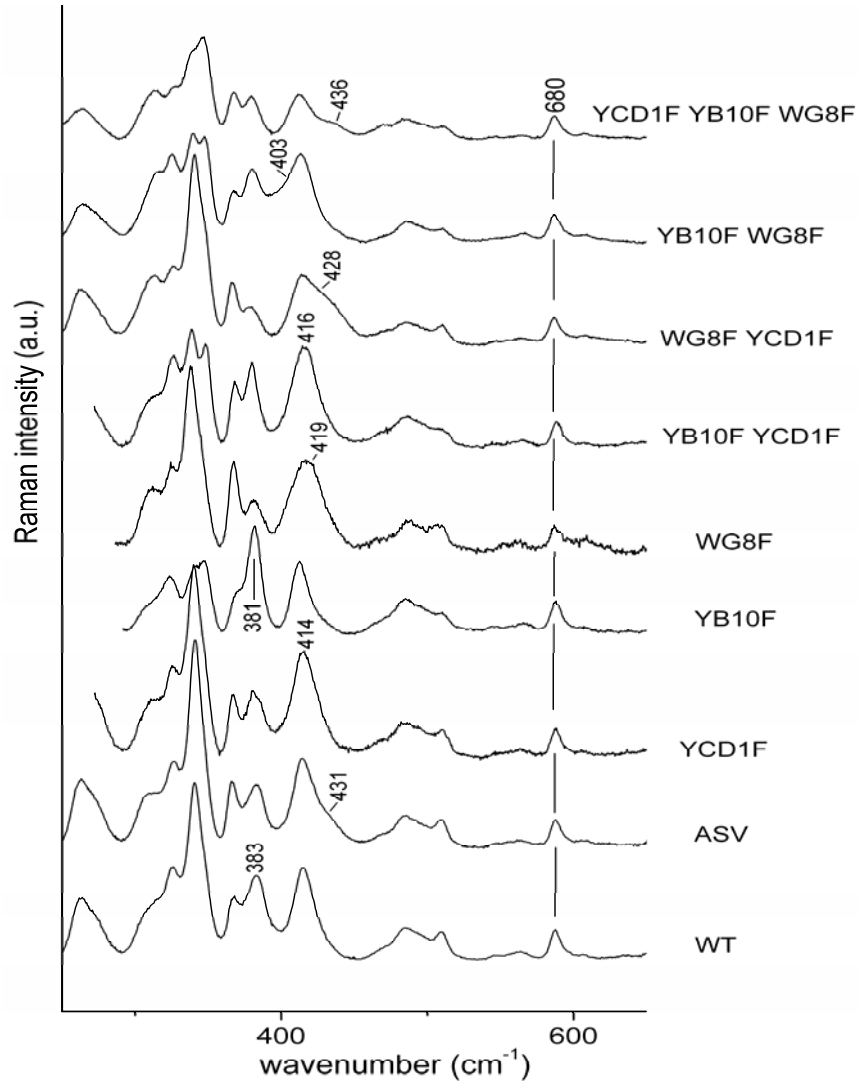

Figure 4.9 RR spectra in the low frequency region of WT, ASV, and mutated Fe^{3+} Tf-trHb, at pH 7 in 0.1 M phosphate buffer, in presence of 0.5 M of fluoride solution. 406.7 nm excitation wavelength, 1.3 cm^{-1} spectral resolution, 10 mW laser power at the sample, 30-35 μM sample concentration, average of eight spectra with 700 s integration time (WT), average of five spectra with 900 s integration time (ASV), average of six spectra with 900 s integration time (WG8F), average of six spectra with 700 s integration time (YCD1F), average of eight spectra with 660 s integration time (YB10F), average of ten spectra with 700 s integration time (YB10F/WG8F), average of nine spectra with 900 s integration time (YCD1F/WG8F), average of eight spectra with 600 s integration time (YB10F/YCD1F), and average of seven spectra with 1000 s integration time (YB10F/YCD1F/WG8F). Spectra have been shifted along the ordinate axis to allow better visualization.

Figure 4.9 shows the RR spectra in the low frequency region obtained for WT Tf-trHbO, ASV and its distal mutants upon Soret excitation. Visual inspection of the spectra clearly indicate marked changes in the 440-380 cm^{-1} region, where the $\nu_{(Fe-F)}$ stretch is expected. In particular, a strong band is observed in the WT protein and in the YB10F mutant at 383 and 381 cm^{-1}, respectively, overlapping with one the propionyl bending mode which, in the free Fe^{3+} protein, gives rise to a weak band at 380-383 cm^{-1} (Figure 4.7). In all the other proteins a new band is observed at higher wavenumbers, at

about 403 (YB10F/WG8F), 414 (YCD1F), 416 (YB10F/YCD1F), 419 (WG8F), 428 (WG8F/YCD1F), 431 (ASV) and 436 cm^{-1} (YB10F/ WG8F/YCD1F).

Table 4.2 Soret, CT1, $\nu_{(C=C)}$, $\nu_{(Fe-F)}$ of WT and mutated Fe^{3+} Tf-trHb, together with Mb, HRP and CCP are reported. The residues involved in the fluoride H-bonding are indicated.

Proteins	**Soret**	**CT1**	$\nu_{(C=C)}$	$\nu_{(Fe-F)}$	**H-bonds with Fluoride**		
	nm	**nm**	cm^{-1}	cm^{-1}			
WT Tf-trHbO	405	613	1629	383		WG8	YCD1
ASV	405	610	1629	≈ 431		WG8	
YCD1F	406	610	1628	≈ 414		WG8	
YB10F/YCD1F	405	610	1628	≈ 416		WG8	
WG8F		609	1627	≈ 419			YCD1
YB10F/WG8F	404	611	1627	≈ 403			YCD1
YB10F	405	614	1627	381		WG8	YCD1
WG8F/YCD1F	404	606	1626	≈ 428			YB10
YB10F/ WG8F /YCD1F	404	603	1627	≈ 436			
CCP(MI) [43]	406	617	1619, 1632		H_2O	W51	R48
W51F CCP(MI) [43]	406	613	1619, 1632		H_2O		R48
HRP [43]	404	611	1621, 1631	385 [44]	H_2O		R38
Mb, pH 6.9 [39]	406 [39]	607 [39]	1622 [46]	461 [39, 42, 45]			
Mb, pH 5.2 [39]		609 [39]		399 [39]		H64 [39, 47]	
Mb, pH 7,0 [39, 45]			1622	422 [39, 45]	H_2O [45]		

Table 4.2 reports a summary of the absorption maxima wavelengths of the Soret and CT1 transitions together with the RR frequencies of the $\nu_{(C=C)}$ and the $\nu_{(Fe-F)}$ stretching modes for the fluoride complexes of WT Tf-trHbO, ASV and its distal mutants compared with selected heme containing peroxidases and Mb. The last column indicates the suggested distal residues hydrogen-bonded to the fluoride ligand.

4.5.2 Discussion

The electronic coupling between the vinyl groups and the porphyrin modulates the energy of the $\pi\rightarrow\pi$ transitions. The vinyl substituents give rise to polarized bands in the 1618-1635 cm^{-1} region. A low frequency is expected to correspond to a higher degree of conjugation between the vinyl group and the porphyrin π system (*48*). Increased conjugation from the vinyl groups should shift the energy of the $\pi\rightarrow\pi$ transitions to lower energy, thus shifting the Soret maximum to the red.

From the RR (Figure 4.9) spectra and Table 4.2, it can be seen that all the fluoride adducts of *Thermobifida fusca* are characterized by an intense single vinyl stretch around 1626-1628 cm^{-1}, Soret maxima between 405 and 407 nm, and CT1 bands between 603 and 614 nm. Conjugation of the vinyl groups with the heme appears to be comparable for these proteins, and the absorption maxima of the proteins are, as a consequence, comparable. Therefore, the 11 nm variability of the CT1 bands observed for the different fluoride adducts, indicates that its transition energy is influenced by an effect other than conjugation. The wavelength of CT1 band [$a'_{2u}(\pi)\rightarrow e_g(d\pi)$] is, in fact, a sensitive probe of axial ligand polarity and of its interaction with the distal amino acids (Chapter 1). In fact, it blue-shifts when the p and/or π donor capability of the axial ligands increases or when the ligand acts as a H-bond donor since the interaction between the p orbitals of the ligand and the iron d_π orbitals raises the energy of the latter (*49-51*). In particular, when the ligand acts as a hydrogen bond donor, the stronger the H-bond and charge donation to the iron atom, the lower is the CT1 wavelength. The opposite effect is observed when the ligand acts as an H-bond acceptor (*43*). This trend has been illustrated by the effect of distal mutations on the CT1 of the fluoride adduct of WT cytochrome c peroxidase (CCP-F). Its CT1, observed at 617 nm, results from H-bonds donated to the fluoride by R48, W51, and a water molecule. A blue-shift of CT1 is observed in the mutant W51F where the replacement of the distal W by a non-hydrogen-bonding F residue reduces the number of hydrogen bonds involving the ligand with the protein matrix from three to two (Table 4.2).

In addition to the UV-Vis spectra, the RR frequency of the $\nu_{(Fe-F)}$ stretching mode in the low-frequency region would provide direct evidence for hydrogen bonding of the fluoride ligand to distal residues. For the fluoride complex of met-Mb, at neutral pH, two bands at about 460-420 cm^{-1} have been assigned to the Fe-F stretch to a non H-bonded form and to a form whose anion, stabilized by H bond with H_2O (*39, 42, 45*), respectively. In particular, based on the X-ray crystal structure (*47*) the band at 420 cm^{-1}

has been assigned to a hydrogen-bonded form to the distal HisE7 and to a water molecule (*43*). The band at 460 cm^{-1} is pH sensitive, as it shifts down by about 60 cm^{-1} upon acidification. This result was interpreted as being due to protonation of the distal His, that directly forms a hydrogen bond to the fluoride ligand (*39*).

Based on the previous findings, we propose that in the WT protein the fluoride is stabilized by two H-bonds which are suggested to be donated by WG8 and YCD1. Accordingly, mutation of the YB10 do not alter significantly the maximum of the CT1 band. This hypothesis is supported by the RR $\nu_{(Fe-F)}$ frequency, observed at 383 and 381 cm^{-1} for the WT and YB10F mutant, respectively. Interestingly this frequency is reminiscent of that found for HRP at 385 cm^{-1} and explained as due to the presence of strong hydrogen bonding between the distal residues (*43, 44*).

Intriguingly, the CT1 band of the ASV protein is found at 610 nm, and a new band at about 431 cm^{-1} is observed in the RR spectrum. These data suggest a weakening of the H-bond interaction. Based on the previous findings, indicating that the YCD1 residue is very flexible (*52*), we suggest that in the ASV protein only a H-bond interaction (probably with the WG8) is present. Accordingly, the CT1 band at 610-611 nm found for the single mutant YCD1F, and the double mutants YB10F/YCD1F and YB10F/WG8F is consistent with the presence of a single H-bond interaction with the WG8 in the first two proteins and by the solely YCD1 in the latter. The 1 nm up-shift together with a frequency at about 403 cm^{-1} found for the YB10F/WG8F, suggest that due to the absence of the side chain interactions of YB10, YCD1 can interact stronger with the ligand as observed in the CO adduct (see below).

On the other hand, YB10 appears to be able to weakly interact only in the absence of the other two polar residues, being the CT1 at 606 nm and the $\nu_{(Fe-F)}$ at 428 cm^{-1} in the double variant YCD1F/WG8F. Finally in the absence of all the polar residues the proteins is not fully bound to the fluoride and both the CT1 (603 nm) and the $\nu_{(Fe-F)}$ (~ 436 cm^{-1}) are consistent with a weak interaction.

4.6 The ferric state at alkaline pH

4.6.1 pH titrations

Figures 4.10-4.11-4.12 show the pH titration of the WT, ASV and distal variants of Tf-trHb. The values underlined in the inset indicate the pH in which the alkaline transition is completed. No further variations are observed at higher pH.

In WT, ASV, YB10F, YCD1F, YB10F/YCD1F (Figure 4.10 and 4.11), isosbestic points are observed. Generally, the presence of at least one isosbestic point means a direct thermodynamic equilibrium between two species. Since in all these samples at pH 7 three species are present (Figure 4.6, see above), the isosbestic point derives from an equilibrium between two absorption spectra that hold up the contribution of the three species. A further condition to explain the presence of the isosbestic points requires a constant ratio between the 5cHS and 6cHS aquo along the pH titration.

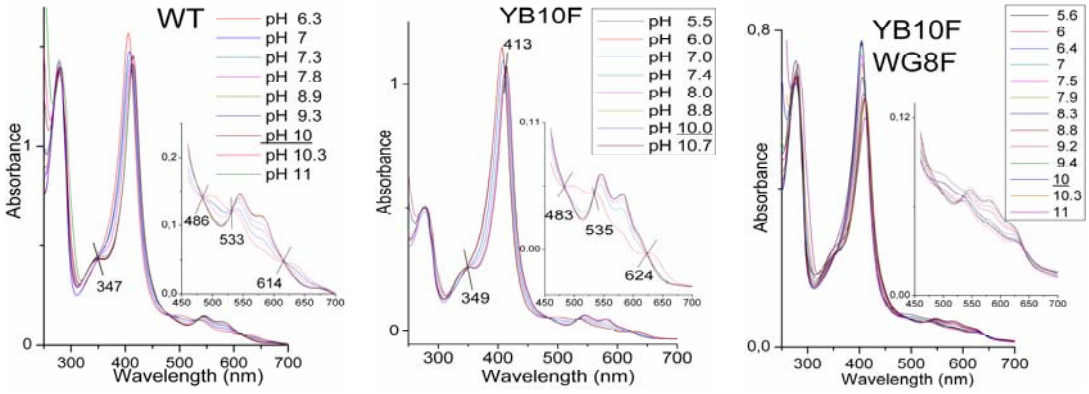

Figure 4.10 Spectrophotometric titration of WT, YB10F, YB10F/WG8F Fe^{3+} Tf-trHb. In the inset the corresponding pH values are reported. Scan time of 600 nm/min, 10-15 μM sample concentration.

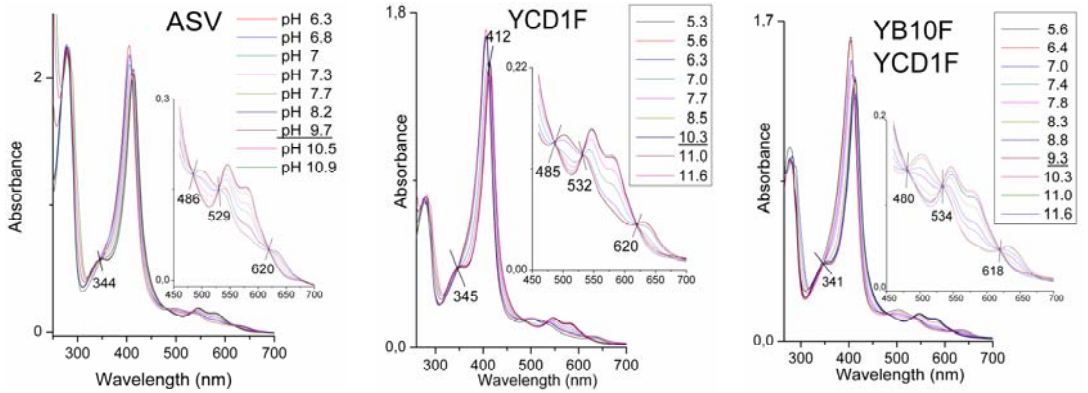

Figure 4.11 Spectrophotometric titration of ASV, YCD1F, YB10F/YCD1F Fe^{3+} Tf-trHb. In the inset the corresponding pH values are reported. Scan time of 600 nm/min, 10-15 μM sample concentration.

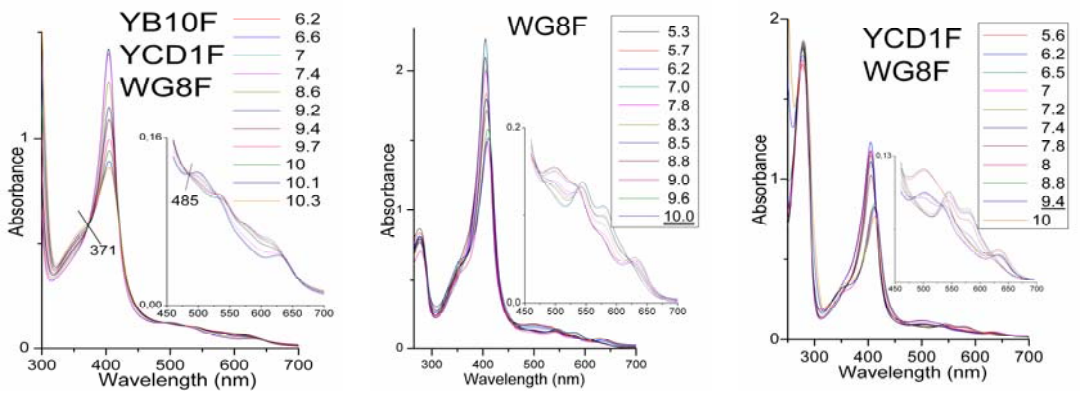

Figure 4.12 Spectrophotometric titration of YB10F/YCD1F/WG8F, WG8F, YCD1F/WG8F Fe^{3+} Tf-trHb. In the inset the corresponding pH values are reported. Scan time of 600 nm/min, 10-15 μM sample concentration.

WG8F and YB10F/YCD1F mutants do not show the presence of isosbestic points since a partially denaturation of the protein occurs, as observed by the slight broadening of the Soret band in the 360-380 nm region (Figure 4.12).

In the case of YB10F/WG8F mutant (Figure 4.10) the absence of a clear isosbestic point is due to a background deriving probably to impurities present in the sample (accordingly, see below, in the RR spectra a high fluorescent background is observed).

Finally, the YB10F/YCD1F/WG8F variant does not experience an alkaline transition and denaturation of the protein occurs. The presence of the isosbestic points at 371 and 485 nm (Figure 4.12) is probably due to the equilibrium between the native and denatured forms.

4.6.2 Room temperature

Figures 4.13 and 4.14 show the UV-Vis and RR spectra of WT, ASV and distal mutants of Tf-trHb at alkaline pH. The UV-Vis of the WT Tf-trHb (Figure 4.13) with the Soret at 413 nm, β and α bands at 545 and 577 nm, and CT1 at ~ 609 nm (black line), indicates that the $–OH^-$ is coordinated in the sixth axial position and gives rise to an equilibrium between an high and low spin species similarly to Mb and human Hb (*19*). Accordingly, the RR spectrum in the high frequency region confirms the equilibrium between a 6cHS (ν_3 at 1478 cm^{-1}, ν_2 at 1560 cm^{-1}, ν_{10} at 1606 cm^{-1}) and a 6cLS species (ν_3 at 1503 cm^{-1}, ν_2 at 1582 cm^{-1}, ν_{10} at 1638 cm^{-1}). Moreover a small amount of unligated (5cHS) species is still present at pH 10 (ν_3 at 1494 cm^{-1}).

The ASV behaves similarly, as revealed by the UV-Vis (only the CT1 is 2 nm blue-shifted) and RR spectra (Figure 4.13).

The other variants retain the $–OH^-$ binding properties as indicated by the Soret band between 410 and 414 nm, β and α bands at 544-545 nm and 577-581 nm, respectively, and a CT1 band in the range of ~ 607-614 nm (Figures 4.13 and 4.14). Moreover, the RR core-size marker band frequencies confirm that the coordination of the $–OH^-$ gives rise to an equilibrium of a 6cHS (ν_3 at 1477-1478 cm^{-1}, ν_2 at 1557-1563 cm^{-1}, ν_{10} at 1601-1607 cm^{-1}) and a 6cLS species (ν_3 at 1501-1503 cm^{-1}, ν_2 at 1582-1584 cm^{-1}, ν_{10} at 1635-1638 cm^{-1}) (Figures 4.13 and 4.14). The $\nu_{(C=C)}$ stretching mode is found between 1627-1630 cm^{-1}.

The 5cHS (ν_3 at 1490-1494 cm^{-1}) is conserved in all variants, except for YB10F and YCD1F mutants, confirming the previous results at pH 7 (see above), that the presence of a W and a Y in the distal cavity markedly favours the $–OH^-$ coordination.

Figures 4.15 and 4.16 show the RR spectra between 425 and 625 cm^{-1}, in buffered H_2O (black line) and D_2O (red line). In this region the $\nu_{(Fe-OH)}$ stretching modes of the HS and LS species were previously reported for Mb and HRP (*19*). The (Fe^{3+}) Mb at alkaline pH shows the presence of two $\nu_{(Fe-OH)}$ at 491 and 550 cm^{-1} (477 and 538 cm^{-1} in D_2O) assigned to the HS and LS species, respectively. On the other side, the HRP-OH complex presents the LS the $\nu_{(Fe-OH)}$ at 503 cm-1 (509 cm^{-1} in D_2O, Chapter 1).

Unfortunately, in spite of the fact that WT and selected of Tf-trHb variants at alkaline pH bind the $–OH^-$ and an equilibrium between an HS and LS species is present, in the low frequency of RR spectra only one band shows a frequency shift in D_2O. Therefore, I am unable to distinguish if this shift corresponds to the HS or the LS species (Table 4.3).

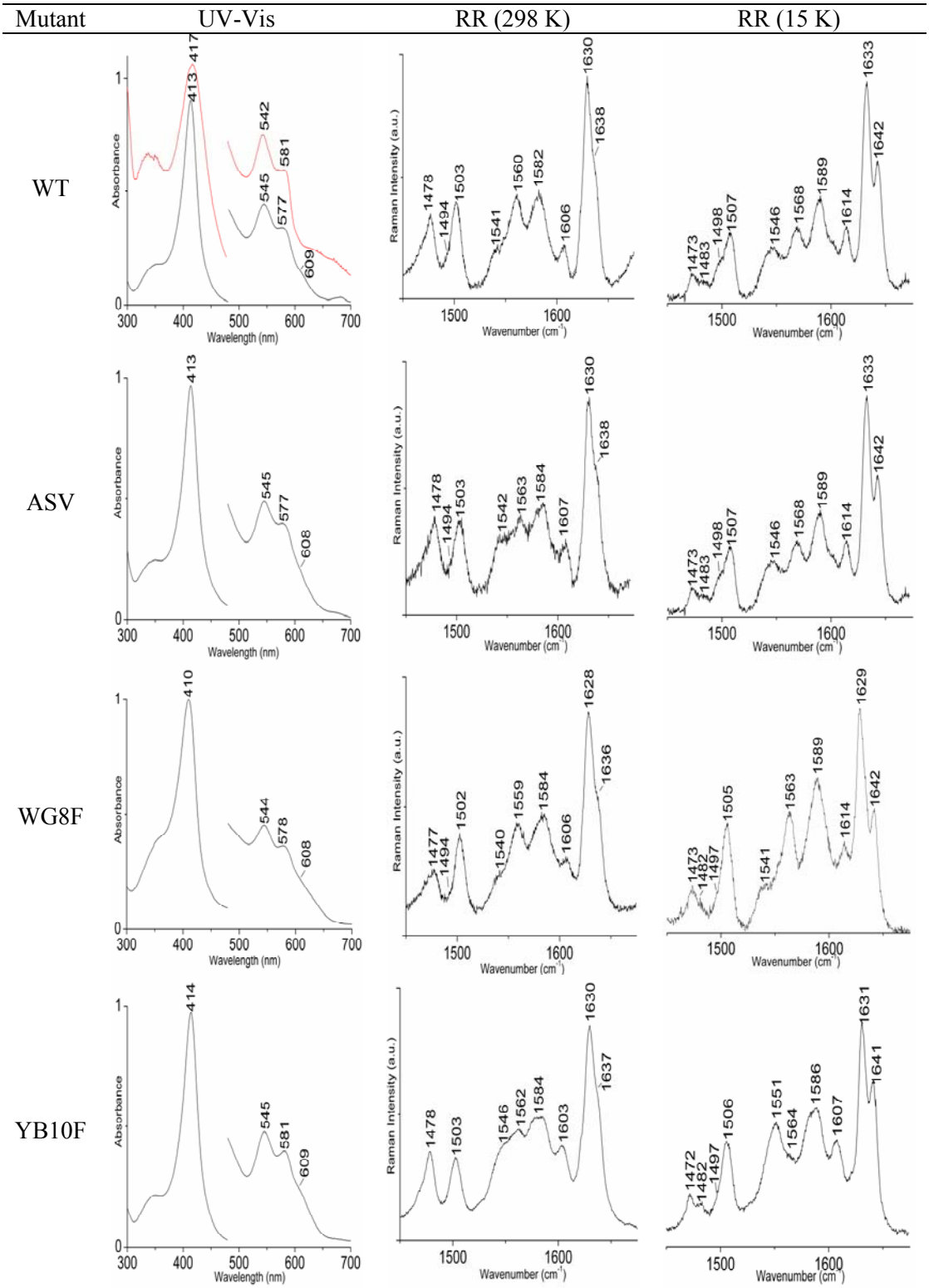

Figure 4.13 UV-Vis and RR (at 298 and 15 K) spectra of WT, ASV, WG8F and YB10F Fe^{3+} Tf-trHb, at alkaline pH (0.1 M glycine buffer). UV-Vis: scan time of 600 nm/min (298 K, black line) and 120 nm/min (15 K, red line), 10-15 μM sample concentration. RR: 413.1 nm excitation wavelength, 1.2 cm^{-1} spectral resolution, 10 mW laser power at the sample, 30-35 μM sample concentration. WT: average of three spectra with 246 s integration time (298 K) and four spectra with 500 s integration time (15 K); ASV: average of two spectra with 900 s integration time (298 K) and three spectra with 300 s integration time (15 K); WG8F: average of six spectra

with 540 s integration time (298 K) and four spectra with 500 s integration time (15 K); YB10F: average of six spectra with 330 s integration time (298 K) and six spectra with 450 s integration time (15 K). Spectra have been shifted along the ordinate axis to allow better visualization.

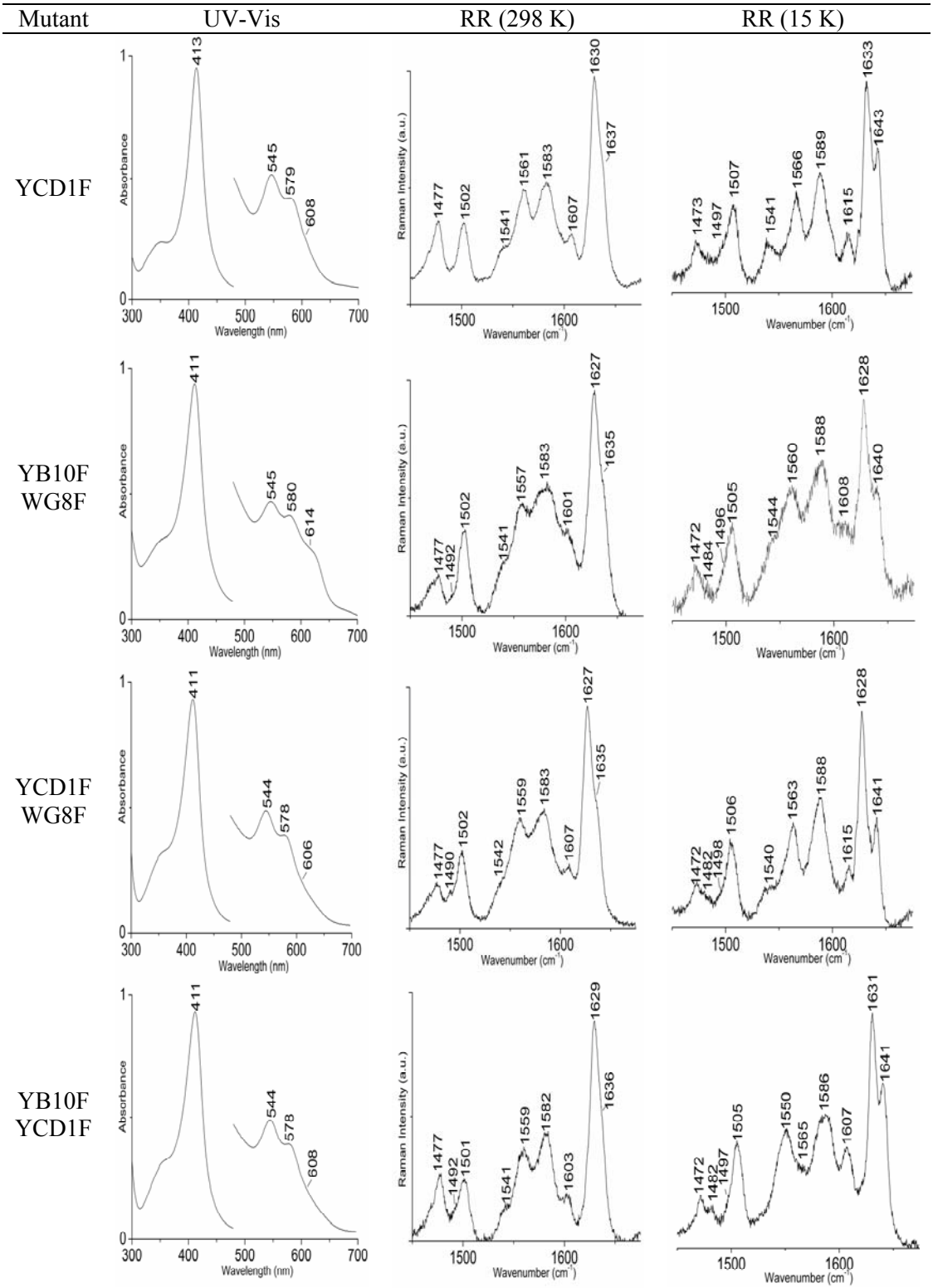

Figure 4.14 UV-Vis and RR (at 298 and 15 K) spectra of YCD1F, YB10F/WG8F, YCD1F/WG8F and YB10F/YCD1F Fe^{3+} Tf-trHb, at alkaline pH (0.1 M glycine buffer). UV-Vis: scan time of 600 nm/min, 10-15 μM sample concentration. RR: 413.1 nm excitation wavelength, 1.2 cm^{-1} spectral resolution, 10 mW laser power at the sample, 30-35 μM sample

concentration. YCD1F: average of four spectra with 300 s integration time (298 K), average of four spectra with 500 s integration time (15 K); YB10F/WG8F: average of four spectra with 700 s integration time (298 K), average of six spectra with 450 s integration time (15 K); YCD1F/WG8F: average of three spectra with 900 s integration time (298 K), average of five spectra with 630 s integration time (15 K); YB10F/YCD1F: average of six spectra with 410 s integration time (298 K), average of seven spectra with 430 s integration time (15 K). Spectra have been shifted along the ordinate axis to allow better visualization.

4.6.3 Low temperature

Upon lowering the temperature to 15 K, the WT Tf-trHb UV-Vis absorption spectrum is characterized by the Soret band at 417 nm, β and α bands at 542 and 581 nm, respectively (Figure 4.13, red line). The corresponding RR spectrum shows that the thermodynamic equilibrium between the HS and LS is shifted in favour of the latter as revealed by the enhancement of the 6cLS modes (ν_3 at 1507 cm^{-1}, ν_2 at 1589 cm^{-1}, and ν_{10} at 1642 cm^{-1}), and the decrease of the 6cHS species (ν_3 at 1483 cm^{-1}, ν_2 at 1568 cm^{-1}, ν_{10} at 1614 cm^{-1}). A significant amount of 5cHS species is present (ν_3 at 1498 cm^{-1}). Moreover as previously noted for other hemoproteins at low temperature (*19*), an increased frequency (of about 4-7 cm^{-1}) of the core size marker bands is observed as a consequence of a contraction of the heme cavity.

The ASV shows an identical behaviour to that observed for the WT.

The other selected variants at 15 K show a predominant 6cLS $–OH^-$ adduct (ν_3 at 1505-1507 cm^{-1}, ν_2 at 1586-1589 cm^{-1} and ν_{10} at 1640-1643 cm^{-1}) and the 6cHS species remains in traces (ν_3 at 1482-1484 cm^{-1}, ν_2 at 1560-1568 cm^{-1}, ν_{10} at 1607-1615 cm^{-1}). Moreover the 5cHS species is markedly decreased respect to WT and ASV.

The $\nu_{(C=C)}$ modes overlap and are between 1628 and 1631 cm^{-1}.

The RR spectra in the low frequency region obtained in buffered H_2O (black lines) and D_2O (red lines) are shown in Figures 3.15 and 3.16. The frequencies of the $\nu_{(Fe-OH)}$ are listed in Table 4.3. WT and ASV LS $\nu_{(Fe-OH)}$ is at 544 cm^{-1} (530 cm^{-1} in D_2O), 14 cm^{-1} lower respect to that of Mb at 20 K (*19*). For the other variants, as observed for the room temperature measurements, the spectra obtained at 15 K reveal the shift of only one mode, and I am not able to assign it (Table 4.3).

Table 4.3 Resonance Raman frequencies (cm^{-1}) of the $\nu_{(Fe\text{-}OH)}$ stretching modes of alkaline pH of WT Tf-trHb and its variants obtained in H_2O and D_2O (in brackets), at 298 and 15 K.

Protein	**298 K**	**15 K**
WT	514 (502)	544 (530) LS
ASV	514 (502)	544 (530) LS
WG8F	501 (487)	~ 502 (493)
YB10F	508 (494)	505 (493)
YCD1F	510 (496)	515 (504)
YB10F/WG8F	/	~ 493 (481)
YCD1F/WG8F	/	515 (502)
YB10F/YCD1F	502 (491)	504 (491)

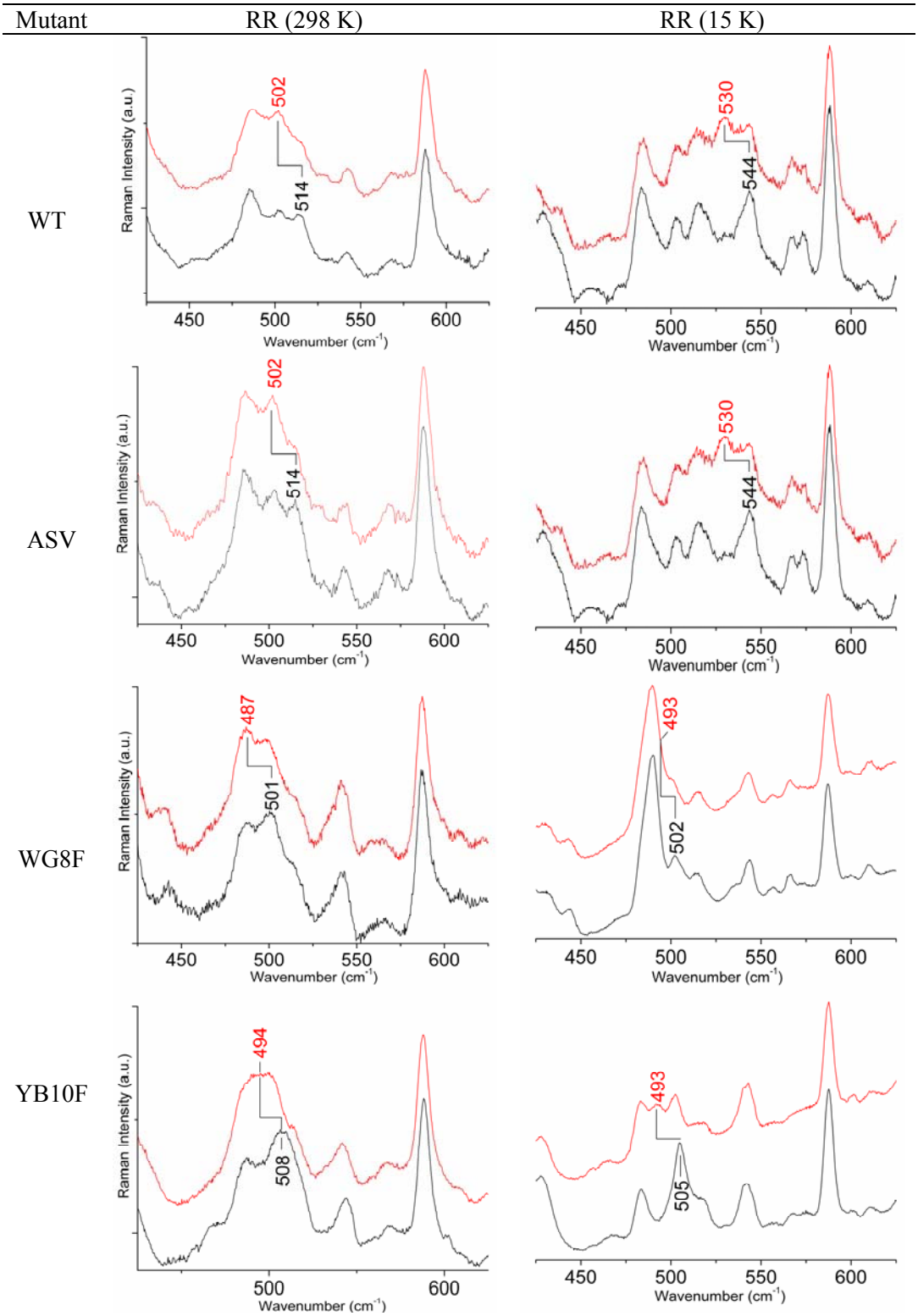

Figure 4.15 RR spectra in the low frequency region (at 298 and 15 K) of WT, ASV, WG8F and YB10F Fe^{3+} Tf-trHb, at alkaline pH (black lines) and pD (red lines) (0.1 M glycine buffer). 413.1 nm excitation wavelength, 1.2 cm^{-1} spectral resolution, 10 mW laser power at the sample, 30-35 μM sample concentration. WT: average of eight spectra with 500 s integration time (298 K), average of six spectra with 650 s integration time (15 K); ASV: average of nine spectra with 700 s integration time (298 K), average of five spectra with 450 s integration time (15 K); WG8F: average of ten spectra with 540 s integration time (298 K), average of five spectra with 600 s integration time (15 K); YB10F: average of nine spectra with 730 s integration time (298 K), average of six spectra with 450 s integration time (15 K). Spectra have been shifted along the ordinate axis to allow better visualization.

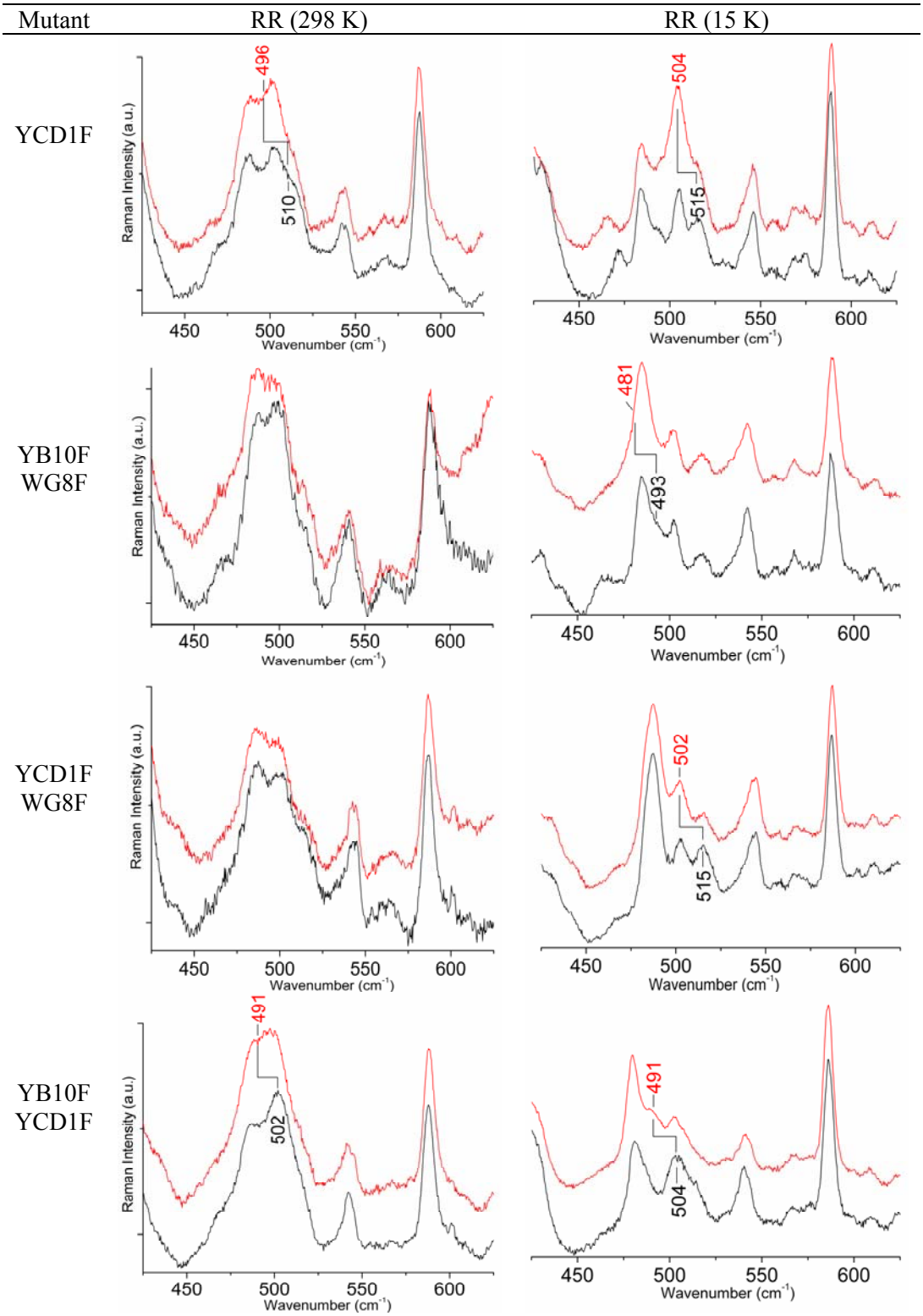

Figure 4.16 RR in the low frequency region (at 298 and 15 K) spectra of YCD1F, YB10F/WG8F, YCD1F/WG8F and YB10F/YCD1F Fe^{3+} Fe^{3+} Tf-trHb, at alkaline pH (black lines) and pD (red lines), in 0.1 M glycine buffer. 413.1 nm excitation wavelength, 1.2 cm^{-1} spectral resolution, 10 mW laser power at the sample, 30-35 μM sample concentration. YCD1F: average of nine spectra with 650 s integration time (298 K), average of six spectra with 800 s integration time (15 K); YB10F/WG8F: average of six spectra with 900 s integration time (298 K), average of seven spectra with 750 s integration time (15 K); YCD1F/WG8F: average of four spectra with 1100 s integration time (298 K), average of nine spectra with 830 s integration time (15 K); YB10F/YCD1F: average of ten spectra with 600 s integration time (298 K), average of

seven spectra with 610 s integration time (15 K). Spectra have been shifted along the ordinate axis to allow better visualization.

4.7 The ferric state in presence of sulfide

WT Tf-trHb has surprisingly shown a high affinity for sulfide anion ($2.8 \cdot 10^{-6}$ M, at pH 7). Previously, the only known heme protein able to bind H_2S with high affinity was Hb I from *L. pectinata*, whose distal cavity bears FCD1, FE11 and a QE7 residues (Chapter 1).

WT Tf-trHb binds sulfide in the Fe^{3+} state, giving rise to a stable 6cLS species (Soret at 425 nm, β and α bands at 550 and 575 nm, respectively), as confirmed by the RR spectrum in the high frequency (ν_4 at 1375 cm^{-1}, ν_3 at 1503 cm^{-1}, ν_2 at 1585 cm^{-1}, ν_{10} at 1636 cm^{-1}). In the low frequency region the band at 375 cm^{-1} was tentatively assigned to the $\nu_{(Fe\text{-}S)}$ stretching mode, in analogy to the Hb I from L. pectinata. Spectroscopic studies of the sulfide binding were extended to theYB10F, WG8F, YCD1F and YB10F/YCD1F7WG8F mutants of the distal cavity. In all cases, upon sulfide binding a 6cLS species occurs, with a $\nu_{(Fe\text{-}S)}$ (at ~ 375 cm^{-1}) not affected by the distal mutation (Chapter 1).

Based on the kinetic experiments (carried out by Prof Boffi et coworker at the University “La Sapienza” of Rome), the overall high affinity resides in the slow rate of sulfide release, attributed to hydrogen bonding stabilization of the bound ligand by distal residue WG8. In fact the set of point mutants in which these residues have been replaced with F indicates that the WG8 residue represents the major kinetic barrier to the escape of the bound sulfide species, whereas the YCD1 and YB10 contributions are negligible.

In summary, the presence of an aromatic cage and a hydrogen bond donor appear to account for the structural determinants that govern the thermodynamic properties of sulfide binding in Tf-trHb. The WG8, YB10, and YCD1 triad provides the first shell of residues surrounding the coordinated sulfide but does not provide multiple H-bond interactions to the iron-bound ligand. In fact, kinetic data indicate clearly that only WG8 residue contributes to the sulfide stabilization through H-bonding interaction. In this manner, the effect of the triple mutation in YB10F/YCD1F/WG8F (10-fold increase in sulfide affinity), which replaces putative hydrogen bonding interactions with a fully

aromatic cage, strengthens the role of sulfide-aromatic interactions with respect to hydrogen bonding contributions (Chapter 1).

The high affinity for hydrogen sulfide in Tf-trHb is thought to have a possible physiological significance since sulfide is produced in bacteria at metabolic steps involved in cysteine biosynthesis and hence in thiol redox homeostasis.

4.8 The ferrous state in presence of CO

WT, ASV and mutants of Tf-trHb were characterized in the (Fe^{2+})-CO adduct by infrared and RR spectroscopy. Among these techniques, the combination RR and infrared spectroscopy of the CO-ligated forms has been successfully employed to characterize the active site of heme proteins (Chapter 1). In fact, when data are available for the WT protein and distal mutants, the vibrational frequencies can be reliably related to specific interactions between the iron- bound CO and the distal residues.

The UV-visible absorption spectra (with Soret, α, β bands in the intervals 420-422 nm, 539-543 nm, 567-570 nm, respectively) and the high-frequency RR spectra obtained with 413.1 nm excitation are characteristic of 6cLS forms, with CO bound as the sixth ligand of the iron atom.

The spectroscopic analysis of the $\nu_{(Fe-CO)}$ and $\nu_{(CO)}$ stretching frequencies allow us to establish the existence of two conformers of both wild-type and ASV protein: form 1 with $\nu_{(Fe-CO)}/\nu_{(CO)}$ at 509/1938 cm^{-1}, and form 2 at 518/1920 cm^{-1}. The spectroscopic results on mutants demonstrate that CO interacts with WG8 in form 1, whereas it interacts with both WG8 and YCD1 in form 2. YB10 plays a negligible role.

The present observations allow us to conclude that the polarity of Tf-trHb distal cavity is intermediate between that of vertebrate hemoglobins and that of heme-containing peroxidases. In particular, the Fe-CO frequencies of form 2 are reminiscent of a peroxidase-like conformer: for instance, *C. cinereus* peroxidase (CIP $\nu_{(Fe-CO)}/\nu_{(CO)}$ at 519/1930 cm^{-1}) (*53*), form 2 of horseradish peroxidas (HRP $\nu_{(Fe-C0)}/\nu_{(CO)}$ at 516/1933 cm^{-1}) (*54, 55*), form 2 of cytochrome c peroxidase (CCP $\nu_{(Fe-CO)}/\nu_{(CO)}$ at 530/1922 cm^{-1}) (*52*,*56*).

4.9 Conclusions

The function of trHbs, after several studies, remain still uncertain. Their high affinity for O_2 allows to exclude a possible role in the gas transport and storage. In the particular case of Tf-trHb, spectroscopic studies elucidate that WG8 is the key H-bonding donor for the exogenous ligand stabilization and YCD1 is a very flexible residue and plays an ancillary role in the ligand binding, if necessary. These structural properties suggest that

Tf-trHb would exert multi-functions in a simple organism such as the *Thermobifida fusca* bacterium. Two hypothetical functions could be: i) involvement in the sulfide metabolism correlated to its high affinity for this ligand; ii) a peroxidase function, in accord with recent findings of the genuine peroxidase activity by Tf-trHb (*57*). The latter hypothesis is also supported by the present findings since the CO and fluoride in WT Tf-trHb experience similar polar interactions to that of heme containing peroxidase in spite of their different distal residues.

References

(1) Vuletich, D. A., and Lecomte, J. T. (2006) A phylogenetic and structural analysis of truncated hemoglobins. *J. Mol. Evol. 62*, 196-210.

(2) Wittenberg, J. B., Bolognesi, M., Wittenberg, B. A., and Guertin, M. (2002) Truncated hemoglobins: a new family of hemoglobins widely distributed in bacteria, unicellular eukaryotes, and plants. *J. Biol. Chem. 277*, 871-874.

(3) Sato, T., and Tamiya, H. (1937) Cytologia, Fujii Jubilee volume. 1133–1138.

(4) Keilin, D., and Ryley, J. F. (1953) Haemoglobin in Protozoa. *Nature 172*, 451.

(5) Iwaasa, H., Takagi, T., and Shikama, K. (1989) Protozoan myoglobin from Paramecium caudatum. Its unusual amino acid sequence. *J. Mol. Biol. 208*, 355-358.

(6) Pesce, A., Couture, M., Dewilde, S., Guertin, M., Yamauchi, K., Ascenzi, P., Moens, L., and Bolognesi, M. (2000) A novel two-over-two alpha-helical sandwich fold is characteristic of the truncated hemoglobin family. *Embo J. 19*, 2424-2434.

(7) Perutz, M. F. (1979) Regulation of oxygen affinity of hemoglobin: influence of structure of the globin on the heme iron. *Annu. Rev. Biochem. 48*, 327-386.

(8) Nardini, M., Pesce, A., Milani, M., and Bolognesi, M. (2007) Protein fold and structure in the truncated (2/2) globin family. *Gene 398*, 2-11.

(9) Milani, M., Savard, P. Y., Ouellet, H., Ascenzi, P., Guertin, M., and Bolognesi, M. (2003) A TyrCD1/TrpG8 hydrogen bond network and a TyrB10TyrCD1 covalent link shape the heme distal site of Mycobacterium tuberculosis hemoglobin O. *Proc. Natl. Acad. Sci. U S A 100*, 5766-5771.

(10) Hoy, J. A., Kundu, S., Trent, J. T., 3rd, Ramaswamy, S., and Hargrove, M. S. (2004) The crystal structure of Synechocystis hemoglobin with a covalent heme linkage. *J. Biol. Chem. 279*, 16535-16542.

(11) Bolognesi, M., Rosano, C., Losso, R., Borassi, A., Rizzi, M., Wittenberg, J. B., Boffi, A., and Ascenzi, P. (1999) Cyanide binding to Lucina pectinata hemoglobin I and to sperm whale myoglobin: an x-ray crystallographic study. *Biophys. J. 77*, 1093-1099.

(12) Ilari, A., Bonamore, A., Farina, A., Johnson, K. A., and Boffi, A. (2002) The X-ray structure of ferric Escherichia coli flavohemoglobin reveals an unexpected geometry of the distal heme pocket. *J. Biol. Chem. 277*, 23725-23732.

(13) Falzone, C. J., Christie Vu, B., Scott, N. L., and Lecomte, J. T. (2002) The solution structure of the recombinant hemoglobin from the cyanobacterium Synechocystis sp. PCC 6803 in its hemichrome state. *J. Mol. Biol. 324*, 1015-1029.

(14) Milani, M., Pesce, A., Ouellet, Y., Ascenzi, P., Guertin, M., and Bolognesi, M. (2001) Mycobacterium tuberculosis hemoglobin N displays a protein tunnel suited for O2 diffusion to the heme. *Embo J. 20*, 3902-3909.

(15) Giangiacomo, L., Ilari, A., Boffi, A., Morea, V., and Chiancone, E. (2005) The truncated oxygen-avid hemoglobin from Bacillus subtilis: X-ray structure and ligand binding properties. *J. Biol. Chem. 280*, 9192-9202.

(16) Bonamore, A., Ilari, A., Giangiacomo, L., Bellelli, A., Morea, V., and Boffi, A. (2005) A novel thermostable hemoglobin from the actinobacterium Thermobifida fusca. *Febs J. 272*, 4189-4201.

(17) Nardini, M., Pesce, A., Labarre, M., Richard, C., Bolli, A., Ascenzi, P., Guertin, M., and Bolognesi, M. (2006) Structural determinants in the group III truncated hemoglobin from Campylobacter jejuni. *J. Biol. Chem. 281*, 37803-37812.

(18) Pesce, A., Nardini, M., Milani, M., and Bolognesi, M. (2007) Protein structure in the truncated (2/2) hemoglobin family. *IUBMB Life 59*, 535-541.

(19) Feis, A., Marzocchi, M. P., Paoli, M., and Smulevich, G. (1994) Spin state and axial ligand bonding in the hydroxide complexes of metmyoglobin, methemoglobin, and horseradish peroxidase at room and low temperatures. *Biochemistry 33*, 4577-4583.

(20) Hu, S., Morris, I. K., Singh, J. P., Smith, K. M., and Spiro, T. G. (1993) Complete assignement of Cytochrome c resonance Raman spectra via enzymatic reconstitution with isotopically lebeled hemes. *J. Am. Chem. Soc. 115*, 12446-12458.

(21) Cerda-Colon, J. F., Silfa, E., and Lopez-Garriga, J. (1998) Unusual rocking freedom of the heme in the hydrogen sulfide-binding hemoglobin from Lucina pectinata. *J. Am. Chem. Soc. 120*, 9312-9317.

(22) Peterson, E. S., Friedman, J. M., Chien, E. Y., and Sligar, S. G. (1998) Functional implications of the proximal hydrogen-bonding network in myoglobin: a resonance Raman and kinetic study of Leu89, Ser92, His97, and F-helix swap mutants. *Biochemistry 37*, 12301-12319.

(23) Smulevich, G., Mauro, J. M., Fishel, L. A., English, A. M., Kraut, J., and Spiro, T. G. (1988) Heme pocket interactions in cytochrome c peroxidase studied by site-directed mutagenesis and resonance Raman spectroscopy. *Biochemistry 27*, 5477-5485.

(24) Razzera, G., Vernal, J., Baruh, D., Serpa, V. I., Tavares, C., Lara, F., Souza, E. M., Pedrosa, F. O., Almeida, F. C., Terenzi, H., and Valente, A. P. (2008) Spectroscopic characterization of a truncated hemoglobin from the nitrogen-fixing bacterium Herbaspirillum seropedicae. *J. Biol. Inorg. Chem. 13*, 1085-1096.

(25) Howes, B. D., Giordano, D., Boechi, L., Russo, R., Mucciacciaro, S., Ciaccio, C., Sinibaldi, F., Fittipaldi, M., Marti, M. A., Estrin, D. A., di Prisco, G., Coletta, M., Verde, C., and Smulevich, G. (2010) The peculiar heme pocket of the 2/2 hemoglobin of cold-adapted Pseudoalteromonas haloplanktis TAC125. *J. Biol. Inorg. Chem*., in press.

(26) Eaton, W. A., and Hochstrasser, R. M. (1968) Single-crystal spectra of ferrimyoglobin complexes in polarized light. *J. Chem. Phys. 49*, 985-995.

(27) Que, L. (1988) Metal-tyrosinate proteins. In: Spiro TG (ed) Biological Applications of Raman Spectroscopy, Vol. 3. Wiley, New York pp 491–521.

(28) Adachi, S., Nagano, S., Ishimori, K., Watanabe, Y., Morishima, I., Egawa, T., Kitagawa, T., and Makino, R. (1993) Roles of proximal ligand in heme proteins: replacement of proximal histidine of human myoglobin with cysteine and

tyrosine by site-directed mutagenesis as models for P-450, chloroperoxidase, and catalase. *Biochemistry 32*, 241-252.

(29) Egeberg, K. D., Springer, B. A., Martinis, S. A., Sligar, S. G., Morikis, D., and Champion, P. M. (1990) Alteration of sperm whale myoglobin heme axial ligation by site-directed mutagenesis. *Biochemistry 29*, 9783-9791.

(30) Liu, Y., Moenne-Loccoz, P., Hildebrand, D. P., Wilks, A., Loehr, T. M., Mauk, A. G., and Ortiz de Montellano, P. R. (1999) Replacement of the proximal histidine iron ligand by a cysteine or tyrosine converts heme oxygenase to an oxidase. *Biochemistry 38*, 3733-3743.

(31) Nagai, K., Kagimoto, T., Hayashi, A., Taketa, F., and Kitagawa, T. (1983) Resonance raman studies of hemoglobins M: evidence for iron-tyrosine charge-transfer interactions in the abnormal subunits of Hb M Boston and Hb M Iwate. *Biochemistry 22*, 1305-1311.

(32) Nagai, M., Yoneyama, Y., and Kitagawa, T. (1989) Characteristics in tyrosine coordinations of four hemoglobins M probed by resonance Raman spectroscopy. *Biochemistry 28*, 2418-2422.

(33) Pond, A. E., Roach, M. P., Sono, M., Rux, A. H., Franzen, S., Hu, R., Thomas, M. R., Wilks, A., Dou, Y., Ikeda-Saito, M., Ortiz de Montellano, P. R., Woodruff, W. H., Boxer, S. G., and Dawson, J. H. (1999) Assignment of the heme axial ligand(s) for the ferric myoglobin (H93G) and heme oxygenase (H25A) cavity mutants as oxygen donors using magnetic circular dichroism. *Biochemistry 38*, 7601-7608.

(34) Blackwood, M. E., Jr., Rush, T. S., 3rd, Romesberg, F., Schultz, P. G., and Spiro, T. G. (1998) Alternative modes of substrate distortion in enzyme and antibody catalyzed ferrochelation reactions. *Biochemistry 37*, 779-782.

(35) Kitagawa, T. (1988) in: T.G. Spiro (Ed.), Biological Applications of Raman Spectroscopy: Resonance Raman Spectra of Hemes and Metalloproteins, Wiley, New York,. 97-131.

(36) Couture, M., Das, T. K., Lee, H. C., Peisach, J., Rousseau, D. L., Wittenberg, B. A., Wittenberg, J. B., and Guertin, M. (1999) Chlamydomonas chloroplast ferrous hemoglobin. Heme pocket structure and reactions with ligands. *J. Biol. Chem. 274*, 6898-6910.

(37) Samuni, U., Ouellet, Y., Guertin, M., Friedman, J. M., and Yeh, S. R. (2004) The absence of proximal strain in the truncated hemoglobins from Mycobacterium tuberculosis. *J. Am. Chem. Soc. 126*, 2682-2683.

(38) Smulevich, G., Feis, A., and Howes, B. D. (2005) Fifteen years of Raman spectroscopy of engineered heme containing peroxidases: what have we learned? *Acc. Chem. Res. 38*, 433-440.

(39) Asher, S. A., Adams, M. L., and Schuster, T. M. (1981) Resonance Raman and absorption spectroscopic detection of distal histidine--fluoride interactions in human methemoglobin fluoride and sperm whale metmyoglobin fluoride: measurements of distal histidine ionization constants. *Biochemistry 20*, 3339-3346.

(40) Asher, S. A., and Schuster, T. M. (1981) Differences in iron-fluoride bonding between the isolated subunits of human methemoglobin fluoride and sperm whale metmyoglobin fluoride as measured by resonance Raman spectroscopy. *Biochemistry 20*, 1866-1873.

(41) Asher, S. A., Vickery, L. E., Schuster, T. M., and Sauer, K. (1977) Resonance Raman spectra of methemoglobin derivatives. Selective enhancement of axial ligand vibrations and lack of an effect of inositol hexaphosphate. *Biochemistry 16*, 5849-5856.

(42) Desbois, A., Lutz, M., and Banerjee, R. (1979) Low-Frequency Vibrations in Resonance Raman Spectra of Horse Heart Myoglobin. Iron-Ligand and Iron-Nitrogen Vibrational Modes. *Biochemistry 18*, 1510-1518.

(43) Neri, F., Kok, D., Miller, M. A., and Smulevich, G. (1997) Fluoride binding in hemoproteins: the importance of the distal cavity structure. *Biochemistry 36*, 8947-8953.

(44) Yu, N. T. (1986) Resonance Raman studies of ligand binding. *Methods Enzymol. Vol. 130*, pp. 350-409.

(45) Asher, S. A., and Schuster, T. M. (1979) Resonance Raman examination of axial ligand bonding and spin-state equilibria in metmyoglobin hydroxide and other heme derivatives. *Biochemistry 18*, 5377-5387.

(46) Choi, S., Spiro, T. G., Langry, K. G., Smith, K. M., Budd, D. L., and La Mar, G. N. (1982) Structural correlations and vinyl influences in the Resonance Raman spectra of protoheme complexes and proteins. *J. Am. Chem. Soc. 104*, 4345-4351.

(47) Aime, S., Fasano, M., Paoletti, S., Cutruzzola, F., Desideri, A., Bolognesi, M., Rizzi, M., and Ascenzi, P. (1996) Structural determinants of fluoride and formate binding to hemoglobin and myoglobin: crystallographic and 1H-NMR relaxometric study. *Biophys. J. 70*, 482-488.

(48) Marzocchi, M. P., and Smulevich, G. (2003) Relationship between heme vinyl conformation and the protein matrix in peroxidases. *J. Raman Spectr. 34*, 725-736.

(49) Howes, B. D., Rodriguez-Lopez, J. N., Smith, A. T., and Smulevich, G. (1997) Mutation of distal residues of horseradish peroxidase: influence on substrate binding and cavity properties. *Biochemistry 36*, 1532-1543.

(50) Smulevich, G., Mantini, A. R., Paoli, M., Coletta, M., and Geraci, G. (1995) Resonance Raman studies of the heme active site of the homodimeric myoglobin from Nassa mutabilis: a peculiar case. *Biochemistry 34*, 7507-7516.

(51) Smulevich, G., Paoli, M., De Sanctis, G., Mantini, A. R., Ascoli, F., and Coletta, M. (1997) Spectroscopic evidence for a conformational transition in horseradish peroxidase at very low pH. *Biochemistry 36*, 640-649.

(52) Droghetti, E., Nicoletti, F. P., Bonamore, A., Boechi, L., Arroyo Manez, P., Estrin, D. A., Boffi, A., Smulevich, G., and Feis, A. (2010) Heme Pocket Structural Properties of a Bacterial Truncated Hemoglobin from Thermobifida fusca. *Biochemistry in press*.

(53) Feis, A., Santoni, E., Neri, F., Ciaccio, C., De Sanctis, G., Coletta, M., Welinder, K. G., and Smulevich, G. (2002) Fine-tuning of the binding and dissociation of CO by the amino acids of the heme pocket of Coprinus cinereus peroxidase. *Biochemistry 41*, 13264-13273.

(54) Feis, A., Rodriguez-Lopez, J. N., Thorneley, R. N., and Smulevich, G. (1998) The distal cavity structure of carbonyl horseradish peroxidase as probed by the resonance Raman spectra of His 42 Leu and Arg 38 Leu mutants. *Biochemistry 37*, 13575-13581.

(55) Uno, T., Nishimura, Y., Tsuboi, M., Makino, R., Iizuka, T., and Ishimura, Y. (1987) Two types of conformers with distinct Fe-C-O configuration in the ferrous CO complex of horseradish peroxidase. Resonance Raman and infarared spectroscopic studies with native and deuteroheme-substituted enzymes. *J. Biol. Chem. 262*, 4549-4556.

(56) Smulevich, G., Evangelista-Kirkup, R., English, A., and Spiro, T. G. (1986) Raman and infrared spectra of cytochrome c peroxidase-carbon monoxide adducts in alternative conformational states. *Biochemistry 25*, 4426-4430.

(57) Torge, R., Comandini, A., Catacchio, B., Bonamore, A., Botta, B., and Boffi, A. (2009) Peroxidase-like activity of Thermobifida fusca hemoglobin: The oxidation of dibenzylbutanolide. *J. Mol. Catalysis B: Enzymatic 61*, 303-308.

Chapter 5

Dehaloperoxidase from *Amphitrite ornata*: a detoxifying enzyme

Francesco P. Nicoletti, Matthew K. Thompson, Barry D. Howes, Stefan Franzen, and Giulietta Smulevich.
New Insights into the Role of Distal Histidine Flexibility in Ligand Stabilization of Dehaloperoxidase-hemoglobin from Amphitrite ornata.
Biochemistry (2010), 49, 1903-1912.

Matthew K. Thompson, Michael F. Davis, Vesna de Serrano, **Francesco P. Nicoletti**, Barry D. Howes, Giulietta Smulevich, and Stefan Franzen.
Two-site competitive inhibition in dehaloperoxidase-hemoglobin.
Biophys. J. (2010), 99, 15, 1586-1595.

5.1 Dehaloperoxidase: a peroxidase hemoprotein with a globin fold

5.1.1 The high flexibility of the distal histidine

The dehaloperoxidase (DHP) from the terebellid polychaete *Amphitrite ornata* is an enzyme that converts para-halogenated phenols to the corresponding quinones in the presence of hydrogen peroxide (*1*). Its enzymatic activity is similar to that of heme peroxidases such as horseradish peroxidase (HRP) (*2*), yet it has the structural characteristics of the globin family of proteins, the main functions of which are oxygen transport and storage. In order to investigate the dual function of this hemoglobin-peroxidase, the enzyme was expressed in *Escherichia coli* as a recombinant protein in

its wild-type form and experiments in presence of exogenous ligands (fluoride, and hydroxide) and mono- and tri-halo-phenols (4XP and TXP) have been carried out (*3*).

For native DHP, the room temperature X-ray crystal structure (pdb 1ew6, (*4*)) (Figure 5.1 A) showed that there are two conformations of the distal histidine (His55) at pH 6.0, suggesting an unusual flexibility of this residue: i) in the closed conformation the His55 is orientated toward the heme iron and H-binds the water molecule coordinated as the sixth axial ligand (6cHS); ii) in the opened conformation His55 moves to the solvent, and the water molecule coordination to the iron is prevented giving rise to a 5cHS species. These two conformations are in a thermal equilibrium as indicated by the 100 K structure, revealing only the closed conformation with His55 positioned in the distal pocket and H-bonded with the distal water molecule in the metaquo form (pdb 2qfk, (*5*)) (Figure 5.1 B). These results have been confirmed in this thesis by acquiring UV-Vis and RR spectra at 298 and 12 K.

On the other hand typical peroxidases are characterized by an increased polarity of the distal cavity compared to globins, and however, a distal Arg, which is a key residue in peroxidases promoting heterolysis of hydrogen peroxide during the catalytic cycle (*6*), is missing in DHP (*5*).

It is well-known that heme pocket distal amino acid residues control ligand binding in hemoproteins. In fact, the comparison of the UV-Vis and RR spectra of the fluoride and hydroxide complexes of various peroxidases and selected mutants has highlighted the complex mechanism of stabilization of anionic ligands exerted by the distal amino acids (*7-10*). Moreover, this process resembles that of compound I formation during peroxidase catalysis, where ligand stabilization by the distal arginine is coupled to protonation of the distal histidine (*11*).

It is of interest, therefore, to understand whether the different cavity characteristics of DHP, globins and peroxidases are also reflected in the binding of exogenous ligands, and in the present thesis I focus my interest on the RR and electronic absorption spectra of the fluoride and hydroxide adducts of DHP. In general, the DHP secondary structure is very similar to that of SWMb (*12*) with the overall disposition of the key α-helices (B, C, D, E, and F) nearly identical. However, on the distal side, His55 in DHP has been reported at different distances from the heme iron, ranging from 5.4 A° (*4*) to 4.8 A° (*5*). While the first reported distance is more similar to the distal cavity of peroxidases than globins, the second structure reports a distance closer to that observed in other globins including SW Mb, where the distal His64 is 4.3 A° from the heme iron and H-

bonded to a distal water molecule (Figure 5.1 B). Nevertheless, the close similarity of the frequencies of the $\nu_{(Fe-F)}$ (462 cm^{-1}) and $\nu_{(Fe-OH)}$ (491 and 551 cm^{-1} for the HS and LS forms, respectively) stretching modes in the fluoride and hydroxide adducts of DHP and Mb (*7, 13*) but markedly different from the corresponding frequencies observed in peroxidases ($\nu_{(Fe-F)}$ at 385 cm-1 for HRP (*14*) and only a LS $\nu_{(Fe-OH)}$ around 500-507 cm^{-1} for various peroxidases (*7, 15-17*)) clearly indicates that these ligands bind the heme iron in a similar manner in both DHP and Mb but quite different from that of peroxidases. In particular, in peroxidases, the Arg is determinant in controlling the ligand binding via a strong hydrogen bond between the positively charged guanidinium group and the anion (*7, 9, 10, 18*). On the basis of the spectroscopic results and by analogy with Mb, I suggest that a hydrogen bond network may exist between the His55, the hydroxide, and the fluoride in DHP. However, this conclusion implies that the distal His, similarly to Arg48 in CCP, may undergo a conformational change that places it within hydrogen-bonding distance of the anionic ligand. This high flexibility might serve as the acid-base catalyst necessary for heterolytic O-O bond cleavage, which constitutes the activation of bound hydrogen peroxide.

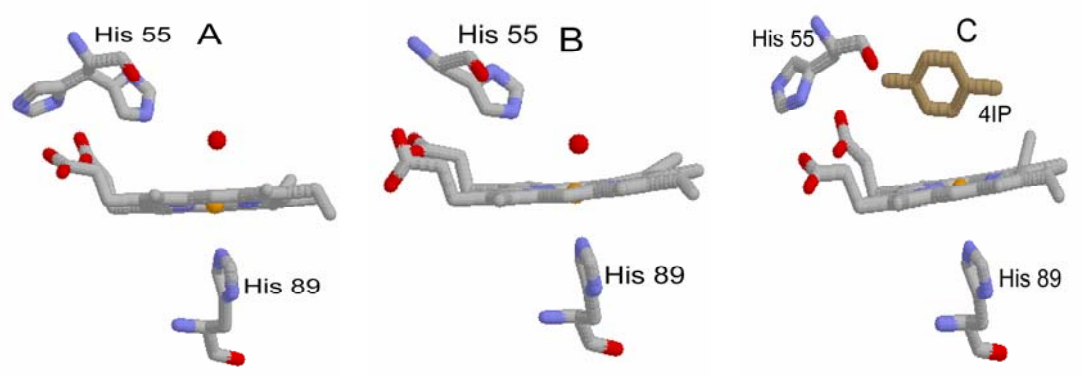

6cHS/5cHS (298 K) *6cHS (100 K)* *5cHS (298 K)*

Figure 5.1 View of the distal histidine (His55) conformations in the wild type form at 298 K (pdb 1ew6 (*4*)) and 100 K (pdb 2qfk (*5*)), and in presence of 4IP (pdb 1ewa (*19*)).

5.1.2 An example of two-site competitive binding inhibition

The DHP structure in complex with the substrate analog 4IP (PDB code 1ewa, (*19*)) revealed that the substrate analog is bound in an internal binding pocket and forces H55 into a solvent-exposed position preventing coordination of the water molecule (Figure 5.1 C), in accord with spectroscopic data that show the presence of a pure 5cHS species (open conformation) (*3*).

This led to the proposal that the internal binding site is the active site for phenol oxidation. However, the native substrate for DHP is 2,4,6-tribromo phenol (2,4,6-TBP), and all attempts to crystallize 2,4,6-TBP (or any other TXP) in the internal site under physiological conditions have failed, so that the only data available for DHP in presence TXP are in solution. The binding of TFP (more soluble respect to the native substrate TBP) to DHP has a quite different effect on the RR spectrum respect to 4IP. In fact the presence of a 320-fold excess of TFP at 298 K determines a slight increase of 6cHS aquo species (closed conformation) (*3*) and favours the His orientation in the closed conformation.

Enzymatic assays performed by Thompson et coworkers (*20*) have revealed that the peroxidase activity and the formation of the corresponding benzo-quinone occur only upon TXP binding and are not observed when 4XP interacts with the protein. Furthermore the binding of 4XP in the internal pocket inhibits the enzymatic function and the oxidation of TXP.

On the basis of these results, and in agreement with the known mechanism for the peroxidase family members, the proposal is that enzymatic oxidation of substrates such as TXP occurs at an external site. Recent ^{1}H-^{15}N HSQC experiments on $^{13}C/^{15}N$-labeled DHP clearly indicate different binding interactions between 4-BP inhibitor and 2,4,6-TCP substrate (*21*).

Hence, DHP has a unique two-site competitive binding mechanism in which the internal (inhibitory) and external (active) binding sites communicate through two conformations of the distal histidine of the enzyme, resulting in non classical competitive inhibition. The same distal histidine conformations involved in DHP function regulate oxygen binding and release during transport and storage by hemoglobins and myoglobins.

5.2 State of art of sulfide interaction with hemoprotein

Hydrogen sulfide (H_2S) is a well known poisonous gas whose cytotoxic effects have been studied for more than 300 years (*22*). It has been found that the reactivity of hemeproteins in the presence of sulfide is quite complex since this ligand may coordinate to the Fe^{3+} iron or, alternatively, form a covalent linkage with the porphyrin. For metmyoglobin and methemoglobin sulfide, active either as H_2S or HS^-, in the presence of O_2 or H_2O_2, gives rise to a covalent modification of the pyrrole ring bearing the 4-vinyl group, generating the so-called sulfmyoglobin and sulfhemoglobin, respectively (*23, 24*). The sulfheme complex has a characteristic absorption band at 620 nm and has been described as a chlorin with sulfide added across the β–β double bond of the pyrrole ‘‘B” (*25*). It has been proposed to protect the cell from sulfide toxicity (*26*). However, since the sulfheme has been found in a number of human diseases involving poisoning with sulfide containing drugs and not with sulfide itself, a protective role of the sulfheme compounds is controversial (*27, 28*).

Several hemeproteins bind sulfide (as H_2S or HS^-) in their Fe^{3+} state. The ambiguity regarding the exact form of sulfide arises from the fact that the pK_a for H_2S is 6.9, leading to a significant fraction of HS^- at physiological pH. The first evidence of the existence of a high affinity sulfide binding hemoglobin was found in the clam *Lucina pectinata* (*L. pectinata*), an invertebrate that, living in sulfide-rich mangroves, is characterized by the presence of symbiotic sulfide-oxidizing bacteria that need to be supplied with both H_2S and O_2 (*29, 30*). The protein responsible for delivering sulfide to the bacteria is hemoglobin I (Hb I) which binds and transports sulfide to sulfide-oxidizing chempautotropic bacteria to maintain a symbiotic relationship and protects the mollusc from sulfide toxicity. This monomeric protein binds sulfide in its Fe^{3+} state, giving rise to UV-Vis and RR spectra characteristic of a low-spin adduct (*29, 31*). Recently, it has been shown that human Fe^{3+} neuroglobin tightly binds sulfide, suggesting a cytoprotective role of neuroglobin in the brain when levels of sulfide increase (*32*). Furthermore, the truncated hemoglobins (trHbs) from *Bacillus subtilis* (Bs) and *Thermobifida fusca* (Tf) have been shown to form high-affinity complexes with sulfide in their Fe^{3+} state (*33*). Sulfide binding to Bs-trHb and Tf-trHb has been demonstrated to occur in vivo within the E. coli host cells in which both proteins are recombinantly expressed. Therefore, the high affinity for sulfide is thought to have a possible physiological significance as sulfide is produced in bacteria at metabolic steps involved in cysteine biosynthesis and hence in thiol redox homeostasis (*33*).

Interactions of sulfide with heme proteins have been recognized and studied for many years in marine invertebrate organisms that live in sulfide-rich environments (*34*). These organisms have evolved strategies for avoiding sulfide toxicity, including the binding and oxidation of sulfide by hemoglobins and symbiotic bacteria, respectively. The giant tubeworm *Riftia pachyptila*, which lives in deep sea hydrothermal vents, supplies O_2 and sulfide to the endosymbionts by binding both ligands simultaneously at two different sites on their extracellular hemoglobins (*27, 34*). The bacteria living inside the tubeworm oxidize sulfide in the presence of O_2 and utilize this energy to synthesize organic nutrients for the invertebrate. In this context we have studied the possibility that dehaloperoxidase-hemoglobin (DHP) from the annelid *A. ornata*, an organism that normally lives in benthic ecosystems, may bind sulfide and exert a detoxifying activity (*35*). DHP is known as a dual-function enzyme that works either as a hemoglobin or peroxidase. In fact, the protein is an oxygen carrier and converts 2,4,6-tribromo phenol to the corresponding 2,6-benzoquinone in the presence of hydrogen peroxide (*35*). While its enzymatic activity is similar to that of the heme containing peroxidases, such as cytochrome c peroxidase (CCP) and horseradish peroxidase (HRP) (*2, 19, 36-39*), its structural characteristics are typical of the proteins from the globin family, whose main function is oxygen transport and storage (*1*). DHP shows maximum turnover of substrate at physiological pH 7.5 (*40*) and has exhibited allosteric interactions of substrate and inhibitor binding both internal and external to the protein, which are regulated by the unusually flexible distal histidine in this globin (*3, 20, 21, 41-43*). Given the simplicity of the structure of *A. ornata*, it is entirely possible that DHP plays a more general role in detoxification that includes sulfide commonly found in coastal estuaries.

In order to investigate the sulfide binding properties of DHP, we undertook a detailed spectroscopic investigation of the protein in the presence of sulfide to highlight if and how the distal heme protein cavity interacts with the exogenous ligand compared to Hb 1 from *L. pectinata* and Tf-trHb. We found that the protein binds sulfide in its Fe^{3+} state. However, upon sulfide binding the protein is fully reduced and in the presence of oxygen it forms the Fe^{2+}-O_2 species. The reaction has been, therefore, monitored in the presence and in absence of oxygen, and the final forms have been compared with those of pure deoxy and DHP-O_2 species. Hence, considering that DHP possesses a significant peroxidase activity under physiological conditions and protects *A. ornata*

from potential toxic molecules such as 2,4,6-tribromophenol (*1, 20*), it is quite possible that this protein also plays a sulfide detoxifying role.

5.3 Results

5.3.1 Deoxy and ferrous-O_2

DHP-O_2. Figure 5.2 A shows the UV-Vis spectrum of deoxy DHP characterized by a Soret band at 432 nm and β band at 557 nm. This spectrum is typical of a 5cHS species with the proximal histidine as the fifth iron ligand. Accordingly, the corresponding RR spectrum in the high frequency region (Figure 5.2 B) confirms the presence of a 5cHS species (ν_3 at 1469 cm^{-1}, ν_2 at 1564 cm^{-1}, ν_{10} at 1602 cm^{-1}, $\nu_{(C=C)}$ at 1619 cm^{-1}). The low-frequency RR spectrum is shown in the inset of Fig. 5.2 C. The prime interest in this region for 5cHS heme proteins is the presence of a strong band due to the iron imidazole stretching mode, $\nu_{(Fe\text{-}Im)}$, which occurs in the range 200-250 cm^{-1} (Chapter 1). The $\nu_{(Fe\text{-}Im)}$ stretching mode frequency is very sensitive to H-bonding and, therefore, to the protein matrix surrounding the proximal histidine (*44, 45*). The $\nu_{(Fe\text{-}Im)}$ is assigned to the strong band at 229 cm^{-1}, previously reported at 233 cm^{-1} (*46*) (inset of Figure 5.2 C). Its frequency is 8 cm^{-1} higher than that of deoxy Mb, suggesting stronger Fe-His bond. Since the crystal structure shows that the N_δ atom of the proximal His (His89) interacts with the carbonyl group of a Leu residue (Leu83) (pdb 3dr9 (*41*)) similar to Mb (His93N_δ-Leu89 carbonyl 2.8 Å (pdb 1a6n (*12*))), the increased $\nu_{(Fe\text{-}Im)}$ frequency cannot result from a strong H-bonding interaction as observed in peroxidases (*11*). The different $\nu_{(Fe\text{-}Im)}$ frequency may derive from the different orientation of the proximal histidine plane with respect to the pyrrole nitrogens, being eclipsed in Mb and staggered in DHP (Figure 5.3) (*12, 41*). Therefore, in DHP a reduction of the repulsive interaction between the imidazole ring and the pyrrole nitrogen atoms might be responsible for a decrease of the (Fe^{2+})-His bond length with the concomitant increase of the $\nu_{(Fe\text{-}Im)}$ stretching frequency. A similar conclusion has been drawn for truncated hemoglobins whose proximal histidines are in a staggered orientation (Figure 5.3). In particular, in the case of trHbN from *Mycobacterium tuberculosis* and trHbC from green unicellular

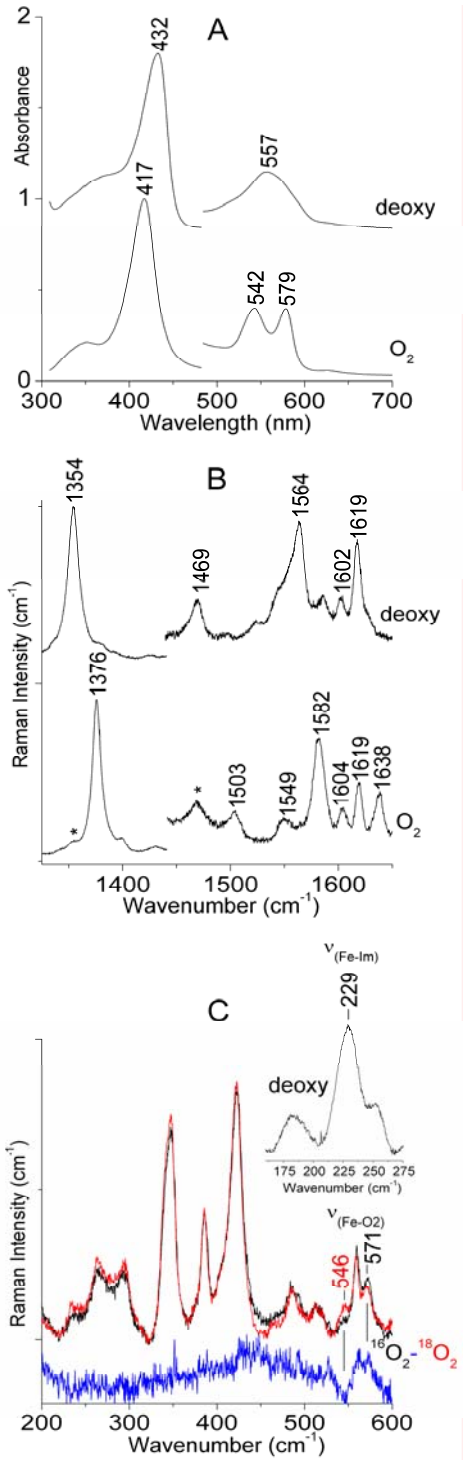

Figure 5.2 UV-Vis (A) and RR spectra in the high (B) and low frequency regions (C) of deoxy and DHP-O_2 ($^{16}O_2$ black line, $^{18}O_2$ red line, and $^{16}O_2$ - $^{18}O_2$ blue line) at pH 6 in 0.1 M phosphate buffer. Experimental conditions: (UV-Vis) Scan rate of 600nm/min. The 450-700 nm region has been expanded of 5-fold. (RR) Deoxy: 441.6 nm excitation wavelength, 0.9 cm^{-1} spectral resolution, 10 mW laser power at the sample, average of 6 spectra with 300 s integration time (high frequency), average of 4 spectra with 300 s integration time (low frequency, in the inset of Panel C). DHP-O_2: 413.1 excitation wavelength, 1.2 cm^{-1} spectral resolution, 1 mW laser power at the sample, average of 15 spectra with 300 s integration time (high frequency), average of 8 spectra with 480 s integration time (low frequency). The asterisks indicate spurious bands due to the deoxy form following to oxygen photolysis under laser irradiation. The 1450-1700 cm^{-1} region has been expanded of 3-fold. Spectra have been shifted along the ordinate axis to allow a better visualization.

alga *Chlamydomonas Eugametos* the $\nu_{(Fe-Im)}$ were found at 226 and 232 cm^{-1}, respectively (*47, 48*).

In the presence of oxygen, the UV-Vis spectrum of DHP-O_2 (Figure 5.2 A) shows a Soret band at 417 nm, and β and α bands at 542 and 579 nm, respectively, similar to that reported for the DHP B isoenzyme (*49*). Accordingly, the high frequency RR spectrum (Figure 5.2 B) is characteristic of a 6cLS species (ν_3 at 1503 cm^{-1},ν_{38} at 1549 cm^{-1}, ν_2 at 1582 cm^{-1}, ν_{37} at 1604 cm^{-1}, $\nu_{(C=C)}$ at 1619 cm^{-1} and ν_{10} at 1638 cm^{-1}). The ν_3 band at ca. 1469 cm^{-1} indicates the presence of a 5cHS Fe^{2+} form due to the unavoidable photolysis of the oxygen under laser irradiation. In order to give insight on the interaction between the diatomic ligand and the distal residues, we studied the low frequency RR region where the $\nu_{(Fe-O2)}$ mode is found. The $\nu_{(Fe-O2)}$ stretching frequency is sensitive to the nature of the H-bond involving the oxygen atoms. In trHbs it was found between 554 and 560 cm^{-1} since the heme-bound ligand is stabilized by interactions with the distal residues through an interlaced H-bonding network with the distal as well as the proximal oxygen (i.e. the oxygen directly coordinated to the iron) atoms of the dioxygen, resulting in a very strong H-bond (*50*). In mammalian globins, such as Mb and Hb, the frequency increases to 568-570 cm^{-1} since the oxygen is H-bonded only to the distal His (*51-53*). In the low frequency RR region of the DHP-O_2 adduct (Figure 5.2 C) the $\nu_{(Fe-O2)}$ mode, on the basis of the isotopic shift observed in $^{18}O_2$ ($\nu_{(Fe-^{18}O2)}$ at 546 cm^{-1}), is assigned to the band at 571 cm^{-1}. Furthermore, no $\nu_{(O-O)}$ stretching mode has been observed in the 1100-1150 cm^{-1} range (Figure 5.4). In fact, this mode is rarely characterized in the RR spectra of heme proteins with a proximal histidine ligand and it has only been observed in trHbs (*54, 55*). The $\nu_{(Fe-O2)}$ stretching mode at 571 cm^{-1} is very close to that observed in Mb (569 cm^{-1}) (*53*) suggesting a similar stabilization played by the distal His and possibly related to the common oxygen transport and storage functions (*49*). Similar environments of the oxyferrous heme moieties in Mb-O_2 and DHP-O_2 has been suggested by the EPR and ENDOR study of the latter adduct cryoreduced at 77 K (*56*). Accordingly, the crystal structures of the Cys73Ser DHP-O_2 mutant (pdb 2qfn, (*5*)) and Mb-O_2 (pdb 1ltw, (*57*)) reveal that both O atoms of the diatomic gas may form H-bonds to $N_{\varepsilon 2}$ of the distal histidine, with distances of 2.8-2.7 Å for the distal and a longer 3.2-3.0 Å bond distance for the proximal oxygen in DHP and Mb, respectively. The slight difference in the H-bonding may support the 2 cm^{-1} frequency variation observed for the $\nu_{(Fe-O2)}$ stretches. Nevertheless, the close similarity of the frequencies of the $\nu_{[Fe-O2]}$ between the two

proteins implies that the distal His in DHP may undergo a conformational change that places it within H-bonding distance of the ligand. In fact, His55 in Fe^{3+} DHP has been reported at distances from the heme iron in the range 5.5-4.8 Å (pdbs 2qfk, 1ew6 (*4, 5, 19*)), longer than in sperm whale Mb (4.3 Å (pdb 1a6k, (*12*))). The same conclusion has been drawn for the stabilization of the fluoride and hydroxide adducts (*3, 7, 13*). Therefore, the data suggest that in DHP the distal His stabilizes the incoming oxygen (O_2 transport) and facilitates both the deprotonation and heterolytic O-O bond cleavage of hydrogen peroxide (peroxidase activity).

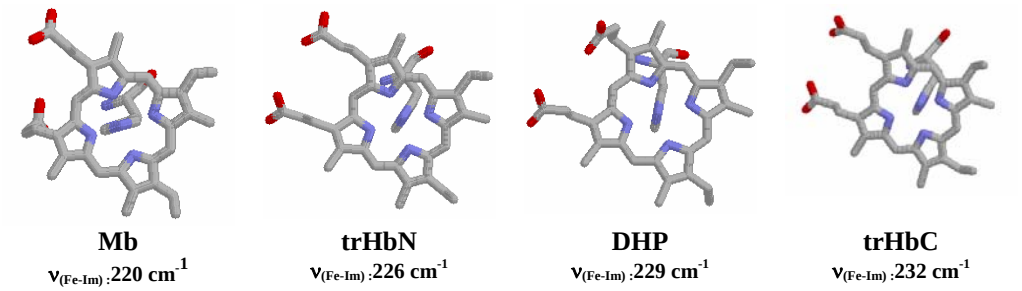

Figure 5.3 Comparison of the proximal histidine orientation with respect to the heme for: deoxy Mb (pdb 1a6n (*12*)), trHbN from *Mycobacterium tuberculosis* (pdb 1idr, (*58*)), DHP (pdb 3dr9, (*41*)), and trHbC from Alga *Chlamydomonas Eugametos* (pdb 1dly, (*59*)).

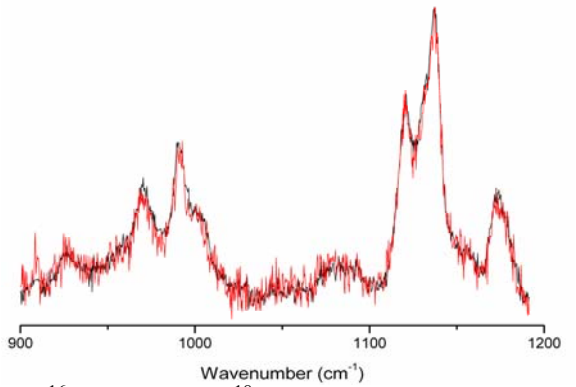

Figure 5.4 RR of DHP-O_2 ($^{16}O_2$ black line, $^{18}O_2$ red line) at pH 6.0, in 0.15 M phosphate buffer. Experimental conditions: 35 μM sample concentracion, 413.1 nm excitation wavelength, 1 mW laser power at the sample, 1.2 cm^{-1} spectral resolution, average of eight spectra with 480 s integration time ($^{16}O_2$) , avergage of three spectra with 300 s integration time ($^{18}O_2$).

5.3.2 Sulfide binding to ferric DHP

As previously reported (*3*), the electronic absorption spectrum of Fe^{3+} DHP at pH 6.0 (Figure 5.5 A a) (Soret band at 406 nm and charge transfer (CT1) band at 637 nm) and the RR spectrum (Figure 5.5 B a) indicate an equilibrium between a predominant hexacoordinated high-spin aquo species (6cHS) (ν_3 at 1483 cm^{-1}) and a 5cHS species

(ν_3 at 1494 cm^{-1}). In the low frequency region (Figure 5.5 C a) the propionyl bending modes overlap at 381 cm^{-1} (*60*). Upon addition of 200-fold excess of sulfide, the UV-Vis spectrum (Figure 5.5 A b) is characteristic of the 6cLS sulfide adduct, with a Soret band centred at 427 nm and β and α bands at 544 and 574 nm, respectively. Accordingly, the RR spectrum (Figure 5.5 B b) shows the typical 6cLS core size marker bands (ν_3 at 1504 cm^{-1}, ν_2 at 1583 cm^{-1}, and ν_{10} at 1637 cm^{-1}) and, in the low frequency region (Figure 5.5 C b) a strong band at 375 cm^{-1} is tentatively assigned to the $\nu_{(Fe\text{-}S)}$ stretching mode by analogy with Tf-trHb (*33*). The band at 385 cm^{-1} is assigned to the heme propionyl bending vibrations (δ(CβCcCd)) (*60*), and similarly to Tf-trHb (*33*), their frequencies upshift by 4 cm^{-1} upon sulfide binding (Figure 5.5 C a-b).

A complete reduction of the protein occurs after exposure to sulfide, either in anaerobic or in aerobic conditions (Figure 5.5 c-d). The reduction is very fast upon gently shaking the sample and it is completed in 2 hrs.

In the absence of oxygen, the appearance of the Soret band at 432 nm, the β band at 557 nm (Figure 5.5 A c), as well as the ν_4 and ν_3 bands at 1354 and 1469 cm^{-1}, respectively (Figure 5.5 B c) and the $\nu_{(Fe\text{-}His)}$ mode at 229 cm^{-1} (Figure 5.5 C c), clearly indicate the formation of the deoxy species. The Fe^{2+} form is then re-oxidised to the Fe^{3+} native form in a week. A complete reduction is also obtained in presence of a substrate (2,4,6-tri-fluoro-phenol) or an inhibitor (4-iodo-phenol) (Figure 5.6), but in these cases the reduction is followed by a fast oxidation to the Fe^{3+} form, probably due to the presence of the disulfide products generated by the oxidation of sulfide (*61*) which appears to be accelerated by the presence of the halo-phenols. In aerobic conditions (Figure 5.5 d) the UV-Vis spectrum maxima (Soret at 418 nm, and β and α bands at 542 and 577 nm, respectively) (Figure 5.5 A d), the RR core size marker frequencies (Figure 5.5 B d) and the presence of the $\nu_{(Fe\text{-}O2)}$ mode at 571 cm^{-1} (Figure 5.5 C d) confirm the formation of the DHP-O_2 adduct. However, in the presence of oxygen, it is important to emphasize the presence in the UV-Vis spectrum (Figure 5.5 A d) of a band at 620 nm due to a small amount of sulfheme which is formed, in analogy to previous findings, by addition of sulfide across the β-β bond of the B pyrrole ring (*24, 62*). Higher amount of sulfheme is readily formed (Figure 5.7) in the presence of sulfide and H_2O_2, however, the protein in the presence of excess of H_2O_2 is unstable and precipitates in a few minutes. According to recent findings it appears that the generation of the sulfheme derivative requires the presence of peroxo or ferryl species and a His (His55) in the distal cavity

(Figure 5.1) properly oriented to form the active ternary complex (*24*). According to this hypothesis,

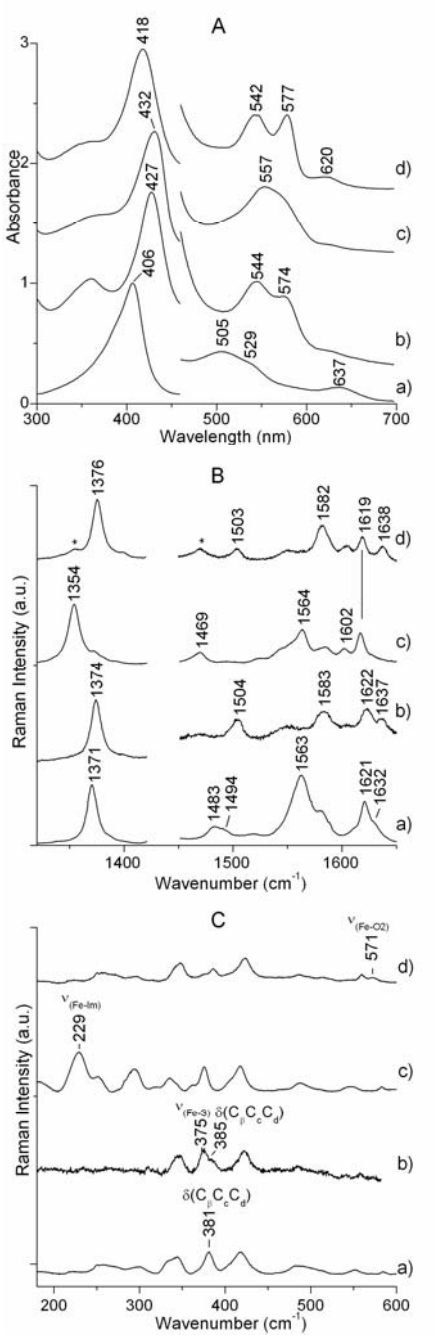

Figure 5.5 UV-Vis (A) and RR spectra in the high (B) and low frequency regions (C) of Fe^{3+} DHP at pH 6 in 0.1 M phosphate buffer. (a) without sulfide; (b) with sulfide, immediately after preparation; (c) after shaking the solution in anaerobic and (d) in aerobic conditions. Experimental conditions: (UV-Vis) Scan rate of 600nm/min. The 450-700 nm region has been expanded of 5-fold. (RR) 413.1 excitation wavelength, 1.2 cm^{-1} spectral resolution (a, b, d); 441.6 nm excitation wavelength, 0.9 cm^{-1} spectral resolution (c). Panel B: 5mW laser power at the sample, average of 6 spectra with 300 s integration time (a), 2mW laser power at the sample average of 3 spectra with 300 s integration time (b); 10 mW laser power at the sample, average of 8 spectra with 300 s integration time (c); 1 mW laser power at the sample, average of 15 spectra with 250 s integration time (d). Panel C: 5mW laser power at the sample, average of 8 spectra with 420 s integration time (a); 2mW laser power at the sample average of 3 spectra

with 300 s integration time (b); 10 mW laser power at the sample, average of 8 spectra with 420 s integration time (c); 1 mW laser power at the sample, average of 15 spectra with 450 s integration time (d). The asterisks indicate spurious bands due to deoxy form. The 1450-1700 cm^{-1} region has been expanded of 3-fold. Spectra have been shifted along the ordinate axis to allow a better visualization.

no sulfheme formation was observed upon sulfide binding to Tf-trHb, since no His residue is present in the distal cavity (*33*). It is noteworthy to mention that in the presence of H_2O_2 and H_2S, HbI from *L. pectinata* forms stable Compound I species without generating the sulfheme derivative (*63*).

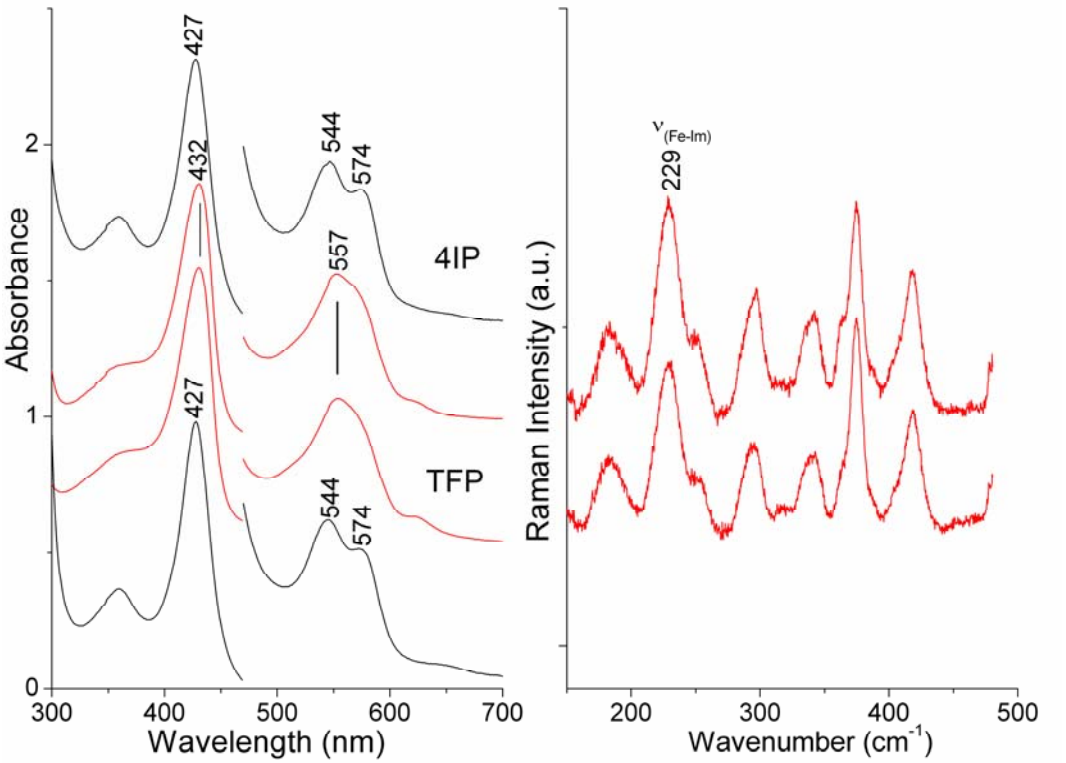

Figure 5.6 UV-Vis (left) and RR spectra in the low frequency regions (right) of DHP-4IP (1:30 molar ratio) and DHP-TFP (1:320 molar ratio) at pH 6 in 0.1 M phosphate buffer, with sulfide (black line), after shaking the solution in anaerobic conditions (red line). Experimental conditions: (UV-Vis) Scan rate of 600 nm/min. The 450-700 nm region has been expanded of 5-fold. (RR) 441.6 excitation wavelength, 0.9 cm^{-1} spectral resolution 10 mW laser power at the sample, average of 8 spectra with 420 s integration time. Spectra have been shifted along the ordinate axis to allow a better visualization.

5.4 Discussion

Structural properties controlling sulfide binding

The data clearly indicate that DHP is able to bind sulfide. Sulfide may coordinate to the heme iron in the monoprotonated (HS^-) or diprotonated (H_2S) form since the pK_a for this equilibrium is reportedly 6.9. The structural determinants for sulfide binding in

DHP can be traced back to the properties of the distal heme cavity. The presence of an aromatic cage and a H-bond donor appear to account for the structural determinants that govern the thermodynamic properties of sulfide binding in hemoglobins. The structure of the sulfide avid HbI from *L. pectinata* has shown that two phenyalanine residues occupy the positions corresponding to CD1 and E11 in myoglobin and the distal E7 residue is glutamine instead of the common histidine of vertebrate myoglobins and

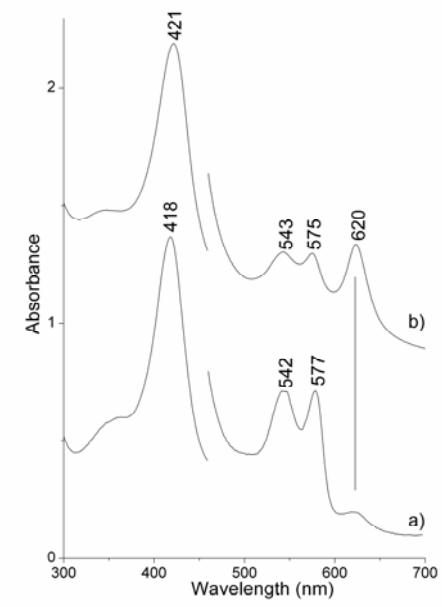

Figure 5.7 Electronic absorption spectra of Fe^{3+} DHP at pH 6 in 0.15 M phosphate buffer in presence of 20-fold excess of sulfide, (a) after shaking the solution in anaerobic and, (b) in presence of 0.1 equivalent of H_2O_2. Scan rate of 600 nm/min. The 450-700 nm region has been expanded 5-fold.

hemoglobins (*64*). The structure of sulfide-bound HbI suggest two different kinds of interactions between the bound ligand and the relevant residues within the distal heme pocket, namely, H-bonding between sulfide and Gln64, and sulfide-aromatic ring electrostatic interactions with Phe43 and Phe68 (*29, 65*). The electrostatic interactions can be regarded as a major determinant of the high H_2S affinity of HbI on the basis of the reported weakness of H-bonds involving S atoms (*66*). On the other hand, Fe-sulfide has been described as a relatively strong H-bond acceptor in DFT calculations on thiolate-bound model porphyrins (*67*). Moreover, molecular dynamics studies of the binding of sulfide to *L. pectinata* HbI suggested that contributions to sulfide affinity come from differences in hydrogen bonding between the heme propionate groups and nearby amino acid residues (*68*). The dynamic model entails a high mobility of the propionate carbonyls that are suggested to be loosely H-bonded to the polypeptide chain and rearrange considerably upon sulfide binding.

The presence of an aromatic cage (Trp119, Tyr54 and Tyr67) and a H-bond donor (Trp119) appear to account for the structural determinants that govern the thermodynamic properties of sulfide binding in Tf-trHb. Furthermore, the RR spectra of Tf-trHb showed an upshift in frequency by 6 cm^{-1} of the band assigned to heme propionyl bending vibrations, as a consequence of sulfide coordination. A shift to a higher frequency indicates a strengthened H-bonding between the propionyl groups of the heme and nearby amino acid side chains (*69*). Therefore, also in Tf-trHb, a substantial rearrangement of the heme propionate geometry was inferred to occur upon sulfide binding.

By analogy to the other sulfide binding heme proteins, the ligand binding to DHP is favoured by an array of aromatic residues. Based on the X-ray structures of Fe^{3+} DHP (*4, 5, 19*), the bound sulfide ligand would be surrounded by four Phe (in positions 21, 24, 35 and 60), and the distal His55 (Figure 5.8). The four Phe residues and the His55 provide the first shell of aromatic residues and, in addition, the His55 may H-bind and stabilize the ligand in the distal cavity. Moreover, the upshift of the heme propionyl bending vibrations upon sulfide addition (Figure 5.5 a-b), suggest a rearrangement of the heme propionate geometry resulting in the formation of stronger H-bonds not present in the unligated protein. Inspection of the X-ray structure of the Fe^{3+} DHP (*5*) indicates that hydrogen bonding between the heme-6-propionate group and amino acid residues is absent, while the presence of moderate hydrogen bonding between a water molecule (H_2O 826) and the heme-7-propionate group can be inferred based on distance criteria [3.1 Å].

Reduction of the heme iron by sulfide

The sulfide complex of DHP is a very reactive system since, after shaking, a complete reduction of the heme iron is observed. Partial heme reduction was previously detected in *L. pectinata* HbI and in some selected variants (*70*) in the presence of sulfide. Pietri and coworkers (*70*) proposed that the presence of a H-bond acceptor is fundamental in order to induce a deprotonation of H_2S, stimulating, in turn, the formation of a ferrous-$SH^{\bullet}$ radical intermediate by one electron transfer from the ferric-SH^{-} moiety. In the presence of a slight excess of ligand, as in the present study, sulfide can react with the ferrous-$SH^{\bullet}$ radical intermediate, producing, in turn, the final deoxy-DHP (or alternatively DHP-O_2) and various disulfide species. This reduction reaction is supported by the observation that interaction of sulfide with other hemeproteins, such as

cytochrome c oxidase (*71, 72*) and flavocytochrome c sulfide dehydrogenase (*73*), induces heme reduction and generates $SH^{\bullet}$ radical intermediates and finally disulfide or elemental sulfur.

Hence, the presence of the highly flexible His55 (*3*) appears to favour the deprotonation of the bound sulfide and thus to trigger the reduction of the heme iron. This mechanism is similar to the role played by the distal histidine in the activation of H_2O_2 for binding to Fe^{3+} heme, which may explain how a peroxidase function is compatible with the observations made in this study. In addition, the complete reduction of the protein upon sulfide binding might be a consequence of the extremely high $E^0(Fe^{3+}/Fe^{2+})$ (200 mV) redox potential of DHP (*49, 74*). This reduction potential is higher than any known hemoglobin except that of *Lumbricus* (*75*) and, moreover, is completely outside the normal range for peroxidases (*76*).

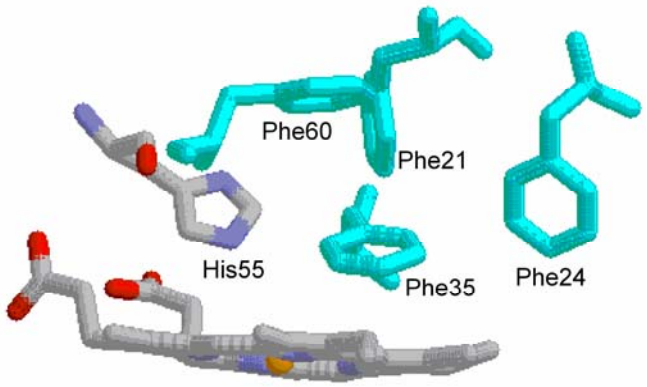

Figure 5.8 Crystal structure of the ferric DHP distal site showing the key aromatic residues involved in sulfide stabilization (pdb 2qfk, (*5*)).

5.5 Conclusions

The chemistry reported herein gives further insight into the function of DHP. The spectroscopic data indicate that the geometry and the high flexibility of the distal histidine, His55, allow DHP to stabilize O_2. More interestingly, the new findings presented here suggest that DHP may play an important role in the catabolism of sulfide, a toxic environmental threat. The flexibility of His55 appears to play a key role in the reactivity of DHP towards sulfide binding as well as for peroxidase activity in the oxidation of highly toxic 2,4,6-tribromophenol to 2,6-dibromo-benzoquinone (*20*). Furthermore, the high redox potential can explain the complete oxidation of sulfide although its high value has not yet been fully explained since all other known

peroxidases show redox potentials significantly negative. The present work suggests that DHP may be tuned for multiple functions required for survival of a relatively simple organism, a stationary terrebellid polychaete, in benthic ecosystems, which has numerous environmental challenges due to both natural and non-natural sources. It is proposed that DHP can work as a detoxifying enzyme with a large spectrum of action.

References

(1) Chen, Y. P., Woodin, S. A., Lincoln, D. E., and Lovell, C. R. (1996) An unusual dehalogenating peroxidase from the marine terebellid polychaete Amphitrite ornata. *J. Biol. Chem. 271*, 4609-4612.

(2) Ferrari, R. P., Laurenti, E., and Trotta, F. (1999) Oxidative 4-dechlorination of 2,4,6-trichlorophenol catalyzed by horseradish peroxidase. *J Biol Inorg Chem 4*, 232-237.

(3) Nicoletti, F. P., Thompson, M. K., Howes, B. D., Franzen, S., and Smulevich, G. (2010) New Insights into the Role of Distal Histidine Flexibility in Ligand Stabilization of Dehaloperoxidase-Hemoglobin from Amphitrite ornata. *Biochemistry 49*, 1903-1912.

(4) LaCount, M. W., Zhang, E., Chen, Y. P., Han, K., Whitton, M. M., Lincoln, D. E., Woodin, S. A., and Lebioda, L. (2000) The crystal structure and amino acid sequence of dehaloperoxidase from Amphitrite ornata indicate common ancestry with globins. *J. Biol. Chem. 275*, 18712-18716.

(5) de Serrano, V., Chen, Z., Davis, M. F., and Franzen, S. (2007) X-ray crystal structural analysis of the binding site in the ferric and oxyferrous forms of the recombinant heme dehaloperoxidase cloned from Amphitrite ornata. *Acta Crystallogr. D Biol. Crystallogr. 63*, 1094-1101.

(6) Smith, A. T., and Veitch, N. C. (1998) Substrate binding and catalysis in heme peroxidases. *Curr. Opin. Chem. Biol. 2*, 269-278.

(7) Feis, A., Marzocchi, M. P., Paoli, M., and Smulevich, G. (1994) Spin state and axial ligand bonding in the hydroxide complexes of metmyoglobin, methemoglobin, and horseradish peroxidase at room and low temperatures. *Biochemistry 33*, 4577-4583.

(8) Howes, B. D., Rodriguez-Lopez, J. N., Smith, A. T., and Smulevich, G. (1997) Mutation of distal residues of horseradish peroxidase: influence on substrate binding and cavity properties. *Biochemistry 36*, 1532-1543.

(9) Neri, F., Indiani, C., Welinder, K. G., and Smulevich, G. (1998) Mutation of the distal arginine in Coprinus cinereus peroxidase--structural implications. *Eur. J. Biochem. 251*, 830-838.

(10) Neri, F., Kok, D., Miller, M. A., and Smulevich, G. (1997) Fluoride binding in hemoproteins: the importance of the distal cavity structure. *Biochemistry 36*, 8947-8953.

(11) Smulevich, G., Feis, A., and Howes, B. D. (2005) Fifteen years of Raman spectroscopy of engineered heme containing peroxidases: what have we learned? *Acc. Chem. Res. 38*, 433-440.

(12) Vojtechovsky, J., Chu, K., Berendzen, J., Sweet, R. M., and Schlichting, I. (1999) Crystal structures of myoglobin-ligand complexes at near-atomic resolution. *Biophys. J. 77*, 2153-2174.

(13) Desbois, A., Lutz, M., and Banerjee, R. (1979) Low-Frequency Vibrations in Resonance Raman Spectra of Horse Heart Myoglobin. Iron-Ligand and Iron-Nitrogen Vibrational Modes. *Biochemistry 18*, 1510-1518.
(14) Yu, N. T. (1986) Resonance Raman studies of ligand binding. *Methods Enzymol. 130*, pp. 350-409.
(15) Nissum, M., Feis, A., and Smulevich, G. (1998) Characterization of soybean seed coat peroxidase: resonance Raman evidence for a structure-based classification of plant peroxidases. *Biospectroscopy 4*, 355-364.
(16) Sitter, A. J., Shifflett, J. R., and Terner, J. (1988) Resonance Raman spectroscopic evidence for heme iron-hydroxide ligation in peroxidase alkaline forms. *J. Biol. Chem. 263*, 13032-13038.
(17) Smulevich, G., Hu, S. Z., Rodgers, K. R., Goodin, D. B., Smith, K. M., and Spiro, T. G. (1996) Heme-protein interactions in cytochrome c peroxidase revealed by site-directed mutagenesis and resonance Raman spectra of isotopically labeled hemes. *Biospectroscopy 2*, 365-376.
(18) Smulevich, G. (1998) Understanding heme cavity structure of peroxidases: comparison of electronic absorption and resonance Raman spectra with crystallographic results. *Biospectroscopy 4*, S3-17.
(19) Lebioda, L., LaCount, M. W., Zhang, E., Chen, Y. P., Han, K., Whitton, M. M., Lincoln, D. E., and Woodin, S. A. (1999) An enzymatic globin from a marine worm. *Nature 401*, 445.
(20) Thompson, M. K., Davis, M. F., de Serrano, V., Nicoletti, F. P., Howes, B. D., Smulevich, G., and Franzen, S. (2010) Internal binding of halogenated phenols in dehaloperoxidase-hemoglobin inhibits peroxidase function. *Biophys. J. 99*, 1586-1595.
(21) Davis, M. F., Bobay, B. G., and Franzen, S. (2010) Determination of Separate Inhibitor and Substrate Binding Sites in the Dehaloperoxidase-Hemoglobin from Amphitrite ornata. *Biochemistry 49*, 1199–1206.
(22) Reiffenstein, R. J., Hulbert, W. C., and Roth, S. H. (1992) Toxicology of hydrogen sulfide. *Annu. Rev. Pharmacol. Toxicol. 32*, 109-134.
(23) Johnson, E. A. (1970) The reversion to haemoglobin of sulphhaemoglobin and its coordination derivatives. *Biochim. Biophys. Acta 207*, 30-40.
(24) Roman-Morales, E., Pietri, R., Ramos-Santana, B., Vinogradov, S. N., Lewis-Ballester, A., and Lopez-Garriga, J. (2010) Structural determinants for the formation of sulfhemeprotein complexes. *Biochem. Biophys. Res. Commun. 400*, 489-492.
(25) Chatfield, M. J., La Mar, G. N., and Kauten, R. J. (1987) Proton NMR characterization of isomeric sulfmyoglobins: preparation, interconversion, reactivity patterns, and structural features. *Biochemistry 26*, 6939-6950.
(26) Szabo, C. (2007) Hydrogen sulphide and its therapeutic potential. *Nat Rev Drug Discov 6*, 917-935.
(27) Bailly, X., and Vinogradov, S. (2005) The sulfide binding function of annelid hemoglobins: relic of an old biosystem? *J. Inorg. Biochem. 99*, 142-150.
(28) Berzofsky, J. A., Peisach, J., and Blumberg, W. E. (1971) Sulfheme proteins. I. Optical and magnetic properties of sulfmyoglobin and its derivatives. *J. Biol. Chem. 246*, 3367-3377.
(29) Kraus, D. W., and Wittenberg, J. B. (1990) Hemoglobins of the Lucina pectinata/bacteria symbiosis. I. Molecular properties, kinetics and equilibria of reactions with ligands. *J. Biol. Chem. 265*, 16043-16053.
(30) Kraus, D. W., Wittenberg, J. B., Lu, J. F., and Peisach, J. (1990) Hemoglobins of the Lucina-Pectinata Bacteria Symbiosis .2. An Electron-Paramagnetic

Resonance and Optical Spectral Study of the Ferric Proteins. *J. Biol. Chem. 265*, 16054-16059.

(31) Boffi, A., Wittenberg, J. B., and Chiancone, E. (1997) Circular dichroism spectroscopy of Lucina I hemoglobin. *FEBS Lett. 411*, 335-338.

(32) Brittain, T., Yosaatmadja, Y., and Henty, K. (2008) The interaction of human neuroglobin with hydrogen sulphide. *IUBMB Life 60*, 135-138.

(33) Nicoletti, F. P., Comandini, A., Bonamore, A., Boechi, L., Boubeta, F. M., Feis, A., Smulevich, G., and Boffi, A. (2010) Sulfide binding properties of truncated hemoglobins. *Biochemistry 49*, 2269-2278.

(34) Weber, R. E., and Vinogradov, S. N. (2001) Nonvertebrate hemoglobins: functions and molecular adaptations. *Physiol. Rev. 81*, 569-628.

(35) Lincoln, D. E., Fielman, K. T., Marinelli, R. L., and Woodin, S. A. (2005) Bromophenol accumulation and sediment contamination by the marine annelids Notomastus lobatus and Thelepus crispus. *Biochem. Syst. Ecol. 33*, 559-570.

(36) Belyea, J., Gilvey, L. B., Davis, M. F., Godek, M., Sit, T. L., Lommel, S. A., and Franzen, S. (2005) Enzyme function of the globin dehaloperoxidase from Amphitrite ornata is activated by substrate binding. *Biochemistry 44*, 15637-15644.

(37) Edwards, S. L., and Poulos, T. L. (1990) Ligand binding and structural perturbations in cytochrome c peroxidase. A crystallographic study. *J. Biol. Chem. 265*, 2588-2595.

(38) Han, K., Woodin, S. A., Lincoln, D. E., Fielman, K. T., and Ely, B. (2001) Amphitrite ornata, a marine worm, contains two dehaloperoxidase genes. *Mar. Biotechnol. (NY) 3*, 287-292.

(39) Weber, R. E., Mangum, C., Steinman, H., Bonaventura, C., Sullivan, B., and Bonaventura, J. (1977) Hemoglobins of two terebellid polychaetes: Enoplobranchus sanguineus and Amphitrite ornata. *Comp. Biochem. Physiol. A Comp. Physiol. 56*, 179-187.

(40) Franzen, S., Gilvey, L. B., and Belyea, J. L. (2007) The pH dependence of the activity of dehaloperoxidase from Amphitrite ornata. *Biochim. Biophys. Acta 1774*, 121-130.

(41) Chen, Z., de Serrano, V., Betts, L., and Franzen, S. (2009) Distal histidine conformational flexibility in dehaloperoxidase from Amphitrite ornata. *Acta Crystallogr. D Biol. Crystallogr. 65*, 34-40.

(42) Davis, M. F., Gracz, H., Vendeix, F. A., de Serrano, V., Somasundaram, A., Decatur, S. M., and Franzen, S. (2009) Different modes of binding of mono-, di-, and trihalogenated phenols to the hemoglobin dehaloperoxidase from Amphitrite ornata. *Biochemistry 48*, 2164-2172.

(43) Nienhaus, K., Nickel, E., Davis, M. F., Franzen, S., and Nienhaus, G. U. (2008) Determinants of Substrate Internalization in the Distal Pocket of Dehaloperoxidase Hemoglobin of Amphitrite ornata. *Biochemistry 47*, 12985-12994.

(44) Kitagawa, T. (1988) in: T.G. Spiro (Ed.), Biological Applications of Raman Spectroscopy: Resonance Raman Spectra of Hemes and Metalloproteins, Wiley, New York,. 97-131.

(45) Smulevich, G., Mauro, J. M., Fishel, L. A., English, A. M., Kraut, J., and Spiro, T. G. (1988) Heme pocket interactions in cytochrome c peroxidase studied by site-directed mutagenesis and resonance Raman spectroscopy. *Biochemistry 27*, 5477-5485.

(46) Franzen, S., Roach, M. P., Chen, Y.-P., Dyer, R. B., Woodruff, W. H., and Dawson, J. H. (1998) The Unusual Reactivities of Amphitrite ornate Notomastus

lobatus Chloroperoxidase Do Not Imidazolate Proximal Heme Iron Ligand. *J. Am. Chem. Soc. 120*, 4658-4661.

(47) Couture, M., Das, T. K., Lee, H. C., Peisach, J., Rousseau, D. L., Wittenberg, B. A., Wittenberg, J. B., and Guertin, M. (1999) Chlamydomonas chloroplast ferrous hemoglobin. Heme pocket structure and reactions with ligands. *J. Biol. Chem. 274*, 6898-6910.

(48) Samuni, U., Ouellet, Y., Guertin, M., Friedman, J. M., and Yeh, S. R. (2004) The absence of proximal strain in the truncated hemoglobins from Mycobacterium tuberculosis. *J. Am. Chem. Soc. 126*, 2682-2683.

(49) D'Antonio, J., D'Antonio, E. L., Thompson, M. K., Bowden, E. F., Franzen, S., Smirnova, T., and Ghiladi, R. A. (2010) Spectroscopic and mechanistic investigations of dehaloperoxidase B from Amphitrite ornata. *Biochemistry 49*, 6600-6616.

(50) Egawa, T., and Yeh, S. R. (2005) Structural and functional properties of hemoglobins from unicellular organisms as revealed by resonance Raman spectroscopy. *J. Inorg. Biochem. 99*, 72-96.

(51) Hirota, S., Ogura, T., Appelman, E. H., Shinzawaitoh, K., Yoshikawa, S., and Kitagawa, T. (1994) Observation of a New Oxygen-Isotope-Sensitive Raman Band for Oxyhemoproteins and Its Implications in Heme Pocket Structures. *J. Am. Chem. Soc. 116*, 10564-10570.

(52) Potter, W. T., Tucker, M. P., Houtchens, R. A., and Caughey, W. S. (1987) Oxygen infrared spectra of oxyhemoglobins and oxymyoglobins. Evidence of two major liganded O2 structures. *Biochemistry 26*, 4699-4707.

(53) Van Wart, H. E., and Zimmer, J. (1985) Resonance Raman evidence for the activation of dioxygen in horseradish oxyperoxidase. *J. Biol. Chem. 260*, 8372-8377.

(54) Das, T. K., Couture, M., Ouellet, Y., Guertin, M., and Rousseau, D. L. (2001) Simultaneous observation of the O---O and Fe---O2 stretching modes in oxyhemoglobins. *Proc. Natl. Acad. Sci. U S A 98*, 479-484.

(55) Mukai, M., Savard, P. Y., Ouellet, H., Guertin, M., and Yeh, S. R. (2002) Unique ligand-protein interactions in a new truncated hemoglobin from Mycobacterium tuberculosis. *Biochemistry 41*, 3897-3905.

(56) Davydov, R., Osborne, R. L., Shanmugam, M., Du, J., Dawson, J. H., and Hoffman, B. M. (2010) Probing the Oxyferrous and Catalytically Active Ferryl States of Amphitrite ornata Dehaloperoxidase by Cryoreduction and EPR/ENDOR Spectroscopy. Detection of Compound I. *J. Am. Chem. Soc. In press*.

(57) Hirota, S., Tiansheng, L., Phillips, G. N., Olson, J. S., Mukai, M., and Kitagawa, T. (1996) Perturbation of the Fe–O2 bond by nearby residues in heme pocket: observation of n_{Fe-O2} raman bands for oxymyoglobin mutants. *J. Am. Chem. Soc. 118*, 7845–7846.

(58) Milani, M., Pesce, A., Ouellet, Y., Ascenzi, P., Guertin, M., and Bolognesi, M. (2001) Mycobacterium tuberculosis hemoglobin N displays a protein tunnel suited for O2 diffusion to the heme. *Embo J. 20*, 3902-3909.

(59) Pesce, A., Couture, M., Dewilde, S., Guertin, M., Yamauchi, K., Ascenzi, P., Moens, L., and Bolognesi, M. (2000) A novel two-over-two alpha-helical sandwich fold is characteristic of the truncated hemoglobin family. *Embo J. 19*, 2424-2434.

(60) Hu, S., Morris, I. K., Singh, J. P., Smith, K. M., and Spiro, T. G. (1993) Complete assignement of Cytochrome c resonance Raman spectra via enzymatic

reconstitution with isotopically lebeled hemes. *J. Am. Chem. Soc. 115*, 12446-12458.

(61) Romero, F. J., Ordonez, I., Arduini, A., and Cadenas, E. (1992) The reactivity of thiols and disulfides with different redox states of myoglobin. Redox and addition reactions and formation of thiyl radical intermediates. *J. Biol. Chem. 267*, 1680-1688.

(62) Evans, S. V., Sishta, B. P., Mauk, A. G., and Brayer, G. D. (1994) Three-dimensional structure of cyanomet-sulfmyoglobin C. *Proc. Natl. Acad. Sci. U S A 91*, 4723-4726.

(63) Gavira, J. A., Camara-Artigas, A., De Jesus-Bonilla, W., Lopez-Garriga, J., Lewis, A., Pietri, R., Yeh, S. R., Cadilla, C. L., and Garcia-Ruiz, J. M. (2008) Structure and ligand selection of hemoglobin II from Lucina pectinata. *J. Biol. Chem. 283*, 9414-9423.

(64) Rizzi, M., Wittenberg, J. B., Coda, A., Ascenzi, P., and Bolognesi, M. (1996) Structural bases for sulfide recognition in Lucina pectinata hemoglobin I. *J. Mol. Biol. 258*, 1-5.

(65) Cerda-Colon, J. F., Silfa, E., and Lopez-Garriga, J. (1998) Unusual rocking freedom of the heme in the hydrogen sulfide-binding hemoglobin from Lucina pectinata. *J. Am. Chem. Soc. 120*, 9312-9317.

(66) Biswal, H. S., Shirhatti, P. R., and Wategaonkar, S. (2009) O-H...O versus O-H...S hydrogen bonding I: Experimental and computational studies on the p-cresol x H2O and p-cresol x H2S complexes. *J. Phys. Chem. A 113*, 5633-5643.

(67) Dey, A., Okamura, T. A., Ueyama, N., Hedman, B., Hodgson, K. O., and Solomon, E. I. (2005) Sulfur K-edge XAS and DFT calculations on P450 model complexes: effects of hydrogen bonding on electronic structure and redox potentials. *J. Am. Chem. Soc. 127*, 12046-12053.

(68) Fernandez-Alberti, S., Bacelo, D. E., Binning, R. C., Echave, J., Chergui, M., and Lopez-Garriga, J. (2006) Sulfide-binding hemoglobins: Effects of mutations on active-site flexibility. *Biophys. J. 91*, 1698-1709.

(69) Peterson, E. S., Friedman, J. M., Chien, E. Y., and Sligar, S. G. (1998) Functional implications of the proximal hydrogen-bonding network in myoglobin: a resonance Raman and kinetic study of Leu89, Ser92, His97, and F-helix swap mutants. *Biochemistry 37*, 12301-12319.

(70) Pietri, R., Lewis, A., Leon, R. G., Casabona, G., Kiger, L., Yeh, S. R., Fernandez-Alberti, S., Marden, M. C., Cadilla, C. L., and Lopez-Garriga, J. (2009) Factors controlling the reactivity of hydrogen sulfide with hemeproteins. *Biochemistry 48*, 4881-4894.

(71) Hill, B. C., Woon, T. C., Nicholls, P., Peterson, J., Greenwood, C., and Thomson, A. J. (1984) Interactions of sulphide and other ligands with cytochrome c oxidase. An electron-paramagnetic-resonance study. *Biochem. J. 224*, 591-600.

(72) Nicholls, P., and Kim, J. K. (1981) Oxidation of sulphide by cytochrome aa3. *Biochim. Biophys. Acta 637*, 312-320.

(73) Steudel, R. (1996) Mechanism for the Formation of Elemental Sulfur from Aqueous Sulfide in Chemical and Microbiological Desulfurization Processes. *Ind. Eng. Chem. Res. 35*, 1417–1423.

(74) de Serrano, V., D'Antonio, J., Franzen, S., and Ghiladi, R. A. (2010) Structure of dehaloperoxidase B at 1.58 A resolution and structural characterization of the AB dimer from Amphitrite ornata. *Acta Crystallogr. D Biol. Crystallogr. 66*, 529-538.

(75) Harrington, J. P., Kobayashi, S., Dorman, S. C., Zito, S. L., and Hirsch, R. E. (2007) Acellular invertebrate hemoglobins as model therapeutic oxygen carriers: unique redox potentials. *Artif. Cells Blood Substit. Immobil. Biotechnol. 35*, 53-67.

(76) Battistuzzi, G., Bellei, M., Bortolotti, C. A., and Sola, M. (2010) Redox properties of heme peroxidases. *Arch. Biochem. Biophys. 500*, 21-36.

Chapter 6

Structural properties of *Eleginops Maclovinus* hemoglobin, a primitive notothenioid fish of temperate latitudines

Antonello Merlino, Luigi Vitagliano, Anna Balsamo, **Francesco P. Nicoletti**, Barry D. Howes, Daniela Giordano, Daniela Coppola, Guido di Prisco, Cinzia Verde, Giulietta Smulevich, Lelio Mazzarella, and Alessandro Vergara.

Crystallization, preliminary X-ray diffraction studies and Raman microscopy of the major hemoglobin from the sub-Antarctic fish Eleginops maclovinus in the carbomonoxy form

Acta Crystallogr. Sect. F: Struct. Biol. Cryst. Commun. (2010) F66, 1536-1540.

6.1 Introduction

The knowledge on protein thermal adaptation and genotypic modifications associated with environmental changes may take advantage of the comparison of differently adapted closely related species. An excellent system for studying hemoglobin (Hb) adaptation to low temperatures is provided by *Notothenioidei*, a group of related species constituting the dominant suborder of teleosts living in Antarctica. The initial diversification of the non-Antarctic notothenioid group, including *Bovichtidae*, *Pseudaphritidae* and *Eleginopidae*, was induced by the cooling of circumpolar waters (*1*) following the fragmentation of Gondwana (*2*). As a consequence, *Bovichtidae* (except one species in the family), monotypic *Pseudaphritidae* and *Eleginopidae* have sub-Antarctic distributions (*i.e.*, north of the Antarctic Polar Front in waters around New

Zealand, Australia and South America) (*1, 2*) and live at temperatures of approximately 5-15 °C (*3*). The members of these three families have never experienced near-freezing water temperatures, and the absence of antifreeze glycoproteins (AFGPs) supports this scenario (*2*).

On the other hand, the high-Antarctic notothenioid group comprises six families, which are highly stenothermal, and their ability to cope with the ongoing increases in environmental temperatures might be reduced, due to the absence of temperature-mediated gene expression, including the heat-shock response (*4*).

Eleginops maclovinus, the sister group of high-Antarctic notothenioids, is the ideal subject for studying the Hb systems that did not undergo historical exposure to the Antarctic climate. It is endemic to the temperate and sub-Antarctic waters of southern South America including the Falkland Islands (*1*). The blood of *E. maclovinus* shows one cathodal (Hb C, accounting for 25%) and two anodal components (Hb 1 and Hb 2, accounting for 70 and 5%, respectively) (*5*).

Although the Fe^{2+} R and T canonical structures of high-Antarctic fish Hbs have been shown to be very close to those of temperate fish, the investigation of their Fe^{3+} forms has recently re-opened the questions on (i) the role of heterogeneity arising from different behaviour of the α and β chains (*6, 7*), and (ii) the landscape of accessible quaternary structures (*7, 8*) potentially relevant in the interpretation of the role of physiological effectors and Root effect in regulating the function of Hb.

In this thesis a spectroscopic characterization of the protein in solution and as single crystal has been carried out. No differences have been found in terms of the spin and the axial coordination between solution and the crystal states.

6.2 Ferric forms: results and discussion

The electronic absorption spectrum of hemoglobin from *E. maclovinus* Hb1 (Fe^{3+}) at pH 7.6 (Figure 6.1) characterized by bands at 407, 493, 531, 557 and 631 nm is indicative of a mixture of a 6cHS aquo form (CT1 at 631 nm) (*9*) and a significant 6cLS component (as previously observed for *P. urvillii* Hb (*10*). Accordingly, the high frequency RR spectrum (Figure 6.2) reveals a 6cHS (1479 cm^{-1} [ν_3], 1562 cm^{-1} [ν_2]) and a 6cLS species (1507 cm^{-1} [ν_3], 1578 cm^{-1} [ν_2], 1607 cm^{-1} [ν_{37}] and 1640 cm^{-1} [ν_{10}]) (*11*). In order to gain insight into the nature of the ligands which give rise to the 6cLS species, we studied *E. maclovinus* Hb1 (Fe^{3+}) in the presence of exogenous ligands such as imidazole and cyanide. The electronic absorption spectrum of the adduct formed

upon imidazole binding at pH 7.6 (Figure 6.1) shows bands at 411, 531 and 557 nm, typical of a bis-His (N-Fe^{3+}-N) 6cLS species (*12*). The corresponding RR spectrum is characterized by bands at 1505 [ν_3], at 1548 [ν_{38}] at 1580 [ν_2], at 1597 [ν_{37}] and at 1640 cm^{-1} [ν_{10}] (Figure 6.2). The similarity of the visible region [bands at 531 nm (β-band) and 557 nm (α-band)] between the spectra of *E. maclovinus* Hb1 (Fe^{3+}) and its imidazole adduct strongly indicates that the *E. maclovinus* Hb1 (Fe^{3+}) 6cLS species results from a bis-histidine hemichrome species, rather than a hydroxide complex as the case of human Hb A (*13*).

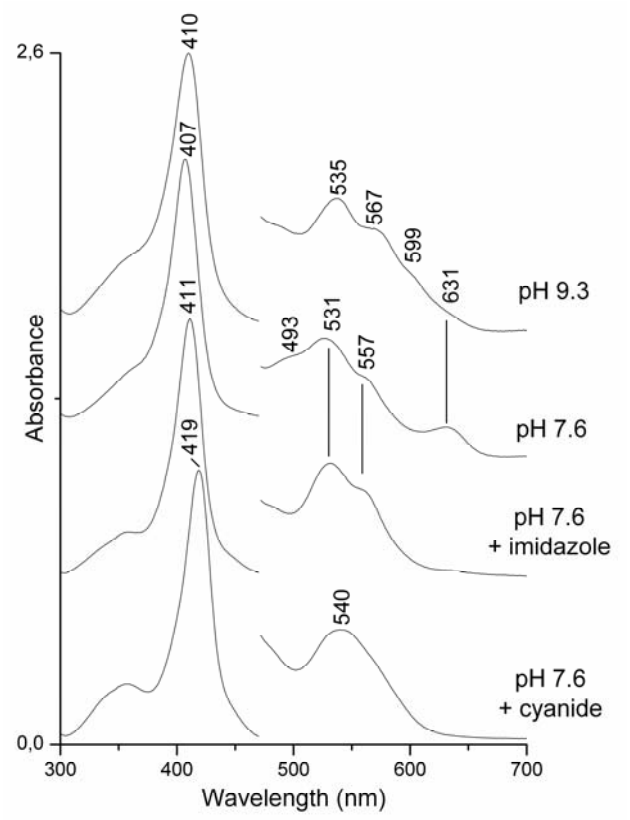

Figure 6.1 UV-Vis spectra of *E. maclovinus* Hb1 (Fe^{3+}) at pH 9.3 (50 mM glycine) and at pH 7.6 (50 mM TRIS), in absence and in the presence of imidazole and cyanide at pH 7.6. The spectra have been shifted along the ordinate axis to allow better visualization. Scan rate of 600 nm/min.

Hemichrome formation in tetrameric Hbs was initially associated only with a partial unfolding of the native structure (*14*). However, it has been recently demonstrated that the hemichrome can also be physiological and functional sub-states of Hbs (*8*) and it is characterized by the reversibility in different environmental conditions and the absence of precipitation and heme release that usually characterize denaturated proteins (*14*). A clear case of a tetrameric Hb in a partial hemichrome state is the air-oxidised Hb from the Antarctic fish *T. newnesi* (*6*). Recently, a detailed analysis of formation and stability

in solution and crystal forms of the hemichrome species found in several Antarctic fish Hbs, has been performed by complementing X-ray crystallography with optical and RR spectroscopy (*7, 15*). Therefore, the hemichrome in Hbs from Notothenioidei fishes living in the Antarctic (*T. bernacchii*, *T. newnesi*) and in temperate climates (*E. maclovinus, P. urvillii*) might have a common origin (*1*).

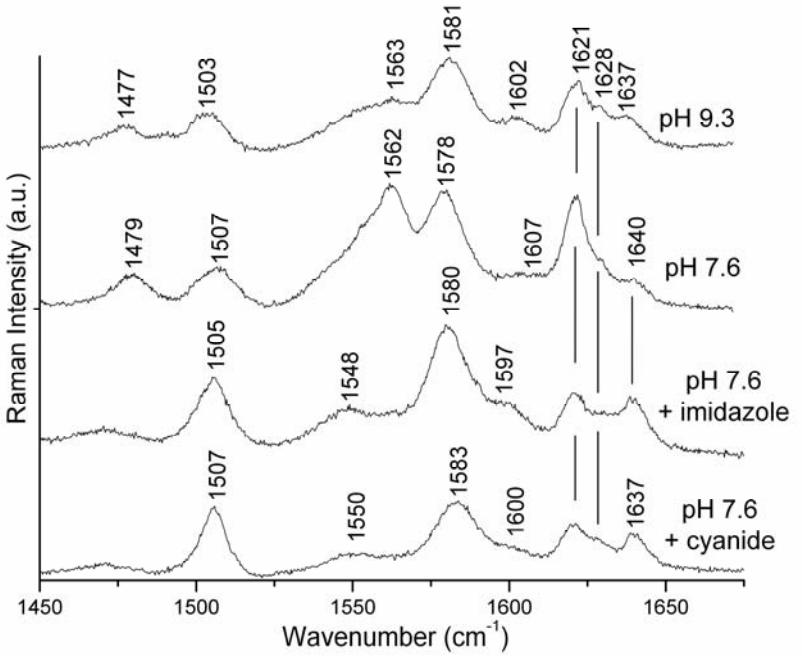

Figure 6.2 High frequency region RR spectra of *E. maclovinus* Hb1 (Fe^{3+}). Experimental conditions: 413.1 nm excitation wavelength, 1.2 cm^{-1} spectral resolution. pH 9.3**:** 4 mW laser power at the sample, average of six spectra with 900 s integration time; pH 7.6: 11 mW laser power at the sample, average of four spectra with 420 s integration time; with imidazole: 8 mW laser power at the sample, average of six spectra with 300 s integration time; with cyanide: 10 mW laser power at the sample, average of four spectra with 960 s integration time. The intensities are normalized to that of the ν_4 band (not shown). The spectra have been shifted along the ordinate axis to allow better visualization.

At pH 9.3 the absorption spectrum of *E. maclovinus* Hb1 (Fe^{3+}) is characterized by bands at 410, 535, 567, 599 and 631 nm (Figure 6.1), indicative of a dominant hydroxide 6cLS with a minor amount of hydroxide 6cHS (CT at about 599 nm), as previously observed for hemoglobin from *P. urvillii* Hb (*10*). The presence at this pH of the HS charge transfer band (CT1) at 631 nm indicates that the alkaline transition to the hydroxide complex is not complete, but the protein denatures at pH values higher than 9.3. The corresponding RR spectrum (Figure 6.2) confirms a mixture of a 6cHS species (1477 cm^{-1} [ν_3], 1563 cm^{-1} [ν_2]) and a 6cLS form (1503 cm^{-1} [ν_3], 1581 cm^{-1} [ν_2], 1602 cm^{-1} [ν_{37}], and 1637 cm^{-1} [ν_{10}]). On the basis of the isotopic shift in D_2O buffer, two $\nu_{(Fe\text{-}OH)}$ stretching modes have been identified at 494 cm^{-1} (481 cm^{-1} in D_2O) and 558

cm^{-1} (548 cm^{-1} in D_2O) (Figure 6.3) and assigned to the high spin and low spin $\nu_{(Fe\text{-}OH)}$ modes, respectively. While the frequency of the high spin $\nu_{(Fe\text{-}OH)}$ stretching mode is similar to that previously observed for human Hb A (Table 6.1) (*16*), the frequency of the low spin $\nu_{(Fe\text{-}OH)}$ stretching mode is 5 cm^{-1} higher suggesting a stronger hydrogen bond.

The UV-Vis spectrum of the cyanide adduct (Figure 6.1), typical of a 6cLS species, has a Soret maximum at 419 nm and a β band at 540 nm. Accordingly, the RR core size marker bands are observed at 1507 [ν_3], 1550 [ν_{38}], 1583 [ν_2], 1602 [ν_{37}], and 1637 cm^{-1} [ν_{10}]) (Figure 6.2). In the low frequency region (Figure 6.3), the $\nu_{(Fe\text{-}CN)}$ stretching mode was observed at 452 cm^{-1} (443 cm^{-1} in presence of $^{13}C^{15}N$). This value is identical to that of human Hb A (*17*), indicating that the strength of ligand coordination to the iron is the same in the two proteins.

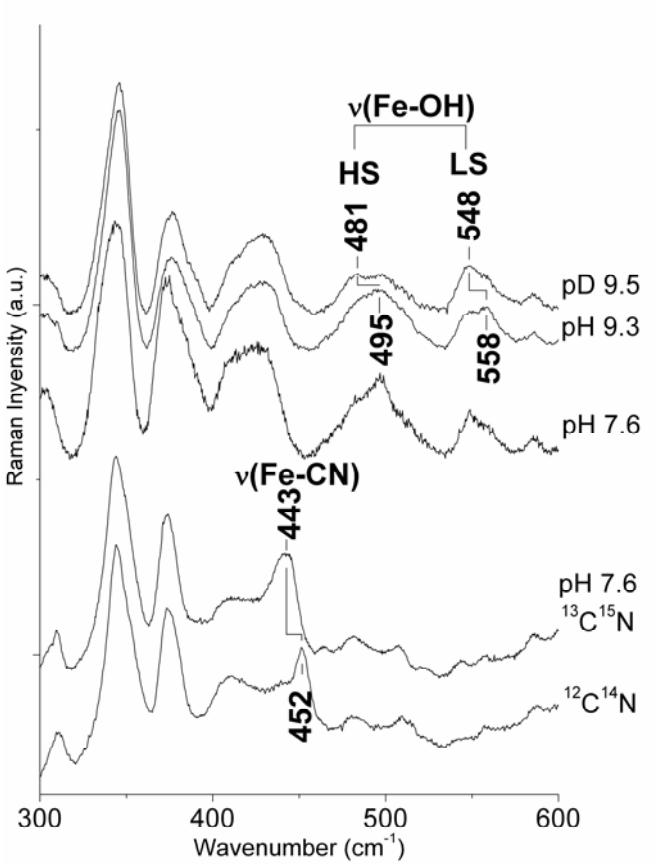

Figure 6.3 Low frequency region RR spectra of *E. maclovinus* Hb1 (Fe^{3+}). Experimental conditions: 413.1 nm excitation wavelength, 1.2 cm^{-1} spectral resolution. From the top to the bottom, pD 9.5: 3 mW laser power at the sample, average of thirteen spectra with 1800 s integration time; pH 9.3: 3 mW laser power at the sample, average of eight spectra with 1920 s integration time; pH 7.6: 11 mW laser power at the sample, average of sixteen spectra with 420 s integration time, with cyanide ($^{13}C^{15}N$ and $^{12}C^{14}N$): 10 mW laser power at the sample, average of seven spectra with 770 s integration time. The intensities are normalized to that of the ν_7 band (not shown). The spectra have been shifted along the ordinate axis to allow better visualization.

6.3 Ferrous forms: results and discussion

6.3.1 Deoxy form

To gain insight into the structure of the proximal heme cavity, the *E. maclovinus* Hb1 was studied in the Fe^{2+} oxidation state at pH 7.6. After reduction, the UV-Vis spectrum (Soret band at 429 nm and β band at 555 nm, Figure 6.4 A) is similar to the deoxy species of *P. urvillii* Hb (Fe^{2+}) (*10*), 3 nm blue shifted respect to human Hb A (*13, 18*) and is characteristic of a 5cHS heme state. Accordingly, the corresponding high frequency RR spectrum is characteristic of a 5cHS species with bands at 1471 cm^{-1} [ν_3], at 1524 cm^{-1} [ν_{38}], at 1564 cm^{-1} [ν_2], at 1604 cm^{-1} [ν_{10}], and at 1618-1627 cm^{-1} [$\nu_{(C=C)}$] (Figure 6.4 B). The presence of two different vinyl stretches respect to human Hb

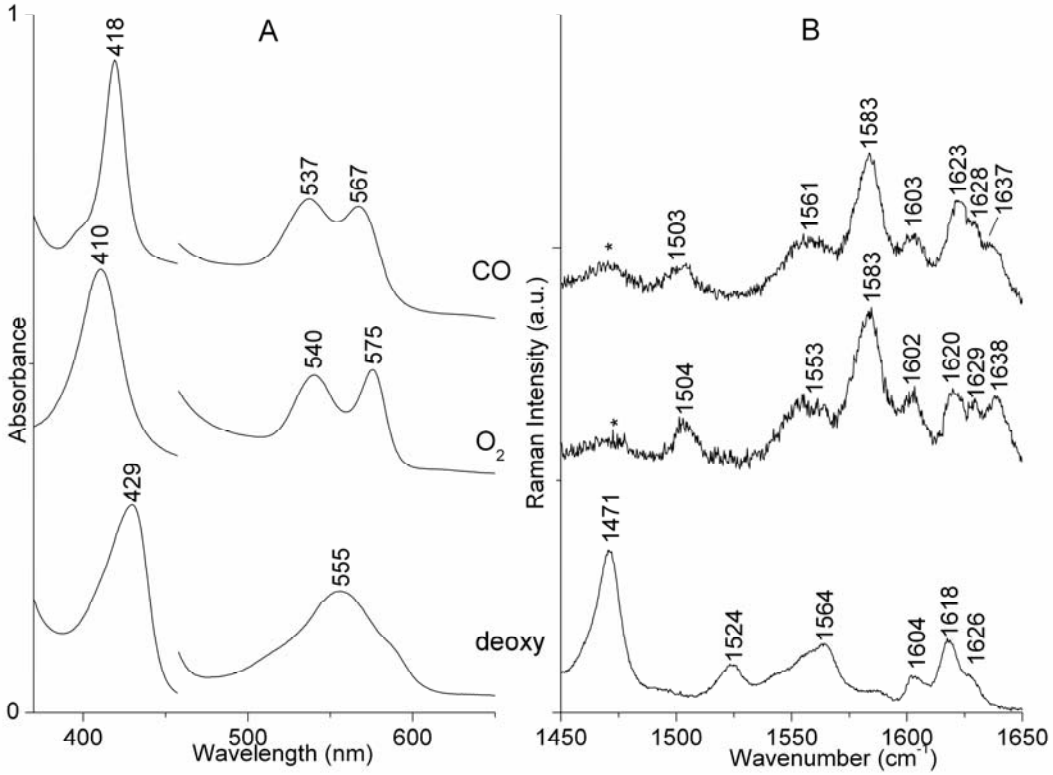

Figure 6.4 UV-Vis (Panel A) and high frequency RR spectra (Panel B) of deoxy, (Fe^{2+})-O_2 and -CO adducts of *E. maclovinus* Hb1 at pH 7.6, in 50 mM Tris buffer. The spectra have been shifted along the ordinate axis to allow better visualization. Experimental conditions. UV-Vis: scan rate of 600 nm/min. RR: Experimental conditions: 441.6 nm excitation wavelength, 0.9 cm^{-1} spectral resolution. (deoxy): 413.1 nm excitation wavelength, 1.2 cm^{-1} spectral resolution (-O_2 and –CO). Deoxy: 13 mW laser power at the sample, average of three spectra with 480 s integration time; (Fe^{2+})-O_2: 10 mW laser power at the sample (using a cylindrical lens to focus the laser beam on the sample), average of eight spectra with 120 s integration time; (Fe^{2+})-CO: 3 mW laser power at the sample (using a cylindrical lens), average of two spectra with 300 s integration time. The intensities are normalized to that of the ν_4 band (not shown). The asterisk indicates the spurious band due to the photolized form.

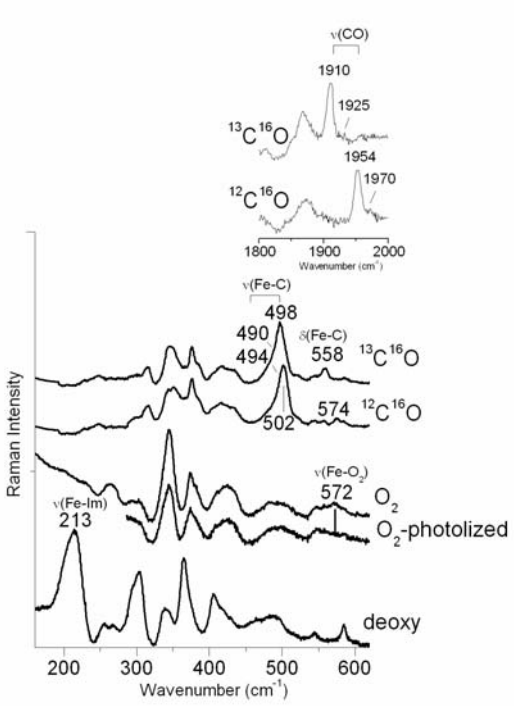

Figure 6.5 RR spectra in the low frequency region of *E. maclovinus* Hb1 in its deoxy, (Fe^{2+})-O_2 and -CO adducts at pH 7.6, in 50 mM Tris-HCl buffer. Experimental conditions: 441.6 nm excitation wavelength, 0.9 cm^{-1} spectral resolution (deoxy); 413.1 nm excitation wavelength, 1.2 cm^{-1} spectral resolution [(Fe^{2+})-O_2 and (Fe^{2+})–CO]. Deoxy: 13 mW laser power at the sample, average of four spectra with 450 s integration time; (Fe^{2+})-O_2: 10 mW laser power at the sample (using a cylindrical lens to broaden the laser beam on the sample), average of six spectra with 420 s integration time; [(Fe^{2+})-O_2 photolized: 5 mW laser power at the sample (using spherical lens to focus the laser beam on the sample), average of three spectra with 300 s integration time; [(Fe^{2+})-CO: 3 mW laser power at the sample (using a cylindrical lens), ($^{13}C^{16}O$) average of three spectra with 700 s integration time, ($^{12}C^{16}O$) average of four spectra with 700 s integration time. The intensities are normalized to that of the ν_7 band (not shown). The inset shows the $\nu_{(CO)}$ stretching mode region, 3.5 cm^{-1} spectral resolution; ($^{13}C^{16}O$) average of two spectra with 3600 s integration time, ($^{12}C^{16}O$) average of three spectra with 2700 s integration time. The intensities are normalized to that of the ν_4 band (not shown). The spectra have been shifted along the ordinate axis to allow better visualization.

(overlapped at 1622 cm^{-1}) (*18*) is due to a different degree of conjugation between the vinyls and porphyrin π group. In particular the presence of an higher stretching frequency corresponds to a lower degree of conjugation, shifting the value of π→π* to higher energy, and thus shifting the Soret maximum to the blue.

The low-frequency RR spectrum is shown in Figure 6.5. In human Hb A, the iron histidine bond is strained by the F-helix due to the T state quaternary interactions, as reflected by a low $\nu_{(Fe\text{-}Im)}$ frequency at 215 cm^{-1} ((*19*), Table 6.1). Similarly, the RR low frequency region of *E. maclovinus* Hb1 (Fe^{2+}) (Figure 6.5) is characterized by the presence of a strong band at 213 cm^{-1}, not present in the Fe^{3+} form, which is assigned to the $\nu_{(Fe\text{-}Im)}$ iron-histidine stretching mode. The absence of significant differences in the

$\nu_{(Fe\text{-}Im)}$ stretching frequencies (Table 6.1) between the deoxy human Hb A, *E. maclovinus* Hb1 (Fe^{2+}) and *P. urvillii* Hb (Fe^{2+}) (*10*) suggests that the proximal cavity in *E. maclovinus* Hb1 is largely unchanged compared to human Hb A and *P. urvillii* Hb.

6.3.2 Fe^{2+}-CO complex

The electronic absorption spectrum of the CO complex of *E. maclovinus* Hb1 (Fe^{2+}) (Figure 6.4 A), similar to that previously reported for human Hb A (*20*), and its corresponding high frequency RR spectrum (Figure 6.4 B) are characteristic of a 6cLS species.

The isotopic shift observed in the ^{13}CO adduct (Figure 6.5) allows us to identify two conformers, form 1 with $\nu_{(Fe\text{-}CO)}/\nu_{(CO)}$ stretching bands at 502/1954 cm^{-1}, and form 2 at 494/1970 cm^{-1}. The band at 574 cm^{-1}, which shifts to 558 cm^{-1} in ^{13}CO, is assigned to the $\delta_{(Fe\text{-}CO)}$ bending mode (Figure 6.5). Both the *E. maclovinus* Hb1 (Fe^{2+})-CO conformers fall on the histidine $\nu_{(Fe\text{-}CO)}/\nu_{(CO)}$ back-bonding correlation line (Figure 6.6). The frequencies of the predominant form (form 1), are close to those observed for *P. urvillii* and *T. bernacchii* Hbs (502, and 1952-1951 cm^{-1}, respectively) (*7, 10*) and slightly different from those of human Hb A-CO (507 and 1951 cm^{-1}) (*20*) (Figure 6.6).

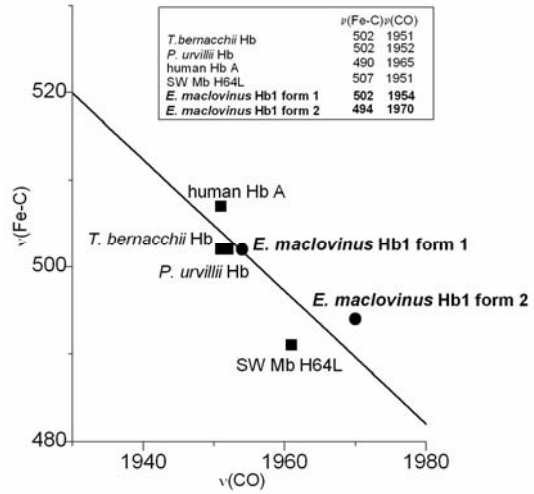

Figure 6.6 Plot of the $\nu_{(Fe\text{-}CO)}$ versus $\nu_{(CO)}$ frequencies observed in the CO complexes of the (Fe^{2+})-CO adducts of the heme proteins mentioned in the text. The line indicates the back-bonding correlation for six-coordinate CO heme proteins with imidazole as sixth ligand, as reported previously (*21*).

On the basis of the $\nu_{(Fe\text{-}CO)}$ and $\nu_{(CO)}$ correlation plot (*21, 22*), form 1 is consistent with a bound CO stabilized by a weaker H-bonding interaction with the distal histidine compared to human Hb A-CO. The small amount of form 2, which has been revealed

only after a band fitting analysis (Figure 6.7) is characterized by $\nu_{(Fe\text{-}CO)}$ and $\nu_{(CO)}$ frequencies similar to those of H64V sperm whale myoglobin (SWMb) (*23, 24*) (Figure 6.6) and therefore, consistent with a conformer having no polar interactions with the surrounding amino acids. Interestingly, forms 1 and 2 are in a thermal equilibrium since upon lowering the temperature of the solution to 15 K only form 1 remains (Figure 6.7).

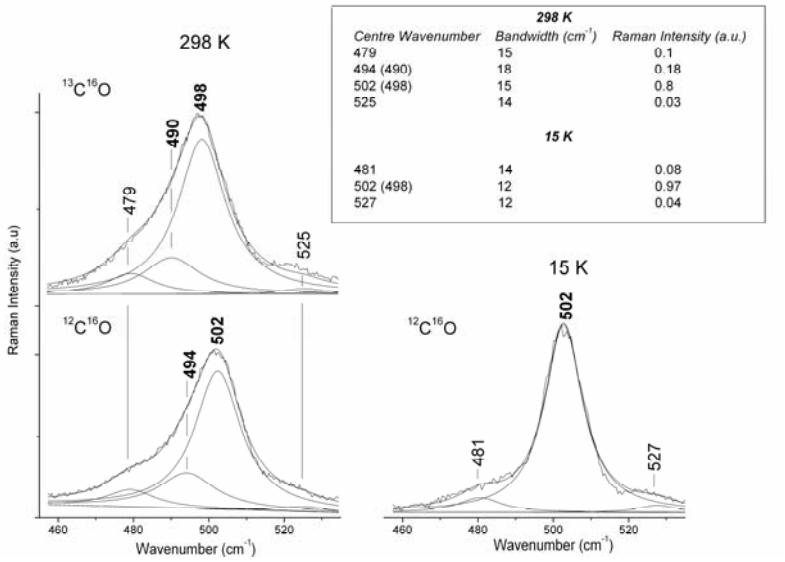

298 K		
Centre Wavenumber	Bandwidth (cm^{-1})	Raman Intensity (a.u.)
479	15	0.1
494 (490)	18	0.18
502 (498)	15	0.8
525	14	0.03
15 K		
481	14	0.08
502 (498)	12	0.97
527	12	0.04

Figure 6.7 RR spectra in the 460-535 cm^{-1} region and corresponding band fitting analysis of the ^{12}CO (298 K and 15 K) and ^{13}CO (298 K) complexes of *E. maclovinus* Hb1 (Fe^{2+})-CO. The spectra have been shifted along the ordinate axis to allow better visualization. Experimental conditions: at 298 K, see Figure 6.5; 15 K: 413.1 excitation wavelength, 5 cm^{-1} spectral resolution, 2 mW power at the sample, 8 s/0.5 cm^{-1} collection interval. The $\nu_{(Fe\text{-}CO)}$ bands are indicated in bold. The band fitting parameters are reported in the table. The ^{13}CO isotope shift is reported in brackets. The band observed at 479 cm^{-1} and at 298 K (481 cm^{-1} at 15 K) has been assigned to the ν_{33} B_{2g} mode, the band at 525 cm^{-1} (527 cm^{-1} at 15 K) to the ν_{25} A_{2g} mode.

A good curve fitting could be achieved either by increasing excessively the bandwidth of the 479 cm^{-1} mode (30 cm^{-1}) or, more reasonable, introducing a new band at 494 cm^{-1} that shifts to 490 cm^{-1} in the ^{13}CO adduct. The corresponding $\nu_{(CO)}$ stretching mode is tentatively placed at 1970 cm^{-1} (1925 cm^{-1} in ^{13}CO, Inset Figure 6.5) in accord with the IR measurements performed by Dr. Vergara at the University of Naples.

No differences have been revealed in the RR spectra in the presence of glycerol (present as a cryo-protector during X-ray diffraction at 100 K on the crystal of *E. maclovinus* Hb1 (Fe^{2+})-CO (*25*)) both at 298 and 15 K (Figure 6.8).

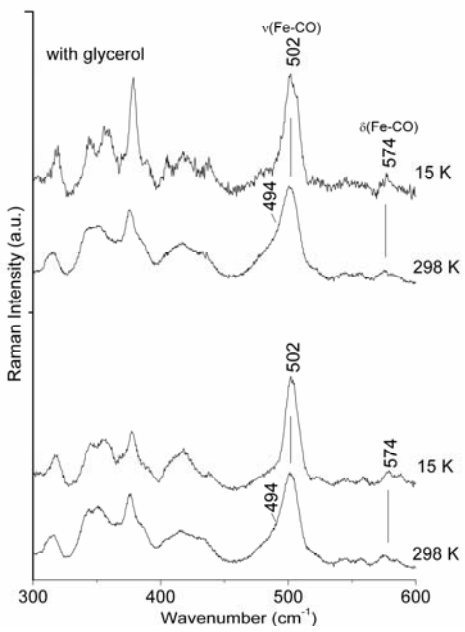

Figure 6.8 RR spectra in the low frequency region of *E. maclovinus* Hb1 (Fe^{2+})-CO adducts at pH 7.6, in 50 mM Tris-HCl buffer, in the absence and presence of 22% (v/v) glycerol, at 298 and 15 K. The spectra have been shifted along the ordinate axis to allow better visualization. Experimental conditions: sample without glycerol see Figure 6.5 and 6.7. With glycerol: 413.1 nm excitation wavelength, 1.2 cm^{-1} spectral resolution, 3 mW laser power at the sample (using a cylindrical lens), average of three spectra with 700 s integration time (298 K); 5 cm^{-1} spectral resolution, 0.8 mW laser power at the sample, collection interval 20 s/0.5 cm^{-1} (15 K).

6.3.3 Fe^{2+}-O_2 complex

E. maclovinus Hb1 (Fe^{2+}) was studied also in the oxy form. The absorption spectrum (Figure 6.4 A) is characterized by bands at 410, 540 and 575 cm^{-1}, which are characteristic of a complex-O_2 (*20*). Accordingly, the corresponding high frequency RR spectrum (Figure 6.4 B) is typical of a 6cLS species (1504 [ν_3], 1553 [ν_{38}], 1583 [ν_2], 1602 [ν_{37}] and 1638 cm^{-1} [ν_{10}]). Since the $\nu_{(Fe\text{-}O2)}$ frequency typically falls in the 550-580 cm^{-1} range depending on the ligand environment, this region was investigated by RR. The band at 572 cm^{-1} (Figure 6.5), which disappears upon photolysis induced by laser irradiation (Figure 6.5), is assigned to the $\nu_{(Fe\text{-}O2)}$ stretching mode. This frequency is slightly higher than human Hb A and *P. urvillii* Hb [568 cm^{-1}] (*26*) but similar to that of horse and elephant Mb [572 cm^{-1}] (*27*), suggesting slightly different hydrogen bonding interactions with distal residues compared to *P. urvillii*.

It is noteworthy that unlike human Hb A, but in common with *P. urvillii* Hb (*10*), all the high frequency RR spectra of *E. maclovinus* Hb1 display two $\nu_{(C=C)}$ vinyl stretching modes at 1621 and 1628 cm^{-1} in the Fe^{3+} species (Figure 6.2) and 1618 and 1626 cm^{-1} in the Fe^{2+} forms (Figure 6.4 B). A direct relationship between $\nu_{(C=C)}$ vinyl stretching frequency and the orientation of the vinyl groups, as induced by specific protein

interactions, has recently been found in heme-containing peroxidases (*28*). The presence of two vinyl bands indicates that the protein matrix does not exert constraints on the vinyl groups. Therefore, in analogy with the conclusion drawn for *P. urvillii* Hb, we suggest that the presence of two distinct vinyl stretches might be related to a reduced steric hindrance of vinyl 4, which is consistent with the replacement of Leu B13 with Cys in the β-chain of both *P. urvillii* Hb and *E. maclovinus* Hb1. A reduced steric hindrance upon replacement of the residue interacting with heme vinyl 4 contributes to the increased mobility of the heme, allowing it to shift to a more exposed position, as required for hemichrome formation.

Table 6.1 Comparison between the RR frequencies (cm^{-1}) of Fe-ligand stretching modes of *E. maclovinus* Hb1, *P. urvillii* Hb, human Hb A and *T. bernacchii* Hb.

	***E. maclovinus* Hb1**[a]	*P. urvillii* Hb [b]	human Hb A	*T. bernacchii* Hb
$\nu_{(Fe\text{-}Im)}$	213	215	215[c]	n.d.
$\nu_{(Fe\text{-}O2)}$	572	568	568[d]	n.d.
$\nu_{(Fe\text{-}CO)}$	502	502	507[e]	502[f]
$\nu_{(CO)}$	1954	1952	1951[e]	1951[h]

[a]This thesis. [b](*10*). [c](*19*). [d](*26*). [e](*20*). [f](*7*). [h] Vergara et al. unpublished data.

6.4 Resonance Raman on crystals

RR spectroscopy is a versatile technique and it can be performed also on protein crystals. To this end, an optical microscope is coupled to a Raman spectrometer to collect Raman signals from sample regions as small as a few micrometers. The advantage of microRR is the opportunity to compare directly crystallographic and spectral data, thus solving the question of whether crystal structure and solution structure are identical in proteins, especially in cases where multiple species are present (*29, 30*). Moreover, proteins might be difficult to crystallize, and often the addition of salts or hydrophilic compounds in the crystallizing medium may help the crystallization process. However, the chemicals can modify the active site of the protein since the structural balance that determines the coordination state in a heme protein can be very delicate.

Therefore, the carbomonoxy form of *E. maclovinus* Hb has been successfully crystallized in two different crystal forms: one form (Ortho) is orthorhombic and the other (Hexa) is hexagonal. Both forms are 6cLS species with His-Fe^{2+}-CO as axial

coordinated ligands, and after treating crystals with degassed stabilizing solutions containing 10 mM sodium dithionite, the Fe^{2+} iron loses the exogenous ligand and remains 5cHS. Furthermore crystals of the Fe^{3+} forms are 6cLS species (His-Fe^{3+}-His), confirming that *E. maclovinus* Hb shows identical iron spin state and axial ligand coordination both on solution and on crystal form.

6.5 Conclusions

1. A hemichrome species is present in *E. maclovinus* Hb1 (Fe^{3+}) around pH 7 as previously observed in the antartic Hbs from *T. Newnesi* and *T. bernacchi*.

2. Unlike human HbA, but in common with Hbs from *T. Newnesi* and *T. bernacchi,* two vinyl stretching modes are observed in all the forms of *E. Maclovinus* Hb1. The same primary structure variation compared to HbA (β chain LeuB13→ Cys), invoked to explain the appearance of two vinyl modes in *P. urvillii* Hb, could be recalled in *E. maclovinus*. The replacement of Leu B13 with Cys increases the distance of the B13 side chain from the heme and, consequently, induces a different conformation of the β heme vinyl 4.

3. The heme cavity properties of *E. maclovinus* Hb1 are essentially identical to those of *P. urvillii* Hb and very similar to human HbA as revealed by the close similarities of the spectroscopic properties of the ligand bound forms.

4. No differences occur in the iron spin state and in the axial ligand coordination of *E. maclovinus* Hb1 both in solution and in the crystal form.

References

(1) Eastman, J. T. (1993) Antartic fish biology: evolution in a unique environment. *Academic Press, Inc., San Diego, CA*.

(2) Cheng, C. H., Chen, L., Near, T. J., and Jin, Y. (2003) Functional antifreeze glycoprotein genes in temperate-water New Zealand nototheniid fish infer an Antarctic evolutionary origin. *Mol Biol Evol 20*, 1897-908.

(3) Johnston, I. I., Calvo, J., and Guderley, Y. H. (1998) Latitudinal variation in the abundance and oxidative capacities of muscle mitochondria in perciform fishes. *J Exp Biol 201 (Pt 1)*, 1-12.

(4) Clark, M. S., and Peck, L. S. (2009) HSP70 heat shock proteins and environmental stress in Antarctic marine organisms: a minireview. *Mar. Geonomics 2*, 11-18.

(5) Coppola, D., Giordano, D., Vergara, A., Mazzarella, L., di Prisco, G., Verde, C., and Russo, R. (2010) The hemoglobins of sub-Antarctic fishes of the suborder Notothenioidei. *Polar Sci. 4*, 295-308.

(6) Riccio, A., Vitagliano, L., di Prisco, G., Zagari, A., and Mazzarella, L. (2002) The crystal structure of a tetrameric hemoglobin in a partial hemichrome state. *Proc Natl Acad Sci U S A 99*, 9801-6.

(7) Merlino, A., Vitagliano, L., Howes, B. D., Verde, C., di Prisco, G., Smulevich, G., Sica, F., and Vergara, A. (2009) Combined crystallographic and spectroscopic analysis of Trematomus bernacchii hemoglobin highlights analogies and differences in the peculiar oxidation pathway of Antarctic fish hemoglobins. *Biopolymers*.

(8) Vitagliano, L., Vergara, A., Bonomi, G., Merlino, A., Verde, C., di Prisco, G., Howes, B. D., Smulevich, G., and Mazzarella, L. (2008) Spectroscopic and

crystallographic characterization of a tetrameric hemoglobin oxidation reveals structural features of the functional intermediate relaxed/tense state. *Journal of the American Chemical Society 130*, 10527-10535.

(9) Smulevich, G. (1998) Understanding heme cavity structure of peroxidases: comparison of electronic absorption and resonance Raman spectra with crystallographic results. *Biospectroscopy 4*, S3-17.

(10) Verde, C., Howes, B. D., De Rosa, M. C., Raiola, L., Smulevich, G., Williams, R., Giardina, B., Parisi, E., and Di Prisco, G. (2004) Structure and function of the Gondwanian hemoglobin of Pseudaphritis urvillii, a primitive notothenioid fish of temperate latitudes. *Protein Sci 13*, 2766-81.

(11) Choi, S., Spiro, T. G., Langry, K. G., Smith, K. M., Budd, D. L., and La Mar, G. N. (1982) Structural correlations and vinyl influences in the Resonance Raman spectra of protoheme complexes and proteins. *J Am Chem Soc 104*, 4345-4351.

(12) Smulevich, G., Miller, M. A., Kraut, J., and Spiro, T. G. (1991) Conformational change and histidine control of heme chemistry in cytochrome c peroxidase: resonance Raman evidence from Leu-52 and Gly-181 mutants of cytochrome c peroxidase. *Biochemistry 30*, 9546-58.

(13) Perutz, M. F., Ladner, J. E., Simon, S. R., and Ho, C. (1974) Influence of globin structure on the state of the heme. I. Human deoxyhemoglobin. *Biochemistry 13*, 2163-73.

(14) Rifkind, J. M., Abugo, O., Levy, A., and Heim, J. (1994) Detection, formation, and relevance of hemichromes and hemochromes. *Methods Enzymol 231*, 449-80.

(15) Vitagliano, L., Bonomi, G., Riccio, A., di Prisco, G., Smulevich, G., and Mazzarella, L. (2004) The oxidation process of Antarctic fish hemoglobins. *Eur J Biochem 271*, 1651-9.

(16) Feis, A., Marzocchi, M. P., Paoli, M., and Smulevich, G. (1994) Spin state and axial ligand bonding in the hydroxide complexes of metmyoglobin, methemoglobin, and horseradish peroxidase at room and low temperatures. *Biochemistry 33*, 4577-4583.

(17) Hirota, S., Ogura, T., ShinzawaItoh, K., Yoshikawa, S., and Kitagawa, T. (1996) Observation of multiple CN-isotope-sensitive Raman bands for CN- adducts of hemoglobin, myoglobin, and cytochrome c oxidase: Evidence for vibrational coupling between the Fe-C-N bending and porphyrin in-plane modes. *Journal of Physical Chemistry 100*, 15274-15279.

(18) Spiro, T. G., and Strekas, T. C. (1974) Resonance Raman spectra of heme proteins. Effects of oxidation and spin state. *J Am Chem Soc 96*, 338-45.

(19) Kitagawa, T. (1988) in: T.G. Spiro (Ed.), Biological Applications of Raman Spectroscopy: Resonance Raman Spectra of Hemes and Metalloproteins, Wiley, New York,. 97-131.

(20) Antonini, E., Brunori, M., and . (1971) Hemoglobin and myoglobin and their reaction with ligands (eds. A. Neuberger and E.L. Tatum), pp. 17-19. North Holland, Amsterdam.

(21) Spiro, T. G., and Wasbotten, I. H. (2005) CO as a vibrational probe of heme protein active sites. *J Inorg Biochem 99*, 34-44.

(22) Vogel, K. M., Kozlowski, P. M., Zgierski, M. Z., and Spiro, T. G. (1999) Determinants of the FeXO (X = C, N, O) vibrational frequencies in heme adducts from experiment and density functional theory. *Journal of the American Chemical Society 121*, 9915-9921.

(23) Li, T., Quillin, M. L., Phillips, G. N., Jr., and Olson, J. S. (1994) Structural determinants of the stretching frequency of CO bound to myoglobin. *Biochemistry 33*, 1433-46.
(24) Ling, J., Li, T., Olson, J. S., and Bocian, D. F. (1994) Identification of the iron-carbonyl stretch in distal histidine mutants of carbonmonoxymyoglobin. *Biochim Biophys Acta 1188*, 417-21.
(25) Merlino, A., Vitagliano, L., Balsamo, A., Nicoletti, F. P., Howes, B. D., Giordano, D., Coppola, D., di Prisco, G., Verde, C., Smulevich, G., Mazzarella, L., and Vergara, A. (2010) Crystallization, preliminary X-ray diffraction studies and Raman microscopy of the major hemoglobin from the sub-Antarctic fish Eleginops maclovinus in the carbomonoxy form *Acta Crystallogr. Sect. F: Struct. Biol. Cryst. Commun.*
(26) Robert, C. H., Fall, L., and Gill, S. J. (1988) Linkage of organic phosphates to oxygen binding in human hemoglobin at high concentrations. *Biochemistry 27*, 6835-43.
(27) Das, T. K., Couture, M., Ouellet, Y., Guertin, M., and Rousseau, D. L. (2001) Simultaneous observation of the O---O and Fe---O2 stretching modes in oxyhemoglobins. *Proc Natl Acad Sci U S A 98*, 479-84.
(28) Marzocchi, M. P., and Smulevich, G. (2003) Relationship between heme vinyl conformation and the protein matrix in peroxidases. *Journal of Raman Spectroscopy 34*, 725-736.
(29) Indiani, C., Santoni, E., Becucci, M., Boffi, A., Fukuyama, K., and Smulevich, G. (2003) New insight into the peroxidase-hydroxamic acid interaction revealed by the combination of spectroscopic and crystallographic studies. *Biochemistry 42*, 14066-74.
(30) Nielsen, K. L., Indiani, C., Henriksen, A., Feis, A., Becucci, M., Gajhede, M., Smulevich, G., and Welinder, K. G. (2001) Differential activity and structure of highly similar peroxidases. Spectroscopic, crystallographic, and enzymatic analyses of lignifying Arabidopsis thaliana peroxidase A2 and horseradish peroxidase A2. *Biochemistry 40*, 11013-21.

Chapter 7

Neuroglobins from icefish *Chaenocephalus aceratus* and from the Antarctic notothenioid *Dissostichus mawsoni*

7.1 Introduction

Neuroglobin (Ngb) is a monomeric globin, expressed in neuronal cells including retinal neurons, which is able to bind oxygen and NO (*1-4*). Although a number of hypotheses [signal transduction (*5*), involvement in Alzheimer's disease (*6*), and protection of neurons against the deleterious effects of hypoxia and ischemia (*7, 8*)] have been proposed, its functional role is still uncertain (*9*). However, Ngbs have essential beneficial effects for the neurons (*10*), supply oxygen to the retina (*11*) and have the ability to neutralise the neurotoxic effects of reactive oxygen species (ROS) (*12*) and reactive nitrogen species (*13*).

In the absence of exogenous ligands, the heme iron of both Fe^{3+} and Fe^{2+} forms are hexacoordinated with the distal His 64 (E7) and proximal His 96 (F8) (Figure 7.1). Nevertheless the physiological function of hexacoordinated hemoglobins is not well understood (*14*).

In human Ngb the structural analysis indicates the presence of a disulfide bond between the Cys residues at the positions CD7 and CD5 (*3*). The disruption of the cystine bond drastically lowers the oxygen affinity by a factor of 10 as it has been observed in both zebrafish Ngb and in murine Ngb (*4*).

Although the physiological role of the disulfide bond in human Ngb is not clear, hypoxia may induce the reduction of the disulfide bond thus allowing the subsequent release of oxygen.

Ngb was originally identified in mammalian species, however, the protein is widespread in all non-mammalian vertebrates including the zebrafish *Danio rerio* (*15*). Mammalian and zebrafish Ngbs share about 50% amino-acid sequence identity and their oxygen-binding properties are similar (*15*). Similar to mammalian Ngb, in zebrafish the oxygen

affinity is about 1 torr. The major differences between the two proteins seem to be related to the effects of disulfide bond on the Ngb function/regulation. The Ngb genes of human and zebrafish contain three conserved introns in the coding regions and four exons encoding compact protein structural modules called M1, 2, 3 and 4, respectively (*15, 16*). The module M1 sequence of zebrafish Ngb shares several amino-acid residues (Arg and Lys) with other fish Ngbs. These residues are replaced by Pro residues in human Ngb suggesting that the protein present in the fish have been mutated during evolution. Wittenberg and Wittenberg in 1975 observed the presence of an extracellular heme protein in the choroid blood from perfused retina of teleosts (*17*). The hemoprotein might correspond to Ngb and in fact only few years ago Ngb has been detected in the serumof gerbils (*18*) and in human cerebrospinal fluid in pain patients (*19*).

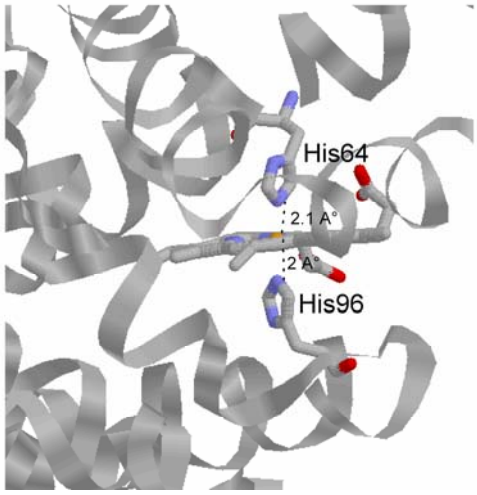

Figure 7.1. Crystal structure of the heme cavity of human Ngb (pdb 1oj6 (*3*)) showing the bis-His coordination to the iron.

The discovery of the Ngb gene in the brain and retina of Antarctic icefish (family *Channichthyidae*) suggests a crucial biological function (*20, 21*). The finding that icefishes retain the Ngb gene despite having lost hemoglobin and myoglobin in most species, may potentially have important implications in the physiology and pathology of the brain. The loss of globin genes in many species of this family together with enhanced lipid membrane densities (accompanied by higher concentrations of mitochondria) become explicable by the exploitation of high oxygen solubility and low metabolic rates in the cold. Oxygen supply largely occurs through circulatory and diffusive oxygen flux (*22*). Therefore, the icefish, as natural knockouts for

hemoglobin/myoglobin, represent a unique example to investigate the role of the protein in vertebrate metabolism.

In collaboration with Dr. Cinzia Verde (CNR of Naples) and Dr. Sylvia Dewilde (University of Antwerp), I have carried out a detailed comparative analysis of Ngbs isolated from the brain of the icefish *Chaenocephalus aceratus*, and from the retina of the closely related, but red-blooded, Antarctic notothenioid *Dissostichus mawsoni* using resonance Raman (RR) spectroscopy.

C. aceratus blood is nearly transparent, and contains leukocytes at <1% by volume, and is iron poor (*23*). In *C. aceratus*, oxygen is carried in physical solution in the plasma, providing ~10% of the carrying capacity of red-blooded notothenioids. *C. aceratus* fails to produce cardiac myoglobin and the mitochondrial density of its cardiomyocytes greatly increased (36% of cell volume) in comparison to the red-blooded, myoglobin-expressing notothenioids (16% of cell volume) (*24*). The expansion of cellular mitochondrial density in *C. aceratus* may enhance oxygen flux in the heart by two different mechanisms (*24, 25*). High densities of mitochondria may reduce the pathway length for diffusion of oxygen. Furthermore, mitochondrial expansion may provide a "lipid highway" to enhance diffusion. Together, these mechanisms may well compensate for the absence of myoglobin (*26, 27*) in the icefish.

7.2 Results and discussion

7.2.1 Ferric and ferrous forms

The UV-Vis and the high frequency region RR spectra of Fe^{3+} and Fe^{2+} *C. aceratus* are typical of 6-coordinate low spin hemes (6cLS) (Figure 7.2). In particular, the UV-Vis spectra of the Fe^{3+} (Soret band at 411 nm, β and α bands at 534 and 557 nm, respectively) and Fe^{2+} forms (Soret band at 425 nm, β and α bands at 530 and 560 nm, respectively), unequivocally indicates the presence of a bis-His heme iron coordination, in analogy with other Ngbs (*2*).

The UV-Vis and RR spectra of *D. mawsoni* are almost identical (1 nm shift of the Soret band in the Fe^{3+} form), and its spectroscopic data are reported in Figure 7.3.

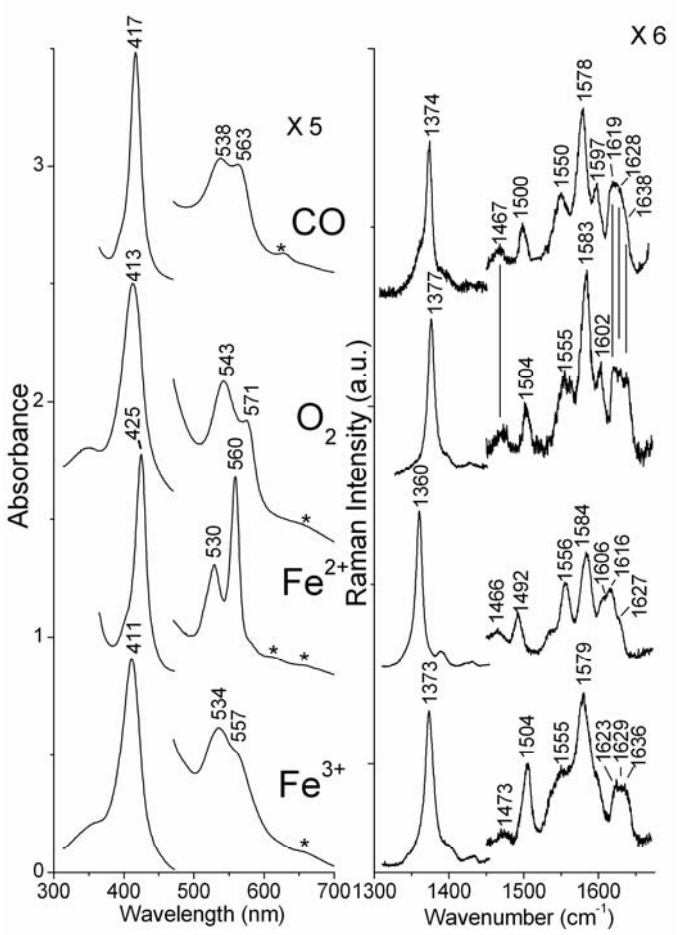

Figure 7.2 UV-Vis (left) and RR (right) spectra of Fe^{3+}, Fe^{2+}, -O_2, and -CO complex of *C. aceratus* Ngb. Experimental conditions: (Left) Scan rate of 600 nm/min. (Right) 413.1 nm excitation wavelength, 1.2 cm^{-1} spectral resolution. Fe^{3+}: 10 mW laser power at the sample, average of twenty spectra with 240 s integration time. Fe^{2+}: 10 mW laser power at the sample, average of ten spectra with 78 s integration time. -O_2: 1 mW laser power at the sample, average of thirty spectra with 180 s integration time. -CO: 900 μW laser power at the sample, average of seven spectra with 160 s integration time. The intensities are normalized to that of the ν_4 band. Spectra have been shifted along the ordinate axis to allow better visualization.

7.2.2 -O_2 and –CO adducts

Upon addition of O_2 e CO to the Fe^{2+} species, the diatomic ligands replace the distal His giving rise to the -O_2 (Soret at 413 nm, β and α at 543 e 571 nm, respectively) and -CO adducts (Soret at 417 nm, β and α at 538 e 563 nm) (*2, 4, 28*). The complete assignment of RR core size bands is reported in Table 7.1.

In the spectrum of the *C. aceratus* Ngb-O_2 adduct the band at 568 cm^{-1} (Figure 7.4 left panel), absent in both the RR spectra of the Fe^{2+} species and in the Fe^{2+}-CO adduct, is assigned to the $\nu_{(Fe\text{-}O2)}$ stretching mode. Its frequency, similar to that of mouse Ngb (571 cm^{-1}) (*29*), suggest the presence of a H-bond interaction between the –O_2 and the distal His (Chapter 1).

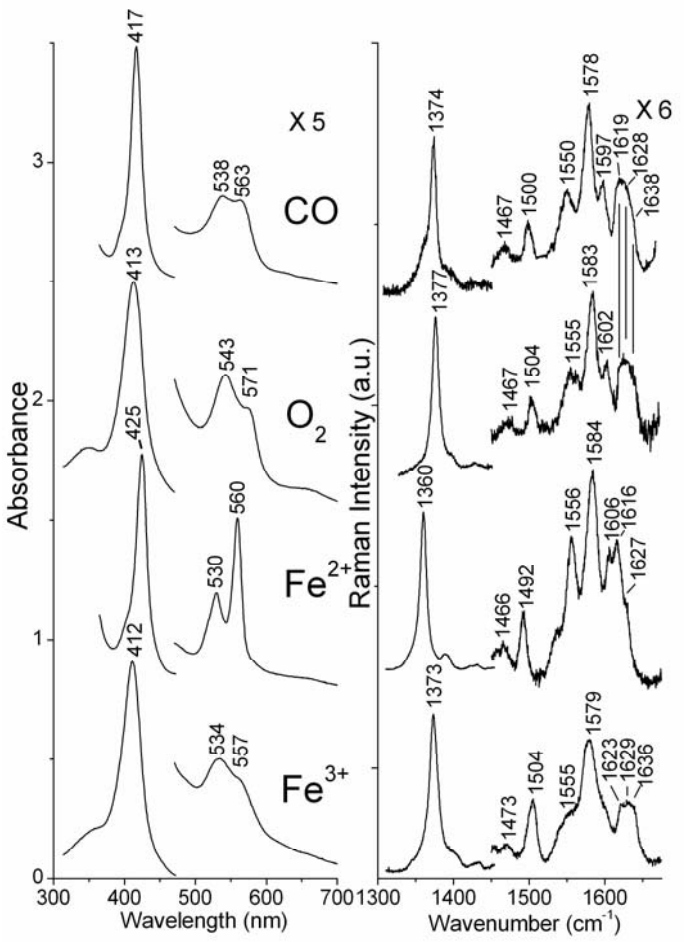

Figure 7.3 UV-vis (left) and RR (right) spectra of Fe^{3+}, Fe^{2+}, -O_2, and -CO complex of *D. mawsoni* Ngb, pH 7.6, in 20 mM TRIS. The asterisks in the spectrum of the CO adduct indicate impurities. Experimental conditions are identical to those of *C. aceratus* Ngb (see Figure 7.2).

Table 7.1 Normal mode assignments of the RR band (in cm^{-1}) observed in the high wavenumber region of the Fe^{3+}, Fe^{2+} forms together with the -O_2 and -CO adducts of *C. aceratus* and *D. mawsoni* Ngb, pH 7.6, in 20 mM TRIS. Sample concentration is about 30-35 μM.

Mode	Sym	**Fe^{3+}**	**Fe^{2+}**	**Fe^{2+}-O_2**	**Fe^{2+}-CO**
ν_{10}	B_{1g}	1636	overlapped[a]	1638	1638
$\nu_{(C=C)}$		1629	1627	1628	1628
$\nu_{(C=C)}$		1623	1616	1619	1619
ν_{37}	Eu		1606	1602	1597
ν_2	A_{1g}	1579	1584	1583	1578
ν_{19}	A_{2g}			1555	1550
ν_{38}	E_u	1555	1556		
ν_3	A_{1g}	1504	1492	1504	1500
ν_{28}	B_{2g}	1473	1466	1467	1467
ν_4	A_{1g}	1373	1360	1377	1374

[a]Overlapped with the $\nu_{(C=C)}$ at 1616 cm^{-1}

Further insight into the distal cavity can be obtained by the study of *C. aceratus* Ngb (Fe^{2+}) in the presence of CO. In analogy with the Fe^{2+}-CO complexes of human and mouse Ngbs (*4, 28*), the isotopic shift observed in the ^{13}CO adduct (Table 7.2) allows us to identify two conformations of the Fe^{2+}-CO unit in *C. aceratus* Fe^{2+}-CO adduct (Figure 7.4, left panel). One arises from an 'open' conformation (Form 1) of the distal histidine which prevents the H-bond with CO [$\nu_{(Fe-CO)}$ and $\nu_{(CO)}$ at 489 and 1965 cm^{-1}, respectively], and the other corresponding to a 'closed' conformation (Form 2) where the close proximity of the dissociated distal histidine to the CO group strongly stabilizes the complex as suggested by the $\nu_{(Fe-CO)}$ and $\nu_{(CO)}$ at 522 and 1934 cm^{-1}, respectively. Thus, the distal histidine can adopt two conformations in agreement with the previous findings for human WT Ngb and its H64V mutant (*4*). Moreover, recently a third conformer (Form 3), weakly H-bonded with a distal residue [$\nu_{(Fe-CO)}$ and $\nu_{(CO)}$ at 505 e 1956 cm^{-1}, respectively], has been identified in the RR spectra of the CO adduct of the recombinant human Ngb (*30*). The comparison of the $\nu_{(Fe-CO)}$ and $\nu_{(CO)}$ frequencies for different Ngbs-CO adducts reported in Table 7.2 clearly indicates that the exogenous ligand binds the proteins in a similar manner. Identical results have been obtained for Ngb from *D. mawsoni* (Figure 7.4, right panel).

Information on the proximal heme cavity cannot be obtained in the RR spectra of Fe^{2+} Ngbs since they are 6cLS species. Therefore the band at 224 cm^{-1} (Figure 7.4) observed also in human Ngb (*4, 30*) is assigned to a γ_{24}, in analogy to cytochrome c (*31*). For mouse Ngb the $\nu_{(Fe-His)}$ has been assigned to a band at 225 cm^{-1} in the RR spectrum of the transient Fe^{2+} photoproduct, obtained upon photolysis of the Fe^{2+}-CO complex (using 400 mW, and 413.1 nm excitation wavelength) (*28*). Unlike the previous experiment where upon CO photolysis the formation of the 5cHS species has been clearly evidenced by the appearance of the RR ν_3 mode at 1470 cm^{-1}, the photolysis of the *C. aceratus* Ngb-CO complex (using 25 mW, and 413.1 nm excitation wavelength), is followed by the immediate distal His rebinding to the heme iron giving rise to a bis-His 6cLS heme (ν_3 = 1492 cm^{-1}, Figure 7.5). As a consequence, in the low frequency region, while the $\nu_{(Fe-CO)}$ stretching mode at 522 cm^{-1} decreases in intensity, no new

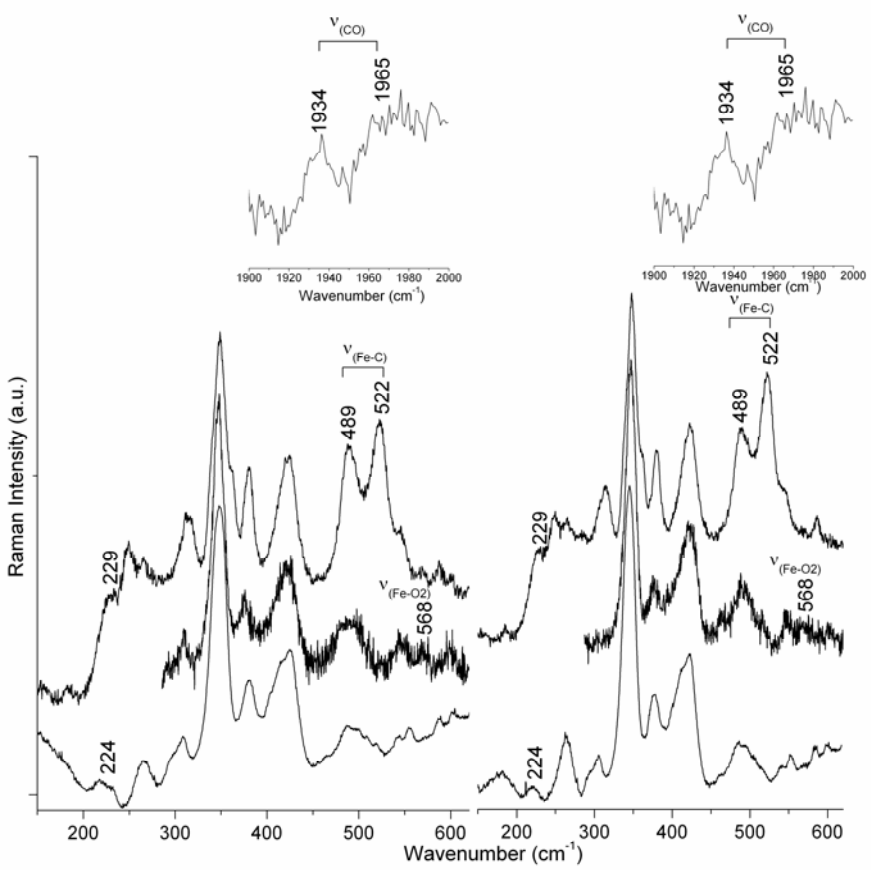

Figure 7.4 RR spectra in the low frequency region of Fe^{2+}, -O_2, and -CO complex of *C. aceratus* Ngb (left) and *D. mawsoni* Ngb (right). Experimental conditions as those reported in Figure 7.2. Fe^{2+}: average of 8 spectra with 300 sec integration time. -O_2: average of 6 spectra with 420 sec integration time. -CO: average of 14 spectra with 522 sec integration time. In the inset: RR spectra of the CO adducts in the $\nu_{(CO)}$ stretching region, average of 3 spectra with 3600 sec integration time, and 3.3 cm^{-1} spectral resolution. Spectra have been shifted along the ordinate axis to allow better visualization. The intensities are normalized to that of ν_7 (not shown).

Table 7.2 $\nu_{(Fe\text{-}CO)}$ and $\nu_{(CO)}$ frequencies (cm^{-1}) of the Fe^{2+}-CO adduct of different Ngbs. The frequencies obtained for the ^{13}CO- adducts are given in parentheses.

	Form 1 (no H-bond)		**Form 3 (weakly H-bond)**		**Form 2 (strongly H-bond)**		*Ref.*
	$\nu_{(Fe\text{-}CO)}$	**$\nu_{(COO)}$**	**$\nu_{(Fe\text{-}CO)}$**	**$\nu_{(CO)}$**	**$\nu_{(Fe\text{-}CO)}$**	**$\nu_{(CO)}$**	
C.aceratus	489	1965			522	1934	This
	(485)	(1918)			(518)	(1888)	thesis
Mouse	492	1969			523	1933	*(29)*
Human	494	1972	505	1956	521	1932	*(30, 33)*

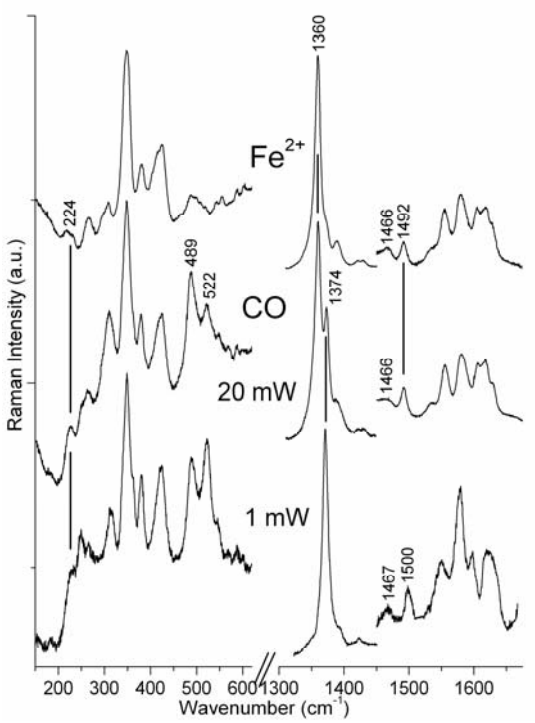

Figure 7.5 RR spectra in the high frequency region of the Fe^{2+} form, its CO complex, and the photolyzed -CO product of *C. aceratus* Ngb, pH 7.6, 20 mM TRIS. Experimental conditions for the Fe^{2+} and CO-adduct are as reported in Figures 7.2 and 7.3. Photolyzed-CO: 20 mW laser power at the sample, average of two spectra with 240 s integration time (high and low frequency regions). Spectra have been shifted along the ordinate axis to allow better visualization. The low frequency region has been expanded 2.5-fold.

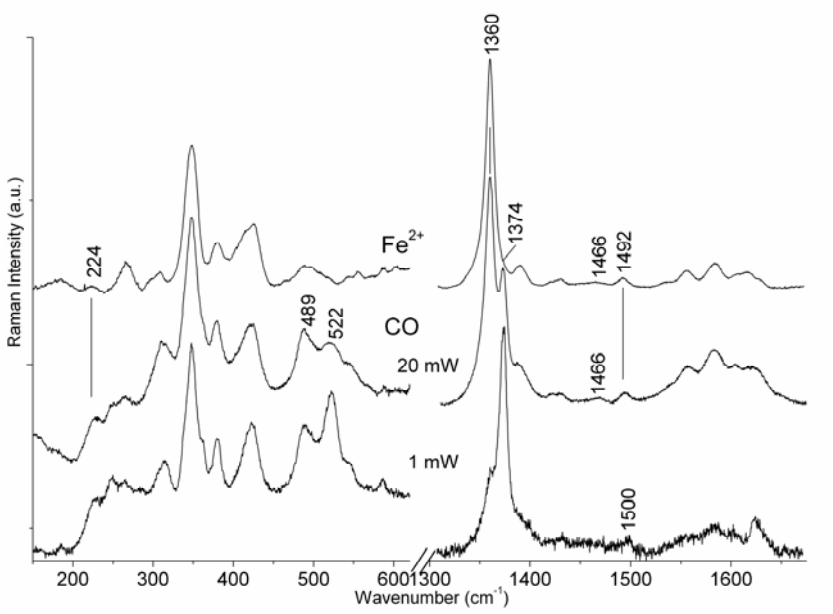

Figure 7.6 RR spectra in the high frequency region of the Fe^{2+} form, its CO complex, and the photolyzed -CO product of *D. mawsoni* Ngb, pH 7.6, 20 mM TRIS. Experimental conditions are identical to those of *C.aceratus* Ngb (Figure 7.5).

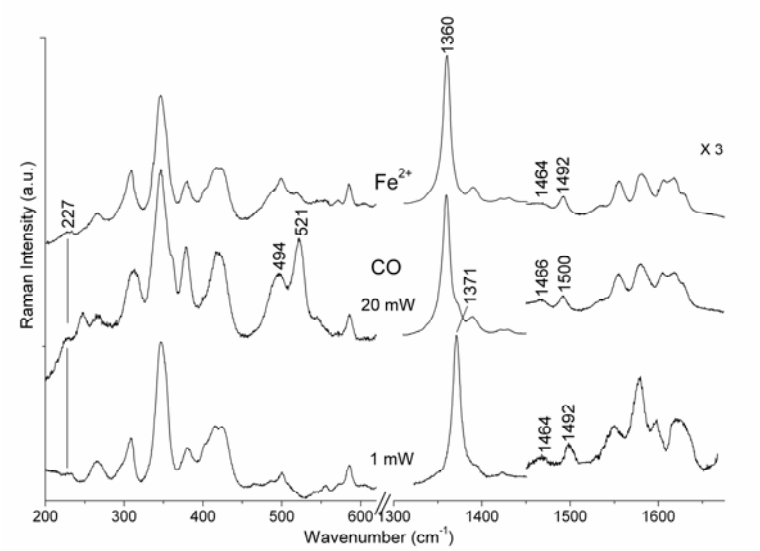

Figure 7.7 RR spectra in the high frequency region of the Fe^{2+} form, its -CO complex, and the photolyzed -CO product of human Ngb, pH 7.6, 20 mM TRIS. Experimental conditions: 413.1 nm excitation walelength, 0.9 cm^{-1} spectral resolution. Fe^{2+}: 15 mW laser power at the sample, average of three spectra with 190 s integration time (high frequency), average of six spectra with 300 s integration time (low frequency); -CO adduct: 1 mW laser power at the sample, average of six spectra with 180 s integration time (high frequency), average of ten spectra with 300 s integration tile (low frequency); photolyzed -CO: 20 mW laser power at the sample, average of 2 spectra with 240 s integration time (high frequency region), average of four spectra with 420 s integration time (low frequency regions). Spectra have been shifted along the ordinate axis to allow better visualization. The low frequency region has been expanded 2.5-fold.

band due to the $\nu_{(Fe\text{-}His)}$ stretch can be observed. Similarly, no $\nu_{(Fe\text{-}His)}$ stretch has been observed in the photolized-CO of Ngb from *D. mawsoni* (Figure 7.6) and human Ngb (Figure 7.7); however, its $\nu_{(Fe\text{-}His)}$ has been recently assigned via time resolved (*30*) and steady-state RR experiments on the distal variant H64V (*4*) at 221 cm^{-1}, a frequency similar to that observed in horse heart Mb (*32*).

7.3 Conclusions

In the absence of exogenous ligands the Fe^{3+} and Fe^{2+} forms of Ngbs from icefish *Chaenocephalus aceratus*, and from the Antarctic notothenioid *Dissostichus mawsoni*, are 6cLS being the distal and proximal histidine coordinated to the heme iron, similar to human and murine Ngbs (*4, 28*). Moreover upon addition of O_2 and CO, the comparison of the $\nu_{(Fe\text{-}XO)}$ stretching frequencies clearly indicate that the exogenous ligands bind the different Ngbs in a similar manner.

References

(1) Burmester, T., Weich, B., Reinhardt, S., and Hankeln, T. (2000) A vertebrate globin expressed in the brain. *Nature 407*, 520-523.

(2) Dewilde, S., Kiger, L., Burmester, T., Hankeln, T., Baudin-Creuza, V., Aerts, T., Marden, M. C., Caubergs, R., and Moens, L. (2001) Biochemical characterization and ligand binding properties of neuroglobin, a novel member of the globin family. *J. Biol. Chem. 276*, 38949-38955.

(3) Pesce, A., Dewilde, S., Nardini, M., Moens, L., Ascenzi, P., Hankeln, T., Burmester, T., and Bolognesi, M. (2003) Human brain neuroglobin structure reveals a distinct mode of controlling oxygen affinity. *Structure 11*, 1087-1095.

(4) Vallone, B., Nienhaus, K., Brunori, M., and Nienhaus, G. U. (2004) The structure of murine neuroglobin: Novel pathways for ligand migration and binding. *Proteins 56*, 85-92.

(5) Wakasugi, K., Nakano, T., and Morishima, I. (2003) Oxidized human neuroglobin acts as a heterotrimeric Galpha protein guanine nucleotide dissociation inhibitor. *J. Biol. Chem. 278*, 36505-36512.

(6) Khan, A. A., Mao, X. O., Banwait, S., Jin, K., and Greenberg, D. A. (2007) Neuroglobin attenuates beta-amyloid neurotoxicity in vitro and transgenic Alzheimer phenotype in vivo. *Proc. Natl. Acad. Sci. U S A 104*, 19114-19119.

(7) Sun, Y., Jin, K., Mao, X. O., Zhu, Y., and Greenberg, D. A. (2001) Neuroglobin is up-regulated by and protects neurons from hypoxic-ischemic injury. *Proc. Natl. Acad. Sci. U S A 98*, 15306-15311.

(8) Sun, Y., Jin, K., Peel, A., Mao, X. O., Xie, L., and Greenberg, D. A. (2003) Neuroglobin protects the brain from experimental stroke in vivo. *Proc. Natl. Acad. Sci. U S A 100*, 3497-3500.

(9) Hankeln, T., Ebner, B., Fuchs, C., Gerlach, F., Haberkamp, M., Laufs, T. L., Roesner, A., Schmidt, M., Weich, B., Wystub, S., Saaler-Reinhardt, S., Reuss, S., Bolognesi, M., De Sanctis, D., Marden, M. C., Kiger, L., Moens, L., Dewilde, S., Nevo, E., Avivi, A., Weber, R. E., Fago, A., and Burmester, T. (2005) Neuroglobin and cytoglobin in search of their role in the vertebrate globin family. *J. Inorg. Biochem. 99*, 110-119.

(10) Burmester, T., and Hankeln, T. (2009) What is the function of neuroglobin? *J. Exp. Biol. 212*, 1423-1428.

(11) Schmidt, M., Giessl, A., Laufs, T., Hankeln, T., Wolfrum, U., and Burmester, T. (2003) How does the eye breathe? Evidence for neuroglobin-mediated oxygen supply in the mammalian retina. *J. Biol. Chem. 278*, 1932-1935.

(12) Brunori, M., Giuffre, A., Nienhaus, K., Nienhaus, G. U., Scandurra, F. M., and Vallone, B. (2005) Neuroglobin, nitric oxide, and oxygen: functional pathways and conformational changes. *Proc. Natl. Acad. Sci. U S A 102*, 8483-8488.

(13) Herold, S., Fago, A., Weber, R. E., Dewilde, S., and Moens, L. (2004) Reactivity studies of the Fe(III) and Fe(II)NO forms of human neuroglobin reveal a potential role against oxidative stress. *J. Biol. Chem. 279*, 22841-22847.

(14) Kundu, S., Trent, J. T., 3rd, and Hargrove, M. S. (2003) Plants, humans and hemoglobins. *Trends Plant Sci. 8*, 387-393.

(15) Fuchs, C., Heib, V., Kiger, L., Haberkamp, M., Roesner, A., Schmidt, M., Hamdane, D., Marden, M. C., Hankeln, T., and Burmester, T. (2004) Zebrafish reveals different and conserved features of vertebrate neuroglobin gene structure, expression pattern, and ligand binding. *J. Biol. Chem. 279*, 24116-24122.

(16) Awenius, C., Hankeln, T., and Burmester, T. (2001) Neuroglobins from the zebrafish Danio rerio and the pufferfish Tetraodon nigroviridis. *Biochem. Biophys. Res. Commun*. *287*, 418-421.
(17) Wittenberg, J. B., and Wittenberg, B. A. (1975) A hemeprotein implicated in oxygen transport into the eye of fish. *Comp. Biochem. Physiol. A Comp. Physiol. 51*, 425-429.
(18) Shang, A., Zhou, D., Wang, L., Gao, Y., Fan, M., Wang, X., Zhou, R., and Zhang, C. (2006) Increased neuroglobin levels in the cerebral cortex and serum after ischemia-reperfusion insults. *Brain Res. 1078*, 219-226.
(19) Casado, B., Pannell, L. K., Whalen, G., Clauw, D. J., and Baraniuk, J. N. (2005) Human neuroglobin protein in cerebrospinal fluid. *Proteome Sci. 3*, 2.
(20) Cheng, C. H., di Prisco, G., and Verde, C. (2009) Cold-adapted Antarctic fish: the discovery of neuroglobin in the dominant suborder Notothenioidei. *Gene 433*, 100-101.
(21) Cheng, C. H., di Prisco, G., and Verde, C. (2009) The "icefish paradox." Which is the task of neuroglobin in Antarctic hemoglobin-less icefish? *IUBMB Life 61*, 184-188.
(22) Cheng, C. H., and Detrich, H. W., 3rd. (2007) Molecular ecophysiology of Antarctic notothenioid fishes. *Philos. Trans. R. Soc. Lond. B Biol. Sci. 362*, 2215-2232.
(23) Ruud, J. T. (1954) Vertebrates without erythrocytes and blood pigment. *Nature 173*, 848-850.
(24) O'Brien, K. M., Xue, H., and Sidell, B. D. (2000) Quantification of diffusion distance within the spongy myocardium of hearts from antarctic fishes. *Respir. Physiol. 122*, 71-80.
(25) Sidell, B. D. (1998) Intracellular oxygen diffusion: the roles of myoglobin and lipid at cold body temperature. *J. Exp. Biol. 201*, 1118-1127.
(26) Merx, M. W., Flögel, U., Stumpe, T., Gödecke, A., Decking, U. K., and Schrader, J. (2001) Myoglobin facilitates oxygen diffusion. *FASEB J. 15*, 1077-1079.
(27) Wittenberg, J. B., and Wittenberg, B. A. (2003) Myoglobin function reassessed. *J. Exp. Biol. 206*, 2011-2020.
(28) Das, T. K., Couture, M., Ouellet, Y., Guertin, M., and Rousseau, D. L. (2001) Simultaneous observation of the O---O and Fe---O2 stretching modes in oxyhemoglobins. *Proc. Natl. Acad. Sci. U S A 98*, 479-484.
(29) Couture, M., Burmester, T., Hankeln, T., and Rousseau, D. L. (2001) The heme environment of mouse neuroglobin. Evidence for the presence of two conformations of the heme pocket. *J. Biol. Chem. 276*, 36377-36382.
(30) Sawai, H., Makino, M., Mizutani, Y., Ohta, T., Sugimoto, H., Uno, T., Kawada, N., Yoshizato, K., Kitagawa, T., and Shiro, Y. (2005) Structural characterization of the proximal and distal histidine environment of cytoglobin and neuroglobin. *Biochemistry 44*, 13257-13265.
(31) Hu, S., Morris, I. K., Singh, J. P., Smith, K. M., and Spiro, T. G. (1993) Complete assignement of Cytochrome c resonance Raman spectra via enzymatic reconstitution with isotopically lebeled hemes. *J. Am. Chem. Soc. 115*, 12446-12458.
(32) Hu, S., Smith, K. M., and Spiro, T. G. (1996) Assignment of Protoheme Resonance Raman Spectrum by Heme Labeling in Myoglobin. *J. Am. Chem. Soc. 118*, 12638-12646.

(33) Uno, T., Ryu, D., Tsutsumi, H., Tomisugi, Y., Ishikawa, Y., Wilkinson, A. J., Sato, H., and Hayashi, T. (2004) Residues in the Distal Heme Pocket of Neuroglobin. *J. Biol. Chem. 279*, 5886-5893.

Conclusions

During my Ph.D. I was involved in several projects regarding the characterization of the heme cavity of new discovered heme proteins, by means of UV-Vis and RR spectroscopic techniques, with the aim of elucidating their functional role.

I studied the Human Serum Albumin (HSA) properties upon binding the heme in the subdomain IB, and ibuprofen and warfarin in the subdomain IIA. I have discovered that the complex of ferric heme with HSA, although this protein, is monomeric, shows allosteric properties. In fact, upon ibuprofen and warfarin binding a conformational change in the heme pocket occurs. The binding induces a 9 Å movement of the His146 which, therefore, coordinates in the 6^{th} coordination position of the iron atom. The link between different binding sites may influence the affinity of different drugs, when simultaneously present, and their pharmacokinetic. Moreover, the complex of the Fe^{2+} heme with HSA at pH 7 shows an equilibrium of two species: a five-coordinate high spin (5cHS) (Tyr-Fe^{2+}) and a six-coordinate low spin (6cLS) (Tyr-Fe^{2+}-His). Upon increasing the pH, the 6cLS species becomes predominant, indicating that HSA is sensitive to the pH effect. This conformational change confirms that the His146 is a very flexible residue.

The truncated hemoglobin (Hb) from *Thermobifida fusca* (Tf-trHb) contains a proximal histidine (His106) in the fifth axial coordination position of the heme iron. The study of the adducts with fluoride (in the Fe^{3+} form) and with CO (in the Fe^{2+} form) of the wild type and of single, double, triple Phe mutants of the distal Tyr54(B10), Tyr67(CD1), Trp119(G8) revealed that the key residues involved in the sixth axial ligand stabilization are the TrpG8 and TyrCD1. Moreover, this latter residue shows a very high flexibility. The TyrB10 does not participate in the distal ligand stabilization since it is far from the heme iron. Nevertheless, when it is the only polar residue present in the distal cavity (i.e. in TrpG8Phe/TyrCD1Phe variant), it appears to be weakly H-bonded with the incoming ligands. The functional role of Tf-trHb is still uncertain, however, the flexibility of the TyrCD1 together with the inter-play showed between the distal residues suggest that the protein might be involved in different functions. We also found that Tf-trHb is endowed with a high affinity for sulfide. The adduct with sulfide gives

rise to a stable 6cLS species in the Fe^{3+} state. In the low frequency region the strong band at 375 cm^{-1} has been assigned to the $\nu_{(Fe-S)}$ stretching mode, in analogy to Hb from *Lucina pectinata*, the only known Hb to posses a high affinity for the sulfide. We suggest that the sulfide binding depends on the properties of the distal heme cavity. In particular, the high affinity is due to the presence of an aromatic cage (TrpG8, TyrCD1 and TyrB10) that allows the interaction between the aromatic π electrons and the sulfur. Since Tf-trHb encoding gene is contained within a thiol redox pathway, we propose that this truncated hemoglobin might be involved in sulfide metabolism and in the biosynthesis of the cysteine.

The spectroscopic characterization of the Dehaloperoxidase-hemoglobin (DHP) in the Fe^{3+} state has revealed the equilibrium of two species: a 5cHS and 6cHS aquo form. The residue that control this equilibrium is the distal histidine (His55), that, in agreement with the X-ray crystal structures, can exist in two conformations: i) an open conformation in which the His55 is oriented towards the solvent and associated to the 5cHS species; ii) a close conformation corresponding to the 6cHS species where the His55 points to the iron and H-binds the water molecule present in the sixth axial position. Studies in presence of halogenated derivatives of phenol have revealed that the mono-halogen-phenols favour the open conformation (5cHS) while tri-halogen-phenols increase the 6cHS species (close conformation). Since enzymatic assays have revealed that the formation of the benzoquinone product occurs only in presence of H_2O_2 and tri-halogen-phenols (substrates of the reaction), and, on the contrary, the mono-halogen-phenol inhibitors reduce the yield amount, we have associated the close conformation to the catalytic species and the open as the inhibited form. The tri-halogen-phenols are toxic molecules and their oxidation is a mean of auto-defence exerted by DHP toward the *Amphitrite ornata* annelid. Recently, we also found that DHP is capable to bind sulfide due to the presence of an aromatic cage (His55 and four Phe). Furthermore, a complete reduction of the Fe^{3+} heme occurs after sulfide addition, due to the high $E°_{(Fe3+/Fe2+)}$ redox potential (200 mV) and the presence of the highly flexible distal histidine, that favours the oxidation of sulfide by accepting a H-bond. In fact, the presence of a H-bond acceptor is fundamental in order to induce a deprotonation of H_2S, stimulating, in turn, the formation of a Fe^{2+}-$SH^{\bullet}$ radical intermediate by one electron transfer from the Fe^{3+}-SH^{-} moiety. In the presence of a slight excess of ligand, the sulfide can react with the Fe^{2+}-$SH^{\bullet}$ radical intermediate, producing, in turn, the final

deoxy-DHP (or alternatively DHP-O_2) and various disulfide species. This behaviour suggest that DHP may have an important role in the catabolism of sulfide, a toxic environmental threat. In conclusion, the present results suggest that DHP is a detoxifying enzyme with a wide range of action being able to oxidise tri-halogen-phenols and sulfide.

I have characterized the tetrameric Hb from *Eleginops maclovinus*, the sister group of high-Antarctic notothenioids, which is the ideal subject for studying Hb adaptation to low temperatures. In fact, this fish lives in temperate waters and did not undergo historical exposure to the Antarctic climate.
Hb 1 from *E. maclovinus* displays functional and structural properties similar to those observed for other temperate and sub-Antartic notothenioid fish Hbs. In particular, similar to Hb of *Nothoteinoidei* fishes that live in cold waters, the Fe^{3+} form of *E. maclovinus* Hb1 is a hemicrome species (His-Fe^{3+}-His). This structural analogy is to be led back to the preservation of the gene encoding for the Hb1 and present originally in Antarctic species. Moreover, the study of the adducts with exogenous ligand such as fluoride, CO and O_2 indicated that *Nothoteinoidei* and human hemoglobins share similar binding stabilization exerted by the distal histidine.

During the last year of my Ph.D., I have characterized the neuroglobins from the Antarctic ice-fishes isolated from the brain of the *Chaenocephalus aceratus* and from the retina of *Dissosticus mawsoni.* Neuroglobin usually are coexpressed with myoglobin and hemoglobin, however, in the case of the *C. aceratus* it is expressed alone.
The two proteins are almost identical, being His-Fe-His both in the Fe^{3+} and Fe^{2+} forms and revealing similar binding properties in presence of exogenous ligand. Moreover, their spectroscopic properties are similar to those of human and murine neuroglobins. The functional significance of the hemicrome species is not well understood. However, neuroglobins are involved in a protective function against the reactive species of oxygen and their expression is upregulated by hypoxia.

Acknowledgements

Science is a team work and I feel indebted to many people who contribute significantly to the success of the work presented in this thesis.

First of all, thanks vey much to Prof. *Giulietta Smulevich* for offering me the possibility to work in her group at the Department of Chemistry, University of Florence. I have greatly benefited from this experience, scientifically and personally.

Grazie di cuore per la fiducia che ha sempre dimostrato nei mìei confronti concedendomi piena autonomia nel mio lavoro, per la comprensione, la pazienza, l'impegno, l'aiuto su tutti i fronti.

Thanks to all my group (Dr. *Alessandro Feis*, Dr. *Barry D. Howes*, Dr. *Enrica Droghetti* and Prof. *Mario Marzocchi*) for the technical and theoretical support and for the nice and friendly work atmosphere.

Grazie a tutti voi che in modi ed in momenti diversi avete contribuito a crescermi scientificamente e a rendere la mia permanenza in questo laboratorio un'esperienza indimenticabile.

I express my gratitude to all people with whom I have collaborated for the interest and fast feedback on the discussion of the data, the organization of all the steps of the scientific research. These collaborations were determinant for the success of this thesis.

Particular thanks to my parents, Gisella, Silvio, Mimmo e Patrizia, who showed interest in my work, offered support in hard times, very patient with my tiredness.

Un grazie non è sufficiente per voi. È al vostro supporto ed aiuto che devo il raggiungimento di questo traguardo. Grazie per avermi sempre incoraggiato anche nei momenti più difficili, per avermi sempre dimostrato fiducia e stima. Grazie per avermi fatto comprendere l'importanza di quello che stavo facendo. Grazie per essere sempre il mio punto di riferimento, il mio sostegno, la mia forza.